NBS SPECIAL PUBLICATION 415

U.S. DEPARTMENT OF COMMERCE / National Bureau of Standards

Biomaterials

NATIONAL BUREAU OF STANDARDS

The National Bureau of Standards[1] was established by an act of Congress March 3, 1901. The Bureau's overall goal is to strengthen and advance the Nation's science and technology and facilitate their effective application for public benefit. To this end, the Bureau conducts research and provides: (1) a basis for the Nation's physical measurement system, (2) scientific and technological services for industry and government, (3) a technical basis for equity in trade, and (4) technical services to promote public safety. The Bureau consists of the Institute for Basic Standards, the Institute for Materials Research, the Institute for Applied Technology, the Institute for Computer Sciences and Technology, and the Office for Information Programs.

THE INSTITUTE FOR BASIC STANDARDS provides the central basis within the United States of a complete and consistent system of physical measurement; coordinates that system with measurement systems of other nations; and furnishes essential services leading to accurate and uniform physical measurements throughout the Nation's scientific community, industry, and commerce. The Institute consists of a Center for Radiation Research, an Office of Measurement Services and the following divisions:

Applied Mathematics — Electricity — Mechanics — Heat — Optical Physics — Nuclear Sciences[2] — Applied Radiation[2] — Quantum Electronics[3] — Electromagnetics[3] — Time and Frequency[3] — Laboratory Astrophysics[3] — Cryogenics[3].

THE INSTITUTE FOR MATERIALS RESEARCH conducts materials research leading to improved methods of measurement, standards, and data on the properties of well-characterized materials needed by industry, commerce, educational institutions, and Government; provides advisory and research services to other Government agencies; and develops, produces, and distributes standard reference materials. The Institute consists of the Office of Standard Reference Materials and the following divisions:

Analytical Chemistry — Polymers — Metallurgy — Inorganic Materials — Reactor Radiation — Physical Chemistry.

THE INSTITUTE FOR APPLIED TECHNOLOGY provides technical services to promote the use of available technology and to facilitate technological innovation in industry and Government; cooperates with public and private organizations leading to the development of technological standards (including mandatory safety standards), codes and methods of test; and provides technical advice and services to Government agencies upon request. The Institute consists of a Center for Building Technology and the following divisions and offices:

Engineering and Product Standards — Weights and Measures — Invention and Innovation — Product Evaluation Technology — Electronic Technology — Technical Analysis — Measurement Engineering — Structures, Materials, and Life Safety[4] — Building Environment[4] — Technical Evaluation and Application[4] — Fire Technology.

THE INSTITUTE FOR COMPUTER SCIENCES AND TECHNOLOGY conducts research and provides technical services designed to aid Government agencies in improving cost effectiveness in the conduct of their programs through the selection, acquisition, and effective utilization of automatic data processing equipment; and serves as the principal focus within the executive branch for the development of Federal standards for automatic data processing equipment, techniques, and computer languages. The Institute consists of the following divisions:

Computer Services — Systems and Software — Computer Systems Engineering — Information Technology.

THE OFFICE FOR INFORMATION PROGRAMS promotes optimum dissemination and accessibility of scientific information generated within NBS and other agencies of the Federal Government; promotes the development of the National Standard Reference Data System and a system of information analysis centers dealing with the broader aspects of the National Measurement System; provides appropriate services to ensure that the NBS staff has optimum accessibility to the scientific information of the world. The Office consists of the following organizational units:

Office of Standard Reference Data — Office of Information Activities — Office of Technical Publications — Library — Office of International Relations.

---

[1] Headquarters and Laboratories at Gaithersburg, Maryland, unless otherwise noted; mailing address Washington, D.C. 20234.
[2] Part of the Center for Radiation Research.
[3] Located at Boulder, Colorado 80302.
[4] Part of the Center for Building Technology.

Biomaterials

Proceedings of a Symposium held in conjunction with the Ninth Annual Meeting of the Association for the Advancement of Medical Instrumentation, New Orleans, April 19-20, 1974

Edited by

Emanuel Horowitz and
John L. Torgesen

Institute for Materials Research
National Bureau of Standards
Washington, D.C. 20234

U.S. DEPARTMENT OF COMMERCE,
NATIONAL BUREAU OF STANDARDS, Richard W. Roberts, *Director*

Issued May 1975

Library of Congress Cataloging in Publication Data

Symposium on Biomaterials, New Orleans, 1974. Biomaterials.

(National Bureau of Standards Special Publication: 415)
Papers presented at the symposium held in conjunction with the 9th annual meeting of the Association for the Advancement of Medical Instrumentation, New Orleans, Apr. 19-20, 1974.
Supt. of Docs. No.: C 13.10:415
1. Biomedical Materials—Congresses. I. Horowitz, Emanuel. Ed. II. Torgesen, John L., Ed. III. Association for the Advancement of Medical Instrumentation. IV. Title. V. Series: United States. National Bureau of Standards. Special Publication; 415.
QC100.U57 No. 415 [R857.M3] 389'.08s [610'.28] 74-30305

National Bureau of Standards Special Publication 415

Nat. Bur. Stand. (U.S.), Spec. Publ. 415, 109 pages (May 1975)

CODEN: XNBSAV

U.S. GOVERNMENT PRINTING OFFICE
WASHINGTON: 1975

For sale by the Superintendent of Documents, U.S. Government Printing Office, Washington, D.C. 20402 (Order by SD Catalog No. C13.10:415). Price $1.75 (Add 25 percent additional for other than U.S. Mailing). Stock Number 0303-01363

Forward

For many years the National Bureau of Standards has conducted a research program for the improvement of dental materials. We are now embarking on a program involving other biomaterials. Our goals are the development of standards, specifications, and data necessary for the creation of improved synthetic implants, improved from the standpoint of increased durability and compatibility in the specialized environment of the body.

Success in such a program can only come from the interaction of our materials experts with the medical profession. We are pleased to cooperate with the Association for the Advancement of Medical Instrumentation, and to have participated in their Symposium on Biomaterials. I welcome such joint efforts, and hope that this publication will increase interest in this vital field.

Richard W. Roberts
Director

Preface

The Association for the Advancement of Medical Instrumentation concerns itself with virtually the complete spectrum of medical measurements and medical devices—the instrumentation involved, the techniques employed, safety, efficacy, and education. Within this broad scope of interest and concern are biomaterials including those used in the fabrication of synthetic implants which are employed to assist or replace body parts. We recognize that biomaterials research is broadly interdisciplinary in nature, requiring medical, surgical, engineering, and materials experts for its advancement. It is necessary that opportunities be provided for these experts to come together to discuss problems, progress, and the potential that biomaterials have in their applications to advances in health care.

We welcome, therefore, a collaboration with the National Bureau of Standards and its materials scientists in organizing and conducting technical sessions at our annual meetings to provide the forums for interchange of ideas between the medical, materials, and engineering communities. The present Symposium on Biomaterials was a feature of the Ninth Annual Meeting of AAMI, held in April, 1974 and is the second in a series organized by NBS on this topic.

We endorse the cooperation of the National Bureau of Standards in publishing this volume of the Proceedings of the Symposium as one in its series of Special Publications. We feel that this form of publication will contribute to a wide circulation of the volume and we pledge the full cooperation of AAMI in the execution of this worthwhile effort.

Harold Laufman, M.D.
President, 1974
The Association for the Advancement
of Medical Instrumentation

Contents

Abstract

This volume is based on papers presented at the Symposium on Biomaterials, held in conjunction with the Ninth Annual Meeting of the Association for the Advancement of Medical Instrumentation, New Orleans, La., April 19–20, 1974. It provides a review of special topics in biomaterials research selected to focus attention on some noteworthy achievements. The topics covered include plasma-polymerized polymers and their application in biomedicine; biocompatibility of ceramic materials and their application both as inert coatings for synthetic implants and as porous materials for bone repair; the selection of metallic implant materials through engineering and medical considerations; in vitro testing of thromboresistance; adsorption of blood proteins on synthetic substrates; a prosthesis for nerve regeneration; and properties of fibrous biomaterials.

Key words: Biocompatibility; biomaterials; blood protein; ceramic implants; implantable electrodes; metallic implants; nerve prosthesis; synthetic implants; thromboresistance.

Introduction

Papers published in this Special Publication of the National Bureau of Standards were presented orally at a Symposium on Biomaterials, held in conjunction with the Ninth Annual Meeting of the Association for the Advancement of Medical Instrumentation, New Orleans, La., April 19–20, 1974.

The aim of the Symposium and this publication is to review some of the important advances that have been made by the medical profession, materials scientists and engineers, and clinicians in the field of materials used for synthetic implants designed to restore body function and activities to patients.

Special topics of general interest were selected for the Symposium in order to focus attention on some noteworthy achievements. Thus, there is reported the plasma-generated synthesis of polymers whose properties are vastly different from those of polymers synthesized by conventional methods and which offer great potential for use in synthetic implants.

An intercomparison of the biocompatibility of certain ceramic materials points to the potential of these inert materials to withstand the body environment. A paper on the application of ceramic materials both as ceramic coatings achieved by a unique flame-spray technique and as porous material for bone repair involving bone ingrowth represents an important contribution to biomaterials research.

Metals and alloys are discussed from the standpoint of their selection for biomedical application based on engineering and biological considerations, the latter emphasizing systemic effects of metal corrosion products.

Thrombogenicity is the subject of two papers, the first describing a reliable *in-vitro* test system for thromboresistance of materials, the second a report on fundamental studies of adsorption of blood proteins on substitutes, which studies are attempting to elucidate the mechanisms of blood clotting.

The fabrication and behavior of implantable porous electrodes are described, work which attempts to decrease polarization losses in galvanic cells used to power pacemakers.

The properties of fibrous biomaterials as dependent on orientation of fibers and layers are discussed as applied to the development of composite biomaterials whose properties approach those of bone.

The final paper discusses the development and application of a prosthesis which is very successfully used in the regeneration of a severed nerve.

In including this symposium in the program of its Ninth Annual Meeting, the Association for the Advancement of Medical Instrumentation is performing an important service to the biomaterials community, as well as to the general public. The Symposium provides a forum for the discussion of progress in research on synthetic implant materials to assist in the development of standards and specification for these materials and improved methods of analysis, characterization and testing leading to improved materials for use by the surgeon to benefit the patient.

Emanuel Horowitz
John L. Torgesen
Institute for Materials Research
National Bureau of Standards

NATIONAL BUREAU OF STANDARDS SPECIAL PUBLICATION 415,
Biomaterials, Proceedings of a Symposium held in conjunction with the Ninth Annual Meeting of the Association for the Advancement of Medical Instrumentation, New Orleans, La., April 19–20, 1974
(Issued May 1975).

Plasma Formed Polymers for Biomedical Application
Part I. Synthesis and Fundamental Studies

K. G. Mayhan

**Graduate Center for Materials Research and Chemical Engineering Department
University of Missouri–Rolla, Rolla, Mo. 65401**

A. W. Hahn

**John M. Dalton Research Center
University of Missouri, Columbia, Mo. 34929**

M. R. Havens

**Graduate Center for Materials Research and Chemical Engineering Department
University of Missouri–Rolla, Rolla, Mo. 65401**

and

B. W. Peace

E. I. du Pont de Nemours, Wilmington, Del. 19898

The deposition of polymeric coatings through Rf plasma techniques is a unique process from several points of view. By introducing monomeric gases into an inert gas Rf plasma, the monomers are converted to ultrathin continuous polymer films. These films can be made to vary in thickness from less than 1 μm to 10 μm or more. These materials are insoluble to common organic solvents and are not attacked by strong mineral acids. In addition, the monomeric materials in the reactor are distilled gases and are therefore quite pure in comparison to monomers used for ordinary linear polymerizations. As a result, the polymer coatings which are formed do not contain residual catalysts or activists and are in a highly purified state. We have utilized the plasma polymerization process to produce polymer films intended for biomedical application. Plasma coatings have been formed from a wide variety of monomers. These coatings have been applied to various nonmetallic, metallic and organic substrates. In each instance it was found that continuous adherent films could be deposited after suitable substrate preparation and reactor operation parameters were established. It has been our experience that a general cleaning procedure for all substrates cannot be dictated and that the preparative steps involved are dictated by the environment to which the final product will be subjected.

Key words: Plasma-formed polymers; polymer films; polymer permeability; polymerization.

1. Introduction

During a recent NSF biomaterials planning session held in Washington, D.C., some basic definitions were laid down to guide research efforts in the biomaterials area. The definition adopted was:

> "Biomaterials are defined as any synthetic or modified natural materials which come into contact with body tissues or fluids. Biomaterials research is aimed toward providing the biomedical community with the best possible materials needed to aid in the restoration of bodily function and/or appearance. This research is directed towards obtaining knowledge which includes any information which may be expected to be useful in the development, synthesis, formulation and characterization of the biomaterials."

Plasma polymers are capable of being an integral part of the materials applications encompassed by this definition.

Research into plasma deposited polymers has grown recently to cover a wide range of topics. The Subcommission on Plasma Chemistry of the International Union of Pure and Applied Chemistry recently released a tabulation showing some 150 investigators, located in Australia, Austria, Belgium, Canada, Czechoslovakia, Denmark, France, Germany, Italy, Japan, The Netherlands, New Zealand, Switzerland, and the United Kingdom, who are actively working on some phase of plasma chemistry

or plasma physics. Also, some 100 investigators in the United States are pursuing similar endeavors. The research topics range from very fundamental mechanistic considerations to plasma technology, processing and applications. This work encompasses almost every field of engineering and science. To date, little has been reported on the application of plasma deposited polymers as a biomaterial. This paper summarizes the authors' bioapplications work which includes three main areas of plasma deposited polymers: (1) synthesis and characterization, (2) polymerization mechanisms and (3) applications.

When discussing biomedical applications, it is important to understand the differences between conventional linear polymers and those polymers formed in a plasma from the same monomers. For instance, conventional linear polymers, such as those derived from styrene, methyl methacrylate, vinyl acetate, and vinyl chloride, are produced by either free radical or ionic mechanisms. The resulting polymers consist of coiled chains having molecular weight distributions as low as two and as high as 10. When these polymers are placed in good thermodynamic solvents, they begin to swell and dissolve. Linear polymers can be melted and extruded and can also be made to decompose at fairly low temperatures. Outside of the normal branching found in most linear polymers, the repeat group is predictable.

By comparison, plasma polymers from the same monomers are formed by a multitude of mechanisms, all occurring simultaneously. The plasma deposited polymers are randomly branched, highly crosslinked, intertwined networks. The polymer resulting from formulation in the plasma is no longer soluble in good thermodynamic organic solvents.

Plasma deposited polymers are not even swollen. In fact, plasma polymers have been refluxed in boiling organic solvents for up to 7 days with only a 1–2 percent weight loss. Plasma deposited polymers do not melt, therefore cannot be extruded, but only decompose at comparatively higher temperatures. Also, plasma deposited polymers have shown considerably higher chemical resistance to reducing or oxidizing environments than conventional polymers. This resistance could be taken, at times, as inertness. Chiefly for the last two properties, minimal solubility and maximum chemical resistance, plasma deposited polymers deserve consideration as biomaterials.

2. Historical

A plasma was first defined by Langmuir in the early 1930's as a state a gas achieves when it is excited to the point of ionization. Plasma is more correctly defined as the region in which the active species are actually formed. Faraday and Crookes are perhaps the first to report observing a plasma glow. De la Rue and Muller reported a relationship between pressure, the type of glow and the resistance of the gas in the discharge. Crookes stated in 1879 that a plasma was a fourth state of matter. C. T. R. Wilson reported in the early 1900's that the electrical conductivity of plasmas was due to ionization of gas molecules by collisions with themselves. In 1910 Dewar and Jones reported the first silent discharge from a DC discharge in an evacuated Wood's tube. The silent discharge operated at much lower temperatures and would prove to be much more useful in chemical synthesis [1].[1]

Shortly after plasmas were observed, fundamental studies of their behavior were carried out primarily by physicists with little regard for the chemical aspects or possible applications of these plasmas. De Wilde [2] and A. Thenard [3] in 1874 reported simultaneously that acetylene reacted readily in a silent discharge leaving no gaseous residue and forming a hard, brittle solid which was insoluble in common solvents. This was the first report of plasma polymerization; however, no effort was made to study the phenomenon beyond this point. At this point in the history of chemistry, polymers were considered to be undesirable by-products and were of no interest.

The first and the oldest form of a plasma is the disruptive discharge, the arc and spark. These discharges produce very high temperatures since they operate with a high voltage source at either atmospheric or higher pressures. They are not useful in organic chemical synthesis since they operate at several thousand degrees Kelvin.

The other type of plasma is the silent plasma which operates in a vacuum and over a large temperature range which may be controlled by the power input to the plasma generator. There are five important types of the silent or nondisruptive discharge. The first is the *glow discharge* which is established in low pressure gases by low frequency rf applied across electrodes sealed into the reaction tube. Second is the *electrodeless discharge* which is formed by passing radio frequency current through a coil surrounding the tube. Third, the *point discharges* are established between conductive points operating at a high voltage, but arranged so as not to cause an arc. Fourth is the *corona discharge* which is similar to the point discharge except a fine wire is used in place of a conductive point. The fifth type is a variation of the corona and is widely used to produce ozone and thus is known as an *ozonizer*.

Both the glow and electrodeless discharge can operate at rather high power levels and remain at essentially ambient temperatures. For this reason they are usually chosen for organic synthesis studies.

Plasma Mechanisms. The initial discharge occurs as a result of the free electrons being acceler-

[1] Figures in brackets indicate the literature references at the end of the paper.

ated in an electric field until they can cause the gas molecules to ionize. The electrons that are released as a result of this ionization are further accelerated and cause subsequent ionization. This type of chain reaction will soon cause the gas to become conductive; the current or flux in the gas rises and a discharge is started. An equilibrium is established almost immediately where rate of ion formation is equal to the rate of recombination of the species. For an example of these reactions, let us consider the possible reactions of molecule AB which can be given by the following equations:

$$AB + e \rightarrow A + B^{-} \cdot \quad (1)$$

$$AB + e \rightarrow A^{-} + B \quad (2)$$

$$AB + e \rightarrow A^{+} + B^{-} + e \quad (3)$$

$$AB + e \rightarrow A^{-} + B^{+} + e \quad (4)$$

$$AB + e \rightarrow AB^{+} + 2e \quad (5)$$

$$A^{+} + e \rightarrow A \quad (6)$$

$$A^{-} + B^{+} \rightarrow AB \quad (7)$$

$$AB^{+} + e \rightarrow AB \quad (8)$$

Equations (1–5) represent the formation of active ionic species while (6–8) represent recombination reactions to form neutral species.

Free radicals are another type of active species formed and are of special importance in polymerization reactions. Radicals are formed when a molecule dissociates into two species in the discharge as given in eqs (9–12).

$$AB \rightarrow A \cdot + B \cdot \quad (9)$$

$$AB^{+} \rightarrow A^{-} + B^{+} \quad (10)$$

$$RH \rightarrow R \cdot + H \cdot \quad (11)$$

$$C_2H_5H \rightarrow C_2H_5 \cdot + H \cdot \quad (12)$$

Equation (12) is an example of an organic radical that has been observed by spectroscopy techniques. The radicals can propagate polymer chain growth until they combine to form a neutral species. This can occur in the gaseous phase by two mechanisms:

1. Disproportionation

$$2C_2H_5 \cdot \rightarrow C_2H_4 + C_2H_6 \quad (13)$$

2. Combination

$$2C_2H_5 \cdot \rightarrow C_4H_{10} \quad (14)$$

Chemical Synthesis in Plasmas-Organic. The early work in cold plasmas dealt with the transformation of a small organic molecule to different molecules. For example, Coats [4] identified 25 different hydrocarbon compounds after passing *n*-hexane through a microwave discharge plasma.

Two free radical reactions, disproportionation and combination, have already been discussed. Some additional free radical reactions will be given now. Hydrogen abstraction occurs via the free radical route and an example given by eq (15) was reported by Cher.

$$\text{Ø-}CH_3 + CH_3 \cdot \rightarrow CH_4 + \cdot CH_2\text{-Ø} \quad (15)$$

Here a methyl radical removes a hydrogen from toluene to form another free radical. Tomkinson [5] reported halogen abstraction could occur in like manner.

A reaction which can lead to polymerization was reported by Brinton and is given in eqs (16–18).

$$\text{Ø-}CH_3 + C_2H_4 \rightarrow \cdot C_3H_7\text{-Ø} \quad (16)$$

$$\text{Ø-}C_3H_7 \cdot + C_2H_4 \rightarrow \cdot C_5H_{11}\text{-Ø} \quad (17)$$

$$C_nH_{2n+1} \cdot + nC_2H_4 \rightarrow C(C_2H_4)_nC \cdot \quad (18)$$

Brinton's reactions terminated before polymer was formed; however, there seems to be no reason why eq (18) could not occur.

Investigations involving polymer plasma chemistry reported to date fall into two classifications: treatment of conventional polymer films in a plasma [6, 7] and actual polymerization of monomers using the plasma as an initiator [8–11].

Hanson et al. [12], reported that when several polymers (polyethylenes) were treated in a mild oxygen plasma, the bulk properties of the polymers were unaltered as the penetration was restricted to the first few hundred Angstroms of the films. In other cases surface ablation of the polymers was reported. With alkane polymers a highly oxidized surface was created which had vastly improved wettability characteristics. Hanson and Schonhorn [13] reported that treatment of polymer films of polyethylene and teflon in an oxygen plasma increased their adhesion properties. Weininger [14, 15] studied the effect of active nitrogen on polyethylene and polypropylene and found increased cross-linking and increased unsaturation resulting from the treatment. Hollahan, Stafford, Balk and Payne [16] reported that amino acid groups could be attached to polymer surfaces by treating the films with nitrogen and hydrogen plasmas. Bazzarree and Lin [17] treated fiberglas filaments with various vinyl type monomers (vinyltriacetoxysilane and vinyltriethoxysilane) in an attempt to increase their tensile strengths.

Shaw polymerized a silicone oil on the surface of small electronic devices and produced an im-

permeable, insulating, thin film. He used a medium power four megahertz capacitively-coupled plasma [18]. Ozawa [19] employed plasma polymerization techniques using styrene and tetrafluoroethylene to make thin film insulators for micro capacitors. He used an alternating current (low frequency) electrode discharge plasma in a long glass tube. He found a more uniform coating was formed when the substrates to be coated were placed away from the electrodes in the plasma glow. Mearns [20] published a review which includes the use of plasma polymerization in the production of thin insulating films.

Some work with vinyl type monomers has been reported. Goodman [21] described the formation of uniform thin (0.1 to 2 μm) polymer films with a plasma from a high voltage alternating current discharge between two parallel plates. Some of the monomers used were styrene, methyl methacrylate, tetrafluoroethylene, monochlorotrifluoroethylene, and difluoroethylene as well as some nonvinyl compounds such as benzene, toluene, and chlorodifluoromethane. Williams and Hayes [22] also reported the flow discharge polymerization of several vinyl type monomers. Denaro, Owens, and Crawshaw [23] investigated the flow discharge polymerization of styrene. This is the more comprehensive plasma polymerization study reported.

The initial work summarized above led to many investigations both basic and applied. The following investigations represent only those which interface the work of the authors and, thus, are not to be considered as a comprehensive list. Several books [24–26] and one general review [27] related to plasma chemistry have been published. Suhr [28] and Stille, [30–31] among others, have investigated some basic organic synthesis using plasmas. Other investigations have looked into oxidation [32] and decomposition [33–36] of various materials in plasmas. A number of investigators have looked into the polymerization aspects of plasma chemistry [37–44]. Others have looked at specifics in the polymeric films which are usually produced [45, 46]. Some specific applications of these films have recently begun to appear in the literature [47–49]. The authors and others [50] have been investigating acceptability of the plasma-deposited polymeric films to biomedical applications.

3. Plasma Reaction Procedures

Before discussing some of the specifics of biomaterials work with the plasma polymers, the actual physical and chemical processes involved in their formation should be described in general terms. Figures 1 and 2 show block diagrams of the reactor system. Figure 3 is a photograph showing one of our more refined reactor systems where basic studies are performed. Figure 4 shows a low cost reactor which was designed and constructed in our laboratories to be utilized in the applications research.

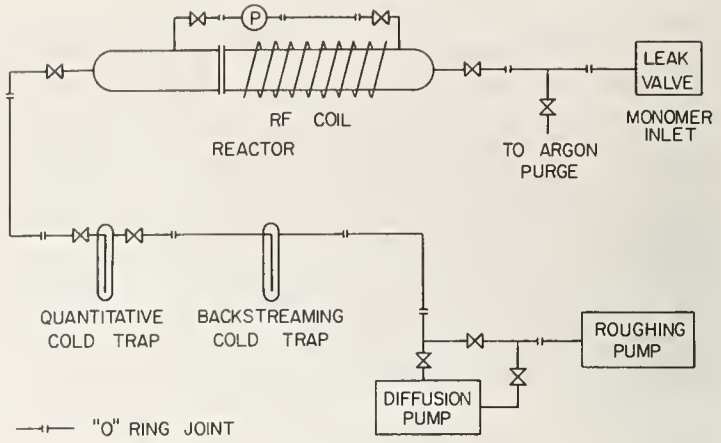

FIGURE 1. *Schematic of reactor system.*

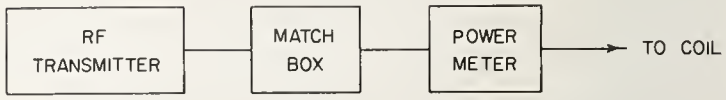

FIGURE 2. *Schematic of power input to load coil.*

The reactors can all be characterized simply as glass tubes wrapped with a copper coil which serves to direct the incident rf power into the tube volume. One end of the reactor contains the inlet system which is one or more leak valves. The other end is connected to a cold trap and then to a vacuum system. The electronics for the rf power are a straightforward application of conventional ham radio parts.

The first step in the process involves consideration of the type of substrate to be either coated, cleaned, or converted. Substrate preparation and cleaning procedures used vary considerably with the type of material to be coated. The cleaning procedures may vary from rinsing with residue free solvents to chemical etching followed by thorough distilled water rinses. In some cases we have resorted to ESCA and Auger spectroscopy to determine the effectiveness of overall surface preparation prior to deposition of plasma polymer films with regard to resulting film adhesion. An example would be a glass substrate. The structure of the cleaned glass substrate and subsequent adherence of the plasma polymer is a function of the chemical composition of the glass. Each material (metals, ceramic, polymer) presents its own unique problems which must be worked out for each application. After the samples to be coated have been cleaned, care is taken not to contaminate the surface through improper storage or handling.

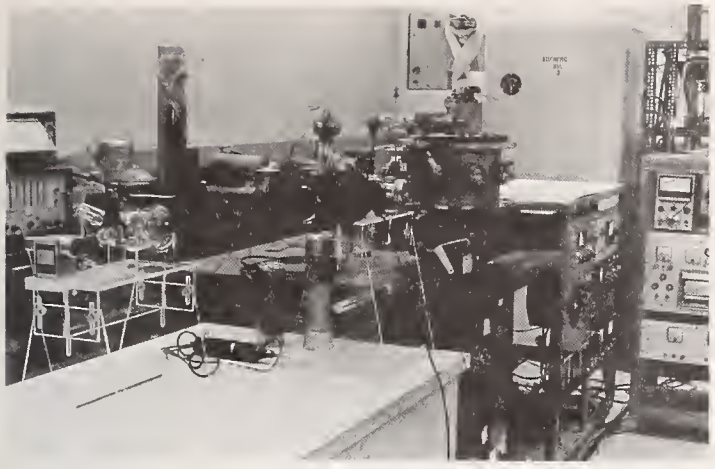

FIGURE 3. *Research reactor.*

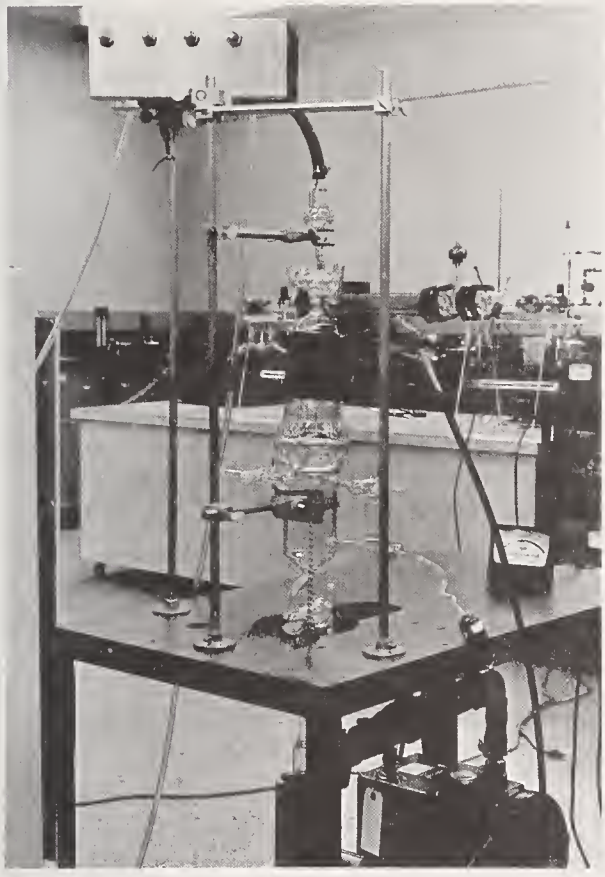

FIGURE 4. *Applications reactor.*

The substrate is then loaded into the reactor either for further cleaning or to be coated. The reactor is then secured and evacuated to a vacuum of below 10^{-4} torr. A prepurified gas (Argon, Helium, Nitrogen, etc.) is bled into the system to achieve a desired pressure. The rf power is tuned up and followed by initiation of the plasma by means of a Tesla coil. By utilizing the initial gas at a higher power level than for polymerization, it is possible, in many instances, to obtain additional substrate cleaning through the interactions of the ionized gas and the substrate. Similar treatments have also been effective in removing impurities from the surfaces of implant devices. This interaction step can be a prelude to sterilization. At this point the monomeric gas of choice can be introduced simultaneously with the inert gas flow or the inert gas can be discontinued and simply replaced with monomeric gas. The pressure and power are adjusted to their final values, respectively, by setting the leak valves and tuning and matching the rf transmitter and load.

The coating process then proceeds until the desired thickness of material is obtained. Relatively pure polymer films with thicknesses of 0.5 to 10 μm can be formed effectively by this means. These films, as will be noted in part 2, have little or no tissue reactions. Any tissue reactions which may occur can be assigned to the polymer structure itself and not to the impurities present in most conventional polymer systems. This assignment can be made because it is inherent to this coating process that all monomers enter the reactor as gases. Thus, the gases can be considered to be essentially purified by their being distilled away from any initiators, catalysts, or inhibitors which normally appear as contaminants in the product. Also, no sensitizers, initiators or catalysts are needed in the reaction.

The total time for deposition can vary from 15 minutes to 12 hours. The rate of polymer deposition is largely dependent on the power input to the load coil, the effective concentration of the monomer gas or gases and reactivity of the particular monomer involved. After polymerization, the reactor is returned to atmospheric pressure by slowly introducing the desired terminating gas.

Recent work in the authors' laboratories has shown that an alternate embodiment of the above procedure can also lead to useful polymer films. After proper cleaning, the substrate is coated with a thin film of a nonvolatile low molecular weight polymer or a nonvolatile high molecular weight monomer where both are generally in the form of a liquid. After evacuation of the reaction vessel, a nonpolymerizing gas is introduced into and excited in the rf field through proper adjustment of the reaction parameters. The liquid film is converted to a solid insoluble polymer having properties similar to those contained in the gas phase deposition. Several interesting systems have been developed through this special synthesis technique.

Other related work has been completed recently which involves linear polymer film interactions with plasmas. Both plasmas of polymerizable and nonpolymerizable gases were used. In both cases, the result is that the surface of the linear polymer film is converted to material similar to that obtained in the previously discussed liquid phase-plasma interactions.

4. Generalized Results

In the authors' laboratories, the tubular type inductively coupled reactors have been found to be superior to the capacitively coupled plate reactors in the applications investigated. Figure 5 (Plasma ethylene) shows the type of polymer distribution obtained for one reactor through more refined design techniques. The bell-shaped curve may be further flattened allowing more uniform polymer deposition.

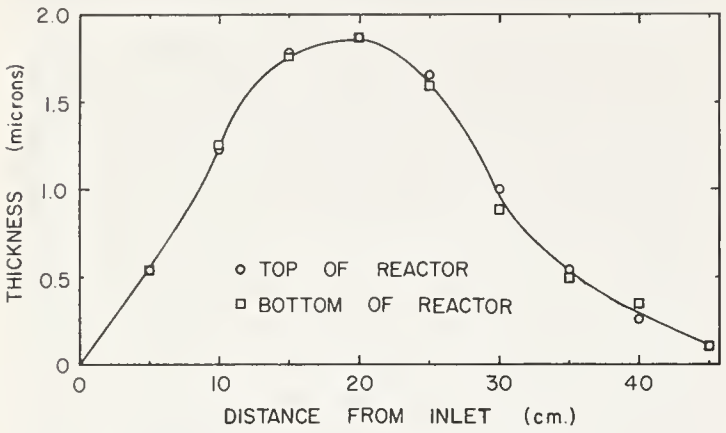

FIGURE 5. *Polymer formation distribution.*

It should be noted that equal deposition around the circumference of the reactor is observed. Kinetic studies have revealed that the rate of polymer deposition at any point in the reactor is constant with time with all other reaction parameters being constant. Figure 6 illustrates the temperature rise in the reactor as a function both of power input and thermocouple position in the reactor. General experience shows that acceptable polymer films can be obtained outside of the reactor volume circumscribed by the coil with little or no temperature rise while operating at fairly high power levels. It has also been shown that monomeric conversion can be controlled by adjusting power inputs and monomer concentration.

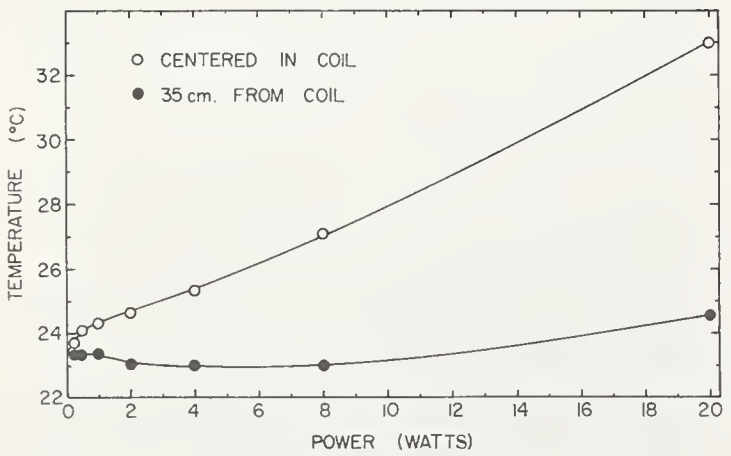

FIGURE 6. *Temperature rise as a function of power input and reactor position.*

At first glance, it would appear that plasma polymerization products possess a much greater thermal stability than corresponding linear polymers. Indeed, this is true after a fashion. Figure 7 shows thermograms for linear and plasma polystyrene heated in air to 700 °C. The plasma polystyrene still retains 40 percent of its initial weight whereas all of the linear polystyrene has decomposed below 400 °C. However, a closer look at these thermograms indicated that the plasma polymer actually began to lose weight initially at a considerably lower temperature than the linear polymer. Therefore, any statements about thermal stability must take into account the temperature range under consideration. The four curves of plasma polystyrene in figure 7 show the effect of polymer film thickness. It becomes apparent that the rate of escape of the decomposition products from the thicker films is a diffusion controlled process. Work currently underway is designed to determine the nature of the apparent instability of these materials. Ways and means are being sought to stabilize the plasma polymer films through quenching techniques in order to flash off any low molecular weight volatiles.

In one aspect of application, some work has been completed recently in investigating plasma deposited polymers for use as membranes. The pur-

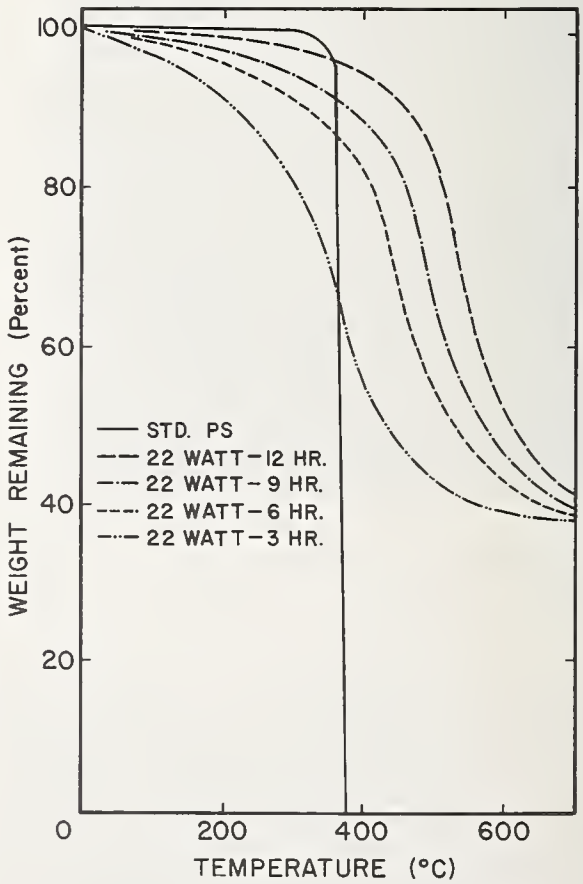

FIGURE 7. *Thermogram of plasma polystyrene.*

TABLE 1. *Permeability of gases through uncoated and coated films*

Gas	Permeability $\left(\frac{\text{cm}^3\ (\text{STP})\ \text{cm}}{\text{cm Hg-cm}^2\text{-s}}\right) \times 10^{10}$ [a]	
	Uncoated 1 mil (25 μm) polyethylene film	1 mil (25 μm) polyethylene film coated with 1–2 micrometers polypropylene
Helium	6.290	3.33
Neon	2.070	0.72
Oxygen	3.250	1.00
Argon	0.375	[b]
Carbon dioxide	9.290	1.93

[a] For conversion to SI units (mol·cm·cm^{-2}·Pa^{-1}·s^{-1}), multiply values by 3.3×10^{-8}.

[b] Permeation rates were too slow for satisfactory measurements.

pose of this work was to show that adherent plasma polymer films could be deposited on smooth polymer membrane surfaces thereby altering the membrane's permeability characteristics. Unplasticized linear polyethylene membranes 1-mil (25 μm) thick, were chosen at the start of the experiments. On these membranes was deposited a 1–2 micrometer film of adherent polypropylene.

The permeability of the coated and uncoated membranes to He, Ne, Ar, O_2, and CO_2 was measured. The results are tabulated in table 1. In comparing the data for coated and uncoated membranes, it is plain that the thin (2 μm) film of plasma deposited polypropylene considerably reduced the permeability constants. These permeability constants are plotted against the square root of the permeating gas' molecular weight in figure 8. Both oxygen and carbon dioxide show a definite dissolution in the uncoated membrane but appear to approach Graham's law behavior with the coated membrane. The slight change in slope between helium and neon in both coated and uncoated cases indicates that some pores have been altered or plugged in the coating process.

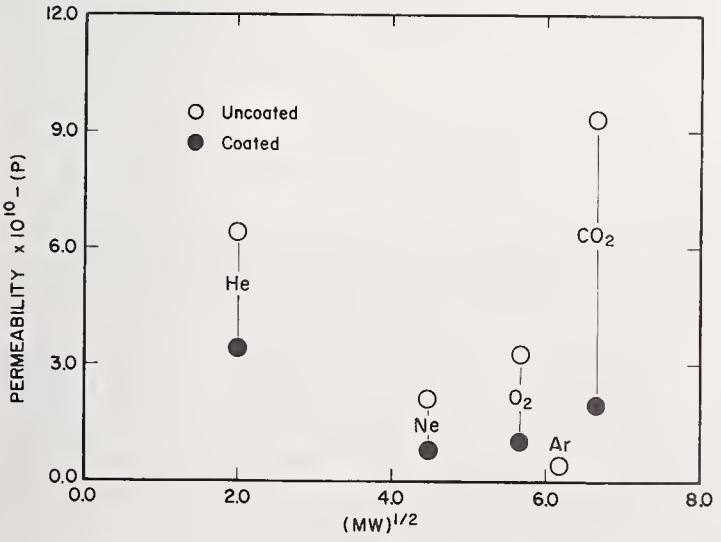

FIGURE 8. *Permeability of uncoated and coated 1-mil polyethylene*

The significance of this data must be evaluated by taking into account the two terms of the permeability constant. This constant is the product of the diffusion constant and solubility constant, $P = DS$. The large reduction in the permeability cannot be explained wholly by the reduction in diffusion through pores which have been altered or plugged by the plasma deposited film. It is known that plasma deposited films are highly cross-linked into a tight three-dimensional network. For example, plasma polypropylene samples have been refluxed in aliphatic and aromatic hydrocarbons, chlorinated hydrocarbons, esters, and ketones for up to a week without appreciable changes in solubility. Thus, the plasma deposited film reduces the solubility of O_2 and CO_2 which allows diffusion to be the predominant transport mechanism, although it is also significantly reduced. The result is to approach Graham's law.

For these reasons, plasma deposited polymer films may have certain advantages as membrane materials. It appears possible that by tailoring thickness and/or composition of the film, a membrane can be made to very nearly approach Graham's law behavior. Behavior like this could be important in those applications where either a definite ratio of two gases is desired for a particular transfer application or where a specific diffusion rate is required. However, greater film thicknesses could conceivably block gas permeation across the membrane.

A complimentary membrane study involved taking the same membrane material and subjecting it to a high wattage argon plasma. The investigation was aimed at alterations of the permeability constant by interaction of the membrane surface with the nonreactive plasma as opposed to plasma polymer depositions. Results of this work for carbon dioxide and helium permeation are shown in figure 9. Permeability was reduced but not as significantly as was the case with plasma deposited polymer films.

Since the aforementioned properties of plasma deposited polymers are markedly different from

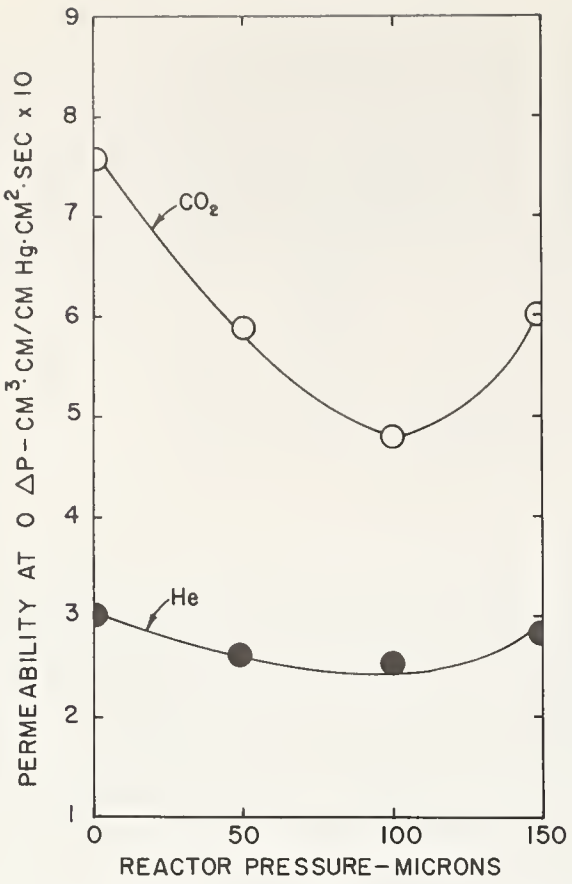

FIGURE 9. *Permeability of gases through plasma treated 1-mil polyethylene.*

those of their generic polymers, an investigation into the more fundamental property of density was initiated. The densities of nine rf plasma produced polymers were determined in a gradient density column. Generally, these polymers were found to be more dense than conventional polymers produced from the same monomer species via common free radical, ionic, or condensation polymerizations. The results of the density determinations are given in table 2. A density range is given for each polymer because the density was found to vary with the monomer concentration, the power level and the position within the reactor. For comparison, the densities of both the single crystal and the amorphous conventional linear polymer are reported. Low angle x-ray diffraction patterns of plasma polystyrene and polyethylene indicated that these materials were amorphous. Since the generic polymers of styrene and ethylene are highly crystalline, this indicates that substantial differences in structure and morphology are present. This density data has been correlated with refractive index measurements of the plasma deposited films. Further probing of these properties has resulted in preliminary data from elemental analysis that indicates oxygen and sometimes nitrogen are incorporated into the plasma deposited films. For example, plasma deposited polyethylene was found to contain from 20 to 30 weight percent oxygen. In addition, the density, refractive index and chemical composition have all been found to vary as functions of both reactor design and operation. Current investigations are aimed at determining the source of these elements and the method of their incorporation into the polymer.

5. Current Problems and Future Work

The early work of the authors involving the coating of bioelectrodes and various implantable substrates went well and yielded promising results. It appears that this early work stayed within the then undefined tolerance limits of substrate preparation, reaction parameters and coating techniques. Reports of dissimilar results from other laboratories for the same monomers regarding both changes in the polymers after formation and elucidation of different reaction mechanisms were disturbing since these phenomena had not been observed in our laboratories. However, these problems and many more began to surface once a realistic approach was

TABLE 2. *Polymer densities*

Starting monomer	Density range of plasma polymer (g/cm^3)	Crystal density [3] of linear polymer (g/cm^3)	Amorphous density [3] of linear polymer (g/cm^3)
Styrene	1.332–1.408	1.126	1.04
Ethylene	1.141–1.231	1.014	0.852
Vinyl chloride	1.463–1.499	1.44–1.522	1.39
Vinyl fluoride	1.341–1.395	1.44	—
Benzene	1.331–1.364	—	—
Acrylonitrile	1.402–1.436	1.11 syndiotactic 1.54 isotactic	— —
Allene	1.195–1.203	—	—
Methylvinyl-dichlorosilane	1.435–1.454	—	—
Allylamine [4]	1.212	—	—

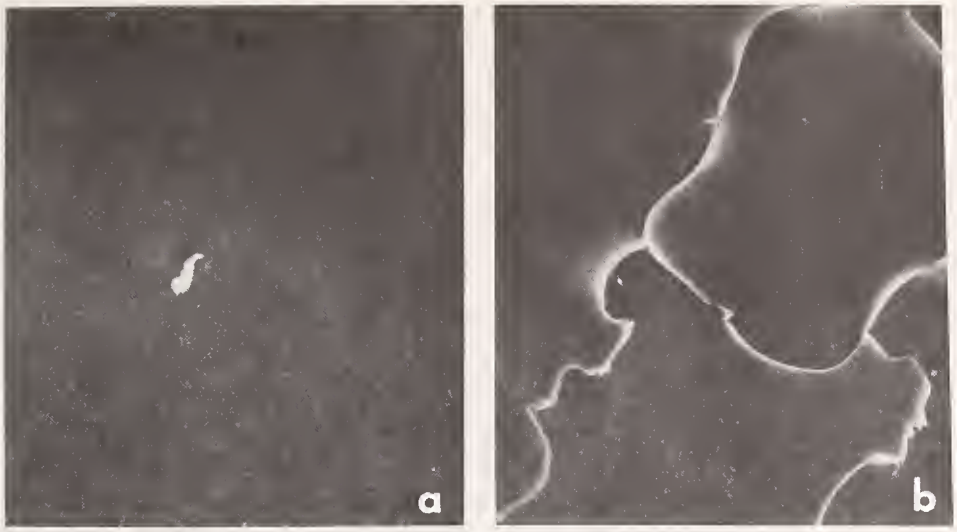

FIGURE 10. *Electronmicrographs of plasma deposited polymers.*

taken to the biocompatibility and use applications of these polymers. After several changes in reactor design, more sophistication in electronics and modifications to both the vacuum system and process procedures, it became apparent that experiments were being run out of control. Results which were favorable during one experiment were not favorable during another experiment, although both were run under presumably identical conditions. Most of the problems involved adhesion of the thin polymer films to the substrates. An extreme example of the differences in adhesion is shown in figure 10. Both films were deposited on glass. In micrograph A, a 2 μm plasma polypropylene film is adherent and so smooth that an artifact had to be introduced onto the surface in order to locate the surface in the SEM. Micrograph B shows cracking of another 2 μm plasma polypropylene deposited under the same conditions but in another run. A series of studies involving both the changing of reaction conditions and the effects of position within the reactor upon adhesion led to the conclusion that more reproducible results were obtained with lower power inputs and where the substrates were positioned toward the trailing edge of the plasma field. These findings only partially eliminated the adhesion problem.

It finally became necessary to curtail all routine experiments and launch a full scale investigation (basic studies have been in progress for 2 years) into the cause and effect of the various parameters upon the final properties of the polymer films. Elemental analyses of the plasma polymer films confirmed that the polymer structure contained elements not present in the original monomer. Specifically, oxygen and nitrogen were contained in the final polymer structure. Figure 11 gives some typical results. This investigation is continuing in conjunction with a more fundamental study. Additional studies are underway to determine whether

ELEMENTAL ANALYSIS OF PLASMA & CONVENTIONAL POLYMERS

	PLASMA POLYMER				CONVENTIONAL POLYMER			
	% C	% H	% O	% N	% C	% H	% O	% N
POLYETHYLENE, 10 W, 80 μM	76.46	8.28	15.3	-	85.71	14.29	-	-
10 W, 60 μM	77.42	8.37	14.2	-				
10 W, 40 μM	73.96	8.36	17.7	-				
10 W, 20 μM	76.72	8.20	15.1	-				
POLYSTYRENE, 10 W, 40 μM	52.20	4.68	24.5	18.63	92.31	7.69	-	-
26 W, 40 μM	55.69	5.26	24.7	14.35				
	51.32	4.67	24.0	19.97				
POLYACETONITRILE	55.81	3.95	11.8	28.39	58.54	7.31	-	34.14
POLYVINYL CHLORIDE, 17 W, 25 μM	46.10	3.44	-	0.46	38.40	4.80	-	-
POLYACRYLONITRILE, 17 W, 27 μM	48.60	4.73	25.5	21.22	67.92	5.17	-	26.91
POLYVINYL FLOURIDE, 16 W, 25 μM	62.88	5.82	-	1.73	52.17	6.52	-	-

FIGURE 11. *Elemental analysis of plasma polymers.*

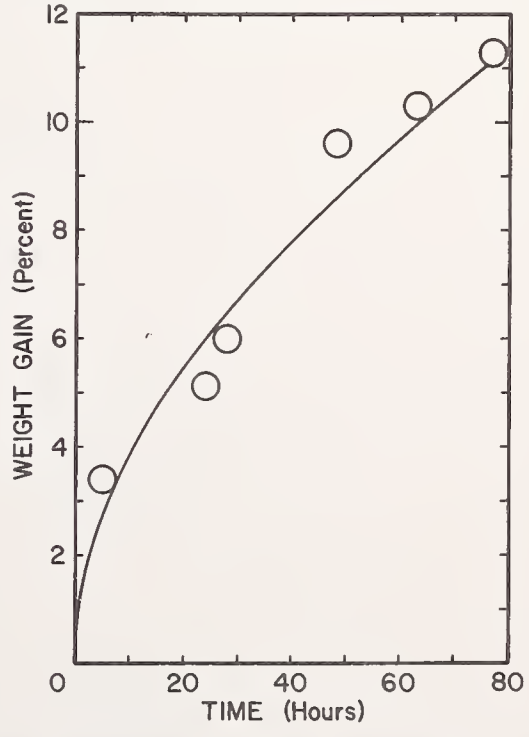

FIGURE 12. *Weight gain of plasma polyethylene as a result of atmospheric exposure.*

or not the source of these elements is contamination of the monomers, perpetual leaks in the system, or whether the polymer is reacting with atmospheric gases after formation. A quartz crystal microbalance was set up in the reactor shown in figure 3 to follow the rate of polymerization and also to follow gas adsorption after polymerization. Figure 12 shows the weight gained by a plasma polyethylene sample deposited on one of the quartz crystals. It is evident that the polymer film is indeed reacting with atmospheric gases.

In conjunction with the quantitative data from this quartz crystal, qualitative data on the species involved was obtained by depositing the plasma polymer films on sodium chloride crystals for IR spectroscopy. Figures 13 and 14 show the IR spectra of such a film and the changes which it has undergone. Preliminary identification of the new absorption peaks indicated the presence of both nitrogen-bearing compounds and cyclic oxygen compounds. It should be noted that this particular film was not adherent and after 7 days exposure to the atmos-

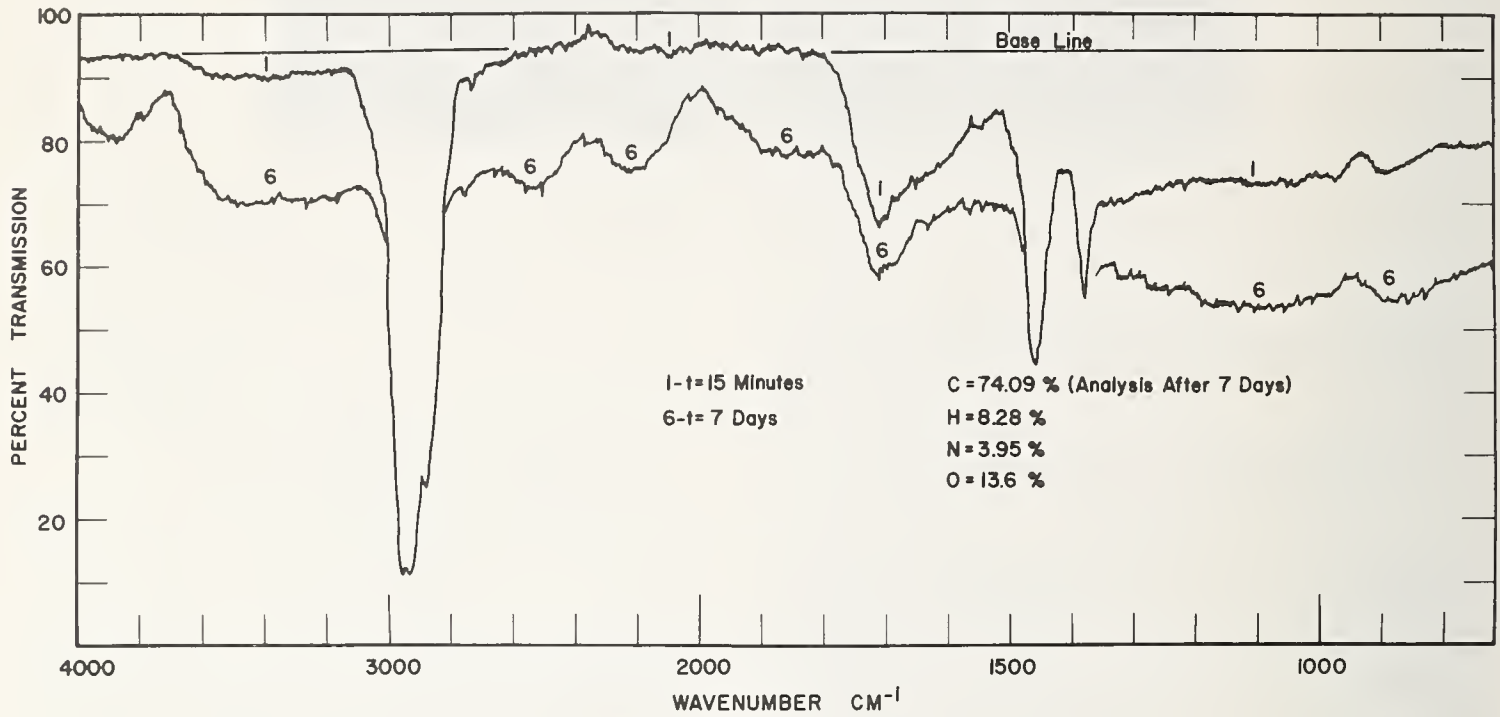

FIGURE 13. *Infrared absorption, atmospheric quenched polyethylene.*

INFRARED ABSORPTION SPECTRA
ATMOSPHERIC QUENCHED POLYETHYLENE

SPECTRUM NO.	ELAPSED TIME	COMMENTS
2	30 MIN.	-
3	90 MIN.	-
4	5 DAYS	NEW ABSORPTION PEAKS EVIDENT AT 3900-4100, 3100-3300, 2400-2600, 2000-2400, 1800-2000, 700-1350 WAVE NUMBERS. PEAKS AT 3200-3700, 1600-1800 MORE INTENSE. COATING LOSING ADHESION.
5	6 DAYS	SAME AS SPECTRUM 4.
6	7 DAYS	COATING PEELED - ADDITIONAL SPECTRA NOT POSSIBLE.

FIGURE 14. *Absorption data associated with figure 13.*

phere had completely peeled from the sodium chloride crystal. Elemental analyses of the peeled film showed the presence of both oxygen and nitrogen. Another experiment was run in which the finished plasma polymer film was allowed to soak in an ethylene atmosphere in the reactor for 8 hours prior to being removed and exposed to the atmosphere. This film has not shown a tendency to peel. Looking at its spectra in figures 15 and 16, it is obvious that the hydroxyl and carbonyl regions have become more intense during observation for a period of 61 days. However, the new adsorption peak previously noted in figures 13 and 14 have not appeared.

Additional experiments are underway to determine how the elemental composition of the polymer changes as a function of length of time that it is exposed to the atmosphere. These experiments are being run whereby the plasma films are being soaked or quenched with reactive and nonreactive gases, as well as being subject to thermal treatments. Studies are also being conducted to follow the decay, of the active species by means of electron spin resonance spectroscopy over a similar period of time.

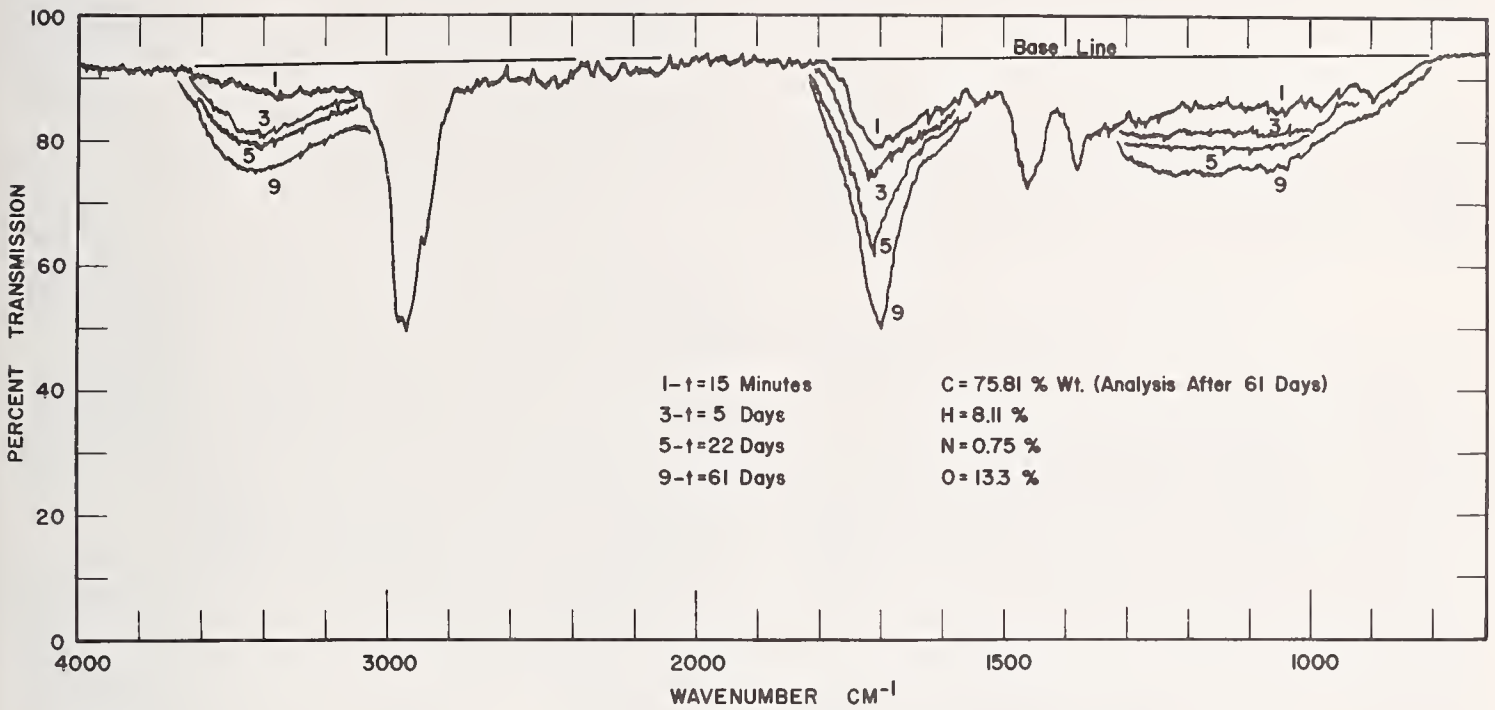

FIGURE 15. *Infrared absorption curves, ethylene quenched polyethylene*

INFRARED ABSORPTION SPECTRA
ETHYLENE QUENCHED POLYETHYLENE

SPECTRUM NO.	ELAPSED TIME	COMMENTS
1	20 MIN.	-
2	1 DAY	-
3	5 DAYS	ABSORPTION PEAKS AT 3200-3700 1600-1800 AND 800-1300 MORE INTENSE. NO OTHER PEAKS DETECTED. ADHESION UNEFFECTED.
5	22 DAYS	3200-3700, 1600-1800 AND 800-1300 MORE INTENSE
6	25 DAYS	NO CHANGE.
7	26 DAYS	NO CHANGE.
8	60 DAYS	3200-3700, 1600-1800 AND 800-1300 MORE INTENSE.
9	61 DAYS	NO CHANGE. TEST CONCLUDED.

FIGURE 16. *Absorption data associated with figure 15.*

6. Summary

Plasma polymerization constitutes a unique technique for forming thin polymer films on a variety of substrates. In most instances the polymers formed by these techniques are more uniform and more stable than conventional polymer films. There is a great deal to be investigated concerning the mechanism by which these polymers are formed. In addition, the kinetic and thermodynamic variables must be understood before one can hope to deposit adherent films on substrates intended for biomedical applications. Preliminary results have indicated that these polymers are potential candidates for biomedical purposes.

We wish to acknowledge the advice and assistance of Dr. Theodore Wydeven, NASA Laboratories, Moffett Field, California. We also wish to acknowledge The National Science Foundation who partially funded this work.

7. References

[1] McTaggart, F. K., Plasma Chemistry in Electrical Discharges, (Elsevier Publishing Company, New York, N.Y., 1967).
[2] de Wilde, P., Ber. **7**, 4658 (1874).
[3] Thenard, A., Comp. Rend. **78**, 219 (1874).
[4] Coats, A. D., U.S. Dept. Comm. Office Tech. Serv. A. D., 419–618 (1962).
[5] Tomkinson, D. M., Galvin, J. P., and Pritchard, H. O., Free radical dissociation of halogenated aromatics in a plasma. J. Phys. Chem. **68**, 541 (1964).
[6] Ogurtsoua, N. N., and Podmosleineskll, J., Zh. Prikl. Spektrosk. **8**, 1043 (1968).
[7] Sacher, E., J. Polym. Sci. Part A, **6**, 1813 (1968).
[8] Sakurada, I., Macromolecules **1**, 265 (1968).
[9] Bashara, N. M., and Doyty, C. T., Appl. Phys. **35**, 3498 (1964).
[10] Kronick, P. L., and Jesch, K. F., J. Polym. Sci. Part A, **7**, 767 (1963).
[11] Bradley, A., and Hammes, J. P., J. Electrochem. Soc. **110**, 15 (1963).
[12] Hanson, R. H., Pascale, J. V., de Benedictis, T., and Rentzepis, P. M., J. Polym. Sci. Part A **3**, 2205 (1965).
[13] Hanson, R. H., and Schonhorn, H., Polym. Letters **4**, 203 (1966).
[14] Weininger, Nature **186**, 546 (1960).
[15] Weininger, J. L., The reaction of active nitrogen with polyolefins, J. Phys. Chem. **65**, 941 (1961).
[16] Hollahan, J. R., Stafford, B. B., Balk, R. D., and Payne, S. T., J. Appl. Polym. Sci. **13**, 807 (1969).
[17] Bazzarree, D. F., and Lin, L. J., Quarterly report to Naval Ordnance Systems Command. No. N00017–69–C–4424, (1969).
[18] Shaw, W., Personal Communication, Western Electric Co., Kansas City, Mo., (1970).
[19] Ozawa, P. J., IEEE Trans. PMP–5, 112 (1969).
[20] Mearns, A. M., Thin solid films **3**, 201 (1969).
[21] Goodman, J., J. Polym. Sci. **44**, 552 (1960).
[22] Williams, T., and Hayes, M. W., Nature **209**, 769 (1966).
[23] Denaro, A. R., Owens, P. A., and Crawshaw, A., Eur. Polym. J. **4**, 93 (1968).
[24] Venugopalan, M., Reactions Under Plasma Conditions, (Two Volumes), (Wiley-Interscience, New York, N.Y., 1971).
[25] Nasser, E., Fundamentals of Gaseous Ionization and Plasma Electronics, (Wiley-Interscience, New York, N.Y., 1971).
[26] Gould, R. F. (Ed.), Chemical reactions in electrical discharges, (American Chemical Society, Washington, D.C., 1969).
[27] Kolotyrkin, V. M., Gilman, A. B., and Tsapuk, A. K., Russian Chem. Rev. **36**, No. 8, 579 (1967).
[28] Suhr, H., Naturwissenschaften **55**, 168 (1968).
[29] Swift, F., Sung, R. L., Doyle, J., and Stille, J. K., J. Org. Chem. **30**, 3114 (1965).
[30] Stille, J. K., Sung, R. L., and Vander Kool, J., J. Org. Chem. **30**, 3116 (1965).
[31] Stille, J. K., and Rix, C. E., J. Org. Chem. **31**, 1591 (1966).
[32] Lawton, E. L., J. Polym. Sci. A–1, **10**, 1857 (1972).
[33] Taki, K., Bull. Chem. Soc. of Japan **43**, 1574 (1970).
[34] Taki, K., Bull. Chem. Soc. of Japan **43**, 1578 (1970).
[35] Taki, K., Bull. Chem. Soc. of Japan **43**, 1580 (1970).
[36] Simionescu, C., Asandei, N., Denes, F., Sandulouici, M., and Popa, G., Eur. Polym. J. **5**, 427 (1969).
[37] Yasuda, H., and Lamaze, C. E., J. Appl. Polym. Sci. **15**, 2277 (1971).
[38] Westwood, A. R., Eur. Polym. J. **7**, 363 (1971).
[39] Westwood, A. R., Eur. Polym. J. **7**, 377 (1971).
[40] Brown, K. C., Eur. Polym. J. **8**, 117 (1972).
[41] Thompson, L. F., and Mayhan, K. G., J. Appl. Polym. Sci. **16**, 2291 (1972).
[42] Thompson, L. F., and Mayhan, K. G., J. Appl. Polym. Sci. **16**, 2317 (1972).
[43] Brown, K. C., and Copsey, M. J., Eur. Polym. J. **8**, 129 (1972).
[44] Kronick, P. L., Jesch, K. F., and Bloor, J. E., J. Polym. Sci. A–1, **7**, 767 (1969).
[45] Tkachuk, B. V., et al., Vysokomol. soyed., A9–9. 2018 (1967), Transl. K. A. Allen.
[46] Wendel, C. T., and Wiley, M. H., J. Polym. Sci. A–1, **10**, 1069 (1972).
[47] Thompson, L. F., and Smolinsky, G., J. Appl. Polym. Sci. **16**, 1179 (1972).
[48] Bradley, A., and Fales, J. D., Chem. Tech., p. 232 (April 1973).
[49] Final Tech., Report F–C2260, The Franklin Institute Research Lab., (NIH) (1969).

NATIONAL BUREAU OF STANDARDS SPECIAL PUBLICATION 415,
Biomaterials, Proceedings of a Symposium held in conjunction with the Ninth Annual Meeting of the Association for the Advancement of Medical Instrumentation, New Orleans, La., April 19–20, 1974
(Issued May 1975).

Plasma-Formed Polymers for Biomedical Applications
Part II. Biocompatibility and Applications*

A. W. Hahn

John M. Dalton Research Center
University of Missouri, Columbia, Mo. 65201

K. G. Mayhan

Graduate Center for Materials Research and Chemical Engineering Department
University of Missouri–Rolla, Rolla, Mo. 65401

and

J. R. Easley and C. W. Sanders

John M. Dalton Research Center
University of Missouri, Columbia, Mo. 65201

Different polymer films generated by rf plasma techniques and deposited on glasses of varying chemical composition, on implant alloys, and on formed prosthetic polymers have been implanted in New Zealand white rabbits and various canine species and have shown minimum tissue reactions after periods of time up to six months. It has further been found that the substrates upon which the plasma polymers are formed are more detrimental to cell cultures than the polymers themselves. These findings, along with other implant work, indicate that plasma-formed polymers will play a definite role as biocompatible materials in the future.

Key words: Biocompatibility; inflammatory response; plasma polymers; tissue reaction.

1. Introduction

In Part I of this joint paper [1],[1] Mayhan et al. have reviewed the fundamentals of the synthesis and deposition of the plasma polymerized films on various surfaces. Our studies were undertaken to explore the compatibility of these polymers with biological tissues and some selected applications to the fields of biology and medicine.

2. Compatibility Studies

Our investigation of compatibility with biological tissues has taken two forms. First, the polymers, coated on a suitable substrate, were exposed to tissue culture. To date we have conducted these tissue culture exposures for the following plasma polymerized materials: polyvinyl chloride, polyethylene, polyallene, polytetrafluroethylene, polychlortrifluroethylene, polystyrene, polyacyrilonitrile, and polyvinyl fluoride.

The procedure used for studying these materials was to obtain various thicknesses of coatings on both glass and commercially available polystyrene cover slips especially made for tissue culture. These 5×10 mm slips were coated, on one side only, under varying reactor conditions. The materials were then brought to our laboratory at University of Missouri–Columbia where the glass cover slips were exposed to autoclaving at standard conditions for sterilization and the polystyrene cover slips were exposed to ethylene oxide sterilization under appropriate conditions.

Control slides of both glass and polystyrene were also sterilized under identical conditions. Each of the study materials was then placed in Leighton tubes which had been previously sterilized, and 5 ml of cells and a standard tissue culture media were added to each tube. The cells used were the HEP–2 cell line which has been well developed and standardized for tissue culture studies. Approximately 10^6 cells were added to each tube. These were then placed in a carbon dioxide incubator at 37 °C and

*Supported in part by grants from the National Science Foundation (#NSF GK 38957) and the National Aeronautics and Space Administration (#NASA NGR 26–004–099).

[1] Figures in brackets indicate the literature references at the end of the paper.

observed at both 24 and 48 h for cell attachment to the particular polymer coated (or control) slide, for attachment to the Leighton tube itself and for metabolism (i.e., or utilization) of the media in the tube. The utilization of the media would determine whether or not the cells were undergoing rapid growth, free from any products which might inhibit this growth.

Figure 1a is a low power photomicrograph of the growth of these cells at 24 h in the control tube. This particular tube (all tubes were done in triplicate) is an uncoated glass slide. Note the stellate appearance of the cell types indicating good attachment and growth at 24 h. Figure 1b is a photomicrograph of the same tube at 48 h, again showing a high concentration of the cells and the beginnings of the development of a monolayer of cells over the slide. During this time it was also noted that there was change in the indicator to a more acid state indicating utilization of energy products within the media. The uncoated polystyrene control slides showed the growth similar to those on the glass slides.

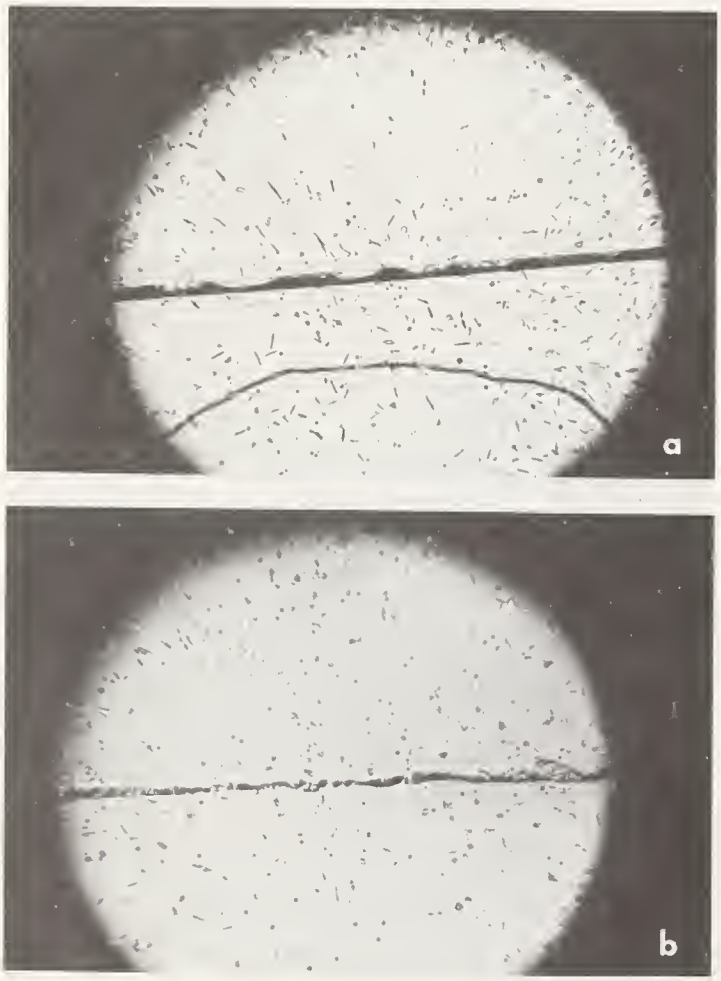

FIGURE 1. *Low power (× 40) photomicrographs of HEP–2 cell growth in the control tube; (a) 24 hours post-inoculation; (b) 48 hours post-inoculation.*

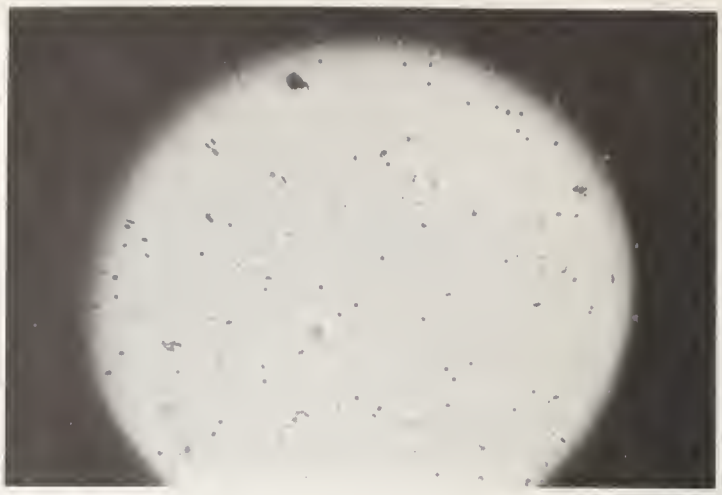

FIGURE 2. *Low power (× 40) photomicrograph of HEP–2 cell growth on a poly-TFE coated cover slip. This represents a 4+ toxic reaction.*

Figure 2 is a photomicrograph of a polymer that is considered to have some form of toxic byproducts inhibiting both growth of the cells within the media and their attachment to the slide. This is considered to be a 4+ toxic reaction. There is a very sparse number of cells throughout the media and all of these have a rounded appearance. This rounded appearance is indicative of a resting phase of the tissue culture cells showing that there is some form of growth inhibitor within the media.

Earlier preliminary studies showed that none of the polymers that were subjected to this form of screening markedly inhibited the growth of the HEP–2 cells. Both the 24 and 48 h examinations of the cells showed that the monolayers appeared normal when compared with controls. An exception to this rule was that polyallene material did show a slight inhibition of growth.

With these encouraging preliminary data, these studies were repeated on a new batch of polymers that had been synthesized in Dr. Mayhan's laboratory by slightly different techniques. Five different batches (TFE–3 and 4 in table 1) of polytetrafluroethylene were examined. It was found that at both 24 and 48 h there were few or no attached cells, and there was little, if any, metabolism in the tubes. Only one of these forms of poly-TFE showed itself to be less toxic at 24 h, but at 48 h it appeared that there were fewer cells attached than earlier. On the other hand, other forms of polymers examined, with the exception of polyvinylfluoride, showed themselves to allow normal attachment and metabolism when compared with the controls at both 24 and 48 h. All of these data are summarized in table 1.

These recent results were disturbing. At the present time it is felt that the post-synthesis treatment of, particularly, poly-TFE is of a high order of significance. It would appear, although not yet established conclusively, that a large number of

Table 1. *Summary of tissue culture results*

Material	Slide growth		Tube growth		Comments
	24 h.	48 h.	24 h.	48 h.	
Control–A	0	0	0	0	
Control–B	0	0	0	0	
TFE(1)	0	0	0	1	
TFE(2)	0	0	0	1	
TFE(3)	4	4	4	4	
TFE(4)	3	1	3	4	
PVC	0	0	0	0	
PE(1)	0	0	0	0	
PE(2)	0	0	0	0	
Polyallene	1	1	0	0	
C–TFE	—	0	—	0	
Polystyrene(1)	—	0	—	0	Polymer peeled.
Polystyrene(2)	—	0	—	0	
Acrilonitrile	0	0	0	0	Polymer surface crazed.
PVF	—	3	—	0	

Code: 0; normal cell attachment to surface
1; approximately half of cells attached
2; approximately one-quarter of cells attached
3; most cells *not* attached
4; no cell attachment
—; slow early growth

Polymer abbreviations:
TFE; Polytetrafluorethylene
PVC; Polyvinylchloride
PE; Polyethylene
C–TFE; Polychlortrifluorethylene

free radicals are present in the plasma synthesized polymer. These probably are responsible for the inhibition of growth in the tissue culture medium. Dr. Mayhan and his group at University of Missouri – Rolla are presently pursuing these findings and attempting to neutralize the active sites that may be contributing to the tissue culture dilemma.

It is interesting to note that in the same reactor and under nearly identical polymerization conditions, the polychlorotrifluorethylene, the polystyrenes and polyacyrilonitriles had little adverse effect on the replication and attachment of the HEP–2 cells in tissue culture.

3. *In Vivo* Studies

Immature New Zealand white rabbits were used to evaluate the tissue reaction to these polymeric films. Various types of polymeric films were deposited on 1×2 cm section of flat Silastic [2,3] sheeting of medical grade quality. Silastic was used because of its universal use and known tissue compatibility.

After anesthetizing the animals with Halothane-oxygen, the implants were sutured with 3/0 silk to the paravertebral muscle fascia 2 cm from the dorsal midline between the last rib and the sacrum. Two implants were placed in a retroperitoneal position without sutures through a small paracostal incision made posterior to the kidney. Sterile technique was used in all surgical procedures. Most animals received four implants, two on either side of the midline approximately 5 cm apart. The experiments are summarized in table 2.

At necropsy the tissues and attached implants were recovered and fixed in 10 percent neutral buffered formalin. Thin tissue sections were embedded in paraffin and cut at 6 μm and stained with hematoxylin and eosin.

Necropsy revealed no systemic effects to the implants, and local gross tissue reaction was limited to encapsulation by connective tissue. The tissue reaction to the implants was deter-

[2] Dow Corning, Midland, Mich.

[3] Certain commercial materials may be identified in this publication in order to adequately specify the experimental procedure. In no case does such identification imply recommendation or endorsement by the National Bureau of Standards, nor does it imply that the material are the best available for the purpose.

Table 2

Implant	Number of animals	Number of implants	Length of study (days)	Reaction	
				Connective tissue	Inflammatory
Polyethylene	4	4	403–432	2.0	1.0
Polyvinyl chloride	1	1	432	1.0	0
TFE	7	14	296–418	2.8	1.3
Allene	2	4	403–418	1.5	1.5
Siallene	3	3	296–352	2.0	0.3
Polypropalene	3	12	209–230	2.9	2.2
Control	8	8	296–432	3.3	1.4

The average connective tissue reaction was graded on a scale of 1–5 as follows: (1) Grade 1: $\leq 1/4$ low power field (lpf) (100×) in diameter; (2) Grade 2: $> 1/4 \leq 1/2$ lpf; (3) Grade 3: $> 1/2 \leq 3/4$ lpf; (4) Grade 4: $> 3/4 \leq 1$ lpf; and (5) Grade 5: > 1 lpf.

The inflammatory reaction was graded on a scale of 0–3 as follows: (1) Grade 0: minimal, ≤ 1 cell/high power field (400×); (2) Grade 1: mild, $> 1 \leq 3$ cells/hpf: (3) Grade 2: moderate, $> 3 \leq 10$ cells/hpf; and (4) Grade 3: severe, > 10 cells/hpf. The grade was based on the average of 10 representative high power fields.

mined by measuring the connective tissue and inflammatory cell response histologically. The results are summarized in table 1. Figures 3a and 3b are photomicrographs of typical responses. In all the experiments the connective tissue reaction was less than that produced by the control (uncoated) strips, and the inflammatory cell reaction to about two-thirds of the polymer strips was less than that of the control.

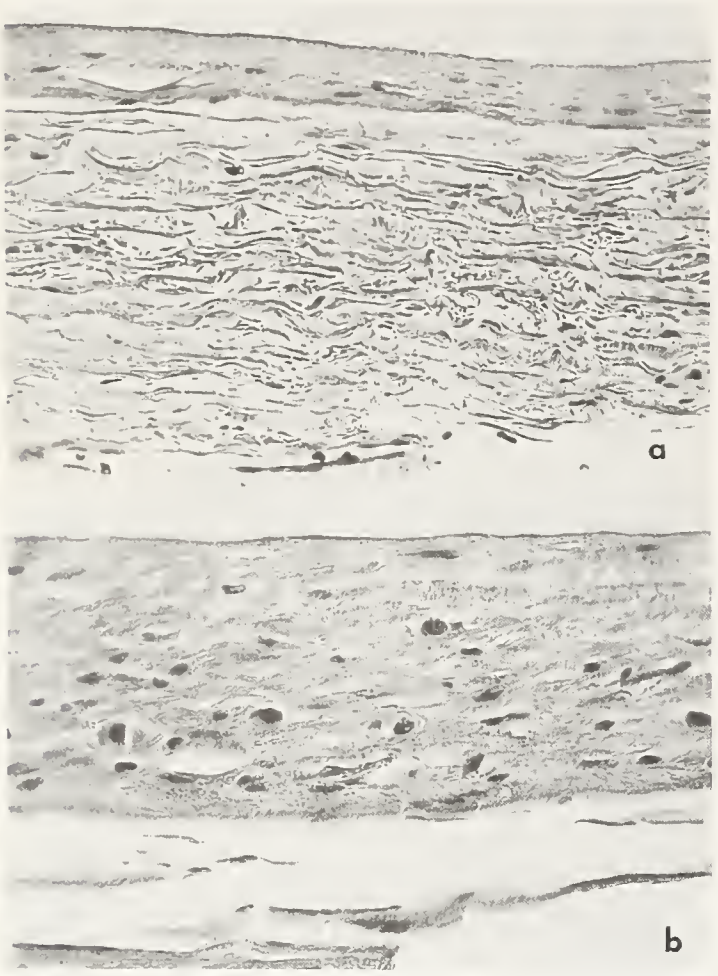

FIGURE 3. *Low and high power photomicrographs of a typical polymer implant capsule given grade one connective tissue reaction and grade one inflammatory cell reaction; (a) 100× magnification of the capsule surrounding polymer implant. The capsule is composed basically of acellular connective tissue matrix with minimal inflammatory cell reaction.*

The dense layer in the upper part of the field is the tissue in direct contact with the polymer implant: (b) 430× magnification of the dense layer of the same capsule. The tissue is composed basically of acellular connective tissue matrix, but a few large inflammatory cells are noted.

Applications

The results of our *in vitro* and *in vivo* studies have shown that, while certain polymeric forms can be rejected because of cytotoxicity, a number are acceptable as candidates for implant applications. Certainly, the *in vivo* studies to date have revealed a paucity of problems. With these encouraging results, our attention was then directed to actual applications for these types of unique polymers.

The biomedical scientist can immediately conceive of numerous potential uses for this type of material, ranging from the coatings of vascular protheses (assuming antithrombogenic properties can be engineered), the protection of implantable electronic devices and the coating of various types of *in vivo* sensing devices. Efforts of our laboratories have concentrated on the coating of implantable oxygen sensing electrodes in order to obviate the problems inherent in the use of polarography; i.e., long-term instability of O_2-sensing surfaces and poisoning of the electrode surfaces.

Principally through the efforts of our colleagues, R. E. Barr and V. G. Murphy [2], our laboratory has undertaken a group of studies aimed at a better understanding of the electrochemical phenomena taking place at these sensing surfaces, *in vivo*, and at the use of the conformal polymerized coatings to obviate certain of the problems encountered.

A particular problem with O_2-sensing polarographic electrodes which utilize O_2 reduction on noble metal surfaces has been with the poisoning of these surfaces by macromolecules, particularly those associated with the sulfur containing amino acids. It was felt that if these surfaces could be protected with a membrane that was permeable to oxygen, but impermeable to the large macromolecules, a far more stable sensing electrode for modestly long-term totally implantable use might be possible.

Figure 4 is a low power scanning electron micrograph of the particular form of oxygen sensing electrode that we are presently using. This is a very thin platinum wire which has been coated with glass. It is the flat surface that is coated with the polymer film.

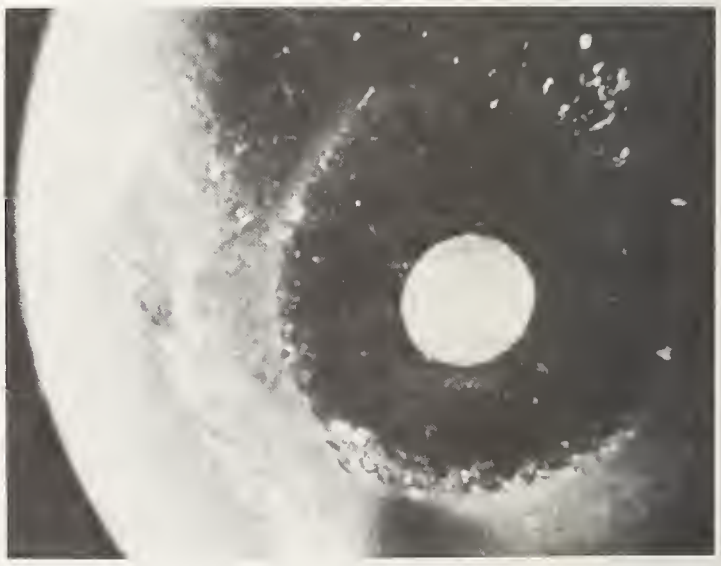

FIGURE 4. *Low power (×300) scanning electron micrograph (SEM) of an uncoated platinum-iridium oxygen electrode used in the studies.*

The sensing surface is the disc in the center of the photograph.

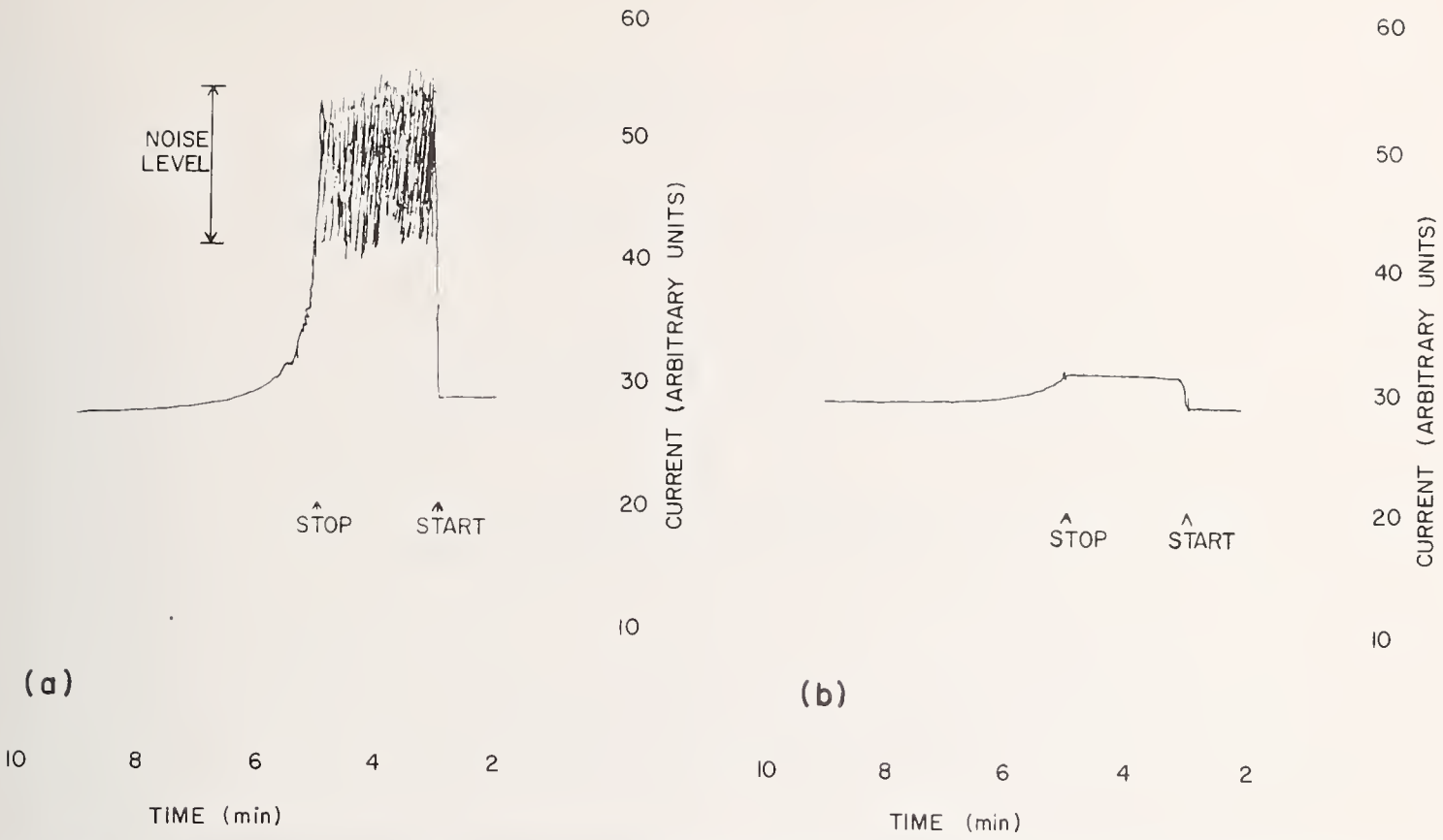

FIGURE 5. *Current generated from Pt-Ir oxygen electrodes during stirring; (a) uncoated (Note the high noise level of the current); (b) coated (poly-ethylene) electrode of the same design.*

While the magnitude of the current has decreased, the noise level is now quite acceptable.

We have found that by coating this sensing surface with a uniform polymer membrane that is tough and firmly applied, we can almost negate the starting artifact that is present around each of these electrodes. Figures 5a and 5b show a recording of the currents generated by polargraphic oxygen electrodes with both uncoated and coated sensing surfaces. Note that the uncoated sensing surface (fig. 4a) when placed in a media which is stirred, is strongly sensitive to stirring artifact; in other words, the platinum surface is seeing random concentrations of local oxygen. With the polymer film on the surface, it may be noted in figure 5b that, while the overall current is cut down in magnitude, there is almost no noise present in this particular recording. This is due to the uniform oxygen boundary layer that the oxygen reducing surface of the platinum sees rather than being bombarded by random concentrations of oxygen even in a highly turbulent medium. The useful life of O_2-sensing electrodes is prolonged to days rather than hours by the use of the film coatings.

While there is certainly a large amount of work remaining to be done in the area of precoating preparation of these electrodes and of their durability in long-term tissue applications, there is much to be gained by the application of a uniform film to the sensing surfaces to allow for protection of the sensing surface from tissue macromolecules and other poisoning effects. It is our opinion at this time that the potential for oxygen sensing in tissues, insofar as long periods of time is concerned, is greatly enhanced by the applicability of these particular forms of membranes.

4. References

[1] Mayhan, K. G., Havens, M. R., Peace, B. W., Hahn, A. W.; Plasma Formed Polymers and Biomedical Applications—Part I: Synthesis and Fundamental Studies, this volume, page 1.

[2] Mayhan, K. G., Hahn, A. W., Barr, R. B.; A New Approach to Coating Oxygen Electrodes. Proc. 25th A.C.E.M.B. (Annual Conference on Engineering in Medicine and Biology), Miami Beach, Fla., p. 85, 1972.

NATIONAL BUREAU OF STANDARDS SPECIAL PUBLICATION 415;
Biomaterials, Proceedings of a Symposium held in conjunction with the Ninth Annual Meeting of the Association for the Advancement of Medical Instrumentation, New Orleans, La., April 19–20, 1974
(Issued May 1975).

Interfacial Behavior of Ceramic Implants

L. L. Hench

**Department of Materials Science and Engineering
University of Florida, Gainesville, Fla. 32611**

H. A. Paschall

**College of Medicine
J. Hillis Miller Health Center and Chief of Orthopaedics
Veterans Administration Hospital, Gainesville, Fla. 32610**

W. C. Allen

**College of Medicine
Department of Orthopedic Surgery
J. Hillis Miller Health Center, Gainesville, Fla. 32611**

and

G. Piotrowski

**Department of Mechanical Engineering,
University of Florida, Gainesville, Fla. 32611**

Recent studies of bioglass, bioglass-ceramic, and alumina implants have produced an understanding of the chemical nature of interfacial tissue reactions to bioceramics. Significant differences between hard and soft tissue reactions are due to the influence of surface chemical reactivity on the ultrastructural histology as revealed by transmission electron microscopy. Modern surface characterization of the implants correlates with the histological reactions. Applications of the results to a variety of orthopaedic prostheses show promise in animal experiments. Biomechanical analyses of interfacial bonding between bioceramic prostheses and tissues are presented.

Key words: Bioglass-ceramic; ceramic implants; flame spray coating; hip prosthesis; segmental bone replacement.

1. Introduction

Two years ago a review article on ceramics in medicine by one of the authors reported that such materials are seldom used for chronic applications in medicine [1].[1] However, pioneering efforts of the last few years have changed this situation. Dr. P. Boutin of Pav, France recently reported over 500 successful cases of total hip replacements using high density, high purity Al_2O_3 components over a 4 year period [2]. Application of the alumina ceramic joint was based upon studies of very low wear rates of alumina in contact with alumina when both ball and socket are finely polished to a 1 μm surface finish. Biocompatibility of the high purity (99.3%) alumina was first established in dogs and humans using both acicular and button configurations of the ceramic. Only a thin fibrous membrane several cell layers deep was present at the implant-tissue interface. Similar results of tissue response and low rates of wear of dense high purity Al_2O_3 implants have been demonstrated by a West German research team [3–5]. These efforts have led to a systematic development of a total hip prostheses that is all Al_2O_3 ceramic. This is in contrast to the Boutin prostheses that utilizes a Ti metal femoral stem pressure fitted onto an alumina ball for the femoral portion of the hip prostheses.

A combined West German and Austrian research team reports total replacement of vertebrae, humerus, and radius in humans with high density, high purity Al_2O_3 ceramics [6]. Successful use of the implants for times in excess of 1 year are recorded.

With application of ceramics in humans commencing, it becomes imperative to understand fully interfacial reactions between ceramic materials

[1] Figures in brackets indicate the literature references at the end of the paper.

and bone. The studies reported by Hulbert and Klawitter et al. [7–10], and those cited above have demonstrated that very close apposition of mineralized bone occurs at the implant interface. However, if dense implants are used, taking advantage of the 40,000 psi (0.28 GPa) tensile strength of high density alumina, a thin fibrous membrane is always observed. The presence of the membrane causes one to reflect on the possibility of implant loosening during long term application with attendant stress localization and bone resorbtion currently characteristic of long term metallic implants. Will the membrane remain firmly attached to the ceramic interface or will interfacial fluids develop with stress-corrosion fatigue at the ceramic grain boundaries? Can compositional, microstructural, or surface modifications be made to the alumina ceramics to avoid fibrous membrane formation without degrading strength? Answers to these and other fundamental questions are only beginning to be obtained. Alumina with 200 μm pore diameters and 50 percent porosity appear to be limited to 10,000 psi (0.07 GPa) tensile strength. Will 10,000 psi tensile be strong enough at the interface to transmit the loads required in weight bearing applications? Successful load bearing segmental bone replacements tested in monkeys in our laboratory using a bioglass-ceramic of less than 10,000 psi tensile strength suggest that mechanical design limits for such materials are presently not understood [11]. In other words, we do not know how strong a ceramic prosthesis must be to withstand chronic applications in humans. The data in animals is only beginning to be achieved in spite of much recent effort [1–15]. Much additional effort directed toward understanding interfacial reactions, strength requirements, and strength deterioration [16–19] must be completed before large scale chronic human applications seem warranted.

Alternative directions towards achieving satisfactory ceramic prostheses also continue to show promise. The research of Graves et al., at the University of Dayton has demonstrated considerable control over osteogenesis in monkeys using variable P_2O_5 content in calcium-aluminate ceramics [12]. Strength enhancement in this system also seems quite probable.

The efforts of our laboratories have concentrated on the investigation of specially designed bioglass and bioglass-ceramic compositions [20–25]. This research will be reviewed in the remainder of this paper. Special emphasis will be placed upon the results of combining the osteogenic features of the surface active bioglass system with the high mechanical strength of 316L surgical stainless steel. The results indicate that flame spray coatings of bioglass on stainless steel or high density Al_2O_3 may provide a solution to many of the interfacial tissue and strength problems described above.

2. Bioglass-Steel Flame Spray Concept

Previous studies in this laboratory have resulted in the development of a nonporous glass and glass-ceramic composition which is compatible with bone on an ultrastructural scale [20–25]. The bioglass and bioglass-ceramic contains Ca, Na, and P ions (table 1) which are slowly leached from the surface of the implant material during the healing process.

TABLE 1. *Bioglass compositions developed for orthopaedic prostheses*

Code number	Weight percentage					
	SiO_2	Na_2O	CaO	CaF_2	P_2O_5	B_2O_3
45S5	45.0	24.5	24.5		6.0	
45S5F	43.0	23.0	12.0	16.0	6.0	
$45B_{15}S5$	30.0	24.5	24.5		6.0	15.0

The surface ion release leaves behind a polymerizing SiO_2-rich gel [22, 23, 26, 27]. The surface gel appears similar in composition to that preceding hydroxyapatite mineralization in normal bone growth [28]. As a consequence of the surface activity, collagen bonding and bone mineralization are initiated at the implant surface [20–25]. The bone growth from the implant-bone interface results in an interfacial chemical bonding which is sufficiently strong that the bone or the implant will fracture before the interface does [11].

Although the tensile strength of the bioglass-ceramic material is in the range of 10,000 psi when crystallized in a controlled manner [29], there are numerous prostheses applications where even greater strength or impact resistance may be desirable. This is especially true for plates, nails, pins, and femoral head shafts where a small cross-sectional area of the implant is required. Stainless steel devices satisfy the strength requirement for these applications. However, a fibrous tissue reaction at the steel interface results in loosening of the implant with time and corrosion of the implant produces metallic particles which become incorporated in the neighboring tissues.

An investigation was conducted to combine the superior strength and impact resistance of surgical stainless steel with the biocompatibility of Na, Ca, P containing bioglasses. This combination is achieved by applying the bioglass as an intimate coating on the surface of stainless steel prostheses. The coating is applied by a flame spraying method developed in collaboration with the ceramics group at IITRI.[3] This paper presents the development of

[3] Illinois Institute of Technology Research Institute, Ceramics Division, Chicago, Ill., S. W. Freiman and E. J. Onesto, Investigators.

the bioglass flame spray coating process, the design of a flame spray coated partial hip prosthesis, surgical results, and a histological comparison of tissue responses adjacent to the partial hip prostheses with those of a standard surgical stainless steel screw.

Flame Spray Process

Flame spraying has been in use for well over half a century in the application of metallic coatings while efforts to apply ceramic coatings, with emphasis on refractory crystalline oxides, began about 20 years ago. The flame spray process consists of passing a material in powder form through a flame where it is heated to a temperature at which it becomes plastic and is readily deformed. The molten material is then impinged onto a substrate at high velocity with consequent deformation and adherence of the particles. The combination of heat and impact which is available in flame spraying permits rapid particle-to-particle sintering at temperatures and times where normal sintering would not be obtained. Consequently, the substrate does not reach a high temperature. For this reason, substrates can be flame spray coated without deformation and loss of tolerance. Diffusion processes between the substrate and the coating are also retarded. Both of these factors are important in producing a high quality coated medical prosthesis.

The spray efficiency and the quality of adherence of a flame sprayed coating depends on many factors, but of particular importance are the thermophysical properties of the sprayed material, and the surface conditions, thermal conductivity and thermal expansion of the substrate. For a given material and substrate, spray conditions are readily optimized empirically as to spray distance, gas flows, powder feed rate, etc.

3. Flame Spray Equipment

The flame spray apparatus consists of an oxyhydrogen torch[4,5] in conjunction with a powder feed hopper, shown schematically in figure 1. The oxygen line to the torch passes through the feed hopper which is equipped with a variable speed screw-feed mechanism to regulate powder flow. The powder is entrained in the oxygen stream and passes through the torch. The powder laden oxygen is combined with the hydrogen at the torch, the powder passing through the resulting oxyhydrogen flame. Since the theoretical flame temperature is approximately 3000 °C, the powder is rapidly heated and becomes molten.

[4] Continental Coatings Corporation.

[5] Certain commercial materials and instruments may be identified in this publication in order to adequately specify the experimental procedure. In no case does such identification imply recommendation or endorsement by the National Bureau of Standards, nor does it imply that the equipment or instruments identified are necessarily the best available for the purpose.

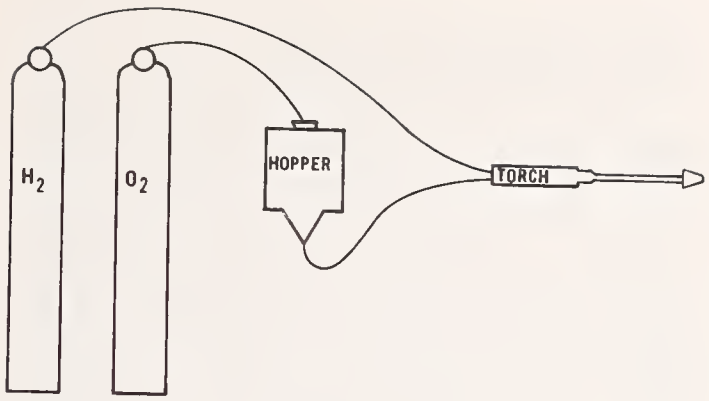

FIGURE 1. *Schematic representation of flame spray apparatus.*

4. Materials Factors in Flame Spraying Glass

When the material being sprayed is a glass, a special situation exists. Glasses differ markedly from metals and most crystalline ceramics in that they display high optical transparency and relatively high viscosity above the softening temperature. These differences are very significant to the flame spraying process, as was observed in previous work at IITRI [30].

As the particles are projected through the flame, they are heated by convection from the hot gases and by radiation from neighboring particles. The lack of the radiation component to heat transfer in the case of transparent glasses results in the evident low temperature of the glass particles relative to spray particles of opaque metals and ceramics. On the other hand, too high a particle temperature may destroy the glass, particularly compositions containing phosphate such as the bioglasses. This is due to the high vapor pressure of the phosphate groups. Also, the low thermal emittance of the particles imparts a slow cooling rate, hence more deformation and flow after impact (provided that the viscosity is sufficiently low).

The long softening range of glasses is advantageous where the substrate is hot or where the thermal conductivity is low because flow can continue for a longer period, resulting in better adherence and a tighter structure. A glass with high viscosity will not flow even when well over the softening temperature. The more rapid the quench rate of the particle, the lower the viscosity must be.

It has been found that a low viscosity is required for sintering as well as for flow of glass particles. Because of the smoothness of the molten glass surface the free energy is small, and the material must flow in order to sinter. This situation is not observed with metal and ceramic particles at high

temperature where surface defects give rise to a high free energy for sintering [31].

The relationship between softening range, quench rate and viscosity of a glass important to flame spraying is shown in figure 2. The volume decrease associated with the cooling of the molten droplets is shown as dark curves in the figure. If the liquid does not crystallize upon cooling to T_m, it can retain its random, liquid-like structure through a supercooled liquid regime, B, and solidify into a glassy material within the transformation range, T_g. The transformation temperature of a given flame sprayed glass is dependent upon its quench rate. A rapid quench produces a high T_g and a less dense glass, curve C. Likewise, a slower quench rate results in high densities and lower transformation temperatures, curves D and E.

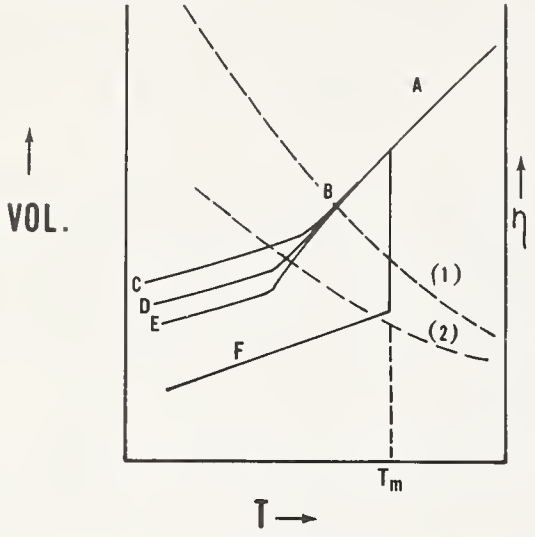

FIGURE 2. *Volume-temperature relations for a liquid (A), supercooled liquid (B), glasses (C, D, E), and crystal (F), all shown in solid lines.*
Viscosity-temperature dependence for two glasses shown as dotted curves.

If a glass has a high viscosity before the glass transformation occurs, such as the dashed curve #1, the flame sprayed particles cannot flow and create a uniform glassy coating on the substrate. However, when the viscosity of the glass is low (curve #2), spreading and interparticle flow occurs prior to solidification of the glass. This condition must be achieved by adjusting the glass composition. There is a limit on compositional adjustment, however. since crystallization at T_m will occur if sufficient three-dimensional network formers are not present in the molten glass particles. Because of the large volume change associated with crystallization (curve F) it is very difficult to obtain a smooth, coherent crystalline coating.

To supplement the low viscosity, a low surface tension of the glass is also required for good wetting of the substrate. Particle flow and sintering after impact will be a function of both viscosity and interfacial tension.

It is most important that the coefficient of thermal expansion of the glass sprayed on a relatively cold substrate be nearly the same as the substrate or slightly lower. A lower expansion will provide thermal shock resistance and a minimum of tensile stress established within the glass when the coating shrinks on cooling. However, as shown in figure 3, if there is large expansion mismatch between the glass and the substrate, tensile stresses will develop at the interface when the glass cools below its transformation temperature. Cracking will result if the stresses become too large [32].

FIGURE 3. *Development of interfacial stresses between a flame spray coating and a prosthesis due to thermal expansion mismatch.*

5. Development of Bioglass Composition for Flame Spraying

Initial flame spraying experiments were conducted using flat plates of 316L surgical stainless steel as the substrate for the 45S5 bioglass (table 1) originally developed for bulk glass-ceramic prostheses. All substrates were grit blasted with 20 mesh SiC at a pressure of 80 psi to completely roughen the surface before spraying. The devices were then thoroughly scrubbed in a detergent solution and rinsed first in water and then in isopropyl alcohol to remove any grit, blasting debris, dirt and oils picked up in handling the devices.

A variety of experimental variables were examined in an effort to achieve a high adherence coating of the 45S5 bioglass [33]. None succeeded. It was concluded that the major reason for the lack of success in flame spraying the 45S5 glass was its very high viscosity at the spraying temperature. This high viscosity prevented the sprayed material from flowing and forming an adherent glassy layer. The high viscosity of the glass is probably due to its relatively high silica content. Previous studies had shown that glasses which form the best flame sprayed layers are those that are low ($<5\%$) in SiO_2 [30].

This interpretation was borne out by an analysis of the thermal expansion coefficient of the 45S5 bioglass and the dilatometric softening point. As shown in figure 4 (determined on 2-inch specimens with an Orton Automatic Recording Dilatometer), the expansion of the 316L stainless steel substrate and the 45S5 bioglass are well matched. However, the softening of the glass under stress, revealed by the hump in the curve, occurs at a relatively high temperature (530 °C) for this composition. Thus, the glass viscosity is too high for a successful flame sprayed coating.

Two approaches were taken to decrease the glass viscosity; substituting B_2O_3 for SiO_2 in the glass and CaF for CaO (table 1). Both changes decreased the viscosity as shown by the lower softening points in figure 4. The decrease in softening point to 470 °C was the same for both the fluorine and boron containing bioglasses. The magnitude of the thermal expansion coefficient was also the same for both compositional series. However, the higher temperature fluidity of the fluorine-containing bioglass 45S5F was less under the flame spraying conditions and produced a smooth, uniform glassy coating on the stainless steel with excellent adherence.

Since it is required that implant devices be virtually encapsulated in a glass coating, it was necessary to flame spray each device individually. Samples were hand held in forceps modified to grip them with minimum contact. In this manner, front, back, and interior surfaces (in the case of cylinders) could be uniformly preheated and coated with a well fused, glassy appearing coating.

Coatings on the prostheses were obtained by preheating the substrate above the softening point of the glass, then initiating the powder feed through the torch and allowing the glass particles to flow, rather than quench, as they struck the surface.

Altering the bioglass composition in order to obtain suitable flame spray behavior does not yield a unilateral change in properties. Consequently, evaluation of solubility characteristics and *in-vivo* responses of the new compositions were necessary before it was justified to produce and test coated prostheses. Previous publications show that the *in-vivo* behavior of both the fluorine and boron containing compositions were suitable for prostheses applications [21–25].

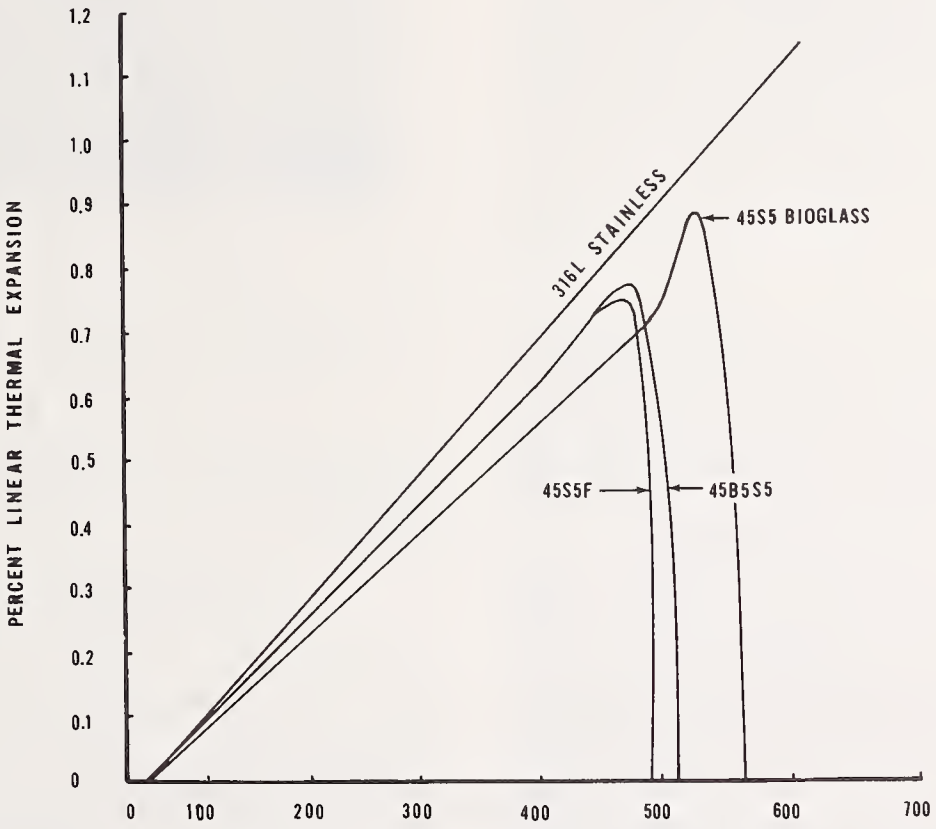

FIGURE 4. *Thermal expansion and softening points of 316L stainless steel and three bioglasses.*

6. Bioglass Flame Spray Application to Prostheses

Several configurations of prostheses and test samples have been flame coated with the 45S5F and $45B_{15}S5$ glass compositions discussed above. Figure 5 shows an array of flame spray coated 316L stainless steel prostheses and test samples. Several bone bridges, rat cortex inserts and a tissue culture blank are shown. Both the 45S5F and $45B_{15}S5$ bioglasses have been used for flame spraying such samples.

FIGURE 5. *A variety of flame spray coated prostheses, $45B_{15}S5$ composition. On the left are segmental bone replacements for rats; at center is a tissue culture substrate, and at right are rat bone chips.*

A femoral head replacement for a Rhesus monkey was selected as the test model for a major prosthetic implant made of 316L stainless steel and flame sprayed with a bioglass coating. The objective of such a composite design is to combine the strength of the stainless steel core with the biocompatible surface properties of the glassy coating.

A prosthetic femoral head replacement is comprised of three major segments: the head, which replaces the head of the femur, the stem, which anchors the device in the shaft of the femur, and the junction between the head and the stem. These three parts are pointed out in figure 6, which is a photograph of the completed prosthesis. The head ideally should be an exact copy of the femoral head, but this is not practical. It was therefore decided to manufacture the head of the prosthesis as a sphere, with a diameter closely matched to the mean diameter of the femoral head.

The stem of the prosthesis anchors the device by fitting snugly into the marrow cavity of the femur. The stem needs to be quite long, so that bending loads may be resisted with a minimum of contact stress developed at the extremes of the stem. The stem should not be circular in cross section, so that the prosthesis cannot rotate about the long axis of the stem. The stem must also be designed to allow itself to be driven into the medullary canal without splitting the femoral cortex. The junction between the head and the stem must not interfere

FIGURE 6. *A prosthetic femoral head replacement for a Rhesus monkey is labeled to show the three segments of the device.*

The stainless steel prosthesis has been flame sprayed with a glass-ceramic coating.

with muscle attachments at the greater and lesser trochanters. The junction also prevents the prosthesis from migrating distally along the shaft of the femur.

7. Design of the Prosthesis

The geometric constraints imposed by the monkey's anatomy are illustrated in the x-ray (fig. 7). The head appears to be a sphere of about 14 mm (0.56 in). The inner diameter of the marrow cavity is about 6 mm (0.24 in) at a point about halfway down the femur. The proximal end, being narrower, is to be reamed out to an inner diameter of about 6 mm as well. Since the smallest outer diameter at about the level of the isthmus, is over 10 mm (0.40 in), the proximal femoral cortex is not greatly weakened by the reaming of the bone.

To prevent rotation of the stem within the marrow cavity, the stem was designed with a square cross section, 5 mm (0.20 in) square. Since a diagonal of the cross section is 7.1 mm (0.28 in) long, the stem must be driven into the marrow cavity and cut four grooves, triangular in shape and approximately 0.5 mm (0.02 in) deep, into the endosteal surface. The end of the stem was cut off square, essentially providing four cutting corners with zero rake angle.

FIGURE 7. *The design for the prosthesis was evolved directly on this x-ray of a Rhesus monkey pelvis.*

Note that the design of the device does not interfere with muscular attachments to the lesser and greater trochanters.

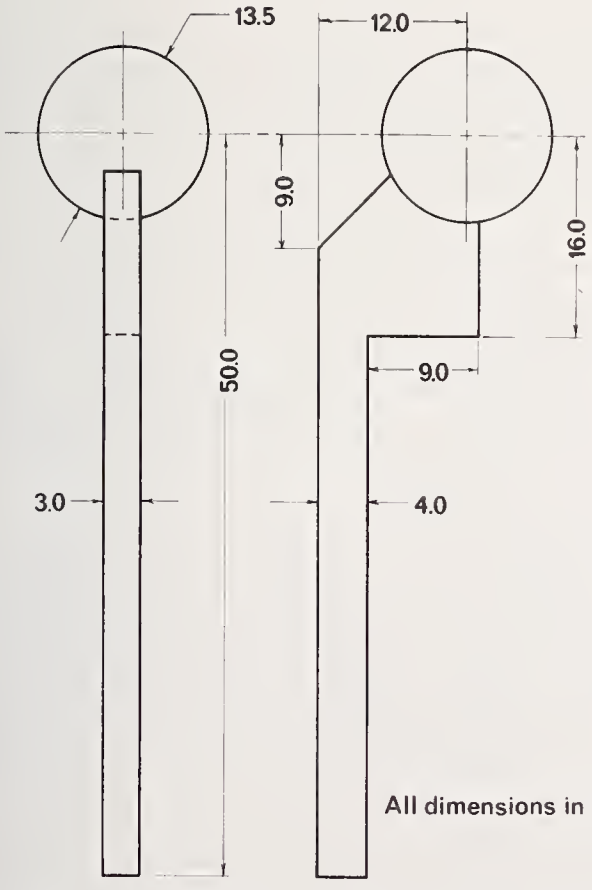

FIGURE 8. *The final design of the metal portion of the prosthesis compensates for the ceramic coating, which is of the order of 0.5 mm thick.*

The thickness of the stem and junction was reduced to 3.0 mm to reduce the danger of splitting the femur during insertion.

The length of the stem was made as great as possible. A length of 43 mm (1.69 in) was selected; a longer length would have no effect in terms of anchoring the prosthesis since the distal portion of the stem would have protruded into the flared region of the distal femur and not be in contact with any cortical bone.

The junction between the head and stem was designed so that both the greater and lesser trochanter would be left undisturbed. Thus, neither the major flexors nor abductors of the hip would be affected.

The thickness of the ceramic coating of the prosthesis is about 0.5 mm (0.02 in). Therefore, the metal portion of the device is 0.5 mm smaller all around, as shown by figure 8. Note that the complete device fits entirely within the original volume of the femur. Thus the range of motion available after implantation is not compromised by the design of the implant.

8. Mechanical Factors

Once the geometry of the implant was established, a series of calculations were performed to compare the strength and rigidity of the intact monkey femur and the prosthesis. The calculations are based on the following assumptions. (1) The femur is a hollow cylinder of constant cross-sectional geometry, with an outer diameter of 10 mm (0.40 in) and an inner diameter of 5 mm (0.20 in). Use of this model to determine the mechanical parameters of the femur assures that the values of strength and rigidity will be lower than the actual values. (2) The modulus of elasticity of the bone was estimated at 2×10^5 kgf/cm^2 (2.5×10^6 psi), while the ultimate tensile strength was estimated to be about 1000 kgf/cm^2 (15,000 psi). (3) The effect of the ceramic coating on the strength and rigidity of the prosthesis were ignored, which is justified considering the small thickness and low modulus of the coating.

The rigidity of the stem of the prosthesis, defined as the product of the modulus of elasticity and the area moment of inertia, was computed to be of the order of 4500 kgf-cm^2 (1530 lb-in^2), while the rigidity of the femoral shaft is approximately 8250 kgf-cm^2 (2760 lb-in^2).

Thus, the shaft of the monkey femur is approximately twice as rigid as the stem of the prosthesis in bending. Bending loads applied to the femur will therefore be primarily carried by the bone rather than the implant. This tends to inhibit disuse osteoporosis in the femur.

Based on a yield strength of 5300 kgf/cm^2 (75,000 psi) for 316L stainless steel, the strength of the stem of the prosthesis is approximately 57 kgf-cm (50 in-lb). The femur, however, can withstand a bending load of 132 kgf-cm (112 in-lb) before fracture. Thus the bone is also twice as strong as the implant. The superior strength and rigidity of the bone, despite the lower modulus of elasticity and failure stress, arises from the fact that the bony

material is distributed much farther away from the axis of the femoral shaft than the implant material.

It is generally accepted that a load of about three times body weight acts on the head of a human femur during single-legged stance. If this same proportion is applied to the Rhesus monkey, a bending load of about 21 kgf-cm (18 in-lb) is seen by the prosthesis at the upper end of the stem. The maximum contact stresses developed by the junction bearing on the bone just above the lesser trochanter are of the order of 70 kgf/cm^2 (1000 psi), far short of the failure stresses of either bone or steel.

If contact between the stem and the femur is assumed to occur in a strip 0.5 mm (0.02 in) wide along each edge of the stem, a torque of 29 kgf-cm (25 in-lb) is required to raise the contact stress to 700 kgf/cm^2 (10,000 psi). The muscles around the hip are not capable of producing such torsional loads. Thus this mode of failure would come about only through accidental application of very large external forces.

Figure 6 shows the device after coating with the 45S5F bioglass. Most of the surface is covered with a clear transparent glass which appears mottled and gray because of the oxidized steel surface underneath. A portion of the end of the femoral shaft shown in figure 6 is more transparent and therefore gives the illusion of the coating being missing.

9. Surgical Procedure

The bioglass flame sprayed monkey hip prosthesis was placed in two stump tail monkeys for a period of 14 months. The monkeys were adult females taken from the colony of stump tails at the animal farm and operated on under aseptic surgical conditions.

After the monkeys were anesthetized, their right hips were shaved and prepped in the usual manner, and a posterior lateral approach used to expose the hip. Through this approach, the gluteus maximus was partially split with the majority of the muscle retracted toward the midline. The gluteus medius and minimus muscles were then defined and retracted superiorly. This allows visualization of the sciatic nerve, which is located just posterior to the greater trochanter. The nerve was protected and the short rotators of the hip cut through an arc of 180° to allow exposure of the femoral head and the labrium cut transversely to allow dislocation posteriorly. Following good hemostosis, the base of the neck was osteotomized, and using a small Hoke osteotome the greater trochanter was notched so as to accomodate the neck of the prosthesis. The femur shaft was reamed using a twist drill and the prosthesis introduced into the femur. With proper notching and reaming, the prosthesis was seen to fit snugly. This is shown in figure 9. The prosthesis was then reduced into the acetabulum, and the labrum and capsule repaired using chromic sutures. The short rotators were sewed to their insertion making no particular effort to reposition them anatomically. The wound was then closed in layers using absorbable sutures on the skin.

FIGURE 9. *Bioglass flame spray coated femoral stem replacement as inserted in femur at time of operation.*

Although the procedure is analagous to the human procedure, there are two notable differences. These are: (1) the close proximity of the sciatic nerve to the posterior capsule of the hip, and (2) the shape and more proximal position of the greater trochanter relative to the base of the neck of the femur.

10. Histological Evaluation

The objective of this part of the study was to evaluate the histological response of the soft tissue reactions about one of the bioglass flame spray coated partial hip prosthesis. The histology of the soft tissue removed from a corroded area about a metallic bone screw on a fixation device is presented for comparison.

Soft tissue used to demonstrate the effects of corrosion upon the soft tissues was taken from an area of black discoloration of the soft tissues beneath a bone plate and adjacent to the bone surrounding a screw which demonstrated corrosion with metallic scarring between the screw and the plate (fig. 10A). The internal fixation device had been used in a 58-year old woman who had undergone an osteotomy of the femur for degenerative arthritis of the hip. The implant had been in place for approximately 18 months at the time of removal.

The second specimen was soft tissue removed from the bioglass flame spray hip prosthesis described above at the location shown in figure 10B. The prosthesis had been experimentally inserted as a replacement device in a stumptailed monkey, and had been in place 14 months at the time of

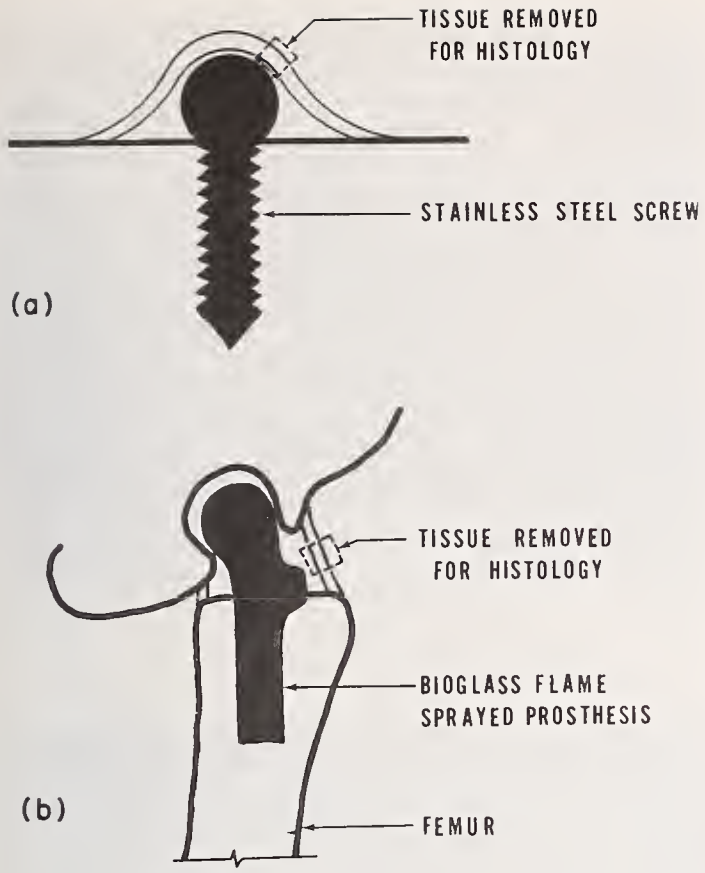

FIGURE 10. *Schematic of the location of soft tissues for histology evaluation.*

A. Tissue adjacent to a stainless steel screw.
B. Tissue adjacent to the bioglass flame sprayed partial hip prosthesis.

sacrifice. This soft tissue showed no evidence of discoloration and appeared healthy and normal in all respects.

In each instance the tissue was taken fresh from the operating room and placed immediately in cold buffered gluteraldehyde. Tissues were fixed for 2 hours in the gluteraldehyde, then washed with additional buffer and fixed an additional hour in 1 percent osmium tetroxide buffered to a pH of 7.4. The tissues were then dehydrated in graded alcohols and then embedded in Epon 812[6].

Sections one micrometer in thickness were taken for routine histology and orientation for sectioning for electron microscopy. The blocks were then further trimmed for electron microscopy and the blocks were sectioned on an MT–2 Porter Blum microtome using a diamond knife, and the sections collected on carbon-stabilized collodian-coated grids. The sections for electron microscopy were stained with lead citrate and uranyl acetate.

Figure 11a is a photomicrograph of soft tissue surrounding the corroded metal screw. This is normal dense collagenous connective tissue and the cells which are seen are fibroblasts. However, one notes in the fibroblasts that there are dense collections of dark staining material which one may assume to be metal particles.

Figure 11b is a photomicrograph of soft tissues surrounding the bioglass coated implant. This tissue is also dense collagenous connective tissue and one sees numerous fibroblast and fibrocyte-like cells surrounded by a dense collagen matrix. These cells do not demonstrate any abnormal inclusion at this magnification.

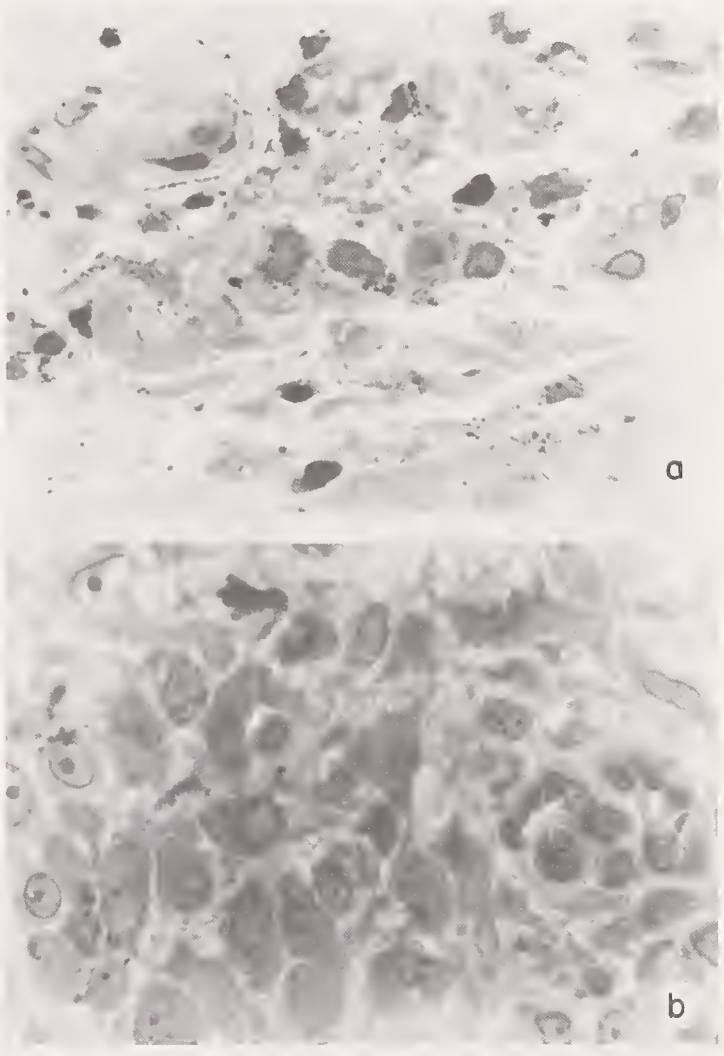

FIGURE 11. a. *Light micrograph of reaction to metallic implant. Note black particle in cytoplasm of fibroblasts.* (1,300×)
b. *Light micrograph of area surrounding bioglass-coated implant.* (1,300×)

[6]Shell Chemical Company.

Figures 12 through 15 are representative electron micrographs of the soft tissue seen in figure 11a. With the resolution afforded by electron imaging, one can now easily discern that the dark staining inclusions within the fibroblasts are made up of aggregations of metallic particles. These particles are enclosed in smooth-walled vesicles. These particles are very densely packed in some of the vesicles so that one cannot distinguish the individual particles but in others there is less dense packing and the individual metal particles are easily visualized.

Figures 16 through 19 are representative electron micrographs of the soft tissue removed from the bioglass-coated implant. In this tissue the cellular morphology is undisturbed. The cells are all typical of fibroblasts actively producing collagen or fibrocytes which are mature and which are enclosed in a very dense collagen matrix. In none of the sections of this tissue were there any inclusions within the cytoplasm containing inorganic crystalline material.

From these observations one can conclude that the material removed from the surface of the metallic implant by corrosion is taken into the fibroblasts of the soft tissue surrounding the implant. These metallic particles are apparently

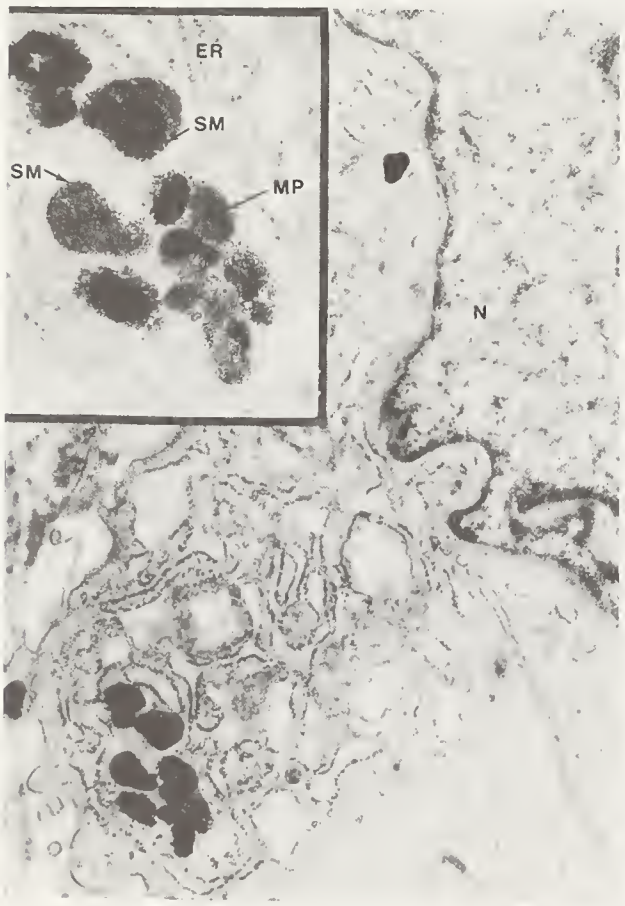

FIGURE 12. *Fibroblast-like cell containing aggregates of metallic particles in cytoplasmic vacuoles.* (23,000×)

Inset—High magnification electron micrograph to demonstrate metallic particles within membrane-bound vacuoles. (55,000×)

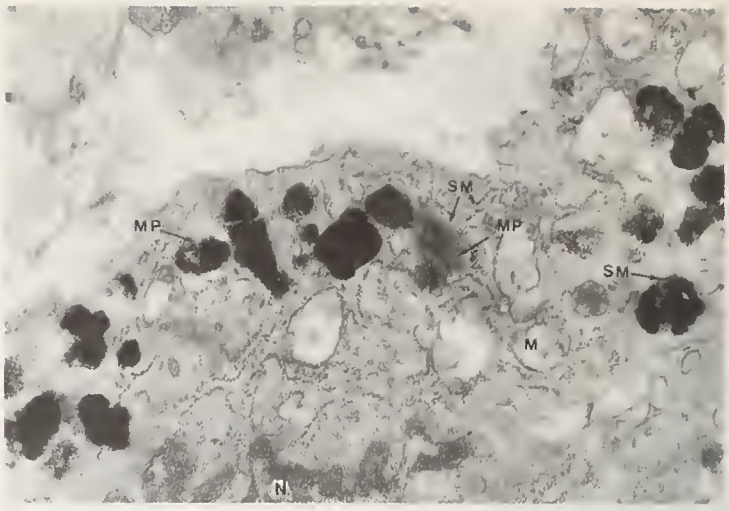

FIGURE 13. *Multiple smooth-walled vacuoles containing metallic particles.*

Note density of packing in some vacuoles. (43,750×)

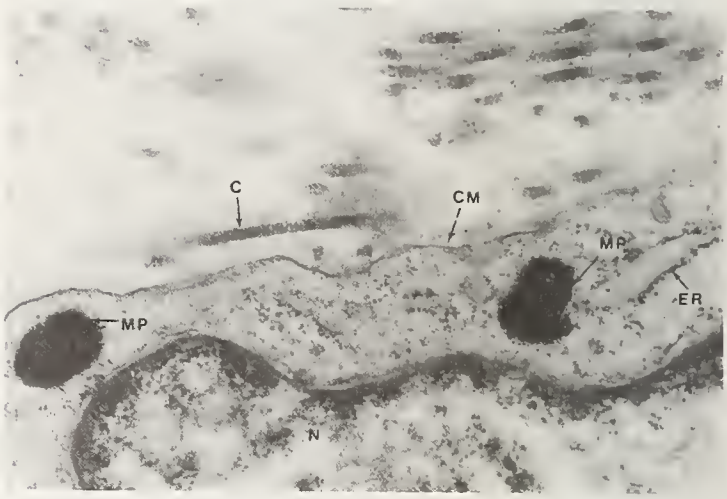

FIGURE 14. *Fibroblast containing two dense aggregations of metallic particles.* (23,900×)

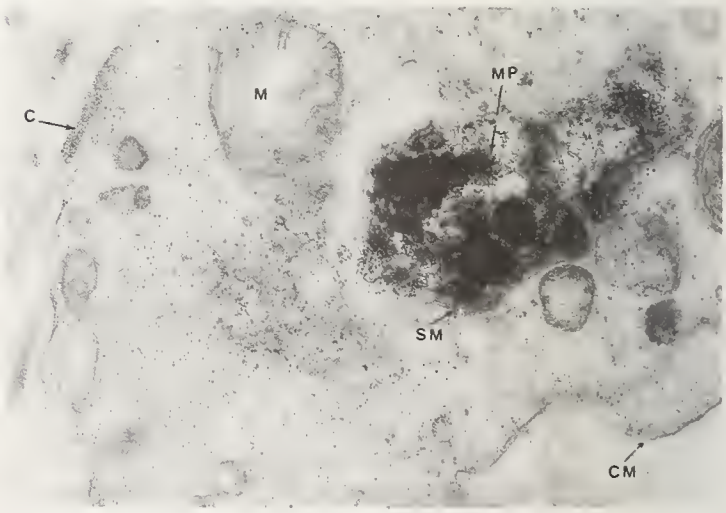

FIGURE 15. *Metallic particles from implant enclosed in smooth-walled vacuoles.* (23,200×).

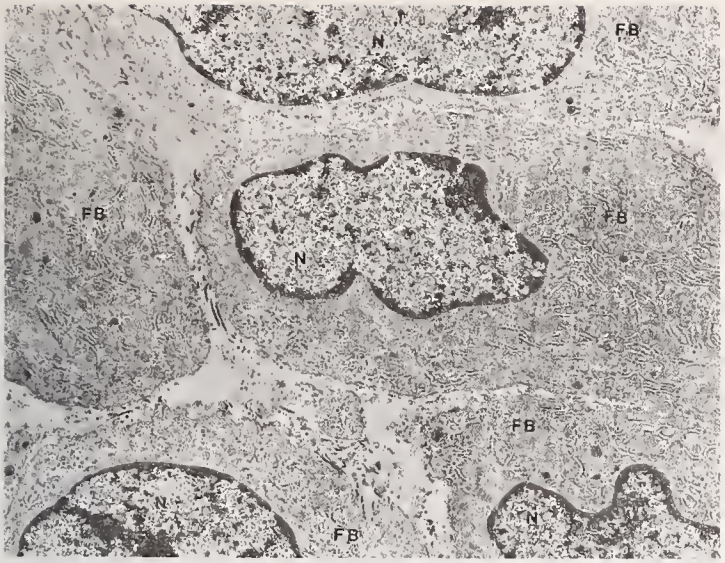

FIGURE 16. *Representative field from tissue surrounding bioglass-coated implant.*

Note absence of cytoplasmic vacuoles containing inorganic material. (12,600 ×)

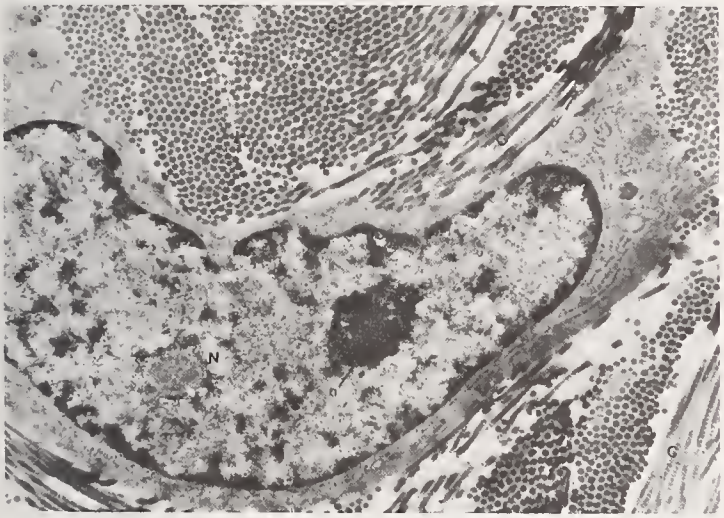

FIGURE 17. *Mature fibrocyte with large nucleus and scant cytoplasm.*

Cell is completely surrounded by mature collagen fibers cut both longitudinally and in cross-section. (21,700 ×)

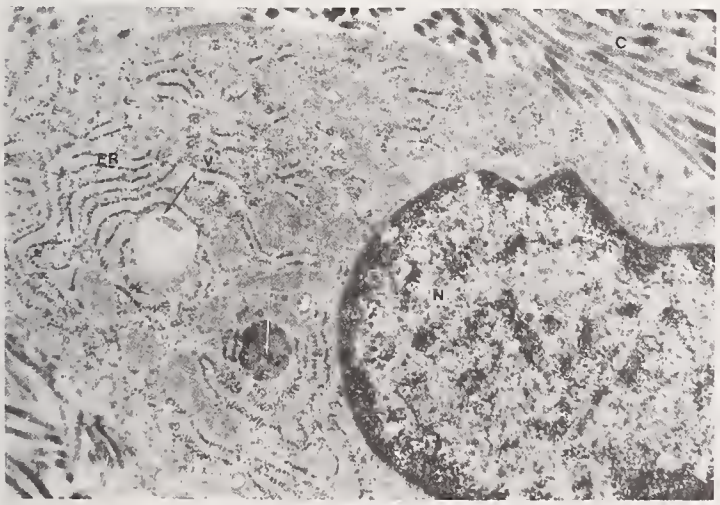

FIGURE 18. *Mature fibrocyte.*

Smooth-walled vesicles do not contain any inorganic material. (29,000 ×)

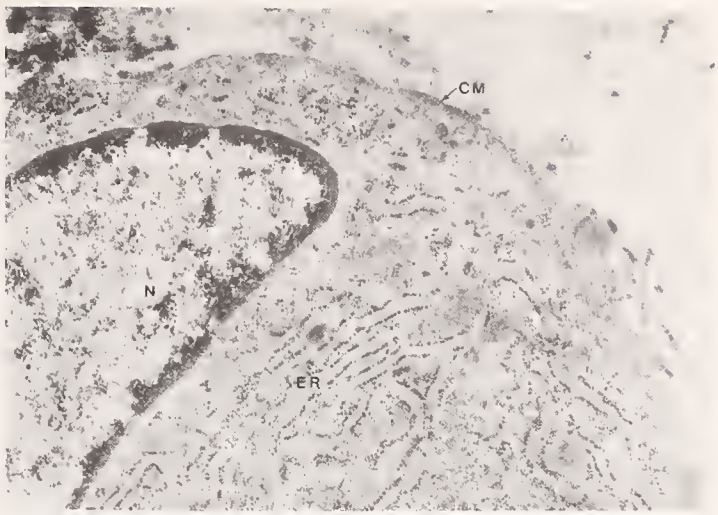

FIGURE 19. *Fibroblast with normal-appearing cytoplasm.*

Note abundant rough endoplasmic reticulum without cytoplastic inclusions of inorganic material. (33,000 ×)

insoluble and are removed as foreign bodies and packeted in the fibroblasts. It is noteworthy that in the soft tissue surrounding the bioglass coated implant, no similar inorganic particles were noted within the cytoplasm of the cells. This would suggest that any elemental constituents released from the ceramic are totally soluble in body fluids and are released into the circulation rather than retained within the cells surrounding the implant. Another obvious conclusion is that the stainless steel implant was protected from corrosion and that no metallic particles were released to be phagocytized by the cells of the surrounding soft tissues.

This report demonstrates a histological comparison between soft tissues removed from a metallic implant and about a bioglass coated stainless steel implant. The evidence supports the conclusion that by coating the stainless steel with a low reactivity biocompatible glass coating, the stainless steel implant is protected from corrosion. Complete mechanical stability of the bioglass flame spray implant after 14 months also demonstrates the potential of using biocompatible coatings to provide orthopaedic device stabilization without resorting to polymer injection. No fibrous capsule was observed at the bioglass coating-bone interface and the implant could not be forcibly extracted from the femoral shaft.

Key to Symbols

C = collagen
CM = cell membrane
ER = endoplasmic reticulum
FB = fibroblast
MP = metallic particles
N = nucleus
n = nucleolus
SM = smooth membrane
V = vacuole

11. Development of a Segmental Bone Replacement: Rats

Application of the bone-bonding bioglass-ceramic material as a segmental replacement for bone has involved three stages of development. The first study involves the use of small bioglass-ceramic washers, ~2 mm thick, as a replacement for a total cross section of rat femur. In the second study, larger segments of bioglass-ceramic, ~7 mm long, were used to replace total cross sections of monkey femora. In the third program bioglass flame spray coated stainless steel segments, ~10 mm, were evaluated. Comparisons of the interfacial strengths developed for the three types of implants, the animal models, and the strength data of the opposite bones of the femoral pairs follow.

The rats were anesthetized with sodium pentabarbital. After a longitudinal incision was made in the right thigh, the femur was exposed by separating the muscles along a fascial plane. The femoral diaphysis was cleaned of soft tissue at the midpoint and osteotomized with a circular dental saw. A Kirschner wire was inserted into the medullary canal of the distal half of the femur, drilled through the condyles, and bent to a right angle with a 1/8 in (3 mm) leg at the distal end. The fracture was reduced after placement of a bioglass-ceramic washer over the wire and against the osteotomy surface by inserting the proximal end of the wire into the medullary canal of the proximal fragment and drilling it through the greater trochanter. The bent end of the wire was placed so it ran subcutaneously down the anterior surface of the tibia and between the lateral and medial condyles of the femur. Apposition of the fracture site was achieved by pulling on the proximal end of the wire, which protruded from the bone (fig. 20, x-ray). The skin was closed with metal wound staples after apposing the muscles over the fracture site with two silk sutures.

FIGURE 20. *A typical animal specimen from the initial series of rat femoral segmental replacement experiments.*

Sixteen rats received the bioglass-ceramic washers, which completely separated the two femoral fragments. Thirteen other rats were subjected to the same operative procedure, but did not receive a bioglass-ceramic implant and thus served as controls for the fracture healing process.

Animals in both groups were sacrificed at varying time intervals, ranging from 6 to 28 weeks. The specific durations are listed in table 2. At sacrifice,

TABLE 2. *Summary of the results of the mechanical testing of pairs of rat femurs*

In all cases the right femur was osteotomized

Duration	With implant				Without implant			
	Animal Number	T_L kgf·cm	T_R kgf·cm	d_T	Animal Number	T_L kgf·cm	T_R kgf·cm	d_T
6 weeks	43	4.8	0.1	0.96	40	5.1	3.9	0.13
	44	4.4	0.5	0.80	41	5.2	1.8	0.49
	45	nonunion		—	48	5.1	1.6	0.52
	46	5.3	0.6	0.80	49	6.6	1.8	0.57
	47	nonunion		—	50	nonunion		—
8 weeks	13	nonunion		—	14	4.2	1.8	0.40
	16	4.4	0.6	0.76	15	6.6	1.4	0.65
	18	nonunion		—	19	4.6	3.8	0.10
	20	nonunion		—	23	nonunion		—
	25	nonunion		—	26	5.0	4.5	0.05
17 weeks	4	nonunion		—	9	4.7	3.2	0.19
	5	fibrous-union		—	11	4.6	1.4	0.53
	7	fibrous-union		—	12	5.0	4.2	0.09
	10	nonunion		—				
28 weeks	33	4.2	3.9	0.04				
	34	5.3	1.8	0.49				

both femurs were removed from the animals and all soft tissue removed from them. Any callus bridging a washer was carefully removed, so that the bioglass-ceramic washer completely separated the two femoral fragments. The left femurs, which were not operated on served as additional controls. A block of metal-plastic potting compound was cast around each specimen end, so that the bones could be gripped securely for the subsequent torsional test. The configuration of the torsional test specimens is shown in figure 21. All femurs were loaded to failure in torsion in the Rapid Loading Torsional Tester, which is described in detail by Frankel and Burstein [34]. The instrumentation yielded the fracture torque for each specimen. Cross-sections of the reconstructed femurs were used to calculate shear stresses at failure, using the computer program developed by Piotrowski and Wilcox [35].

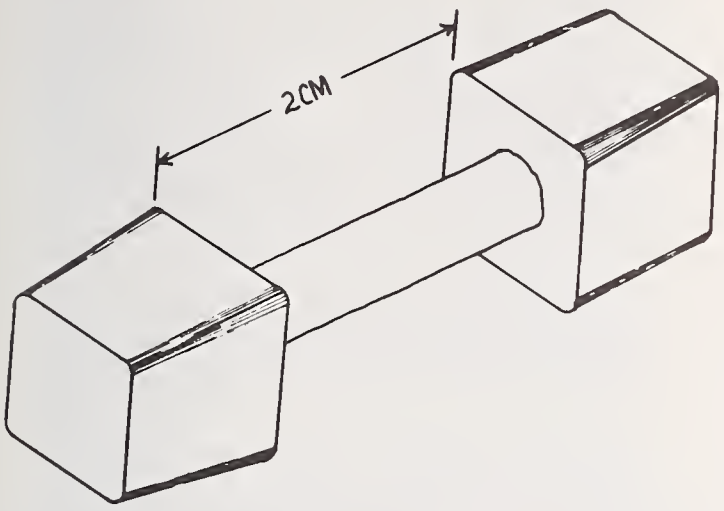

FIGURE 21. *Arrangement of bone test specimen, in center, with ends embedded to facilitate gripping for torsional testing.*

The torques required to fracture all of the rat femurs are summarized in table 2. The percent side-to-side difference of the fracture torques is defined by

$$d_T = \frac{T_L - T_R}{T_L + T_R}$$

where T_L and T_R are the torques required to fracture the left and right femurs of a given animal, respectively. Values for d_T are also tabulated in table 2.

Two studies of the normal side-to-side differences in the fracture torques of paired rat femurs show that there is no significant left-right bias (average value of $d_T = -0.015$ for the 27 pairs, with a standard deviation of 0.110). One should expect that about 30 percent of all rat femur pairs normally will exhibit a side-to-side difference in fracture torque greater than 0.110. This finding is consistent with normal side-to-side differences found for canine fibulas and monkey tibias as well [12].

Figure 22 summarizes the side-to-side differences for the animals receiving bioglass-ceramic implants and the control animals. Superposed over the diagram is the distribution of the side-to-side differences in 27 normal rat femur pairs. A positive value of d_T indicates that the right femur, which was fractured, is weaker than the left femur, which serves as a control.

In the group without implants, two nonunions occurred, as listed in table 2. The relative strengths of the healed bones compared to the intact controls as indicated in figure 22, where a histogram of the d_T's is plotted. In the group with the bioglass-ceramic washer implants, 10 femurs failed to unite by the time the animals were sacrificed.

For both groups, the right femurs, by and large, failed to recover structural integrity. The large

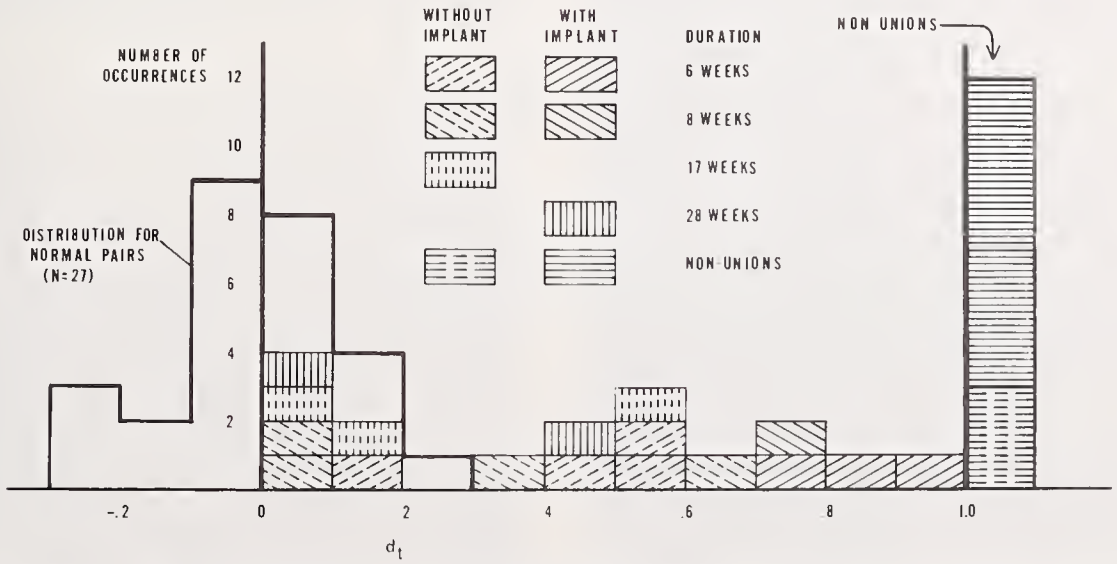

FIGURE 22. *Bar graph showing the percent side to side differences,* d_T, *in the fracture torques of both normal pairs of rat femurs, pairs with sham operations (without implant), and pairs with implants in the right femur.*

degree of scatter in the relative strength, as well as the large number of nonunions, appear to be due to the fact that the fixation used affords no resistance to torsional loading of the fractured femur. Fewer nonunions were observed with the control group because the rough bony surfaces acting on each other provide more friction than the bone-implant interface.

The maximum shear stresses experienced at fracture were calculated for 12 left femurs. The distribution of these stresses is presented in figure 23. The mean value for the computed fracture stress was 1040 kgf/cm², with a standard deviation of 397 kgf/cm².

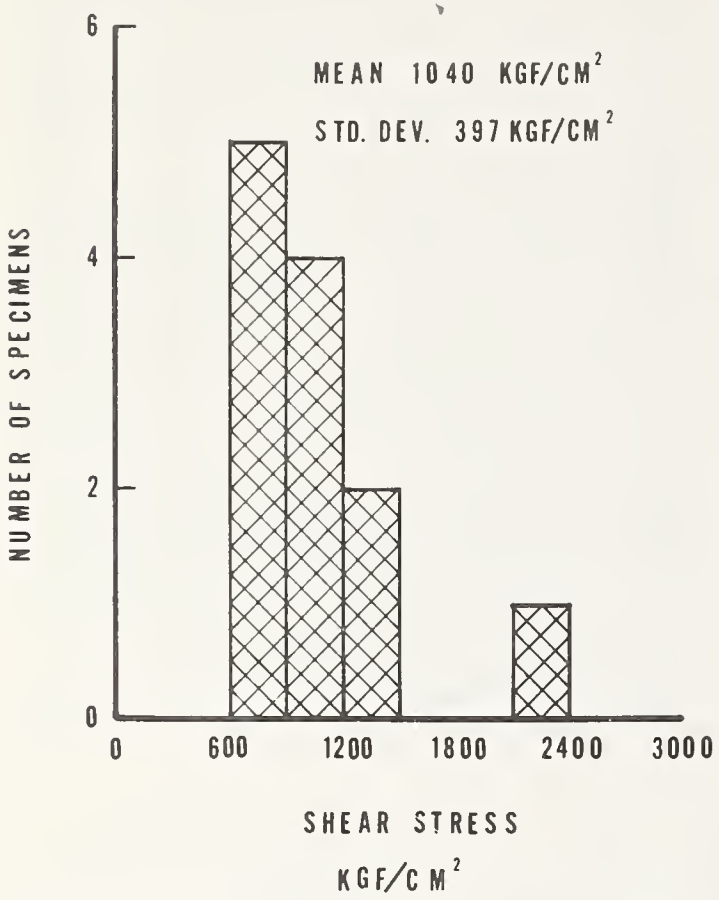

FIGURE 23. *Distribution of fracture shear stresses for normal rat femora.*

All but one of the right femurs containing the implants failed at the bone-implant interface. The femurs of animal 33, shown in figure 24, clearly show that fracture occurred away from the interface, and in fact backed away from the interface after approaching it. Shear stresses for bone 33R were computed to be about 515 kgf/cm² at the fracture site, and 150 kgf/cm² at the bone-bioglass interface. Thus the interface was subjected to a stress equal to 29 percent of the fracture stress of the same bone.

The results of this study were rather inconclusive due to the small number of specimens. However,

FIGURE 24. *Femurs of animal number 33 after mechanical testing.*

Note that the right femur did not fracture at the surface of the ceramic washer.

the striking success of animal 33 stimulated further interest in the determination of the strength of the bone-bioglass bond. A subsequent series of rat implants failed to generate a technique for rigid fixation in both bending and rotational modes. The rat studies were then abandoned in favor of segmental replacement study involving monkey femurs.

12. Development of a Segmental Bone Replacement: Monkeys

Segments of monkey femurs were surgically removed and replaced by either a solid bioglass-ceramic implant, or a flame-sprayed metallic implant, as shown in the accompanying x-rays (figs. 25 and 26). The compositions involved are listed in table 1. All but two of the implants were gas sterilized and conditioned in a buffered solution for 24 h prior to implantation. Fixation of the implant is provided by a 3 mm Schneider nail which spans the length of the femur. Periodic x-rays were used to evaluate the post operative progress.

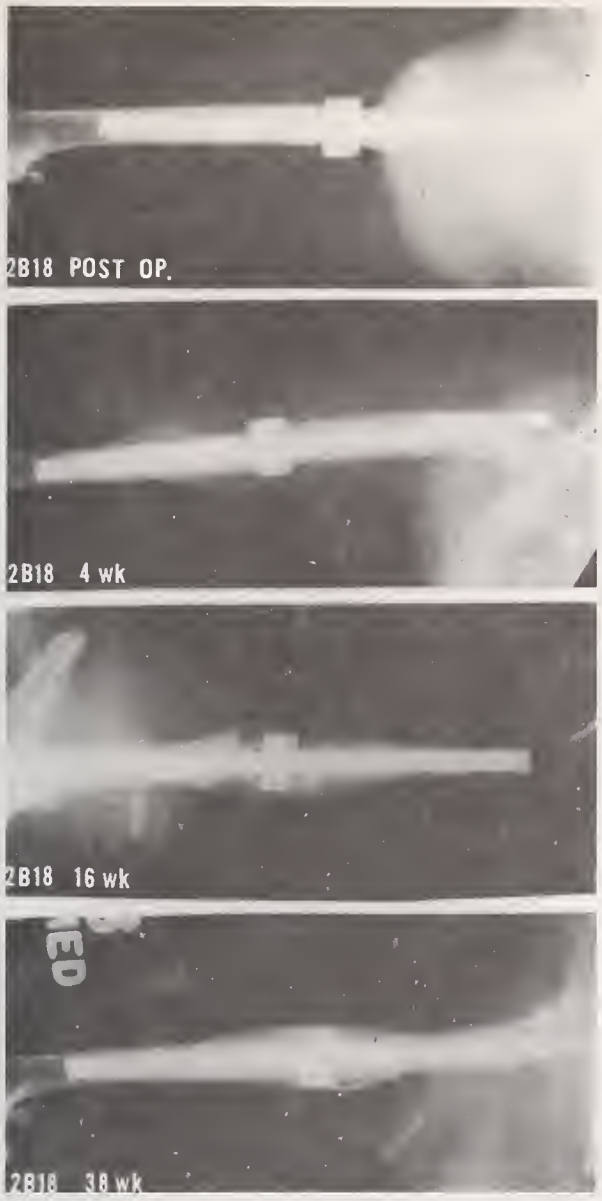

FIGURE 25. *Development and remodeling of a normal callus at a 45S5 bioglass-ceramic segmental bone replacement in a monkey femur.*

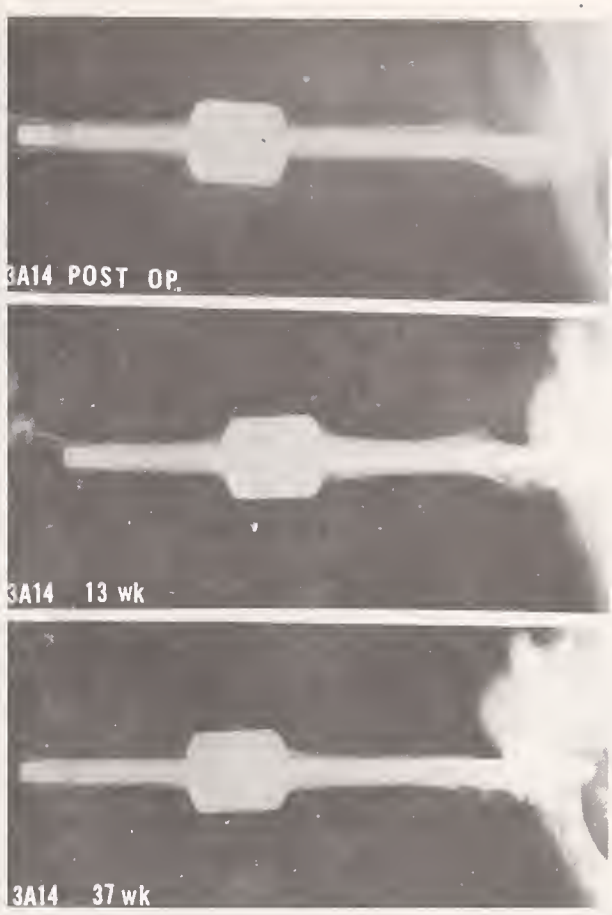

FIGURE 26. *Development and remodeling of a callus at the extremity of a 45S5F bioglass flame sprayed 316L stainless steel segmental bone replacement.*

In one monkey (fig. 27) paralysis of the right limb occurred when the sciatic nerve was engaged by the drill during the reaming operation. Of the 20 other monkeys that were implanted, four animals died within 1 week post op. One monkey fractured both bones of the lower right leg and succumbed to the subsequent complications. One monkey escaped. Of the remaining 14 monkeys eight received bulk bioglass-ceramic implants and six received bioglass flame-sprayed steel implants. One of the animals with a bulk bioglass-ceramic implant was sacrificed for histologic studies.

The progress of the repair processes is illustrated by the accompanying x-ray sequences. Animal 2B18 received a bulk bioglass-ceramic implant (fig. 25). The callus is beginning to mineralize at 4 weeks, is fully established at 16 weeks, and is

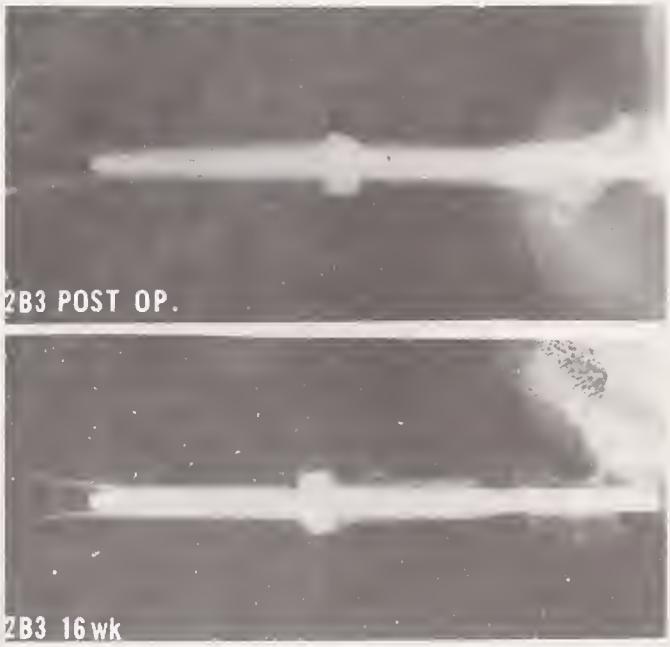

FIGURE 27. *Minimal development of callus at a 45S5 bioglass-ceramic segmental bone replacement on a paralyzed monkey femur.*

to a large extent resorbed by 38 weeks. The larger flame-sprayed implant in animal 3A14 (fig. 26) prevents total encapsulation by the callus (13 weeks) but also appears to form a contiguous structure with the remodeled callus (37 weeks). Animal 2B3 sustained complete paralysis of the right leg during the implantation, and shows a minimal amount of reparative activity at 16 weeks. At 36 weeks little evidence of fracture healing was seen (fig. 27).

The animals were sacrificed at periods between 23 and 50 weeks. All major long bones of the lower extremities were removed, the Schneider nails withdrawn, and the bones tested mechanically to failure in a rapid loading torsion tester [34]. The bones were kept physiologically moist during sacrifice and test. After the torsional tests were completed, the bones were reassembled, embedded in a clear epoxy potting compound, and sectioned. The geometry of these sections was transmitted to the SCADS computer program [35, 36] which was used to determine the torsional stresses generated both at the fracture sites and at the implant surfaces.

TABLE 3. *Mechanical properties of monkey femurs*

In all cases, the right femur contains the implant.

Animal Number	Fracture torques		d_T	Computed stress right femur	
	Right	Left		Fracture	Interface
	(kgf·cm)			(kgf/cm²)	
Bulk bioglass-ceramic					
2B2	9.0	24.0	0.45	*	547
2B5	18.0	30.0	0.25	515	822
2B6	22.0	24.5	0.05	1162	661
2B13	11.0	25.0	0.39	649	615
2B14	33.0	39.0	0.08	1174	955
2B18	10.0	27.0	0.46	*	101
2B19	14.0	30.0	0.36	859	1191
mean			0.29	872	849
Flame-sprayed metal					
2F7	3.0	24.0	0.78	*	150
2F8	4.0	23.0	0.70	*	52
3A13	5.0	18.0	0.57	*	132
3A14	3.5	15.0	0.62	*	150
2G14	5.0	23.0	0.64	*	534
mean			0.66		204

*Failure occured at bone-implant interface.

The results of the mechanical testing are summarized in table 3. The structural integrity of the experimental bone is characterized by the percent difference between it and its opposite, control, bone. This difference, d_T, is defined by the equation $d_T = T_L - T_R/T_L + T_R$, where T_L and T_R are the torques required to fracture the left and right bones respectively. Pairs of tibias were used as controls for this portion of the experiment. The group of tibias exhibits a mean difference of 0.010, indicating that there is no left-right bias, and a standard deviation of 0.07 [37]. The group of femurs containing a bulk bioglass-ceramic implant showed an average difference of 0.29; this difference is quite significant, in that it establishes that the structural integrity of the femurs which were operated on has not recovered fully by approximately 40 weeks. The femurs containing the flame-sprayed implants failed at extremely low torques, resulting in an average difference of 0.66. The torques indicate that the flame-sprayed implant system probably would not be able to sustain severe physiological torques. However, the monkeys used the legs with the flame-spray coated prostheses without difficulty or any noticeable physiological deficit throughout the post-operative period. Close examination of the failure surfaces, which were always near the implant bone interface, showed that the glass coating was still adhering to the bone but that it was torn off the metal substrate during the mechanical testing.

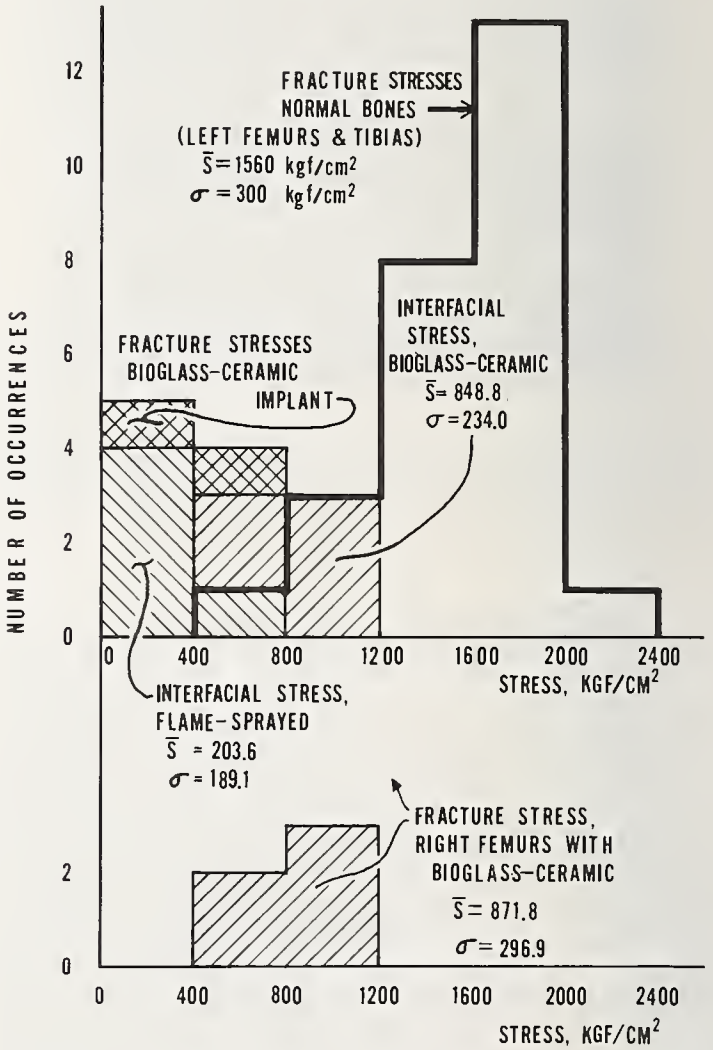

FIGURE 28. *Distribution of computed shear stresses of normal bones at fracture, bone with implants at fracture, and shear stresses developed at bone-implant interfaces in monkeys.*

Figure 28 shows the results of the stress analyses of the various bones involved. The upper histogram shows the distribution of fracture stresses of normal bones, i.e., left femurs and tibias in a bold outline. The average stress required to fracture a normal monkey bone is about 1560 kgf/cm^2 with a standard deviation of 300 kgf/cm^2. No difference was noted in the strength of bone from left femurs and from tibias. Stresses from three groups of bone implant systems are summarized in figure 28: bones with flame sprayed stainless steel implants, bones with bioglass-ceramic implants which broke during the mechanical testing, and bones with bioglass-ceramic implants which fracture through the bone rather than through the implant. The average stress at which the bones containing flame sprayed implants failed was 203 kgf/cm^2. As noted before this is really the stress required to fracture the glass from the metal substrate (see fig. 29). Two

FIGURE 29. *Fractured end of the flame spray coated segmental implant showing the exposed metal surface fracture site (grey areas).*

bulk bioglass-ceramic implants failed through the implant rather than through the bone (fig. 30), and these two are shown as crosshatched blocks in figure 28. This low strength shows that at the present state of the art the bulk material is not of adequate strength to reliably support physiological loads to failure. Five femurs containing bulk bioglass-ceramic implants failed away from the bone implant interface. The lower histogram of figure 28 shows the distribution of the fracture stresses calculated in those bones, with the corresponding region in the upper histogram denoting the interfacial stresses

FIGURE 30. *Failure of bone bioglass-ceramic implant test specimen (2B18) failing within the implant.*

Note the implant bone interface withstands the fracture stress applied.

developed at the surface between the bioglass-ceramic and the newly healed bone. The average stresses in these two distributions are very close to each other, and are not significantly different from each other.

13. Discussion

The structural strength of the monkey femurs was compromised considerably by the presence of the implant. During the torsion tests, fracture occurred at various sites, but appeared to be limited by either the strength of the implant material or the strength of the healing bone near the implant. The fact that the fracture stresses of the right femurs containing bioglass-ceramic implants was considerably lower than the average fracture stress for normal monkey bones was probably due to the fact that the Schneider nails used for fixation were not removed from the animal until just prior to test. This means that a substantial portion of the bending loads to which the bone-ceramic system was subjected was transmitted across the implant site by the nail itself. Thus the bone was protected from full physiologic stress and is therefore probably weaker than normal monkey bone. It should be kept in mind, however, that normal axial compression forces were able to act on the implant-bone interface. This axial compression is probably responsible for the *in-vivo* implant failures.

The distribution of the interfacial stresses calculated for the bulk bioglass-ceramic implants indicates that the strength of the interface is nearly as great as that of the newly healing bone in the same vicinity. The data in figure 28 also indicates that the strength of the interface is at least 75 percent of the strength of normal monkey bone. Due to the fact that failure did not occur preferentially at the interfaces in our study, it must be kept in mind that these figures represent only a lower limit on the strength of the bond developed between the bone and the bioglass-ceramic.

The authors gratefully acknowledge the able assistance of H. Parkhurst, A. W. Smith, and J. McVey of the University of Florida; S. W. Freiman and E. J. Onesto of IITRI, the financial support of U.S. Army Medical R & D Command Contract No. DADA 17–70–C–001 and cooperation of the Gainesville, Florida Veterans Administration Hospital.

14. References

[1] Hench, L. L., Ceramics, glasses and composites in medicine, Med. Instr. **1**, 136–144 (1973).

[2] Boutin, P., Direct attachment of ceramic joints, Symposium on Materials for Reconstructive Surgery, (Clemson University, April 1974).

[3] Griss, P., Heimke, G., von Andrian-Werburg, H., Krempien, B., Reipa, S., Hartung, J., and Lauterbach, J., Morphological and biomedical aspects of Al_2O_3 ceramic joint replacement; experimental results and design considerations for human endoprostheses, Symposium on Materials for Reconstructive Surgery, (Clemson University, April 1974).

[4] Griss, P., von Andrian-Werburg, H., Krempien, B., and Heimke, G., Biological activity and histocompatibility of dense Al_2O_3/MgO ceramic implants in rats, J. Biomed. Res. Symp., No. 4, pp. 453–462, (Interscience, New York, N.Y. 1973).

[5] Griss, P., Krempien, B., von Andrian-Werburg, H., Heimke, G., and Fleiner, R., Experimentelle Utersuchung zur Geivebsuertraglichkeit oxidkeramischer (Al_2O_3) Abriebteilchen, Arch. für orthopädische und Unfall-Chirurgie **76**, 270–279 (1973).

[6] Englehardt, A., Salzer, M., Zeibig, A., and Locke, H., Experiences with Al_2O_3 implantation in humans to bridge resection defects, Symposium on Materials for Reconstructive Surgery, (Clemson University, April 1974).

[7] Klawitter, J. J., and Hulbert, S. F., Applications of porous ceramics for the attachment of load bearing internal orthopedic applications, J. Biomed. Res. Symp., No. 2, Part 1, pp. 161–229 (Interscience, New York, N.Y. 1972).

[8] Hulbert, S. F., Cooke, F. W., Klawitter, J. J., Leonard, R. B., Sauer, B. W., Moyle, D. D., and Skinner, H. B., Attachment of prostheses to the musculoskeletal system by tissue ingrowth and mechanical interlocking, Biomed. Res. Symp. No. 4, pp. 1–23, (Interscience, New York, N.Y., 1973).

[9] Hulbert, S. F., Young, F. A., Mathews, R. S., Klawitter, J. J., Talbert, C. P., and Stelling, F. H., Potential of ceramic materials as permanently implanted skeletal prostheses, J. Biomed. Mat. Res. **4**, 433–455 (1970).

[10] Hulbert, S. F., Klawitter, J. J., and Leonard, R. B., Compatibility of bioceramics with the physiological environment, Ceramics in Severe Environments, W. W. Kriegel and H. Palmour, III (Eds.), pp. 417–434 (Plenum Press, New York, N.Y., 1971).

[11] Piotrowski, G., Hench, L. L., Allen, W. C., and Miller, G., Mechanical studies of the bone-bioglass interfacial bond, Symposium on Materials for Reconstructive Surgery, (Clemson University, April 1974).

[12] Graves, G. A., The influence of compositional variations on bone ingrowth of implanted porous calcium aluminate ceramics, Symposium on Materials for Reconstructive Surgery, (Clemson University, April 1974).

[13] Graves, G. A., Hentrich, R. L., Stein, H. G., and Bajpai, P. K., Resorbable ceramic implants, J. Biomed, Res. Symp. No. 2, Part 1, pp. 91–115 (Interscience, New York, N.Y. 1972).

[14] Bhaskar, S. N., Brady, G. M., Getter, L., Grower, M. F., and Driskell, T. D., Biodegradable ceramic implants in bone, Oral Surg. **32**, 336 (1971).

[15] Bhaskar, S. N., Cutright, D. E., Knapp, M. J., Beasley, J. D., Perez, B., and Driskell, T. D. Tissue reaction to intrabony ceramic implants, Oral Surg. **31**, 282 (1971).

[16] Schnittgrund, G. D., Kenner, G. H., and Brown, S. D., *In vivo* and *in vitro* changes in strength of orthopedic calcium aluminates, J. Biomed. Res. Symp. No. 4, pp. 435–452 (Interscience, New York, N.Y., 1973).

[17] Kenner, G. H., Brown, S. D., Pasco, W. D., and Lovell, J. E., Bull. Amer. Ceramic Soc. **52**, 432 (1973).

[18] Frakes, J. T., Brown, S. D., and Kenner, G. H., Bull, Amer. Ceramic Soc. in press, (1973).

[19] Jecman, R. M., Eggerding, C. L., Brown, S. D., and Schnittgrund, G. D., J. Biomed. Mat. Res. **7**, 369 (1973).

[20] Hench, L. L., Splinter, R. J., Allen, W. C., and Greenlee, T. K., Mechanisms of interfacial bonding between ceramics and bone, J. Biomed. Res. Symp. No. 2, Part 1, pp. 117–143 (Interscience, New York, N.Y., 1972).

[21] Hench, L. L., and Paschall, H. A., Direct chemical bond of bioactive glass-ceramic materials to bone and muscle, J. Biomed. Res. Symp. No. 4, pp. 25–42 (Interscience, New York, N.Y., 1973).

[22] Clark, A. E., Hench, L. L., and Paschall, H. A., The influence of surface chemistry on implant interface hisotlogy: A theoretical basis for implant materials selection, Symposium on Materials for Reconstructive Surgery, (Clemson University, April 1974).

[23] Hench, L. L., and Paschall, H. A., Histo-chemical responses at a biomaterials interface, J. Biomed. Res. Symp. on Prostheses and Tissue: The Interface Problem, (Clemson University, 1973).

[24] Beckham, C. A., Greenlee, T. K., Jr., and Crebo, A. R., Bone formation at a ceramic implant interface, Calc. Tis. Res. **8**, No. 2, 165 (1971).

[25] Greenlee, T. K., Jr., Beckham, C. A., Crebo, A. R., and Malmborg, J. C., Tissue responses at the interface of a ceramic, J. Biomed. Mat. Res. **6**, 244 (1972).

[26] Clark, A. E., and Hench, L. L., Effect of P^{5+}, B^{3+}, and F^- on corrosion of invert soda-lime-silica glasses, Submitted to J. Amer. Ceramic Soc. (1974).

[27] Clark, A. E., Pantano, C. G., and Hench, L. L., Auger spectroscopic analysis of invert glass corrosion films, Submitted to J. Amer. Ceramic Soc. (1974).

[28] Carlisle, E. M., Silicon—a possible factor in bone calcification, Science **167**, 279–280 (1970).

[29] Housefield, L. G., Mechanical property control of a bioglass-ceramic system, Masters Thesis, University of Florida (1972).

[30] Bliton, J. L., Ceramic coatings for cementitious and metallic surfaces, IITRI Final Report, Project No. B8009, (International Lead Zinc Research Organization, 1964).

[31] Oel, H. L., The relationship between free energy and kinetics in sintering processes, Kinetics of High-Temperature Processes, W. D. Kingery (Ed.), (John Wiley and Sons, Inc., New York, N.Y., 1959).

[32] Kingery, W. D., Introduction to Ceramics, pp. 628–647 (John Wiley and Sons, Inc., New York, N.Y., 1960).

[33] Hench, L. L., Onesto, E. J., and Freiman, S. W., Development of a bioglass flame spray coated hip prosthesis, U.S. Army Medical Research and Development Command Contract No. DADA 17–70–C–0001, Report No. 3, 180 pp.

[34] Burstein, A. H., and Frankel, V. H., A standard test for laboratory animal bone, J. Biomech. **4**, 155 (1971).

[35] Piotrowski, G., and Wilcox, G. A., The STRESS program: a computer program for the analysis of stresses in long bones, J. Biomech. **4**, 497 (1971).

[36] Piotrowski, G., and Kellman, G. I., A stress calculator for arbitrarily drawn sections—the S.C.A.D.S. computer program, U.S. Army Medical Research and Development Command Contract No. DADA 17–70–C–0001, Report No. 4, 126 pp. (1973).

[37] Miller, G., and Piotrowski, G., Variability of the torsional strength of paired bones, J. Biomech., **7**, 247 (1974).

NATIONAL BUREAU OF STANDARDS SPECIAL PUBLICATION 415,
Biomaterials, Proceedings of a Symposium held in conjunction with the Ninth Annual Meeting of the Association for the Advancement of Medical Instrumentation, New Orleans, La., April 19–20, 1974 (Issued May 1975).

Soft Tissue Response to a Series of Dense Ceramic Materials and Two Clinically Used Biomaterials

W. C. Richardson, Jr.

Tulane University, New Orleans, La. 70112

S. F. Hulbert

Medical Center, University of Alabama, Birmingham, Ala. 35294

and

J. J. Klawitter, and B. W. Sauer

Clemson University, Clemson, S.C. 29631

Disc-shaped implants of spinel, alumina, mullite, zircon, a cast Co-Cr-Mo alloy, and ultra-high molecular weight polyethylene (UHMWPE) were implanted in the parasipinalis musle of twelve adult, male, White New Zealand rabbits. Prior to implantation the implants were characterized with respect to size and shape, weight and surface roughness. After periods of 1 month, 2 months, and 4 months the rabbits were sacrificed and the tissue specimens were retrieved with the implants still intact. Histological examination of the tissues surrounding the implants along with changes in the size and shape, weight, and surface roughness of the implants were used as criteria for evaluating these materials for implant purposes.

No surface degradation of any of the materials was detected using scanning electron microscopy. Fibrous tissue seems to adhere to the UHMWPE implants more than any other material used in this study. Large amounts of fibrous tissue were also found to adhere to the cast Co-Cr-Mo alloy implants.

The histological results indicated that within the limits of this investigation, the biocompatibility of the ceramic materials used in this study compares favorably with the clinically used cast Co-Cr-Mo alloy implants and the UHMWPE implants.

Key words: Biocompatibility, ceramic implants, histological evaluation; implant characterization.

1. Introduction

Ceramic materials are beginning to find a place in the field of biomaterials as new demands are made for materials that can withstand the highly corrosive environment of the human body [1–26].[1] The physical and chemical properties of ceramics have recently led researchers to consider these materials for use in the replacement of bone [1, 3, 4, 6, 9, 10, 12–16, 19–26] and teeth [17–19].

Ceramic materials have certain advantages and disadvantages as compared to other materials for implantation. The major advantage of ceramics is that they are highly chemically inert in the physiological environment. They are, however, characteristically brittle, notch sensitive materials. Thus, a careful consideration of their mechanical properties will be essential to their applications as biomaterials.

Fixation of orthopedic appliances to bone is a definite problem to the orthopedic surgeon. Some investigators have approached this problem by developing a mechanical interlocking between the implant and the tissue [3, 6, 10, 12–14, 17, 19, 20, 22, 24, 26]. The mechanical interlocking was achieved by tissue growth into the interconnecting pores of porous ceramic materials. Klawitter [10] reported that a minimum pore size of approximately 100 μm is necessary for bone ingrowth.

Hench et al. [21], reported achieving direct chemical bonding of a glass-ceramic material with bone and soft tissues. They accomplished this through the development of a series of surface-active glasses and glass-ceramics.

2. Compatibility Testing

One of the problems of conducting a biocompatibility experiment is that of methodology. Thus far there appears to be no universally accepted method for evaluating tissue compatibility [27–42].

[1] Figures in brackets indicate the literature references at the end of the paper.

There are two main techniques which have been used to evaluate candidate materials for implantation, *in vitro* and *in vivo* studies. *In vitro* studies incorporate the use of tissue culture or simulated body fluids to test the biocompatibility of candidate materials and they have advantages in that they are considerably less expensive. While *in vitro* studies serve as an excellent tool for screening materials, they do not provide conclusive information because the total dynamic physiological environment is not simulated [36, 39, 40].

In vivo biocompatibility studies, most generally, consist of implanting materials of interest into research animals for varying periods of time and subsequently performing a histological evaluation of the adjacent tissues.

There are some inherent problems associated with determining compatibility of biomaterials [44]. When implants are placed into the body, the material is subjected to a barage of rejection and healing mechanisms. As the body reacts to the foreign material, certain histological processes take place which are observable in the tissues surrounding the implant as well as in special organs that are far removed from the implant. The combined activity of the many cell types, tissues, and organ systems produce such a complex sequence of interactions that it is often difficult to explain certain histological observations that occur when an implant is placed in the body [44]. It is essential for the researchers in these types of studies to have a basic understanding of the nature and processes of foreign-body reactions and their characteristic signs. A paper by Hulbert et al. [44], provides a discussion of phagocytosis, the immune response, abscesses, neoplasms, poisons, inflammation and normal wound healing and relates these phenomena to their importance in evaluating the biocompatibility of implant materials.

Many investigators attempt to monitor the biocompatibility of an implant by designing a device of the type desired and to test it in the exact location of the intended application [7, 17, 18, 24, 25, 37, 45]. In an attempt to reduce the number of experimental variables, other researchers have implanted sample materials in various shapes and forms [5, 6, 9–12, 15, 27–30, 33, 34]. Wood et al. [29], reported that an increased tissue response which typically occurs near the ends of rod-shaped implants does not occur around disc-shaped implants.

Autian [38] mentioned that a material implanted in the body may initiate a response in two general ways: (1) the effects of the body on the material and (2) the effects of the material on the body. In view of this fact, it seems that a properly designed compatibility experiment would seek to not only investigate the histological reactions, but would also attempt to monitor changes which may occur to the material. Indeed, material characterization is an extremely important but often neglected portion of biocompatibility studies.

3. Materials and Methods

3.1. Scope of the Research

Disc-shaped implants of spinel[2] ($MgO\ Al_2O_3$), alumina[2] (Al_2O_3), mullite[2] ($3Al_2O_3\ 2SiO_2$), zircon[2] ($ZrSiO_4$), a cast Co-Cr-Mo alloy,[3] and ultra-high molecular weight polyethylene, were implanted in the paraspinalis muscle of twelve adult, male, White New Zealand rabbits. Prior to implantation the implants were characterized with respect to size and shape, weight and surface roughness. After periods of 1 month, 2 months, and 4 months the rabbits were sacrificed and the tissue specimens were retrieved with the implants still intact. Histological examination of the tissues surrounding the implants along with changes in the size and shape, weight and surface roughness of the implants were used as criteria for evaluating these materials for implant purposes.

3.2. Materials Selection

Spinel[2] ($MgO\ Al_2O_3$), alumina[2] (Al_2O_3), mullite[2] ($3Al_2O_3\ 2SiO_2$), and zircon[2] ($ZrSiO_4$), were chosen for this experiment because they represent a group of ceramic materials which are often selected for use in severe environments and which were available from commercial suppliers.[5]

In order to facilitate quality comparisons of these ceramic materials with clinically used biomaterials, this experiment included the implantation of an ultra-high molecular weight polyethylene (UHMWPE)[4] and a cast cobalt-chromium-molybdenum alloy (meeting the ASTM Standard Specification for Surgical Implants, designation number F75–67) as experimental controls.

3.3. Materials Characterization

Each implant was characterized with respect to size and shape, surface roughness, and weight before and after implantation. Scanning electron microscopy was also used before and after implantation. Chemical analysis, x-ray diffraction, and reflected light microscopy were used to characterize the materials before implantation.

---

[2] Supplied by American Lava Corporation, Chattanooga, Tenn.
[3] Zimaloy, Zimmer Manufacturing Company, Warsaw, Ind.
[4] RCH 1000, Hoechst, Supplied by Zimmer Manufacturing Co., Warsaw, Ind.
[5] Certain commercial materials and instruments may be identified in this publication in order to adequately specify the experimental procedure. In no case does such identification imply recommendation or endorsement by the National Bureau of Standards, nor does it imply that the equipment or instruments identified are necessarily the best available for the purpose.

Size and Shape

The disc-shaped implant was chosen for this experiment for reasons demonstrated by Wood et al. [29]. The diameter and thickness of each implant was determined.

3.4. Surface Roughness

Variation in surface roughness from 4 microinches to 25 microinches (0.1–0.6 μm) was shown not to influence the degree of tissue reaction in a preliminary experiment [48].

Attempts were made to achieve a uniform surface roughness on all implants. The ceramics were polished on a 30 μm diamond grinding wheel with a water lubricant. The UHMWPE implants were finished by hand with 320 grit (approximately equal to 30 μm) SiC grinding paper and with a water lubricant. These implants were finished by hand to reduce the degree of feathering along the edges of the implant which occurred using the grinding wheel. The Zimaloy implants were polished on a 320 grit SiC grinding wheel. The surface roughness of the implants was measured using a profilometer [6] before and after implantation.

3.5. Weighing the Implants

Prior to weighing the implants, they were washed in an ultrasonic cleaner in an effort to remove any particulate matter and any organic film which may have been present. The following procedure was used:

Benzene wash	15 minutes
Acetone wash	15 minutes
Absolute Ethanol wash	15 minutes
Dry and desiccate in a Bell Jar	8 hours

From this point on, the implants were only handled with a pair of forceps.

Each implant was characterized with respect to size and shape, surface roughness, and weight prior to being implanted. After the implantation period, the implants were to be characterized in the same fashion to determine any changes in these characteristics due to implantation. A separate experiment was conducted in order to determine the possibility of any changes which may result from cleaning and/or sterilization procedures. The results showed that the sterilization and/or cleaning procedures do not significantly affect the size or shape, the surface roughness or the weight of the implants.

Chemical Composition and Crystal Phase State of the Implants

The chemical composition of the implants was determined by spectrochemical analysis[7] of the materials. X-ray diffraction[8] was used to determine the crystal phase state of the ceramic implants.

Microstructure of the Implants

Photomicrographs and the average crystal size data for the four ceramic materials were acquired from the supplier of these materials.

Metallographic analysis was performed to determine the microstructure of the cast Co-Cr-Mo alloy (Zimaloy) used in this study.

3.6. Surgical Procedure

Three groups of four male White New Zealand rabbits approximately 6–8 months old received six implants and a sham operation (an incision without an implant) in the paraspinalis muscle of each rabbit. The first group of four rabbits received implants for 4 months. The second group were 2-month implants and the third group were 1-month term implants. The relative positions of six implants and the sham were chosen completely at random. This process was carried out for each of the 12 rabbits.

Sodium pentobarbital (approximately 60.0 milligram per kilogram of body weight) was used for induction and maintenance of surgical anesthesia. A large region of hair was clipped to reveal the skin on the back. The skin was then scrubbed with alternating providone-iodine surgical scrub sponges and alcohol sponges approximately three times. A film of providone-iodine surgical preparatory solution was sprayed on the skin and left for surgery.

Sterile technique was used throughout surgery. A midline skin incision approximately 7 cm long was made with an electrocautery unit. The subcutaneous facia was dissected out of the implantation region. Incisions were made with a scalpel approximately 2 cm into the paraspinalis along the longitudinal axis of the muscle and approximately 1 cm long. The implants were placed into the incision using a pair of polypropylene forceps. The muscle tissue was closed with a single horizontal mattress stitch of 000 medium chromic gut. The facia was closed in the same manner. The sham operation was performed in the same fashion except that the forceps were inserted into the muscle without an implant. The subcutaneous tissue was closed with a simple continuous suture pattern of 000 chromic gut. The skin was closed with interrupted 000 monofilament nylon suture material.

3.7. Post Operative Care

Following surgery, a clean bandage was secured

[6] Brush Electronics Co., Cleveland, Ohio. Model BL–110–57–2041.

[7] Spectrochemical Laboratories, Inc., Pittsburgh, Pa.

[8] Norelco Type 42202 Diffractor, North American Philips Co., Inc., Mount Vernon, N.Y.

with adhesive tape over the midportion of the rabbit. Procain Penicillin-G (100,000 units) and dihydrostreptomycin (0.125 g) were administered twice a day for 5 days post-operatively.

3.8. Tissue Preparation

The rabbits were sacrificed using a 1 cm^3 intravenous injection of Barb-Euthol. After sacrifice, tissue specimens measuring approximately 2.5 cm by 1.5 cm by 0.5 cm were retrieved with the implants *in situ* and mounted on a piece of balsa wood before fixation in 10 percent formalin. After at least 2 days in 10 percent formalin, the implants were carefully dissected out of the tissue specimens by making an incision along the midportion of the implant parallel to the longitudinal axis of the muscle fibers. The tissue specimens were infiltrated and embedded in paraffin blocks to facilitate sectioning.

Sections 8 μm thick were taken from the tissue blocks using a rotary type microtome. These sections were mounted on glass slides using an albumin fixative and were dried overnight before staining.

The sections were stained using a normal hematoxylin and eosin staining technique and were covered with microscopic cover glasses for histological examination under a light microscope.

3.9. Post-Implantation Characterization of Materials

Post-implantation characterization of the implants was performed using the same technique as in the pre-implantation characterization.

4. Results and Discussion of Results

4.1. Results of Materials Characterization

Geometric Analysis

The diameter and thickness of each implant was determined before and after implantation. All implants had an approximate diameter of 1 cm and an approximate thickness of 1 mm. When consideration is given to the diameter and thickness of the implants and the sensitivity of the instrument used, the minimum percent change detectable for the thickness is 1 percent and the minimum percent change detectable for the diameter is 0.25 percent. A summary of the data for each material is listed in table 1.

The UHMWPE implants were the only implants to have a noticeable increase in diameter. The increase in thickness can probably be attributed to the fact that some tissue remained attached to the surfaces of the implants after washing the implants in successive washings of benzene, acetone and absolute alcohol. One of the UHMWPE implants was processed through the normal H & E staining procedure in order to identify the tissue which had adhered to these implants. These UHMWPE implants permitted the transmission of light and thus, the histological observation was made with relative ease. These histological results revealed that a thin layer (approximately one cell layer thick) of young fibrous tissue was firmly attached to these implants.

TABLE 1. *Summary of geometric analysis*

Material name	Mean percent change in diameter	Mean percent change in thickness
Alumina (Al_2O_3)	0.0	0.0
Mullite ($3Al_2O_3$ $2SiO_2$)	.0	.0
Zircon ($ZrSiO_4$)	.0	.0
Spinel (MgO Al_2O_3)	.0	.0
UHMWPE	+0.3	+1.0
Cast Co-Cr-Mo alloy	0.0	+1.0

4.2. Weight Determinations

The weight of the implants used in this study was determined before and after implantation. When consideration is given to the weights of the implants and the sensitivity of the instrument used, the minimum percent change detectable for the weights is 0.01 percent. A summary of the data for each material is given in table 2.

The spinel implants were the only implants to have an appreciable change in weight.

The weight changes observed here were biased as mentioned earlier by the fact that some tissues continued to adhere to each sample after the washing sequence.

TABLE 2. *Summary of weight changes*

Material name	Mean weight before implantation (grams)	Mean percent change in weight
Alumina (Al_2O_3)	0.2994	−0.02
Mullite ($3Al_2O_3$ $2SiO_2$)	.2452	+0.01
Zircon ($ZrSiO_4$)	.3211	0.00
Spinel (MgO Al_2O_3)	.2044	−0.38
UHMWPE	.0707	+0.05
Cast Co-Cr-Mo alloy	.6869	−0.01

4.3. Surface Roughness Determinations

The surface roughness of each implant was determined before and after implantation. When consideration is given to the sensitivity of the profilometer, the minimum percent change detecta-

ble for the surface roughness is 1 percent. A summary of the results is presented in table 3.

TABLE 3. *Summary of changes in surface roughness*

Material name	Mean surface roughness before implantation (microinches) [a]	Mean percent change in surface roughness
Alumina (Al_2O_3)	14.9	13
Mullite ($3Al_2O_3\,2SiO_2$)	15.8	21
Zircon ($ZrSiO_4$)	10.6	75
Spinel ($MgO\ Al_2O_3$)	15.1	37
UHMWPE	27.4	6
Cast Co-Cr-Mo alloy	6.1	259

[a] 1 microinch=0.025 micrometers

All of the materials showed an overall increase in surface roughness. The cast Co-Cr-Mo alloy implants showed a considerably larger increase than any of the ceramic materials or the UHMWPE implants. The pre-implantation measurements for the cast Co-Cr-Mo alloy implants indicated a surface roughness of approximately 6 microinches which is considerably less than the surface roughness of the other implants before implantation. The tissue which had adhered to the cast Co-Cr-Mo alloy implants, along with the low before implantation measurements, are probably responsible for the large percent increase in surface roughness.

4.4. Scanning Electron Microscopy

One representative sample of each material was observed under a scanning electron microscope[9] (SEM) before and after implantation.

After removing the implants from the tissue blocks, all of the materials had some tissue which had remained intact. Two specimens of each material (from the 4-month implant group) were chosen to determine an approximate percentage of the surface covered with tissue. An eyepiece objective with grid markings was used to observe the implants under reflected light. Three areas of the surface of each implant were chosen at random and the number of grid blocks falling on the surface with and without tissue was counted and percentages calculated.

The SEM analysis provided supportive evidence in agreement with the data presented in table 4. Very little difference was seen in the SEM photomicrographs of the four ceramic materials before and after implantation. However, the UHMWPE appeared to be entirely covered with tissue.

[9] Mark 2A Stero Scan, Kent Cambridge Scientific Inc., Morton Grove, Ill.

TABLE 4. *Approximate percentages of the surface of the implants covered with tissue*

Material	Approximate percentage of the surface covered with tissue
Alumina (Al_2O_3)	8
Mullite ($3Al_2O_3\,2SiO_2$)	11
Zircon ($ZrSiO_4$)	15
Spinel ($MgO\ Al_2O_3$)	8
UHMWPE	96
Cast Co-Cr-Mo alloy	72

The cast Co-Cr-Mo alloy implants had relatively large amounts of tissue which had remained intact. This is in agreement with observations recorded by Homsy, et al. [49].

4.5. Spectrochemical Analysis

Spectrochemical analysis of the ceramic materials used in this study is given in table 5.

TABLE 5. *Semiquantitative spectrographic analysis [a] (weight percent)*

Constituents	Alumina	Mullite	Zircon	Spinel
Al_2O_3	Major	Major	3.0	20.0
ZrO_2	[b] 0.01	[b] 0.01	Major	0.01
MgO	.15	10.0	2.0	Major
SiO_2	.35	10.0	25.0	0.10
CaO	.05	0.06	1.0	.07
TiO_2	.02	.02	0.25	.05
Fe_2O_3	.15	.15	.25	.15
CuO	.10	.05	.01	.02
CoO	.07	([b])	([b])	([b])
BaO	([b])	([b])	.02	([b])
NiO	.005	.003	.002	.003
PbO	.002	.002		.002
Cr_2O_3	([b])	.001	([b])	([b])
ZnO	.001	.001	([c])	.001
B_2O_3	.001	.001	([b])	([b])
SnO_2	([b])	([b])	([b])	([b])
MnO	.001	.001	.001	.001

[a] Data obtained from Spectrochemical Laboratories, Inc., Pittsburg, Pa.
[b] Not detected.
[c] Zr Interference.

4.6. Crystal Phase State of the Ceramic Materials

The identity of the ceramic materials used in this study was confirmed using x-ray diffraction. A representative specimen of each of the ceramic implants was crushed, ground and a powder x-ray diffraction analysis performed using Cu Kα radiation. No unreacted raw materials were observed in any of the specimen analyses.

Microstructure and Average Crystal Size of the Materials

Photomicrographs of the ceramic materials were provided by the American Lava Corporation. The average crystal size of the ceramic materials is given in table 6.

TABLE 6. *Average crystal size of the ceramic materials* [a]

Material	Average crystal size
Alumina (Al_2O_3)	typically ≤ 2 μm
Mullite ($3Al_2O_3$ $2SiO_2$)	6 μm
Spinel (MgO Al_2O_3)	6 μm
Zicron ($ZrSiO_4$)	typically ≤ 2 μm

[a] Data obtained from American Lava Corporation, Chattanooga, Tenn.

5. Results of Histological Evaluation

Three groups of rabbits received implants for 4 months, 2 months, and 1 month, respectively. One of the rabbits (from the 2 month implant group) died 2 weeks post-operatively. The cause of death was a chronic respiratory infection not related to the implant study. All other rabbits remained healthy the full duration of their implant periods.

Upon sacrifice the implant sites were observed macroscopically. All of the implant sites appeared to be healthy and normal with no incidence of excessive swelling or redness.

The histological sections were evaluated using the following criteria:

slight: thin fibrous tissue capsule with uniform thickness and no inflammatory response evident.

moderate: thin fibrous tissue capsule with some localized thickening and with little or no inflammatory response evident.

severe: uniform thick fibrous tissue capsule associated with a chronic inflammatory response.

A summary of these results appears in table 7.

All of the ceramic materials indicated a tissue compatibility that compared favorably with the compatibility of the clinically used cast Co-Cr-Mo alloy and the UHMWPE. The spinel implants seemed to have a slightly better compatibility than any of the other materials used in this study. The mullite implants indicated a tissue compatibility slightly less than any other material.

Many of the histological sections indicated a much thicker fibrous membrane on one side of the implant site with a very thin membrane on the other side of the implant site. This could probably be attributed to mechanical factors rather than poor compatibility. Wood et al., has described a "clubbing" effect which occurs around rod-shaped implants [29]. This "clubbing" effect is the increased tissue response around the ends of a rod-shaped implant. The effect occurred around many of the implants used in this study. Since this type of increased tissue response is thought to be due to mechanical irritation, these regions of "clubbing" were not considered in the histological evaluation.

There are some inherent advantages and disadvantages in this method of evaluation. The removal of the implants before histological procedures allows the investigator to use a paraffin embedding technique. This technique is an easier and quicker technique than the process of embedding the tissue and implant in poly(methylmethacrylate) [10]. Another advantage in this technique is that it allows pre- and post-implantation evaluation of the implants. The disadvantages in paraffin embedding are twofold. Firstly, the actual tissue-implant interface cannot be observed. Secondly, the criteria for histological evaluation in this study considered the thickness of the encapsulating membrane. Since part of this membrane was removed along with the implant, it seems that the histological evaluation may have been adversely affected.

TABLE 7. *Summary of histological evaluation*

Material	Fraction with a slight response	Fraction with a moderate response	Fraction with a severe response
Alumina (Al_2O_3)	5/12	6/12	1/12
Mullite ($3Al_2O_3$ $2SiO_2$)	4/12	8/12	0
Spinel (MgO Al_2O_3)	9/12	2/12	1/12
Zircon ($ZrSiO_4$)	8/12	2/12	2/12
UHMWPE	5/12	7/12	0
Cast Co-Cr-Mo alloy	8/12	3/12	1/12

NOTE. All of the sham operations indicated a normal wound healing process.

6. Overall Discussion of Results and Recommendations

Changes in weight, size and shape, and surface roughness of the implants have been monitored on a pre- and post-implantation basis. Table 8 serves to summarize the results. The spinel implants were the only implants to exhibit an appreciable weight loss. These implants had the best tissue response of all materials used in this study. No obvious changes were noted in the surface of these spinel implants using scanning electron microscopy.

Within the limits of this investigation, the biocompatibility of the ceramic materials compares favorably with the clinically used cast Co-Cr-Mo implants and the UHMWPE implants.

One of the major disadvantages in this technique of evaluation is that the tissue-implant interface cannot be observed histologically. Future biocompatibility studies could possibly become more significant by implanting two series of implants. One group could be used to evaluate the material on a pre- and post-implantation basis as described in this experiment. Another group could be sectioned with the implant *in situ* in order to observe the actual tissue-implant interface using the technique described by Klawitter [10].

Another recommendation is that future studies include the implantation of a negative control. This would further validate the sensitivity of the implant study.

TABLE 8. *Overall summary of results*

	Alumina (Al_2O_3)	Mullite ($3Al_2O_3\ 2SiO_2$)	Zircon ($ZrSiO_4$)	Spinel ($MgO\ Al_2O_3$)	UHMWPE	Cast Co-Cr-Mo alloy
Mean percent change in weight	−0.02	+0.01	0.00	−0.38	+0.05	−0.01
Mean percent change in diameter	0.0	0.0	0.0	0.0	+0.3	0.0
Mean percent change in thickness	0.0	0.0	0.0	0.0	+1.0	+1.0
Mean percent change in Surface Roughness	+13	+21	+75	+37	+6	+259
Fraction with slight response	5/12	4/12	8/12	9/12	5/12	8/12
Fraction with moderate response	6/12	8/12	2/12	2/12	7/12	3/12
Fraction with severe response	1/12	0	2/12	1/12	0	1/12

7. Conclusions

Within the limits of this investigation, the following conclusions can be drawn:

1. The biocompatibility of the ceramic materials used in this study compares favorably with the clinically used cast Co-Cr-Mo alloy implants and the UHMWPE implants.
2. Fibrous tissue seems to adhere more to the UHMWPE implants than to any other material used in this study.
3. Fibrous tissue seems to adhere more to the cast Co-Cr-Mo alloy than to any ceramic material used in this study.
4. No surface degradation of any of the materials was detected using scanning electron microscopy.

8. References

[1] Ross, G. A., and Smith, L., Cerosium, Symposium on Use of Ceramics in Surgical Implants (Clemson University, 1969).

[2] Helmer, J. D., and Driskell, T. D., Research on Bioceramics, Symposium on Use of Ceramics in Surgical Implants (Clemson University, 1969).

[3] Hentrich, R. L., Graves, G. A., Stein, H. G., and Bajpae, P. K., An evaluation of inert and resorbable ceramics for future clinical orthopedic applications, J. Biomed. Mater. Res. **5**, pp. 25–51 (1971).

[4] Welsh, R. P., and Macnab, Ian., Ceramics in surgery, J. Biomed. Mater. Res. **5**, pp. 231–249 (November 1971).

[5] Davis, S. D., Gibbons, D. F., Martin, R. L., Levitt, S. F., Smith, J., and Harrington, R. W., Biocompatibility of ceramic implants in soft tissue, J. Biomed. Mater. Res. **6**, pp. 425–449 (September 1972).

[6] Hulbert, S. F., Klawitter, J. J., Talbert, C. D., and Fitts, C. T., Materials of construction for artificial bone segments, Research in Dental and Medical Materials, pp. 19–67 (Plenum Press, 1969).

[7] Hulbert, S. F., Morrison, S. J., and Klawitter, J. J., Compatibility of porous ceramics with soft tissue; application to tracheal prostheses, J. Biomed. Mater. Res. Symposium, No. 2, pp. 269–279 (1971).

[8] Hulbert, S. F., Klawitter, J. J., and Leonard, R. B., Compatibility of bioceramics with the physiological environment, Ceramics in Severe Environments—Materials Science Research, **5** (Plenum Publishing Corp., New York, N.Y.)

[9] Rhinelander, R. W., Rouweyha, M., and Milner, J. C., Microvascular and histogenic responses to implantation of a porous ceramic into bone, J. Biomed. Mater. Res. **5**, pp. 81–112 (1971).

[10] Klawitter, J. J., A basic investigation of bone growth into a porous material, Ph.D. Thesis, Clemson University (1970).

[11] Morrison, S. J., Tissue reaction to three ceramics of porous and nonporous structures, M.S. Thesis, Clemson University (1971).

[12] Bowman, L., Characterization of tissue growth into pellets and partial sections of porous ceramics implanted in bone, M.S. Thesis, Clemson University (1971).
[13] Hulbert, S. F., Klawitter, J. J., Sauer, B. W., and Matthews, J. R., Characterization of tissue ingrowth into porous bioceramics, Technical Report No. 2, Office of Naval Research Contract No. N00014-71-A-0339-0001 (May 1972).
[14] Talbert, C. D., A basic investigation into the potential of ceramic materials as permanently implantable skeletal prostheses, M. S. Thesis, Clemson University (1969).
[15] Welsh, R. P., Pilliar, R. M., and Macnab, Ian., Surgical implants, Journal of Bone and Joint Surgery **53-A**, No. 5, pp. 963-977 (July 1971).
[16] Greenlee, T. K., Jr., Beckham, C. A., Crebo, A. R., and Malmorg, J. C., Glass ceramic bone implants, H. Biomed. Mater. Res. **6**, pp. 235-244 (1972).
[17] Hamner, James E., III, Reed, O. M., and Greulich, R. C., Ceramic root implantation in baboons, J. Biomed. Mater. Res. Symposium, No. 3, pp. 1-13 (1972).
[18] Bartels, John C., Dental ceramics, Journal of Prosthetic Dentistry **11**, No 3, pp. 537-551 (1961).
[19] Monroe, E. A., Votava, Ward, Bass, D. B., and McMullen, James, New calcium phosphate ceramic material for bone and tooth implants, Journal of Dental Research **50**, No. 4 (1971).
[20] Benson, J., Elemental carbon as a biomaterial, J. Biomed. Mater. Res. Symposium **5**, No. 2, Part 1, pp. 41-47 (1971).
[21] Hench, L. L., and Paschall, H. A., Direct chemical bond of bioactive glass-ceramic materials to bone and muscle, Symposium on Materials and Design Considerations for the Attachment of Prostheses to the Musculo-Skeletal System, Clemson University (1972).
[22] Klawitter, J. J., and Hulbert, S. F., Application of porous ceramics for attachment of load bearing internal orthopedic appliances, J. Biomed. Mater. Res. **5**, pp. 161-231 (1971).
[23] Peterson, C. D., Miles, J. S., Solomons, C., Predecki, P. K., and Stephen, J. S., Union between bone and implants of open pore ceramic and stainless steel, a histological study, Journal of Bone and Joint Surgery **51-A**, pp. 805 (1969).
[24] Topazian, R. G., Hamner, W. B., Talbert, C. D., and Hulbert, S. F., The use of ceramics in augmentation and replacement of portions of the mandible, J. Biomed. Mater. Res. Symposium, No. 2, pp. 311-332 (1972).
[25] Leonard, R. B., Sauer, B. W., Hulbert, S. F., and Per-Lee, J. H., Use of porous ceramics to obliterate mastoid cavities, Symposium on Materials and Design Considerations for the Attachment of Prostheses to the Musculo-Skeletal System, Clemson University (1972).
[26] Stanitski, C. L., and Mooney, Vert., Osseous attachment to vitreous carbons, Symposium on Materials and Design Considerations for the Attachment of Prostheses to the Musculo-Skeletal System, Clemson University (1972).
[27] Laing, P. G., Ferguson, A. B., and Hodge, E. S., Tissue reaction in rabbit muscle exposed to metallic implants, J. Biomed. Mater. Res. **1**, pp. 135-149 (1967).
[28] Ferguson, A. B., Laing, P. G., and Hodge, E. S., The ionization of metal implants in living tissues, Journal of Bone and Joint Surgery **42-A**, No. 1, pp. 77-90 (January 1960).
[29] Wood, N. K., Kaminski, E. J., and Oglesby, R. J., The significance of implant shape in experimental testing of biological materials: disc vs. rod, J. Biomed. Mater. Res. **4**, pp. 1-12 (1970).
[30] Stinson, N. E., The tissue reaction induced in rats and guinea-pigs by polymethylmethacrylate (acrylic) and stainless steel (18/8/Mo), British Journal of Experimental Pathology **45**, No. 1 (1964).
[31] Cohen, Jonathan, Assay of foreign-body reaction, The Journal of Bone and Joint Surgery **41-A**, No. 1, pp. 152-166 (January 1959).
[32] Brown, D. E., Tissue reaction to plastic and metal implants, Arch Otolaryng. **88**, pp. 283-287 (September 1968).
[33] Fitzpatrick, Barry, A comparative study of some implant materials, Australian Dental Journal **13**, pp. 422-434 (December 1968).
[34] Roydhouse, R. H., Implant testing of polymerizing materials, J. Biomed. Mater. Res. **2**, pp. 265-277 (1968).
[35] Johnsson-Hegyeli, R. I. E., and Hegyeli, A. F., Interaction of blood and tissue cells with foreign surfaces, J. Biomed. Res. **3**, pp. 115-144 (1969).
[36] Johnsson, R. I., and Hegyeli, A. F., Tissue culture techniques for screening of prosthetic materials, Annals of the New York Academy of Sciences **146**, pp. 66-76 (1968).
[37] Homsy, C. A., McDonald, K. E., Akers, W. W., Short, C., and Freeman, B. S., Surgical suture-canine tissue interaction for six common suture types, J. Biomed. Mater. Res. **2**, pp. 215-230 (1968).
[38] Autian, John, Toxicologic aspects of implants, J. Biomed. Mater. Res. **1**, pp. 433-449 (1967).
[39] Rosenbluth, S. A., Weddington, G. R., Guess, W. L., and Autian, J., Tissued culture method for screening toxicity of plastic materials to be used in medical practice, Journal of Pharmaceutical Sciences **54**, No. 1, pp. 156-159 (January 1965).
[40] Homsy, C. A., Ansevin, K. D., O'Brannon, W., Thompson, S. C., Hodge, R., and Estrella, M. E., Rapid in vitro screening of polymers for biocompatibility, J. Macromol. Sci.—Chem. **A4**, No. 3, pp. 615-634 (May 1970).
[41] Cohen, Jonathan, Tissue reactions to metals—the influence of surface finish, The Journal of Bone and Joint Surgery **43-A**, No. 5, pp. 687-699 (July 1961).
[42] Evarts, C. M., Steffee, A. D., and McCormack, L. J., Investigation of canine tissue reaction to TEE-fluorocarbon resin, to high-density polyethylene and to vitallium, Journal of Surgical Research **10**, No. 2, pp. 91-94 (February 1970).
[43] Ludwigson, D. C., Today's prosthetic metals, Journal of Metals **16**, pp. 226-231 (1964).
[44] Hulbert, S. F., Morrison, S. J., and Klawitter, J. J., Problems associated with determining compatibility of biomaterials, Symposium-Workshop on Research Techniques in Biomaterials Evaluation, Clemson University (March 1971).
[45] Richbourg, Henry Leroy, Evaluation of a metal-ceramic composite hip prosthesis, M.S. Thesis, Clemson University (1973).
[46] Laing, P. G., Ferguson, A. B., and Hodge, E. S., Spectrochemical determination of trace metals in normal striated muscle in the rabbit, The Journal of Bone and Joint Surgery **41-A**, No. 4, pp. 737-744 (June 1959).
[47] Ferguson, A. B., Akahoshi, Y., Laing, P. G., and Hodge, E. S., Trace metal ion concentration in the liver, kidney, spleen, and lung of normal rabbits, The Journal of Bone and Joint Surgery **44-A**, No. 2, pp. 317-322 (March 1962).
[48] Hulbert, S. F., Klawitter, J. J., and Richardson, W. C., Jr., Soft tissue response to a dense ceramic and varying surface characteristics, 3rd Annual Meeting of the Biomedical Engineering Society, Baltimore, Maryland (April 7, 1972).
[49] Homsy, Charles A., Stanley, Rufus F., Anderson, M. Sidney, and King, Joe W., Reduction of tissue and bone adhesion to cobalt, alloy fixation appliances, J. Biomed. Mater. Res. **6**, pp. 451-464 (1972).

NATIONAL BUREAU OF STANDARDS SPECIAL PUBLICATION 415,
Biomaterials, Proceedings of a Symposium held in conjunction with the Ninth Annual Meeting of the Association for the Advancement of Medical Instrumentation, New Orleans, La., April 19–20, 1974
(Issued May 1975).

Engineering and Biological Studies of Metallic Implant Materials

Norbert D. Greene, Claude Onkelinx, Leon J. Richelle, and Peter A. Ward

Schools of Engineering, Dental Medicine, Medicine, and the Institute of Materials Science, The University of Connecticut, Storrs, Conn., Box U-136 06268

The aim of this investigation is the development of improved alloys for short term (0.5 to 5 years) orthopaedic implants. The program is interdisciplinary in nature—simultaneous studies of corrosion, inflammatory response, and systemic effects of iron, nickel, cobalt, titanium, and tantalum base alloys are being determined. Corrosion tests under *in vitro* and *in vivo* conditions have been performed via linear polarization and other electrochemical methods.

The inflammatory responses of various implant alloys are being determined by both *in vivo* and *in vitro* experiments. *In vitro* chemotactic assays on rabbit neutrophilic granulocytes and mononuclear cells are performed in the presence and absence of appropriate metal ion concentrations. Corrosion rate data described above are employed to select the proper concentrations.

Systemic effects of metallic corrosion products have been determined via radioisotope and analytical techniques. Radioactive metallic salts at appropriate concentrations are injected intravenously in rats of known age and sex. Following this, the concentration of metallic products is determined as a function of time in various biological samples (plasma, urine, feces, etc). These data permit the establishment of models which can predict the distribution of individual elements released from continuously corroding metal implants.

Keywords: Corrosion; inflammatory response; metallic implants; systemic effects.

1. Introduction

A successful orthopaedic implant must possess sufficient mechanical strength to resist the stresses it encounters in service and it should be compatible with its host environment. A yield strength of 100,000 psi (.07 GPa), tensile strength of 150,000 psi (0.1 GPa) and an elongation of 10 percent probably represent minimal characteristics. High yield and tensile strengths are needed to prevent bending and breaking due to tensile overload and fatigue, while adequate elongation is needed to avoid brittleness. In addition, alloys should be easy to fabricate into complex shapes and consequently, those which can be strengthened by heat treatment after machining hold special interest. To be compatible, an alloy should corrode very slowly when implanted and its corrosion products should not affect adjacent tissue (inflammatory response) and produce no adverse reactions in the rest of the organism (systemic effects). It is especially important that the alloy resists crevice corrosion since many implants are multicomponent devices containing shielded areas.

None of the current implant alloys meet the above requirements. Specifically, Type 316 stainless steel lacks sufficient strength and corrosion resistance, especially crevice corrosion. Cast Vitallium [1] although much more inert and consequently more compatible with adjacent tissue, tends to exhibit brittle behavior. Also, the fact that it can be fabricated only by casting is a limitation. Haynes 25 ("Ductile Vitallium") has the strength of cast Vitallium, together with sufficient ductility to prevent brittleness and to permit fabrication by conventional methods. Its corrosion resistance, although not as good as Vitallium, is superior to stainless steel. Ideally, its strength should be somewhat higher. The actual biological compatibility of this alloy is not known since the manufacturer has not distinguished it from cast Vitallium in his products. Titanium is very corrosion-resistant and may be the least toxic although this has not been confirmed by quantitative clinical tests. Unfortunately, the strength of pure titanium is essentially identical to stainless steel.

Summarizing, all of the presently employed implant alloys are inadequate. Alternate materials are needed since only small improvements can be

[1] Certain commercial materials and instruments may be identified in this publication in order to adequately specify the experimental procedure. In no case does such identification imply recommendation or endorsement by the National Bureau of Standards, nor does it imply that the equipment or instruments identified are necessarily the best available for the purpose.

accomplished with current implant alloys. Cold working is utilized by most manufacturers to increase the yield strength of Type 316 stainless steel, but this is done at the expense of decreasing ductility and it cannot be conveniently applied to all devices. Coating stainless steel implants to improve their corrosion resistance is limited by two factors. First, orthopaedic implant surfaces are subjected to high tensile and abrasive forces. Coating failures would most likely occur at the most critical areas (e.g., at bone plate-screw interfaces). More importantly, even if an ideal coating were applied to stainless steel, it would not alter its basically inferior mechanical properties. Similarly, there is no way to significantly increase the ductility of Vitallium or the strength of titanium. The only approach capable of producing a significant improvement is a modification of alloy composition (i.e., substitution).

Historically, the development of implant alloys has utilized empirical *in vivo* implantation tests. The American Society for Testing and Materials (ASTM) is now standardizing such a test for the purposes of evaluating new implant materials [1].[2] Cylindrical specimens are inserted in the muscles and bones of rabbits, rats and/or dogs and histological examinations made at various intervals up to 104 weeks. However, this test is insufficiently sensitive to detect significant differences between any of the present implant alloys, as shown by the studies of Laing et al. [2]. Current implant materials, in the absence of crevices, corrode so slowly that histologically observable tissue reaction does not occur. Thus, crevice-free samples of present orthopaedic alloys are sufficiently inert to render conventional implantation methods obsolete. The solution to this is the implantation of large numbers of multicomponent appliance samples for extended periods (e.g., 5 years or more). This of course would be prohibitively expensive and time-consuming except for more promising candidate materials. Sensitive, accurate screening techniques for selecting potential alloys are therefore required for future implant alloy development. In the future, as implants remain in place for longer periods, the possibilities of local inflammatory complications and toxic systemic effects become increasingly important.

2. Research Approach

New, improved implant alloys together with rapid, sensitive methods for predicting their *in vivo* performances are urgently needed. Actually, a survey of present commercial alloys shows that many materials with properties superior to these now used for implants already exist. This is especially true of the superalloys—high strength, corrosion resistant alloys developed for jet turbine applications. For example, Elgiloy and MP–35N closely resemble wrought Vitallium on the basis of composition and corrosion resistance. Both possess markedly superior strength characteristics. Elgiloy is used as lead wires in cardiac pacemakers because of its high strength, resistance to fatigue fracture and excellent tissue compatibility. There is little doubt that these alloys could function as improved orthopaedic implants.

Although high yield and tensile strengths together with good ductility are desirable for screws and bone plates, there may be optimum limits for these mechanical properties. There is some evidence to indicate that less ductility is required as tensile and yield strength are increased. Also, it is likely that beyond a certain tensile strength level it is impossible to torsionally fracture bone screws during conventional orthopaedic procedures. If so, then higher mechanical properties could be "traded off" for better corrosion resistance, lower toxicity or other features.

Since there are so many potentially useful implant alloys, selection can be made on the basis of minimum long term inflammatory and systemic effects. To accomplish this, three major coordinated research studies are used in this program. Corrosion measurements are being used to determine the rate of metal solution into adjacent tissue. These data are then utilized to determine inflammatory and systemic effects. Also, optimum mechanical properties for bone screws are being determined by laboratory and *in vivo* experiments. The interactions between these different studies is schematically illustrated in figure 1. The corrosion rates of most current and potential implant alloys are so low that loss of mechanical strength is not an important consideration. Consequently, the corrosion rates of most implanted metals are meaningless, *per se*. Corrosion rate only has biological significance, and this can be described in terms of inflammatory and systemic effects. As noted in the diagram, there is feedback between these two general biological effects and the alloy corrosion rate. These effects are influenced by both the specific metallic elements and their rate of discharge (corrosion rate) under *in vivo* conditions.

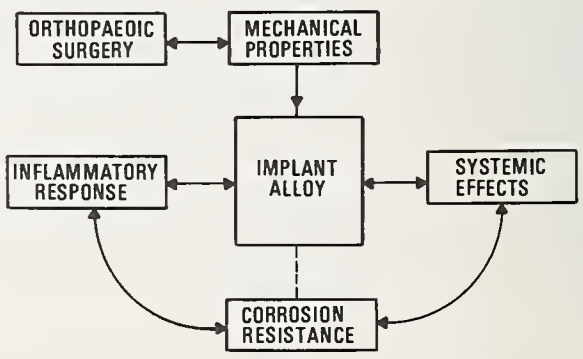

FIGURE 1. *Schematic diagram showing multidisciplinary approach to the selection of new implant alloys.*

[2] Figures in brackets indicate the literature references at the end of this paper.

Although mechanical properties can be used to qualitatively select potentially useful alloys for orthopaedic applications, the optimum properties can only be defined by empirical mechanical tests with actual appliances (e.g., bone screw and plates). Figure 1 illustrates this aspect by showing that mechanical properties can be used to select suitable alloys but the selection process can be improved by feedback dialog between engineers and orthopaedic surgeons. It follows that the selection of new implant alloys requires an interdisciplinary research team, competent in the areas of metallurgy, corrosion, orthopaedic surgery, inflammatory response and systemic effects.

3. Corrosion Studies

3.1. Background

There are two general features important in evaluating the corrosion characteristics of a material. These are the rate and type of corrosive attack. For implant applications, the corrosion rate determines the amount of foreign metal compounds released into surrounding tissues.

To avoid significant local reaction, an implant must corrode at a very slow rate. In general, rates two or three orders of magnitude lower than those commonly employed in conventional industrial practice are necessary [3]. The measurement of such very low rates introduces experimental difficulties since conventional weight loss methods which are usually employed are insufficiently sensitive. Fortunately, electrochemical methods [3–8], particularly linear polarization techniques and charging curve analyses [3], are ideally suited for the measurements of ultra low rates. Briefly, these methods involve the measurement of the potential-current relationships of a corroding specimen near its corrosion potential. Over a potential range of 10 mv or less, there is a linear relationship between voltage and applied current. The slope of this linear region can be used to calculate the instantaneous corrosion rate of a metal or alloy. The accuracy of these techniques have been verified under *in vitro* and *in vivo* conditions. Corrosion rates, especially those of alloys protected by passive films, usually vary with time. Thus, the ability to measure corrosion as a function of time is very valuable in comparing implant performance.

The evaluation of resistance to localized corrosion such as crevice attack can also be accomplished by elcctrochemical techniques. The initiation of crevice attack is readily detected by monitoring the corrosion rate of a sample via linear polarization techniques or charging curve analyses [9]. Also, it has been shown that characteristic changes in the corrosion potential also accompany initiation of localized corrosion [9]. Localized attack, because it is concentrated at isolated points, can be detected by microscopic (light and electron) techniques. Such methods are also very useful for examining specimens after *in vivo* exposure.

3.2. Procedures

Pretreatments of implants, such as sterilization procedures, cause marked changes in the corrosion resistance of a given material under both *in vitro* and *in vivo* environments [8, 10]. Also, the surface finish of an implant (e.g., polished versus grit blasted) has a major influence on corrosion characteristics [11]. Thus, in screening possible implant alloys it is important that they be tested with a representative surface finish after exposure to typical clinical sterilization techniques. Where possible, highly polished surfaces which have been exposed to high temperature steam or dry heat sterilization for long periods have been employed since these conditions yield surfaces with the greatest corrosion resistance [10].

The corrosion rates of various implant alloys are being measured as a function of time using linear and transient linear polarization methods together with charging curve analyses [3]. Also, when applicable, passive current-time measurements [10] are used to monitor corrosion rates. Passive current measurements are simpler than linear polarization techniques and they have the added advantage of permitting continuous monitoring of corrosion rate during the test period. Corrosion rates are monitored for periods ranging between 100 hours and several months depending on the behavior of a particular system. The corrosion rate of most metals decreases exponentially with time [3, 10] in a regular fashion. Therefore, the relative resistances of various materials can be compared on the basis of short time exposures. However, the most promising materials will be subjected to long term tests in both *in vitro* and *in vivo* environments.

Resistance to crevice corrosion can be evaluated with the above electrochemical measurements. Since the corrosion potential must be monitored during linear polarization measurements, potential changes which accompany the initiation of crevice corrosion can be detected. Thus, the experimental procedures used to determine corrosion-time characteristics are also capable of detecting localized attack.

Isotonic saline solutions at average body temperature can be used to qualitatively measure the corrosion rate of implant alloys [8]. Although the absolute value of the corrosion rates measured under these conditions may not correspond to *in vivo* environments, they are sufficiently accurate to determine if a potential alloy has a sufficiently low corrosion rate to be considered for further testing. The most promising materials will be subjected to *in vivo* tests utilizing specially modified electrochemical apparatus and procedures [4, 8]. Rats, rabbits, dogs, and monkeys will be employed. Of special interest are comparisons of different *in vivo*

environments. Previous studies [8] suggest that they are very similar, but additional data are needed.

3.3. Results

Since crevice corrosion is the most common form of corrosion damage observed on surgical implants, we have devoted special attention to this aspect of the program. A new technique for quantitatively evaluating the crevice corrosion susceptibility of alloys has been developed [11] and is presently being refined further. The method employs a paper covered metal sample immersed in a suitable electrolyte. The presence of the paper simulates the restrictive convection conditions within a crevice without the resistance drop ("IR") errors normally associated with shielded areas. Crevice corrosion susceptibility is directly related to the change in dissolution currents observed in the presence of a paper substrate.

Figure 2 illustrates the construction of the paper shielded electrode used in these measurements, and figure 3 shows the effect of paper shielding on Type 304 stainless steel—a material which is very susceptible to crevice attack. Photographic paper with its gelatin coating provides a very effective convective diffusion barrier and its influence on alloy dissolution rate is very pronounced. Titanium, which is almost completely resistant to crevice attack, shows the opposite effect—paper shielding decreases dissolution current (fig. 4). This decrease in current is probably due to the increase in pH caused by the accumulation of sulfate ions. Additional metals and alloys are now being compared using this procedure in several different electrolytes.

Passive currents versus time are being determined in isotonic saline at 37 °C using newly developed mini potentiostats [12]. These devices, based on solid state operational amplifiers, are ideally suited for multiple, long time measurements because of

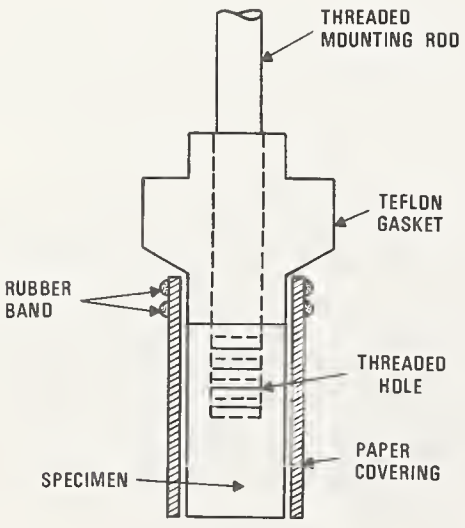

FIGURE 2. *Construction of paper-shielded electrode used to measure crevice corrosion susceptibility.*

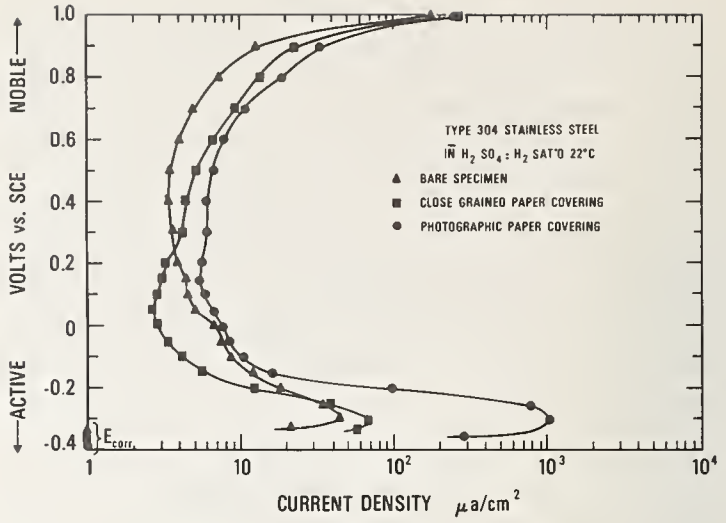

FIGURE 3. *Polarization curves of Type 304 stainless steel in sulfuric acid solution.*

Increased current density in the active region for the specimen covered with photographic paper illustrates the tendency for crevice corrosion.

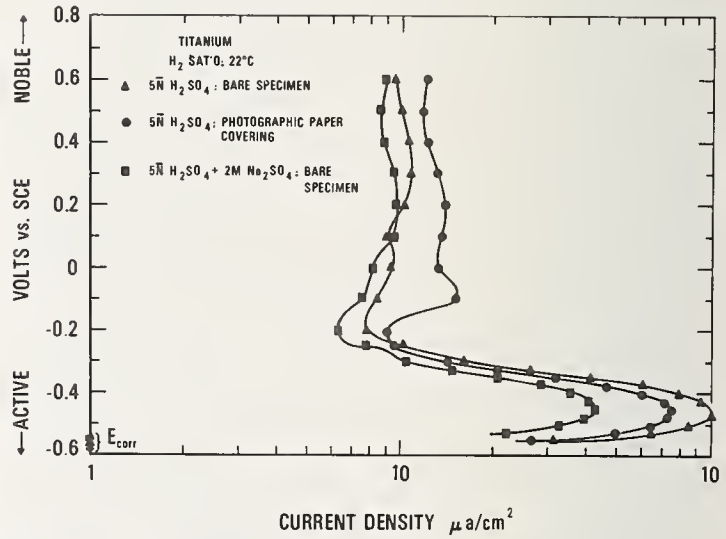

FIGURE 4. *Polarization curves of titanium in sulfuric acid solution.*

No sensitivity to crevice attack in the active region is indicated.

their simplicity and low cost. These potentiostats together with specially designed polarization cells and a shielded wiring system are being used to collect passive current-time data. MP35N alloy possesses passive corrosion characteristics similar to wrought Vitallium (HS–2 alloy). This together with its outstanding mechanical properties indicates potential usefulness as an implant alloy. However, the recent systemic kinetic analyses of nickel distribution (see below) suggest that although nickel base alloys such as MP35N may appear promising, their use should be approached with caution because of possible toxic and carcinogenic effects.

4. Inflammatory Response

4.1. Background

The inflammatory response is, by definition, the reaction of the body to injury. In this context, the most important consideration is the change in the functional behavior of blood vessels, the acute inflammatory response being characterized by an increased vascular permeability with a leakage of fluids into extravascular sites. At the same time that salts, water and proteins begin to leak from blood vessels, a concomitant but independent accumulation of leukocytes (neutrophils or neutrophilic granulocytes) occurs. It seems clear that the localization of neutrophils at a site outside blood vessels is primarily a defensive reaction, since these cells avidly ingest and kill bacteria, providing an important defensive function. This is particularly relevant if there has been a break in the integument, such as a laceration or abrasion in the skin. The inflammatory response then progresses, in the case of wound healing, to the subacute stage at which point collagen is rapidly formed by fibroblasts and a scar is produced. We are primarily concerned at this point with the acute inflammatory response.

Although it is usually beneficial, in some situations the acute inflammatory response goes out of control. The clinical results may be rheumatoid arthritis or glomerulonephritis. One of the ways in which these complications may occur is by the overproduction or the inappropriate production of factors that cause the accumulation of leukocytes.

Why the excessive accumulation of leukocytes at a site outside blood vessels should be deleterious to the tissue is explained by the fact that these cells contain a battery of proteolytic enzymes, and it has been demonstrated that elastin, collagen, basement membrane, and other structural proteins of tissues are suitable targets. Thus, in glomerulonephritis there is actual evidence of basement membrane degradation. In the vascular lesions of serum sickness we find evidence for dissolution of elastic fibers. In such situations where neutrophilic granulocytes appear, it is readily apparent that unless the inflammatory response is carefully controlled, tissue injury may result.

The above discussion points out the proinflammatory effects of chemotactic agents [13–16]. If a compound impairs chemotactic responsiveness, it will have anti-inflammatory effects by preventing the delivery of cells to extravascular sites. This is the way in which several of the potent anti-inflammatory drugs have their effect. Drugs showing antichemotactic effects include corticosteroids, derivatives of various quinolines, and other agents that by clinical evaluation have been shown to be effective anti-inflammatory agents [17]. The significance of knowing a material has chemosuppressive effects on leukocytes, aside from the obvious clinical application, lies in the fact that such agents may render an area of tissue susceptible to invasion by micro-organisms. It seems possible that corrosion products from implanted metals may affect leukocyte migration either positively or negatively as described above.

The possibility that corrosion products from metallic prosthetic devices may suppress the chemotactic responsiveness of leukocytes is of great interest, since in wound healing the arrival (by chemotactic means) of neutrophils, assuming excessive numbers are not delivered, provides the area with a protective shield of phagocytes, whose duty is to ingest and enzymatically degrade bacteria. If, for any reason, inadequate numbers of neutrophils fail to arrive in the vicinity of a surgical wound, serious trouble may develop in the form of a wound infection. The development of this complication in patients receiving metallic implants almost always dictates removal of the prosthesis. The finding of antichemotactic activity in any of the metal salts that represent corrosion products of metallic prosthetic devices is therefore of great clinical significance and it is this part of the program, based on preliminary data, that is described below.

Recent advances in the understanding of agents that affect leukocyte migration have broadened our concepts regarding the control of inflammatory responses [13–16]. For instance, it is now recognized that several of the complement proteins of plasma (and extracellular fluids) are substrates of endogenous enzymes (tissue proteases, plasmin and enzymes derived from the complement sequence), the products of which are the chemotactic factors for leukocytes. The generation of any one of these factors will set the stage for leukocyte accumulation, a hallmark of the inflammatory response. Other agents such as bacterial products are directly chemotactic for leukocytes and require no other proteins for the expression of their biological activity, [18]. If this happens in the context of bone or soft tissues, the outcome will be an inflammatory response that may be inimical to the affected tissue. Conversely, agents that suppress the chemotactic responsiveness of leukocytes are potentially anti-inflammatory agents.

4.2. Procedures

In vitro chemotactic assays on rabbit neutrophilic granulocytes and mononuclear cells have been carried out using modified Boyden chambers [19] that employ micropore filters [20]. In this assay, the leukocyte suspension is placed on one side of the filter, the chemotactic factor on the other side. After a 3–5 hour period of incubation at 37 °C, the chambers are disassembled and the filters fixed, stained, dehydrated and cleared in xylene, then mounted on a glass slide. By conventional light microscopy the number of cells that have migrated in five high power fields (selected at random) is determined. This reflects the chemotactic activity

of the material added to the compartment opposite that containing the leukocyte suspension.

The cells used in this bioassay are rabbit peritoneal cells, the neutrophils collected from exudates 4 hours after the installation of 0.1 percent glycogen in saline into the peritoneal cavity, the mononuclear cells collected 3–4 days after the intraperitoneal injection of mineral oil [20, 21]. For the neutrophil system, micropore filters with pore size 0.65 micrometer are used, while the mononuclear cell system involves the use of filters with 5 micrometer pore size[20, 21].

The following protocol is used for evaluation of a metal compound:

(a) Intrinsic chemotactic activity—test material by itself in medium 199 (see below) is added to the lower compartment (opposite the cell suspension).

(b) Effects on cell function—test material is added to upper compartment containing cell suspension. If the material suppresses chemotactic function, the dose that causes 50 percent inhibition is determined.

(c) Effects of metallic derivates on the chemotactic factor—metal salt is added to the lower compartment containing the chemotactic factor. Of interest are those elements contained in potentially promising alloys. These include chromium, cobalt, molybdenum, nickel, tintalum, tatanium, and tungsten. These are added in the form of an appropriate compound (e.g. chloride).

In all of these studies the chemotactic factor to be employed is the soluble, low molecular weight factor produced by *E. coli* grown in a simple, defined, protein free culture medium (medium 199). If any of the metal derivatives are found to depress chemotactic function of granulocytes, the complement-derived chemotactic factors C3a, C5a, and C567 [22, 23] will also be tested to determine if the suppressive effect is specific for a given chemotactic factor or if it affects a variety of chemotactic factors.

4.3. Results

The data in tables 1 through 3 provide preliminary evidence for the effects of metal salts on chemotactic activity of neutrophilic leukocytes. The findings can be summarized by the following statements: (1) Several of the metal salts have a pronounced antichemotactic effect. None of those studied have a prochemotactic effect. (2) Not all salts are antichemotactic. (3) The mechanism by which the salts exert an antichemotactic function seems to be by a direct, and in some cases irreversible, effect on the leukocytes rather than on the chemotactic factor *per se*.

In table 1 a series of metal salts at varying concentrations have been mixed with the neutrophils obtained from glycogen-induced peritoneal exudates of rabbits. The cell suspensions containing the salts were then placed in the test chamber and a standard chemotactic factor a culture filtrate of the bacterium (*E. coli*) deposited on the opposite side of the filter. Numbers of cells responding chemotactically to the bacterial factor were determined by the standard method. By extrapolation, the dose of metal salt causing 50 percent inhibition of cell migration was determined. The gold salt was the most antichemotactic agent found, inhibiting 50 percent of the cell responsiveness at a concentration of 2.3×10^{-4}M.

TABLE 1. *Inhibitory effects of various metal salts on chemotactic function of neutrophils*

Salt tested	Concentration (M) giving 50% inhibition of chemotaxis
$HAuCl_4 \cdot 3H_2O$	2.3×10^{-4}
$RhCl_3$	3×10^{-4}
$CuCl_2 \cdot 2H_2O$	3×10^{-4}
$CrCl_3 \cdot 6H_2O$	3×10^{-4}
$MnCl_2 \cdot 4H_2O$	5×10^{-4}
$AlCl_3 \cdot 6H_2O$	10^{-3}
$CuCl$	10^{-3}
$FeCl_2 \cdot 4H_2O$	10^{-3}
$FeCl_3 \cdot 6H_2O$	10^{-3}
WO_3	$> 10^{-3}$
$ZnCl_2$	
MoO_3	
$CoCl_2 \cdot 6H_2O$	
$NiCl_2 \cdot H_2O$	

TABLE 2. *Direct inhibitory effect of metal salts on neutrophil chemotactic function*

Salt tested	Inhibition of chemotactic response[a], Percent	
	Salt mixed with factors	Salt mixed with cells
$HAuCl_4 \cdot 3H_2O$	86	100
$RhCl_3$	41	71
$CuCl_2 \cdot 2H_2O$	52	32
$CrCl_3 \cdot 6H_2O$	5	22
$MnCl_2 \cdot 4H_2O$	5	80

[a]Salts added to cell suspension or to chemotactic factor in a concentration of 5×10^{-4}M.

It is interesting to note that gold salts have been used for years to treat patients with rheumatoid arthritis. The mechanism for this action has never been explained. It is quite possible that the antichemotactic, and the anti-inflammatory, effect of gold salts shown in table 1 is the basis for this clinical effect.

As described in table 1, several other metal salts also have an antichemotactic effect, whereas the last five in the list have no demonstrable effect on chemotaxis in doses as high as 10^{-3}M.

In table 2 salts (at 5×10^{-4}M) have been mixed either with leukocytes or with the chemotactic (Bacterial) factor in the chemotaxis chamber and the resulting chemotactic response of the cells assessed. Five different salts were tested, each of which was previously determined to have an anti-

chemotactic effect (table 1). As shown in four of the five cases (cupric chloride excepted) the metal salts had an accentuated effect if mixed with the cell suspension, in contrast to their effects when mixed with the chemotactic factor. These findings indicate that in most cases the antichemotactic effect of the metal salts is the result of a direct action on the cells.

These findings were further explored (table 3) where washing experiments were done. Briefly, cells were treated with various metal salts and then one-half of each suspension was diluted, centrifuged, and the cells suspended in culture medium lacking the particular metal salt. It is evident that in several cases, particularly with the gold and the manganese salts, that substantial inhibitory effects persisted when the salts were removed. These data indicate that in some instances the inhibitory effect on chemotactic responsiveness of leukocytes is irreversible whereas in other cases this is not the case. The data confirm those in table 3 and indicate that the inhibitory effect of the salt is the result of a direct action on the cells.

TABLE 3. *Irreversible inhibitory effect of metal salts on neutrophil chemotactic function*

Salt used[a]	Inhibition of chemotactic response, Percent	
	Cells washed	Cells not washed
$HAuCl_4 \cdot H_2O$	100	100
$RhCl_3$	20	90
$CuCl_2 \cdot 2H_2O$	15	100
$CrCl_3 \cdot 6H_2O$	46	50
$MnCl_4 \cdot 4H_2O$	75	100

[a]At a concentration of 5×10^{-4}M.

5. Systemic Effects

5.1. Background

The study of the systemic effects of any foreign molecules introduced into the body has two fundamental aspects. The first component of such a study attempts to determine the amount of the active form of the molecule which is present, at any given time, in various parts of the body. The second component of the study deals with the interactions between the active form of the molecule and some receptor sites. In general, such interaction will modify one or more physiological or biochemical phenomena, thus leading possibly to the development of a pathological condition.

It is clear that when metallic elements are released into the body by the corrosion of implanted materials, their distribution in time and space is an essential step before conducting any logical study of their potential toxicity. In discussing the limitations of current techniques for the evaluation of new biomaterials, Hegyeli [24] insists on "the lack of willingness to select, adapt and actually conduct objective tests of high predictive value for human patient response". She also suggests that "any implanted device should be considered as a potentially hazardous bulk pharmaceutical." For the study of systemic side effects she notes the shortcomings of *in vitro* methods that result from the fact that physiological conditions in the body are not adequately duplicated. Moreover, some *in vitro* conditions such as gas atmosphere, acidity, evaporation, temperature, etc. are not always controlled as they are *in vivo*. These parameters influence the interactions between implants and the biological environment. In the past, experiments have been carried out to study the distribution of trace elements in the body. For instance, A. B. Ferguson et al. [25, 26] measured the trace metal ion concentrations in various organs of the rabbit. Using those data as a baseline, they were then able to investigate the release of trace ions from embedded metal implants and their subsequent uptake by various organs. These tedious experiments (6 to 16 weeks) did not allow establishing in detail how these ions are distributed in the body. Differences were noted from animal to animal, between various metals, etc. Some organs, like spleen and liver, appeared to pick up more material than other tissues. Sunderman [27] has produced a bibliography that describes how a variety of elements (beryllium, cadmium, chromium, cobalt, iron, lead, nickel, selenium, zinc) find their way into various organs when administered via different routes (dietary, intramuscular, subcutaneous, intravenous, intraperitoneal, etc.). Though these papers are specifically oriented towards carcinogenicity, their content clearly indicates that the systematic approach that we employ for studying the distribution of trace elements released by metallic implants, would provide much needed information.

In toxicology and pharmacology, kinetic analysis [28] is, by now, a classical method to study "drug transference." This term refers to all the phenomena which result in a given drug or molecule being transported between various points in the organism or being transformed from one chemical form into another. Both classes of phenomena are grouped in one general category—transference—because the mathematical analysis of these phenomena is based on a number of common concepts proper to kinetic analysis [29]. Such methods have been used to study the metabolism of calcium, an element normally present in the body, and radioactive strontium, a fallout product resulting from the explosion of nuclear devices [30–33].

The specific aims of this part of the program are:

1. Establish the distribution throughout the body of trace elements released by implanted biomaterials by making use of appropriate kinetic models. Single intravenous injections of radioactive isotopes will be used for this purpose.

2. Predict, using these kinetic models, the time course of the concentration of elements in various parts of the body, when they are released from implants, taking into account the *in vivo* rate of corrosion as determined by the studies described above.
3. Analyze, chemically and radiochemically, those organs and tissues which appeared to retain potentially toxic amounts of the elements for sufficiently long periods of time, after *in vivo* implantation of biomaterials.
4. Study possible interactions between the elements retained in toxic amounts and biological receptor sites in order to determine the precise nature of any pathological process.

5.2. Procedures

The rationale of the methodology is apparent from the above list of specific aims. In a first step, rats of known age and sex are injected intravenously a single dose of a radioactive tracer of the element under study. By sampling blood at regular intervals, the rate at which the serum loses the injected dose is determined. Over the same time period, urine and feces are collected. If most of the loss is found in urine, feces, or both, then the kidneys and/or liver will be considered as likely target organs. If the difference between what is lost from the blood and what is found in both urine and feces is considerable, the skeleton is then sampled and analyzed, since it acts as a sink for many metals.

Once a model is established, it can be used to predict the distribution of the element when, instead of a single intravenous injection, the element is continuously released, at a known rate, by the corrosion of the implanted material. It is also possible to check these predictions, either by continuous perfusion of animals (acute experiments), or by implanting samples of the material containing a radioactive isotope of the element under study (chronic experiments).

6. Results

Nickel was the first metal chosen for study in terms of whole body kinetics. The reasons for this choice were as follows: (a) nickel is a major component of many alloys used in implants; (b) corrosion characteristics of nickel containing alloys have been determined both *in vivo* and *in vitro*, [8, 10]; (c) its potential toxicity is well established particularly in relation to carcinogenesis [35, 36].

Rabbit data were kindly made available to us by Dr. Sunderman (Department of Laboratory Medicine, Health Center, University of Connecticut). The experiments were conducted as follows: 18 albino rabbits were administered radioactive nickel chloride ($^{63}NiCl_2$) in a single intravenous injection of 0.24 mg Ni/kg body weight (equivalent 1.43 mCi/kg). At intervals ranging from 1 hour to 7 days after the injection, blood samples were collected and the concentration of radioactive nickel in the serum was determined. The animals were kept in metabolism cages in order to collect urine in which radioactive nickel was subsequently measured. Similar measurements were also performed in the bile collected from two animals under anesthesia.

The results indicate that nickel is rapidly cleared from the plasma during the first two days after an intravenous injection, but disappears at a much slower rate from 3 to 7 days (fig. 5). An average of 78 percent of the administered ^{63}Ni (i.e. 0.187 μg/kg of rabbit) was recovered in urine during the first 24 hours after the injection. The biliary excretion was estimated at approximately 9 percent (4.6 μg/kg body weight) of the administered dose. No data were available for the net elimination of ^{63}Ni in the feces.

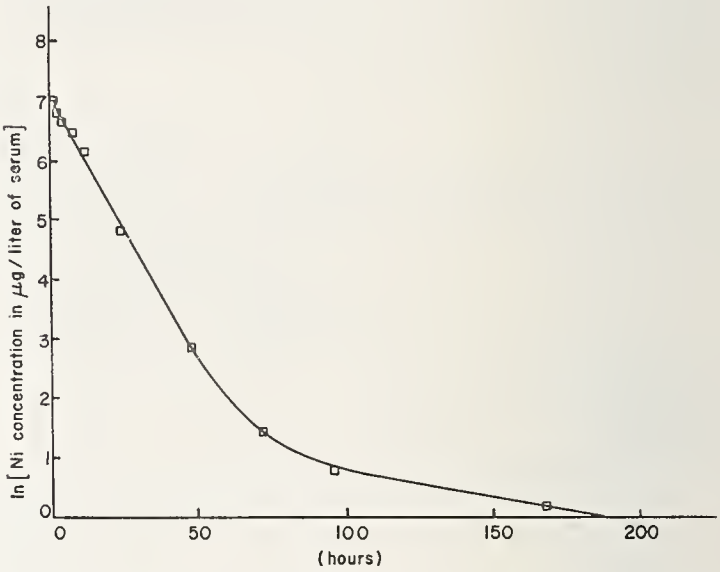

FIGURE 5. *Time-course of* $^{63}Ni(II)$ *concentrations in serum of rabbits following a single i.v. injection of* $^{63}NiCl_2$. *(Each point represents the mean of measurements in at least 3 rabbits.)*

Experiments with rats were conducted as follows. Female Wistar rats, 10 weeks of age, were administered 100 μCi of ^{63}Ni (II) in a single intravenous injection. The injection was performed under ether anesthesia into the left subclavial vein. Immediately thereafter, the animals were placed in metabolism cages in order to collect feces and urine separately. Blood samples were withdrawn from the tip of the tail with the help of capillary tubes at a series of time intervals between 2 hours and 8 days after the injection. Plasma was separated by centrifugation and weighed before radioactive nickel determination. Feces and urine were collected separately for a period of 3 days starting at injection time. They were dried in crucibles then ashed in a muffle furnace (24 hours at 300 °C, followed by 24 hours at 600 °C). The ash was dissolved in 6 N HCl over a hot plate and the solution transferred into a 500

ml volumetric flask. While bringing the solution to volume, the pH was adjusted to 3 with NaOH. Radioactive nickel was measured in all the samples with a TRI–CARB Packard scintillation counter (scintillating mixture: Aquasol, New England Nuclear Co.). The count rate was corrected for quenching using an internal standard.

As was the case with the rabbit, the concentration of ^{63}Ni in the plasma decreased very rapidly during the first 2 days after the injection (fig. 6). Thereafter the decrease took place at a much slower rate. After 5 days, most of the radioactive nickel had been eliminated in the urine and to a lesser extent in the feces.

As demonstrated in figure 5 for the rabbit, and in figure 6 for the rat, the disappearance curve of ^{63}Ni (II) from the plasma can be approximated very closely by a sum of two exponential terms:

$$S = A_1 e^{-a_1 t} + A_2 e^{-a_2 t} \qquad (1)$$

in which S stands for the concentration of nickel in the plasma (in μg/liter) and t is time measured from the time of injection (hours).

This fact strongly suggests that nickel dilutes

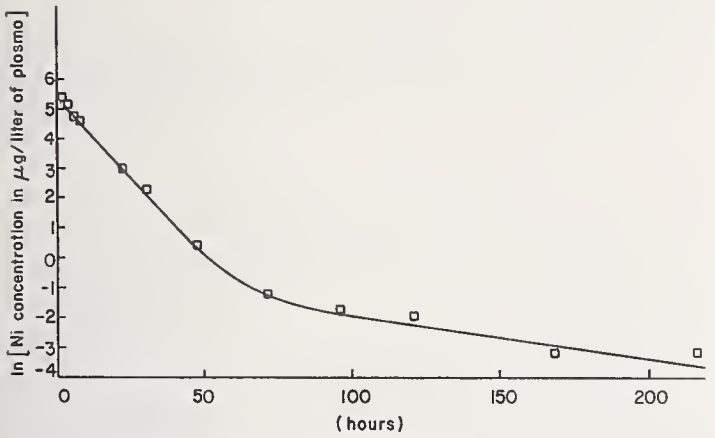

FIGURE 6. *Time-course of* ^{63}Ni(II) *concentrations in plasma of rats following a single i.v. injection of* $^{63}NiCl_2$. *(Each point represents the mean of measurements in at least 15 rats.)*

itself within a distribution volume made up of two compartments and is eliminated from at least one compartment according to first order kinetics (within the range of concentrations observed in these experiments). Compartment I, which includes the plasma is the central compartment in which ^{63}Ni (II) is injected at time $t=0$ and from which elimination takes place. Compartment II represents a hypothetical volume related to the first compartment by an exchange process. We assume that at time $t=0$, ^{63}Ni (II) is rapidly and uniformly distributed within the first compartment.

In the rabbit experiment, the time course of ^{63}Ni (II) concentration in the plasma is very well approximated by the following equation:

$$S = 1165\ e^{-0.0925t} + 4.94\ e^{-0.0084t} \qquad (2)$$

(units: μg/liter; amount injected: 0.24 mg/kg body weight)

whereas in the rat experiment the following equation was determined:

$$S = 226.3\ e^{-0.1103t} + 0.572\ e^{-0.014t} \qquad (3)$$

(units: μg/liter; amount injected: 17.0 μg per animal)

These equations were obtained by fitting expression (1) to the average values of nickel concentration in plasma as a function of time for each group of animals. The degree of fit is demonstrated in figures 5 and 6.

A mathematical analysis of the two-compartment model, based upon the data reported above, can be worked out in terms of differential equations. This allows a complete quantitation of nickel kinetics in the body. In particular, the distribution volume of each compartment as well as the clearances of nickel exchange and excretion can be evaluated.

Furthermore, once the parameters of the model are known, it is possible to predict the time-course of nickel concentration in both compartments when nickel is continuously released into the plasma at a constant rate. From what is known about nickel corrosion, one can estimate that in humans who have implants made of a nickel-containing alloy, the rate of nickel release from the device can range between 5 and 500 mg/year per individual. This corresponds approximately to a range of 0.81–0.0081 μg/h per kg of body weight on the basis of an average body weight of 70 kg for humans. The following table gives the estimated steady state values of nickel concentration in plasma resulting from 3 different input rates within that range.

Infusion rate μg/h per kg of body weight	Steady state Ni concentration μg/liter	
	Rabbit	Rat
0.81	45	19.9
0.081	4.5	1.99
0.0081	0.45	0.20

These figures have to be compared with the normal range of nickel concentration in human plasma. In a recent paper, McNeely et al. [38] reported a value of 2.6 μg/liter ($\pm$0.08) for a presumably normal population sampled from the area of Hartford (Conn.), while in Sudsbury, Ontario, the site of the largest open-pit nickel mines in North America, the plasma level was 4.6 μg/liter ($\pm$1.4). It is quite

clear from the table that an implant can constitute a continuous source of nickel resulting in far higher plasma levels that those due to the heaviest atmospheric pollution.

Although there is no direct evidence as yet that these high levels of plasma nickel are necessarily toxic, one should certainly exercise caution with regard to the potential hazards associated with its use in implants. Indeed our results reinforce the opinion voice by Hueper [35] according to which "the evidence on hand indicates that metal implants which contain nickel and which remain over long periods in human tissues might create delayed potential cancer hazards to their recipients."

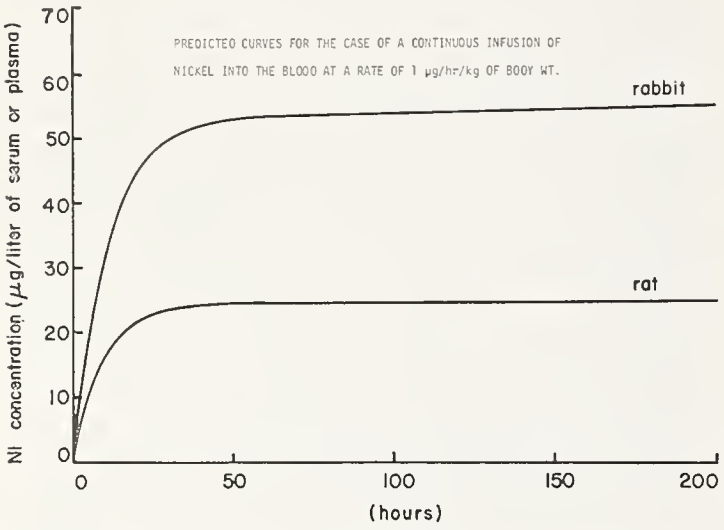

FIGURE 7. *Computer-plotted curves for the predicted concentrations of* ^{63}Ni(II) *in plasma or serum of rats and rabbits, assuming a continuous i.v. infusion of* $^{63}NiCl_2$ *at a rate of 1 μg* Ni/*kgh.*

We can add finally that the steady state under a continuous input is reached very quickly, as illustrated in figure 7 which pictures the transient curve from the time at which the continuous infusion is started. As can be seen from the figures, it takes about 7–8 hours to achieve a plasma concentration half the maximum value.

This research is supported by the National Science Foundation and the Institute of Materials Science, University of Connecticut.

7. References

[1] Recommended Practice for Experimental Testing for Biological Compatibility of Metals for Surgical Implants, ASTM Committee F–4 on Surgical Implants, ASTM, Philadelphia, Pa.
[2] Laing, P. G., Ferguson, A. B., Jr., and Hodge, E. S., J. Biomed. Mat. Res. **1**, 135 (1967).
[3] Jones, D. A., and Greene, N. D., Corrosion **22**, 198 (1966).
[4] Colangelo, V. J., Greene, N. D., Kettelkamp, D. B., Axelander, H., and Campbell, C. J., J. Biomed. Mater. Res. **1**, 405 (1967).
[5] Skold, R. V., and Larson, T. E., Corrosion **13**, 139t (1957).
[6] Stern, M., Corrosion **14**, 440t (1958).
[7] Stern, M., and Weisert, E. D., Proc. ASTM **59**, 1280 (1959).
[8] Revie, R. W., and Greene, N. D., J. Biomed. Mater. Res. **3**, 465 (1969).
[9] Jones, D. A., and Greene, N. D., Corrosion **25**, 367 (1969).
[10] Revie, R. W., and Greene, N. D., Corr. Sci. **9**, 755, 763 (1969).
[11] Picard, R. J., and Greene, N. D., Electrochemical Reactions at Paper Shielded Metal Surfaces to be published.
[12] Greene, N. D., Moebus, G. A., and Baldwin, M. H., The Mini Potentiostat: A Versatile Power Source for Electrochemical Studies, accepted publication in Corrosion.
[13] Keller, H. O., and Sorkin, E., Separatum Experientia **24**, 641 (1968).
[14] Mergenhagen, S. E., Snyderman, R., Gewurz, H., and Shin, H. S., Significance of complement to the mechanism of action of endotoxin, Current Topics in Microbiology and Immunology **50**, 37 (1969).
[15] Tempel, T. R., Synderman, R., Jordan, H., and Mergenhagen, S. E., J. Periodont. **41**, 71 (1970).
[16] Ward, P. A., Arth. & Rheum. **13**, 181 (1970).
[17] Ward, P. A., J. Exp. Med. **124**, 209 (1966).
[18] Ward, P. A., Lepow, I. H., and Newman, L. J., Am. J. Path. **52**, 725 (1968).
[19] Boyden, S., J. Exp. Med. **115**, 453 (1962).
[20] Ward, P. A., Cochrane, C. G., and Muller-Eberhard, H. J., J. Exp. Med. **122**, 327 (1965).
[21] Ward, P. A., J. Exp. Med. **128**, 1201 (1968).
[22] Shin, H. S., Snyderman, R., Friedman, E., Mellors, A., and Mayer, M. M., Science **162**, 361 (1968).
[23] Taubman, S. B., Goldschmidt, P. R., and Lepow, I. H., Fed. Proc. **29**, 434 (1970).
[24] Hegyeli, R. J., Limitations of Current Techniques for the Evaluation of Biohazards and Biocompatibility of New Candidate Materials, Medical Applications of Plastics, H. P. Gregor, Ed. (Wiley, New York, N.Y., 1971) pp. 1–14.
[25] Ferguson, A. B., Akahoshi, Y., Laing, P. G. Hodge, E. S., J. Bone and Joint Surg. **44–A**, 317 (1962).
[26] Ferguson, A. B., Akahoshi, Y., Laing, P. G., Hodge E. S., J. Bone and Joint Surg. **44–A**, 323 (1962).
[27] Sunderman, F. W., Jr., Food and Cosmetics Toxicology **9**, 105 (1971).
[28] Ariens, E. J., Molecular Pharmacology (Academic Press, New York, N.Y., 1964).
[29] Riggs, D. S., The Mathematical Approach to Physiological Problems, (Williams and Wilkins, Baltimore, 1963).
[30] Berman, M., and Weiss, M. F., Users Manual for SAAM, Publication No. 1703, U.S. Public Health Service.
[31] Aubert, J. P., Bronner, F., Richelle, L. J., J. Clin. Invest. **42**, 885 (1963).
[32] Bronner, F., Aubert, J. P., Richelle, L. J., Saville, P. D., Nicholas, J. A., Cobb, J. R., J. Clin. Invest. **42**, 1095 (1963).
[33] Richelle, L. J., Bronner, F., in Proc. First Europ. Symp. Calcif, Tissues, H. J. J. Blackwood, Ed. (Pergamon Press, London, 1964).
[34] Moore, C. V., Dubach, R., in Mineral, Metabolism, and Advanced Treatise, Vol. 3, C. Comar, F. Bronner, eds. (Academic Press, New York, N.Y. 1963).
[35] Heuper, W. E., Carcinogenic hazards from arsenic and metal containing drugs, Potential Carcinogenic Hazards from Drugs, R. Truhart, Ed., (Springer-Verlag, Berlin, 1967), pp. 79–104.
[36] Sunderman, F. W., Jr., The current status of nickel carcinogenesis, Am. Clin. Lab. Sci. (in press).
[37] Van Soestberger, M., and Sunderman, F. W., Jr. ^{63}Ni-complexes in serum and urine after injection of $^{63}NiCl_2$ (in press).
[38] McNeely, M. D., Nechay, M. W., and Sunderman, F. W., Jr., Clinical Chemistry **18**, 992 (1972).

NATIONAL BUREAU OF STANDARDS SPECIAL PUBLICATION 415,
Biomaterials, Proceedings of a Symposium held in conjunction with the Ninth Annual Meeting of the Association for the Advancement of Medical Instrumentation, New Orleans, La., April 19–20, 1974
(Issued May 1975).

Materials Characterization of Implantable Porous Electrodes

R. B. Beard, J. F. DeRosa, S. F. Dubin, L. Sturm, and R. M. Koerner

Drexel University, Philadelphia, Pa. 19104

and

A. Miller

Temple University, School of Dentistry, Philadelphia, Pa. 19122

Porous platinum and palladium black electrodes have been used as cathodes for reducing body oxygen in implantable hybrid cells supplying energy to pacemakers. The power-generating capabilities of a cell are greatly decreased under load, i.e., increased current density, due to polarization at the electrode interface. A greatly increased surface area of the porous electrodes, i.e., number of sites for the electrode reaction, permits a greater current density with lower overpotential or polarization. Similarly, at the pacemaker stimulating electrode and at electrodes used in making electrical impedance measurements there is polarization and a consequent loss of energy in a charge transfer at the electrode interface. Porous electrodes in these cases have also greatly reduced the overpotential. The physical electrochemical properties of the porous electrodes have been characterized by specific adsorption, i.e., BET measurements; scanning electromicrographs; galvanostatic and potentiostatic measurements; and electrical impedance measurements. Histopathological studies have been made in order to determine the biocompatibility of the tissue-electrode interface.

Key words: Implantable hybrid cells; pacemakers; palladium black; platinum black; polarization; porous electrodes.

1. Introduction

Implantable hybrid cells consisting of catalytic cathodes where dissolved oxygen is reduced and sacrificial anodes are galvanically oxidized are capable of powering pacemakers [1–10], [1] carotid-sinus, bladder and electrophrenic stimulators [11]. The implantable hybrid cell has a long shelf life, costs no more than conventional batteries and has a potential for lasting 10 years or longer. The power generating capabilities of the hybrid cell depend upon the cathode electrode potential and current drain. Under zero current drain the electrodes in the body develop an open circuit voltage. When current is drawn through the load, the electrode potential decreases from its open circuit value due to the overpotential developed at the electrode. Higher power outputs are produced by electrodes which can maintain higher potentials for given current drains. *In-vivo* and *in-vitro* studies have demonstrated that the power of the cell is decreased due to the overpotential at the catalytic cathode. There is sufficient oxygen available in the subcutaneous tissue according to Roy et al. [12], to depolarize for current loads in excess of 200 μA which will produce sufficient power to drive pacemakers. At Drexel, implanted hybrid cells powering commercial pacemakers pacing dogs use porous cathodes which have operated with current loads of 610 μA or 25 μA/cm [12, 13].

In-vivo and *in-vitro* studies on platinum and palladium black cathodes consisting of hydrophobic binders of teflon and hydrophilic binders of polyvinyl chloride and silicone rubber have demonstrated considerable overpotential with a resulting power loss [8, 13].

In order to increase the number of available sites for reducing the oxygen and to obtain a more biologically compatible interface [14], platinum and palladium porous cathodes were fabricated using the techniques of powder metallurgy [15, 16]. The polarization or overpotential at the various types of cathodes has been studied using the galvanostatic technique. *In-vivo* studies have been made implanting the electrodes under load subcutaneously in the lateral abdomen and thorax of dogs. Material and biological compatibility characterization studies have been made on the various types of cathodes. The surface areas of the palladium and platinum powders and compacts have been determined using the Brunauer-Emmett-Teller (BET) gas adsorption technique and the scanning electron microscope. The compatibility of the electrodes have been determined by histopathologic evaluation of the

[1] Figures in brackets indicate the literature reference at end of this paper.

tissues surrounding the porous metal implants [15, 16].

Besides the problem of decreasing the electrode polarization (i.e., overpotential) of the power source, there is also the problem of a significant waste of stimulation energy at the cardiac pacemaker electrode surface due to polarization [17, 18, 19, 20]. A decrease in the electrode surface increases the current density, lowering the threshold voltage for stimulation, but increasing the polarization voltage [20]. There is therefore an optimum size electrode and pulse shape [17, 42] from the standpoint of both stimulation threshold and pacemaker energy.

Although a variety of electrodes have been investigated for delivering an electrical stimulus to the heart [17, 18, 20, 21, 22, 23], noble metals such as platinum and platinum alloys are commonly used and recommended because of their inertness to body tissue [17]. Very high thresholds due to infection have been reported [23]. The current threshold is determined by the minimum current density at the electrode required for stimulation of the surrounding myocardium. Fluctuations which occur in the current threshold immediately after implantation are attributed to the process of tissue formation. When the myocardial tissue reaction is complete the threshold stabilizes. Infection around the electrode with tissue degeneration results in a further increase in threshold current [23]. The above investigations [17, 19, 21, 22, 23] have been limited to electrode materials currently used in cardiac pacemaker stimulating electrodes. The polarization that occurs at the smooth platinum electrodes used as pacemaker stimulating electrodes is much greater than in the case of platinum black electrodes.

The porous stimulating electrode on the other hand can be made small with the electrode polarization being reduced without effecting the current density just outside the electrode surface area. The rise in threshold is attributed not to an increase in the electrical impedance of the scar tissue surrounding the electrodes, but rather due to an increase in the size of the electrode surface due to the conductive scar tissue with a resulting decrease in current density [20]. Porous ceramics with 45 to 100 μm pore size have shown thin fibrous encapsulating layers of 4–6 cells in thickness with a good blood supply or no observable encapsulation as contrasted to thick encapsulation around impervious discs [24, 25]. Thus, porous stimulating electrodes should have lower electrode polarization and a lower threshold of stimulation due to tissue ingrowth. Tissue ingrowth will also help to fix the stimulating electrode in place. One of the principal complications remaining with the transvenous technique has been reported to be electrode displacement in the right ventricular inflow tract [26].

Electrode polarization is also a problem in impedance measurements on biological materials, and corrections for this polarization must be made if excessive measurement errors are to be avoided [27]. Corrections are not only large but uncertain at sufficiently low alternating current frequencies where polarization becomes large [28, 29]. At present, electrodes in our laboratory and elsewhere [27] are coated with platinum black by electroplating from a Kohlrausch solution. This normally reduces electrode polarization to a relatively low level for frequencies above 100 kHz. However, for measurements on physiological fluids at lower frequencies, corrections for polarization must be made [18, 19, 28, 29, 30, 31] or different electrode configurations used. For example, the four-electrode null technique [28] has been applied to impedance measurements over the range of 10 Hz to 1 kHz. Here voltage across the sample is applied by one pair of electrodes and another pair of noncurrent-carrying electrodes is used to measure the voltage across the sample. The electrodes have a platinum black coating to further decrease polarization. Platinum black electrodes deteriorate with use in biological fluids which is believed due to macromolecules effecting the platinum black surface [27]. If macromolecules are blocking the sites of the platinum black interface and decreasing the ease of charge transfer, this would account for the increased polarization when the electrodes are used in protein solutions. Again, the development of porous electrodes could be applied to improve biological impedance measurements.

DeRosa and Beard [30, 40] at Drexel have considered polarization in terms of rate determining steps. The effects of electrode d.c. potential, pH and oxygen coverage on the mechanism of cathodic reduction of oxygen and their influence on the cathode polarization has been studied [30]. Anodic polarization under the variation of the above parameters has also been studied. The anodic as well as the cathodic reactions are important in a.c. polarization in electrical impedance measurements and at bipolar pacemaker electrodes.

2. Experimental Procedures

2.1. Modified Transient Galvanostatic Method for Studying Polarization [33]

When using the galvanostatic technique to study the variation of electrode potential as a function of current density, the cell current is changed suddenly from zero to a given value, and the resulting variation of potential with time is recorded. The electrode under test and a counter electrode are placed in a Ringer's solution which has an ionic concentration approximating that of subcutaneous tissue fluid. The potential of test electrodes with reference to a silver-silver chloride electrode is measured as shown in figure 1. The cell current is changed from zero to a given current density by a current pulse of approximately 1 ms. width and 500 μA amplitude. The electrode potential is measured with respect

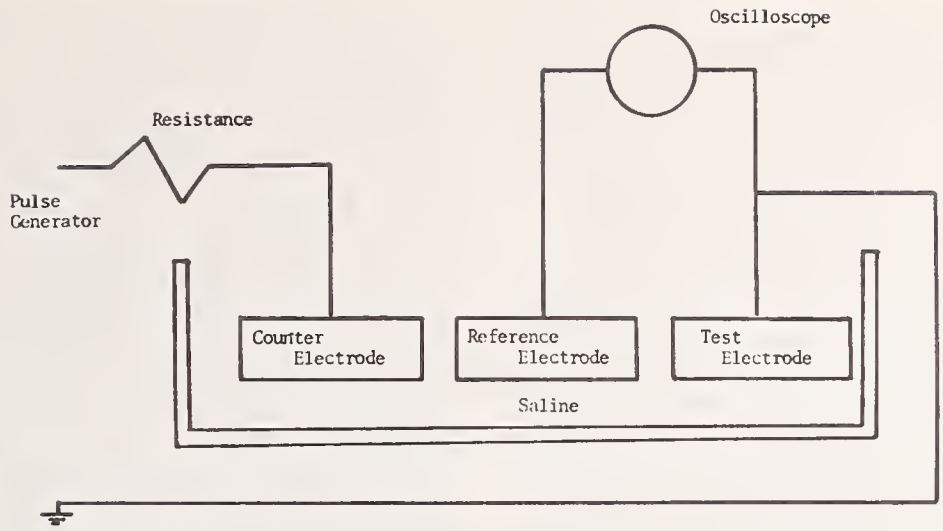

FIGURE 1. *Transient galvanostatic technique.*

to the reference electrode. Since the current through the reference electrode is very small, there is negligible overpotential and voltage drop in the solution between it and the electrode under test.

When a stimulus such as a step current is applied to an electrode interface, most of the initial current is used to charge up the double layer while later on the constant current density is used to promote electronation or a charge transfer reaction [33]. By recording the variation of the potential with time between a nonpolarizable reference electrode and the test electrode, the kinetic parameters of the electrode reaction can be obtained [33, 34].

2.2. The Brunauer, Emmett, and Teller (BET) Gas Adsorption Method

The Brunauer, Emmett, and Teller (BET) Gas Adsorption Method has been used to measure the surface area of porous compacts and powder [16, 35–38]. The utilization of the technique requires one to obtain an experimental gas adsorption isotherm from which the volume corresponding to monomolecular gas coverage is estimated. Once this volume is known along with the average area of the molecules of the adsorbate, the surface area of the specimen can be calculated.

The experimental setup which was used is similar to Kreiger [38] and is basically a combined gas buret and mercury manometer. To obtain more accurate pressure measurements, a thermocouple was also used. Before testing began, the specimens were outgassed at 0.5 μmHg at 200 °C for approximately 16 hours. Helium was used for dead space determination and nitrogen for the adsorbate during the actual measurement portion of the tests. All tests were made with the sample container immersed in a liquid nitrogen bath. The resulting pressure versus volume data results in a Type II Brunauer isotherm [39] in which the "knee" of the curve (fig. 2a) is generally accepted as being monomolecular gas coverage of the surface involved. For both convenience and greater accuracy, this data can be plotted as shown in figure 2(b) with the resulting straight line slope and intercept giving monomolecular coverage directly, i.e., $v_m = 1/(b+m)$.

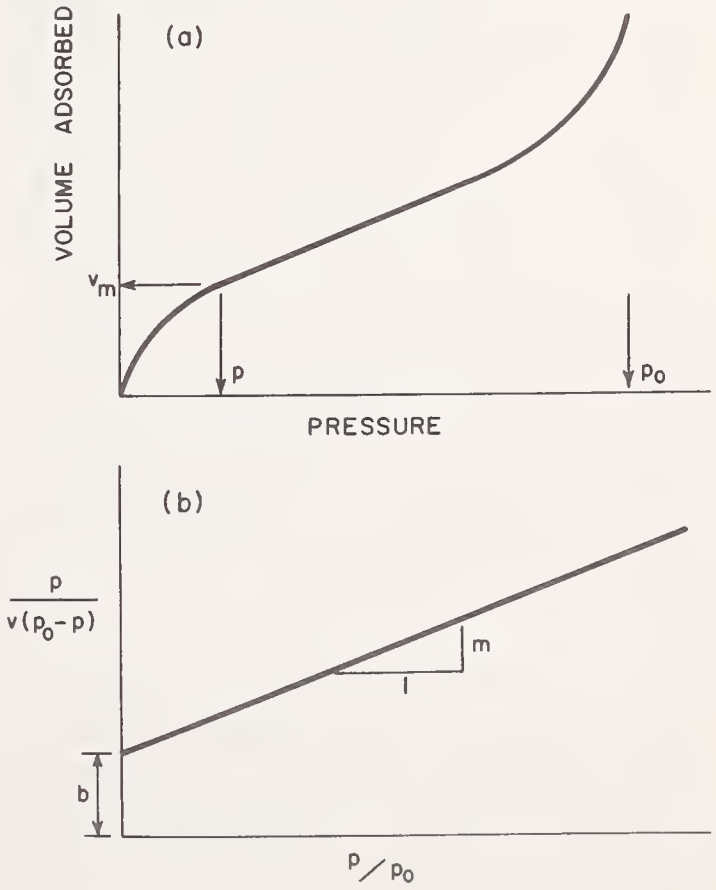

FIGURE 2. *(a) Type II Brunauer isotherm. (b) BET free-surface linear plot.*

The product of V_m, the cross-sectional area of the absorbate and Avogadro's number corrected to standard temperature and pressure gives the surface area, S_{BET}.

2.3. Scanning Electronmicrographs

A scanning electron-microscope [2,3] was used to study the loose powders and compacts. The preparation of biological materials for the scanning electron microscope was as follows: Upon removal from the animal, the sample was washed in saline to remove mucous and fixed in glutaraldehyde. The sample was then using a succession of ethyl alcohol-water baths, i.e., 58, 90, 95, and 100 percent alcohol. The alcohol was dehydrated then replaced with amyl acetate. The samples were then freeze-dried in conventional manner, coated with gold, and examined in the scanning electron microscope.

2.4. Impedance Measurements

Electrode polarization, which greatly influences electrical impedance measurements, can be studied both from time and frequency domain measurements [19, 21, 33, 40]. Plastic cells of poly(tetrafluoroethylene) and poly(methyl methacrylate), consisting of thin-walled measuring chambers surrounded by circulating water for temperature control, were used for studying a variety of porous electrodes. For time domain measurements a constant current pulse source is connected to the electrodes and the amplitude of the current pulse is increased in steps. The potential across the electrodes and current are measured at each level. The impedance measurements were made using a Wayne Kerr B221 Admittance Bridge which measures the parallel conductance and capacitance. The amplitude of the applied sinusoidal voltage is only 25 millivolts RMS which insures the electrical impedances are measured in the linear range, i.e., not in the range where impedance is a function of the amplitude of the applied signal. Measurements were made at 25 °C over the frequency range from 200 Hz to 20 kHz. While cell temperature was controlled and the pH and oxygen concentration was monitored with an oxygen meter.

3. Materials

3.1. Fabrication of Porous Electrodes

Following powder metallurgy techniques, the loose powder is placed in a hardened metal die and is compressed under high pressure. Under pressure, the particles become cold welded together and the magnitude of the compacting pressure greatly influences the density and strength of the resulting compact. The required compacting pressure depends upon the ductility of the base metal from which the powder is formed, e.g., aluminum compacts at 10,000–30,000 psi (0.07–0.2 GPa), ferrous powders at 30,000–60,000 psi (0.2–0.4 GPa), and tungsten at 80,000–150,000 psi (0.5–1.0 GPa). Since no published information was available regarding compacting pressure versus density or strength, a number of platinum and palladium powder electrodes [4] were prepared at different compacting pressures. These pressures were 10,000, 30,000 and 50,000 psi, which resulted in compacts with gradually increasing density. The green strength of the compacts was sufficient to withstand sterilization in a steam autoclave and they were therefore left unsintered.

The stimulating electrodes have been fabricated under a variety of techniques. Some electrodes were fabricated from platinum- and palladium-black powders with an isostatic compaction technique, then sintered. In the fabrication of large pore sizes, poly(methyl methacrylate) (PMMA) powder was blended with the palladium black and compacted under a hot press technique [41].

4. Results

In-vivo results for the porous electrodes used as power source electrodes demonstrated that there was a six-fold increase in power density for these electrodes [15]. Figure 3 shows the comparison between a porous palladium electrode and others with plastic binders. Porous Pd electrodes implanted in dogs over a period of 146 days under loads of 70 $\mu A/cm^2$ had no adverse tissue reactions [43, 44].

Figure 4 illustrates that the surface area of platinum and palladium is of the order of 10^4 times greater than foil. The large surface area, with a large increase in sites, accounts for the marked decrease in overpotential.

Figure 5 demonstrates the decrease in polarization of the porous stimulating electrodes which are compared to the standard platinum-iridium tips. The potential difference versus time across the platinum-iridium electrode has, as shown by its initial jump, a considerable potential across its electrodes and, as shown, in the curve of figure 5, a large overpotential across the interface. The amplitude of the 1 ms. current pulse was held to 200 μA, which gave a current density of 200 $\mu A/cm^2$.

[2] Type JSM–2, Japan Electron Optics Laboratory Company, Ltd.

[3] Certain commercial materials may be identified in this publication in order to adequately specify the experimental procedure. In no case does such identification imply recommendation or endorsement by the National Bureau of Standards, nor does it imply that the material are the best available for the purpose.

[4] The metal powders were obtained from Matthey Bishop, Inc., Malvern, Pa.

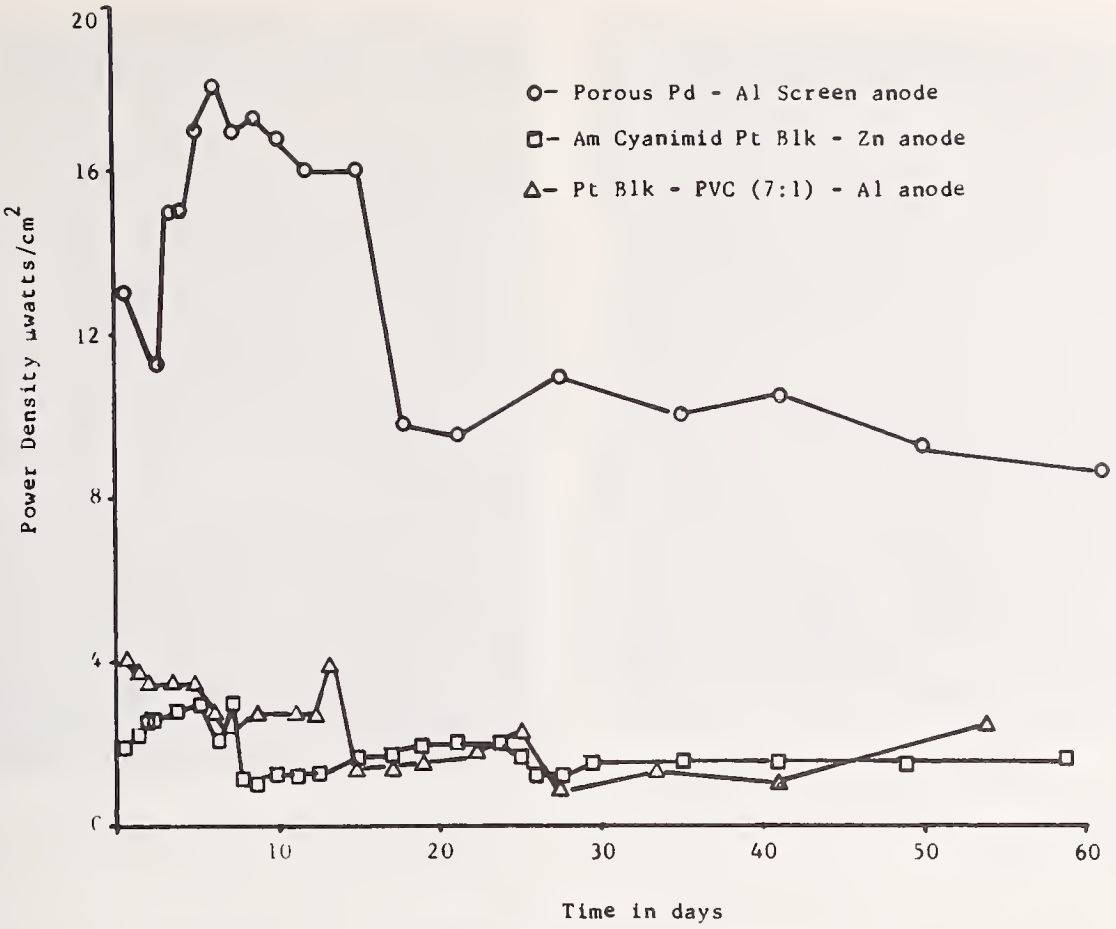

FIGURE 3. *Power density versus time.*

An implanted porous palladium compact and platinum black with poly (tetrafluoroethylene) and poly (vinyl chloride) binders

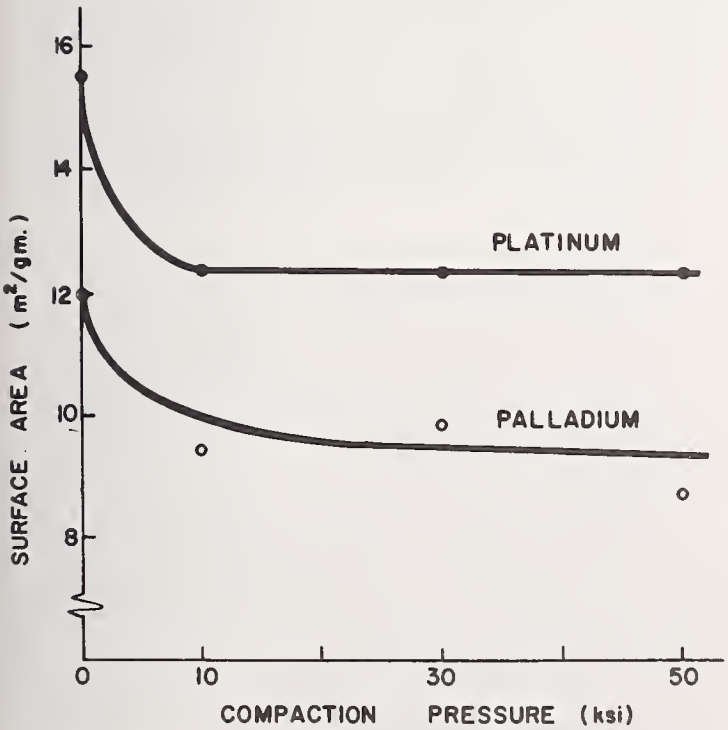

FIGURE 4. *Surface area of platinum and palladium compacts for various compacting pressures.*

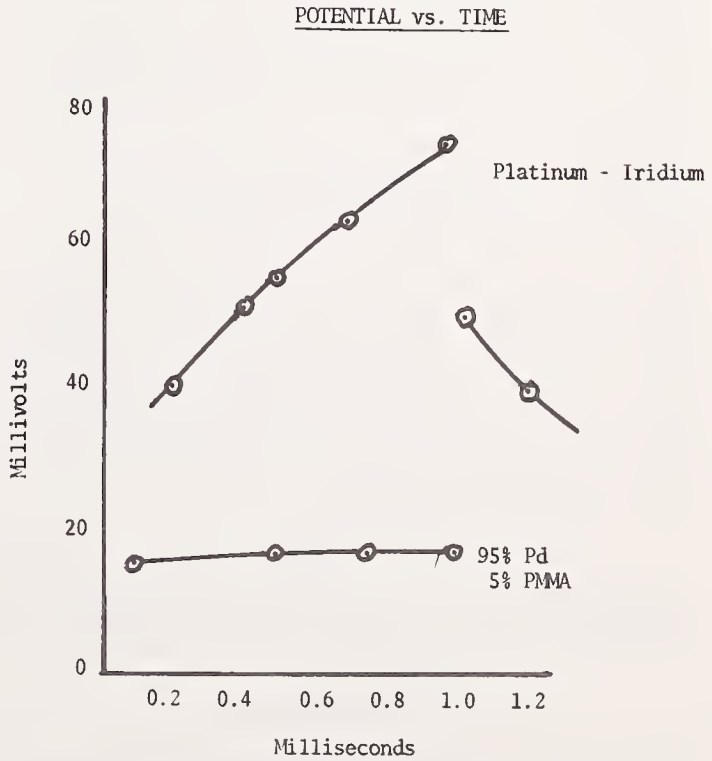

FIGURE 5. *Potential difference versus time across a platinum—iridium electrode and a porous palladium electrode.*

FIGURE 6. *Scanning electronmicrograph of porous palladium electrode; magnification 100; 97 percent palladium 3 percent PMMA; sintered at 450 °C.*

FIGURE 7. *Enlarged scanning electronmicrograph of figure 6 demonstrating tissue ingrowth magnification 300.*

The scanning electromicrographs of figures 6 and 7 demonstrate that the pore sizes are irregular and vary in size, with some pores 70 μm long. Figure 7 shows tissue ingrowth in the larger pores. More recent electrodes have been fabricated with 100 μm pore sizes and are in the process of being evaluated. It appears that porous palladium and platinum structures must, like ceramics, have pores greater than 45 μm for marked tissue ingrowth [25]. Pore sizes above 100 μm produce a weakened structure so that there is a balance between strength and tissue ingrowth.

Additional linear alternating current electrode polarization impedance measurements are being made to determine the effect of various background ligands on the electrode polarization impedance. Ahrland [46] has shown that the tendency of metal ions (acceptors) to form stable complexes depends on the relative coordinating affinities of nonmetal groups (donor atoms). Impedance measurements with various ligands such as iodide, bromide, and chloride appear to influence the electrode polarization in a predictable manner.

This study was made possible by the support of the Biomaterials Program of N.S.F. Grant No. GH 33748.

5. References

[1] Roy, O. Z., Biological Energy Sources: A Review, Bio-Medical Engr. **6,** No. 6, 250–256 (1971).

[2] Schaldach, M., Bioelectric energy sources for cardiac pacing in Part IX of Advances in Cardiac Pacemakers, S. Furman, Editor, Annals of N.Y.A.S. **167,** 016–1024 (1969).

[3] Reynolds, L. W., and Konikoff, J. J., Utilization of Bioelectric Potentials, First Interim Report, 1963, Ames Research Center, NASA Contract NAS–2–1420.

[4] Roy, O. Z., and Wehnert, R. W., Keeping the Heart Alive with a Biological Battery, Electronics, (1966).

[5] Racine, R., Power Generation from Implantable Electrodes, M.S. Thesis, Drexel University, Philadelphia, Pa., (1966).

[6] Massie, H. and Racine, P., Cardiac Pacemaker Without Batteries, 18th Annual Conf. on Engr. in Med. and Biol. (ACEM, Nov. 1965).

[7] DeRosa, J. F., Beard, R. B., Carim, H., and Dubin, S. E., Polarization and corrosion studies of porous and solid anodes for implantable power generating electrodes, IEEE Trans. on Biomed. Engr. **BME–20,** No. 5, 345–349 (1973).

[8] DeRosa, J., Fabrication and evaluation of cathode and anode materials for implantable hybrid cells, M. S. Thesis, Drexel University, Phila., Pa. (1969).

[9] Cooper, J. B. and Hahn, A. W., Hybrid biological power cells for cardiac pacemakers-materials evaluation, IEEE Trans. on Biomed. Engr. **BME–20,** No. 5, (1973).

[10] Satinsky, V., Dreifus, L. S., Racine, P., Massie, H. L. and Reynolds, L., Self-Energizing Cardiac Pacemaker, J.A.M.A., 35, 192–7 (1965).

[11] Tseung, A. C. C., King, W. J., and Wan, X. C., An Encapsulated, Implantable Metal-Oxygen Cell as a Long Term Power Source for Medical and Biological Applications, Med. Biol. Engr. **9,** 175–184 (1971).

[12] Roy, O.Z., Wehnert, R. W., Heggtveit, H. A., and Waddell, W. G., Biological energy sources in Part III of Advances in Cardiac Pacemakers, S. Furman, Editor, Annals of N.Y.A.S. **167,** 645–660 (1969).

[13] DeRosa, J. F., Beard, R. B., and Hahn, A. W., Fabrication and evaluation of cathode and anode materials for implantable hybrid cells, IEEE Trans. on Bio-Med. Engr. **BME–17,** No. 4, (1970).

[14] DeRosa, J. F., Beard, R. B., and Koerner, R. M., Improved Cathodes for Implantable Power Generating Electrodes, 23rd ACEMB, Washington, D.C., (1970).
[15] Beard, R. B. DeRosa, J. F., Koerner, R. M., Dubin, S. E. and Lee, K. J., Porous cathodes for implantable hybrid cells, IEEE Trans. Biomed. Engr. **BME-19,** 233–238 (1972).
[16] Koerner, R. M., Beard, R. B., DeRosa, J. F. and Miller, A. S., Porous Electrode-Tissue Interface Studies for Implantable Power Sources, Letters in Applied and Engineering Sciences **1,** 163–177, (1973).
[17] Greatback, W., Piersma, B., Shannon, F. D., and Calhoon, S. W., Jr., Polarization phenomena relating to physiological electrodes, in Part V of Advances in Cardiac Pacemakers, S. Furman, Editor, Annals of N.Y.A.S. **167,** 722–744 (1969).
[18] Jaron, D., A Study *In-Vivo* and *In-Vitro* of Electrical Correlates of Artificial Cardiac, Ph.D. Thesis, University of Penn., (1967).
[19] Jaron, D., Schwan, H. P. and Geselowitz, D., A mathematical model for the polarization impedance of cardiac pacemaker electrodes, Med. and Biol. Engr. **6,** 579–594 (1968).
[20] Myers, G. H., and Parsonnet, V., Engineering in the Heart and Blood Vessels (Wiley-Interscience, New York, N.Y., 1969).
[21] Jaron, D., Briller, S., Schwan, H. P., and Geselowitz, D., Non-linearity of cardiac pacemaker electrodes, IEEE Trans. in Biomed. Engr. **16,** No. 2, 132 (1969).
[22] Parsonnet, V., Zucker, R., Gilbert, L., Gerhard, L., Myers, G. and Avery, R., Clinical use of a new transvenous electrode, Part V, N.Y.A.S. **167,** 756–760 (1969).
[23] Thalen, T. H. J., van den Berg, J. W., van der Heide, J. N. H., and Nieveen, J., The Artificial Cardiac Pacemaker, C. C. Thomas, Springfield, Ill., (1969).
[24] Hirschhorn, J. A., and Reynolds, J. T., Powder Metallurgy Fabrication of Cobalt Alloy and Surgical Implant Materials in research in Dental and Medical Materials, E. Korostoff, Editor (Plenum Press, New York, N.Y., 1969).
[25] Hulbert, S. F., Morrison, S. J., and Klawitter, J. J., Tissue reaction to three ceramics of porous and nonporous structures, J. Biomed. Materials Res. **6,** 347–374 (1972).
[26] Smith, W. K., Frankl, W. S. and Boland, J. P., Transvenous pacemakers in clinical practice, Medical Clinics of North America **57,** No. 4, (1973).
[27] Schwan, H. P., Determination of Biological Impedances in Physical Techniques in Biological Research, Vol. **VI,** Part B, W. L. Nastuk, Ed. (Academic Press, New York, N.Y., 1963).
[28] Schwan, H. P. and Ferris, C. D., Four electrode null technique for impedance measurement with high resolution, Rev. Sci. Inst. **39,** No. 1, (April, 1968).
[29] Schwan, H. P., Electrode polarization impedance and measurements in biological materials, Ann. N.Y.A.S. **148,** (1968).
[30] DeRosa, J. F., and Beard, R. B., Electrode Polarization Studies on Solid and Porous Platinum and Palladium, Proc. of 26th ACEMB, Minneapolis, Minn., Sept. 30–Oct. 4, 1973.
[31] Ferris, C. D., Further Studies of Signal Distortion by A–C Electrode Polarization and Other Factors In Neurological Recording, Proc. of 26th ACEMB, Minneapolis, Minn., Sept. 30–Oct. 4, 1973.
[32] Pollak, V., An Equivalent Diagram for the Interface Impedance of Metal Electrodes, Proc. of 26th ACEMB, Minneapolis, Minn., Sept. 30–Oct. 4, 1973.
[33] Damaskin, B. D., The Principles of Current Methods for the Study of Electrochemical Reactions (McGraw-Hill, New York, N.Y., 1967).
[34] Bockris, J. O'M. and Reddy, A. K. N., Modern Electrochemistry, Vol. 2 (Plenum Press, New York, N.Y., 1970).
[35] Brunauer, S., Emmett, P. H. and Teller, E. Adsorption of gases and multimolecular layers, Chem. Soc. **60,** 309 (1938).
[36] Emmett, P. H., Measurement of the Surface Area of Solid Catalysts, Chapter 2 of Catalysis, Vol. **I,** Edited by P. H. Emmett (Reinhold Pub. Corp., New York 1954).
[37] Broekhoff, J. C. P. and Linsen, B. G., Studies on Pore Systems in Adsorbents and Catalysts in Physical and Chemical Aspects of Adsorbents and Catalysts, Edited by B. G. Linsen (Academic Press, London, 1970).
[38] Krieger, K. A., Apparatus for surface area measurement, Ind. Chem. Engr. Annl. Ed., 398–399 (1944).
[39] Adamson, A. W., Physical Chemistry of Surfaces (J. Wiley and Sons, New York, N.Y., 1967).
[40] DeRosa, J., Linear Electrode Polarization Studies on Solid and Porous Platinum and Palladium, Dissertation, Drexel University, 1974.
[41] Sturm, L. J., Fabrication and Evaluation of Cardiac Pacemaker Stimulating Electrodes, M.S. Thesis, Drexel University, 1974.
[42] Klafter, R. D., An optimally energized cardiac pacemaker, IEEE Trans. on Bio-Med. Engr. **BME-20,** No. 5 (Sept. 1973).
[43] Beard, R. B., Carim, H. M., Dubin, S. E., DeRosa, J. F., and Miller, A. S., Corrosion and Histopathological Studies on Anode Materials for Implantable Power Sources, J. Electro. Chem. Soc. **121,** No. 8, 277C (1974).
[44] Carim, H. M., Beard, R. B., DeRosa, J. F., and Dubin, S. E., Corrosion Studies on Anode Materials for Implantable Power Sources, ACS Div. of Organic Coatings and Plastic Chem., Symposium on Biomed. Application of Polymers, Chicago, Aug. 26, 1973.
[45] Hoare, J. P., The Electrochemistry of Oxygen (Interscience, New York, 1968).
[46] Ahrland, S., Chatt, J., and Davies, N. R., The relative affinities of ligand atoms for acceptor molecules and ions, Quart. Rev. (Chemical Society London) **12,** 265 (1958).

NATIONAL BUREAU OF STANDARDS SPECIAL PUBLICATION 415,
Biomaterials, Proceedings of a Symposium held in conjunction with the Ninth Annual Meeting of the Association for the Advancement of Medical Instrumentation, New Orleans, La., April 19–20, 1974
(Issued May 1975).

Properties of Fibrous Biomaterials With Statistically Dispersed Orientation*

E. Y. Robinson

Prototype Development Associates, Santa Ana, Calif. 92705

Many factors influence the interaction between bone or soft tissue and implanted synthetic biomaterials, e.g., biocompatibility, implant configuration, functional requirements, bone and tissue structure, and relative mechanical properties. Of the many active factors, one aspect is considered here: the theoretical consequences of the fibrous-lamellar structure of bone, and of the degree of fibrous orientation present in the individual lamellae. This orientation is known to be statistically dispersed about certain preferred directions in each layer, with possible large orientation changes from layer to layer. Analysis of this type of structure is presented with graphical illustration of the effects of orientation and of statistical dispersion of orientation on conventional engineering material parameters.

New biomaterials are being evolved which combine fiber reinforcement with polymer resin matrices (e.g., graphite fibers/polyethylene matrix). Such materials may be tailored to yield certain specific properties by controlling fiber orientation and quantity. Materials of this type are of interest in implants which may be required to behave in a similar fashion to adjacent bone tissue (as in bone splints, hip prostheses, etc.). The analysis presented here provides a rapid and convenient basis for calculating the effect of controlled and dispersed fibrous orientation on material properties.

The methods described lay a base for first approximations and show certain directions which should be followed in further investigation. Graphical results include examples for both fibrous bone tissue models and synthetic types of fiber-reinforced biomaterials.

Key words: Biomaterial properties; biomechanics; composites; fiber orientation; fibrous biomaterials.

List of Symbols

$\sigma(i)$	Stresses
$\epsilon(i)$	Strains
E_1	Principal Young's modulus
E_2	Secondary Young's modulus
ξ	$= E_2/E_1$; anisotropy parameter
ν_1	Primary Poisson ratio
G_1	Shear modulus in 1–2 plane direction; elastic constants without subscripts denote the isotropic asymptotes
$Q(ij)$	Stress-strain matrix
$U(i)$	Coefficients of the multiple-angle formulation for coordinate transformation of $Q(ij)$
θ	Angle of orientation of the natural longitudinal direction measured positive counter-clockwise from the reference coordinate axis; variable of integration
$f(\theta)$	Frequency distribution function of orientation angle
$\bar{Q}(ij)$	Stress-strain (stiffness) matrix of the multilayer laminate, analogous to the single layer properties defined above
$\tilde{Q}(ij)$	Isotropic stress-strain (stiffness) matrix
α	Intended orientation; integration limit for θ
$\pm\delta$	Bounds of orientation dispersion

1. Bone and Soft Tissue as Layered Fibrous Materials

The structure of bone tissue is highly fibrous and the fiber networks are often found in aggregated layers or lamellae. The nature of the lamellar bone structure varies within the musculoskeletal system and also within localized regions. Enlow in Evans [1][1] gave a concise description of several characteristic bone structures, two of which are reproduced here in figure 1.

Various mechanisms of bone development described by Enlow result in generally striated or at least localized layering of bone. In some cases this oriented lamellar structure develops by successive layering around a nucleus, such as an osteon. In other cases the process seems to be a progressive densification, as in cancellous compaction. In still other cases the bone exhibits regular strata with

*This paper presents the results of one phase of research carried out at the Jet Propulsion Laboratory, California Institute of Technology, under Contract No. NAS 7-100, sponsored by the National Aeronautics and Space Administration.

[1]Figures in brackets indicate the literature references at the end of this paper.

apparently aligned vascular channels within each lamella, as in figure 1b.

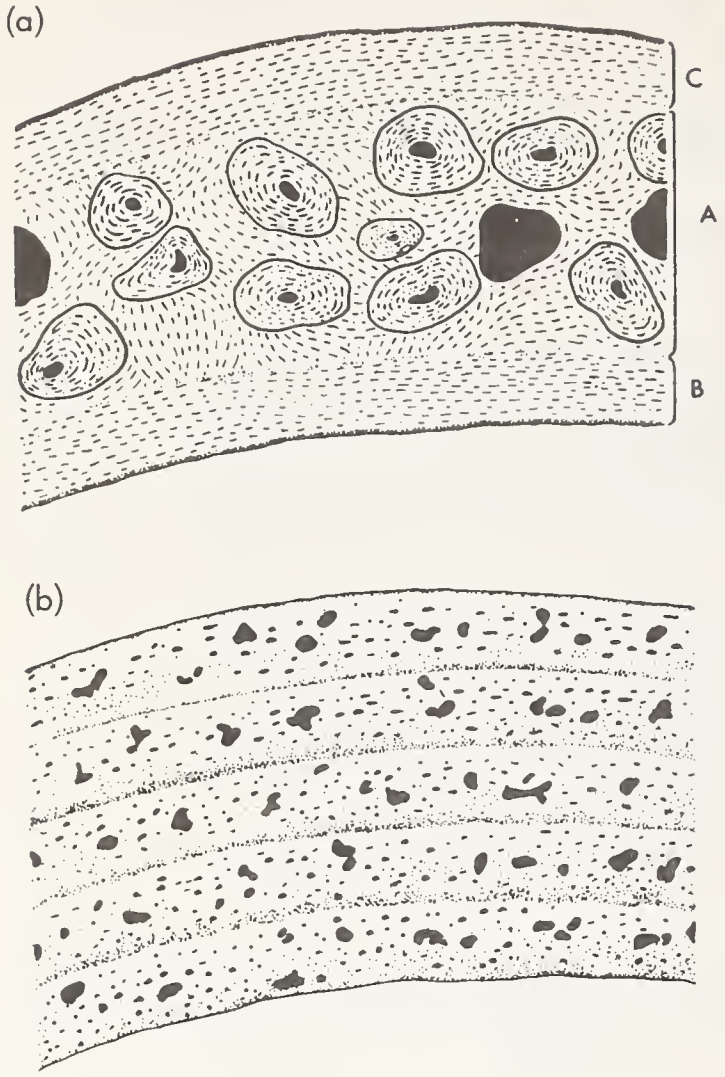

FIGURE 1. *Schematic layered bone structures.*

(a) Zones B and C are surface plates; Zone A shows cancellous compaction.
(b) Laminar bone with stratified vascular canals. (After Enlow in Evans, [1]).

Thus, in one case the material may be laced with highly oriented, dense (and probably strong and stiff) unidirectional structural elements such as osteons, while in another the properties reflect a system of pores which may be highly organized, "en echelon." Each of these structures imparts a particular and peculiar behavior to gross material properties.

Many published studies are devoted to elucidating the fibrous structure not only of bone but soft tissue as well, for example Walton in Buckles [2], Currey [3], Dempster [4], and others. Direct studies of single osteons have been pursued for some time, notably by Ascenzi et al; see for example in Evans [1]. Figure 2a, taken from Ascenzi in Evans [1], shows an osteon segment after fracture testing.

FIGURE 2a. *Tested single osteon sample.*

(After Ascenzi et al., in Evans, [1]).

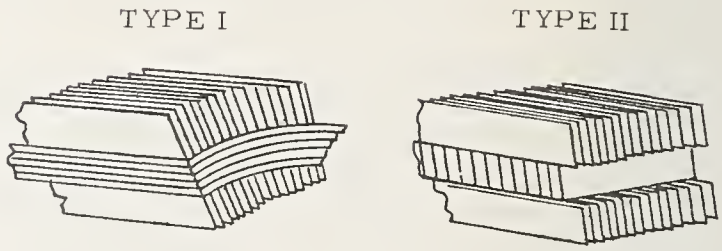

FIGURE 2b. *Schematic of one type of alternating lamellar aggregation.*

The lamellar structure is clearly evident, as well as a change of character in adjacent series of layers. A schematic of lamellar orientation shown in figure 2b shows two types of lamellar arrangement. The properties of the layered structure must depend not only on the lamellar arrangement but also on the details of fibrous orientation within each lamella. Evidence for these types of arrangement has been found in bone tissue. Localized aggregations of

FIGURE 3a. *Fibrous mats and oriented structure of mandibular tissue in cortical plates.*

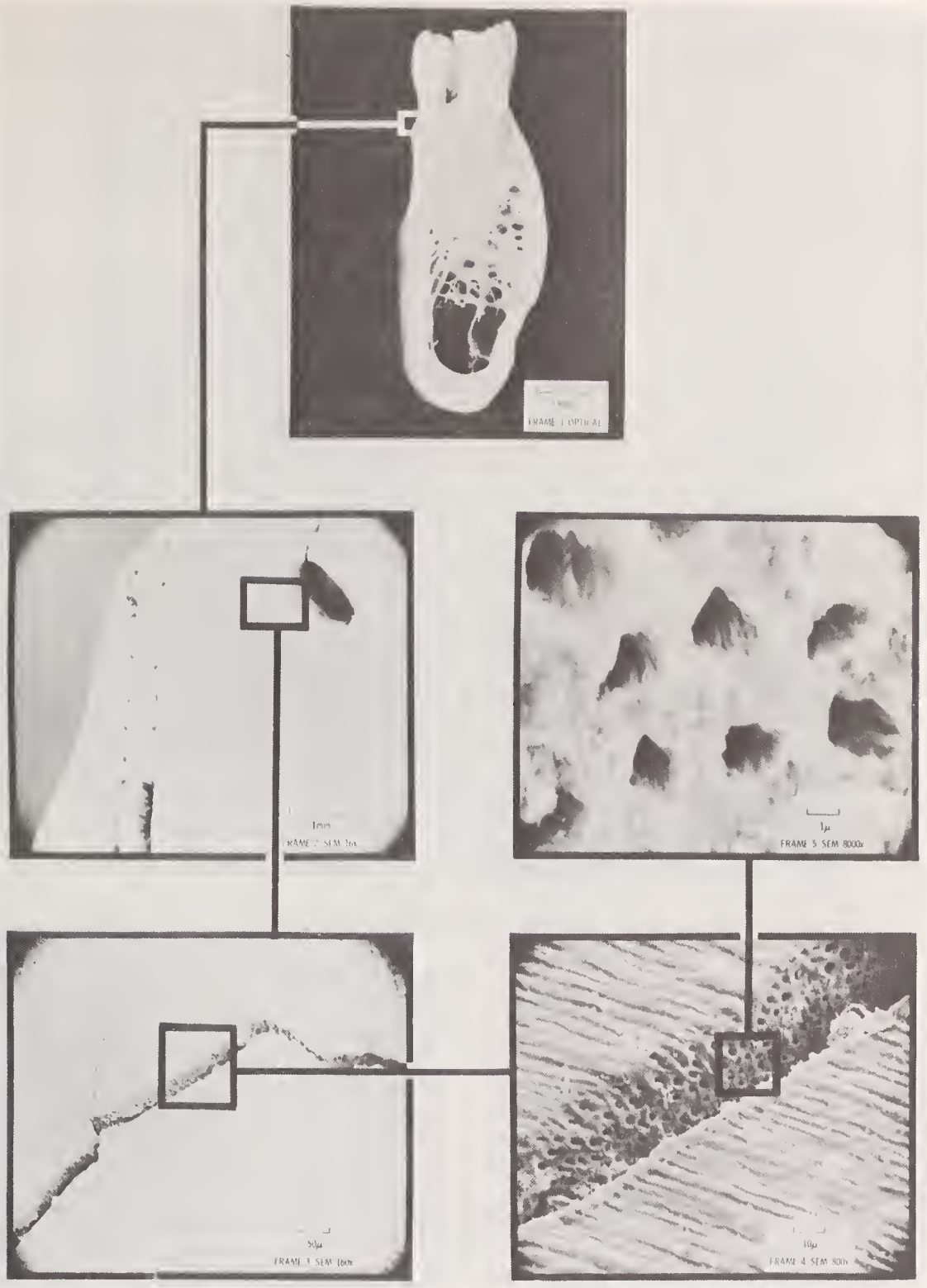

FIGURE 3b. *Fibrous mats and oriented structures in mandibular tissue.*

Successively magnified views of dentin.

Type 1 are shown in figure 2b, in osteons, while Type 2 structure is suggested in the SEM photograph of figure 3a. Implications of bone structure orientations have been considered by Evans and Vincentelli [5], Bonfield [6, 7], Cooke [8], Currey [9], and others. The Type 2 lamellar arrangement, illustrated in figure 2b, is shown in an electron micrograph of mandibular cortical tissue in figure 3a.

Figure 3b shows a sequence of progressive magnifications in dentin. Here the effect of orientation must be attributed to the parallel ranks of tubules (see Lees and Rollins [10]), while fibrous structures around the tubules appear to be quite random, without obvious preferential orientation. However, the highly organized geometry strongly suggests some corresponding fiber orientation.

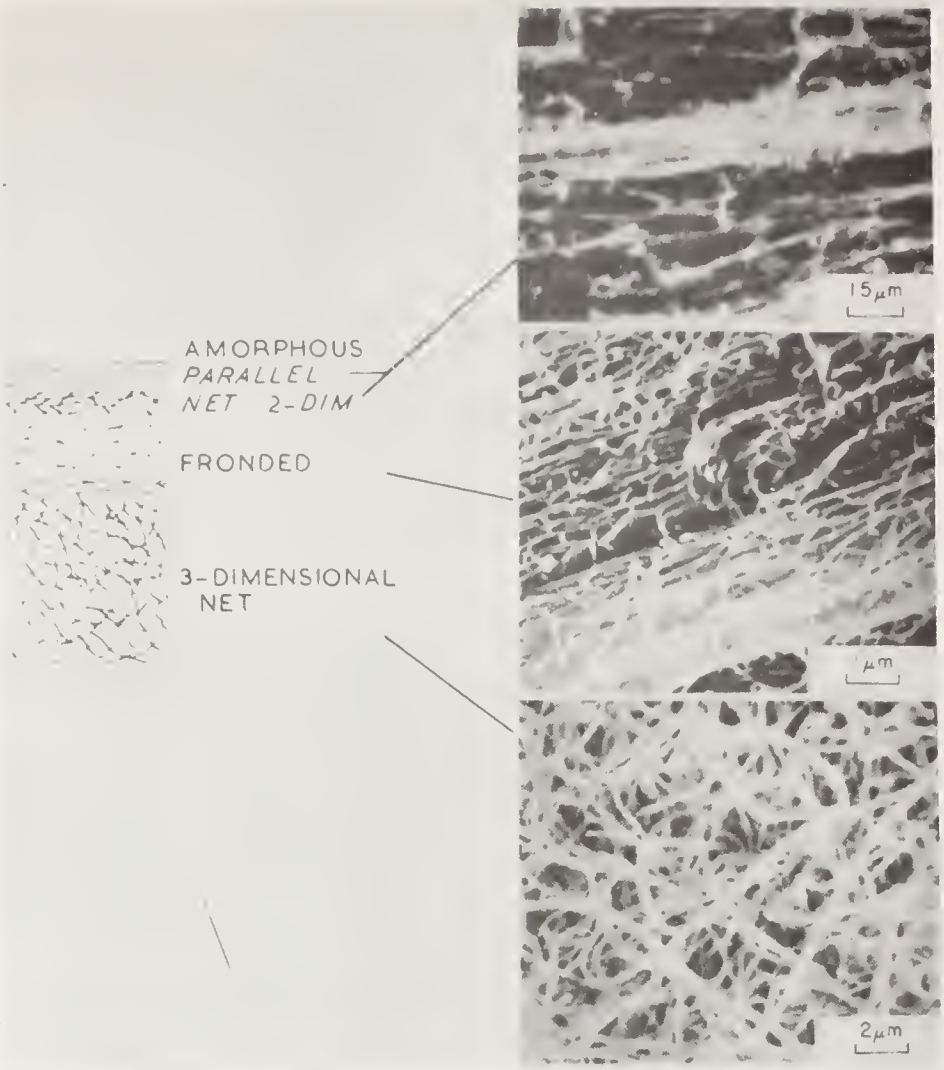

FIGURE 4. *Fiber patterns in femoral cartilage (After Millington et al., in Kenedi,* [11])

Studies of fiber arrangements in soft tissue have yielded many revealing and instructive configurations. Figure 4, from Millington et al., in Kenedi [11], illustrates changes in fiber organization through the thickness of femoral cartilage. Adjacent layering and change in predominant orientation direction between adjacent layers of dermal collagen may be seen in figure 5.

The cross-linking between adjacent layers may not be great, allowing a "scissor" action between such layers. On the other hand, if there is fairly intimate binding between layers, the "scissoring" is inhibited and a reaction stress is induced in each layer. If the fibers are adversely oriented, for example in a highly transverse direction, the induced stress may be intolerable and splitting results, as shown in figure 5b. Figure 6 is a schematic representation of a distended carotid artery, showing relative compaction of the inner collagenous layers and an apparently random arrangement on the outer boundary.

While the bone tissue, characterized by high mineral content, may be analyzed in somewhat simpler terms (linear elastic) than soft tissue, there are evidently many microstructural aspects which are similar, and a properly conceived analytical approach could shed additional light on the behavior of both tissue types.

2. Peculiar Behavior of Anisotropic Materials

Before establishing a simplified fiber-reinforced laminate model for tissue, it is instructive to review briefly some of the peculiar properties which accompany material anisotropy. In engineering structures these properties tend to be of secondary importance and are often avoidable by design. In the case of natural tissue these effects could be of importance and are therefore of interest here.

Consider a single layer of material containing perfectly aligned fibers bonded together by rela-

tively weak cross-link bonds and/or a binder matrix which permeates the layer. The fiber longitudinal and transverse directions are the "natural" directions of the layer, representing axes of elastic symmetry. If forces are applied along these directions, the material behavior is described as orthotropic. If forces act at some arbitrary angle to a natural direction, the material behavior is generally anisotropic. The mathematical implications are shown in figure 7.

FIGURE 5. *Dermal collagen under load (After Millington et al., in Kenedi, [11]).*

(a) "Scissor" action. (b) Transverse splitting.

FIGURE 6. *Schematic representation of distended carotid artery.*

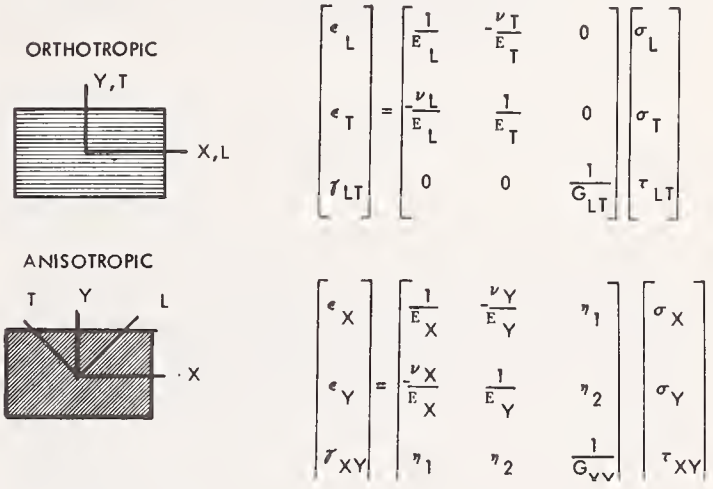

$$\begin{bmatrix} \epsilon_L \\ \epsilon_T \\ \gamma_{LT} \end{bmatrix} = \begin{bmatrix} \frac{1}{E_L} & -\frac{\nu_T}{E_T} & 0 \\ -\frac{\nu_L}{E_L} & \frac{1}{E_T} & 0 \\ 0 & 0 & \frac{1}{G_{LT}} \end{bmatrix} \begin{bmatrix} \sigma_L \\ \sigma_T \\ \tau_{LT} \end{bmatrix}$$

$$\begin{bmatrix} \epsilon_X \\ \epsilon_Y \\ \gamma_{XY} \end{bmatrix} = \begin{bmatrix} \frac{1}{E_X} & -\frac{\nu_Y}{E_Y} & \eta_1 \\ -\frac{\nu_X}{E_X} & \frac{1}{E_Y} & \eta_2 \\ \eta_1 & \eta_2 & \frac{1}{G_{vv}} \end{bmatrix} \begin{bmatrix} \sigma_X \\ \sigma_Y \\ \tau_{XY} \end{bmatrix}$$

FIGURE 7. *In-plane stress-strain relation for orthotropic and anisotropic material.*

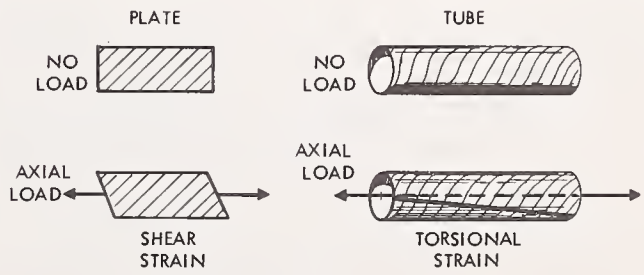

FIGURE 8. *Illustration of shear coupling.*

The nonzero terms of the bottom matrix mean that normal or transverse stress will cause shear strain. This effect is illustrated in figure 8.

Figure 8 shows the shear distortion of an anisotropic sheet subject to axial tension. Similar behavior of a tubular section is manifested by rotation accompanying axial tension. The shear distortion of a single $+\theta$ anisotropic ply is prevented by attaching a second layer oriented at $-\theta$. This is referred to as balanced orientation. However, such a two-layer laminate will tend to twist when axial force is applied, as illustrated in figure 9.

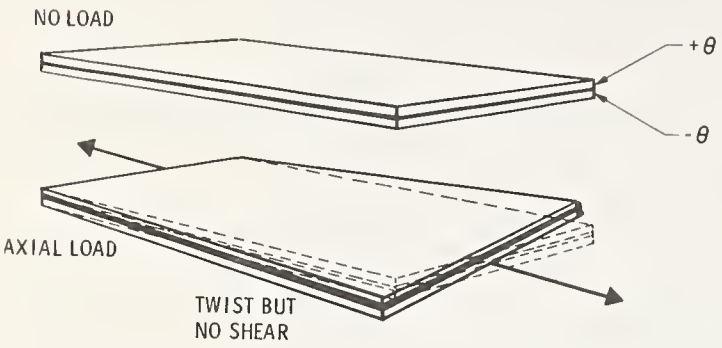

FIGURE 9. *Illustration of twist coupling.*

Combining this two-layer laminate with another two-layer laminate having opposite twist tendencies to form a "symmetric" and balanced laminate will result in conventional, uncoupled deformation under applied tensile or compressive in-plane forces, and the material system will be orthotropic. However, if this symmetric, balanced laminate is subjected to bending, as illustrated in figure 10, the twisting tendencies reappear. Generally speaking, it is not possible to simultaneously eliminate both load-twist and bend-twist coupling.

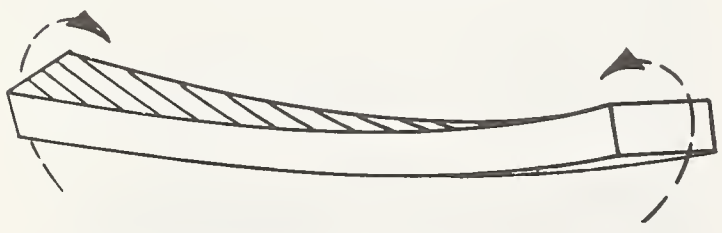

FIGURE 10. *Illustration of bend-twist coupling.*

As the number of layers increases and the orientation patterns become more dispersed, these coupling effects tend to diminish. They should, however, be recognized and may in fact play a significant role in the microscopic behavior of single fibers such as helically configured collagen fibrils.

3. Defining a Simplified Analytical Model

It is clear from even a general perusal of published results that fiber-orientation in layered tissue is not precise. While certain directions predominate, there is dispersion of orientation about these directions. Cox [12] provides a useful and general analysis applicable to a broad class of fiber networks.

For the present purpose the model will be limited to systems of two-dimensional layers. Applied or induced stresses in the transverse "thickness" directions are considered negligible. This assumption can lead to overestimation of elastic modulus of three-dimensional materials.

The effect of fibrous structure in a lamella is approximated by considering the layer to be a homogeneous, orthotropic continuum. The orthotropic properties of this equivalent layer are derived by analytical consideration of individual fiber properties and matrix or cross-linking properties.

All layers in the laminate are assumed to strain contiguously; that is, the strain is uniform through the transverse thickness direction. If "scissoring" and interfacial slippage occur between layers, this assumption will tend toward overestimation of modulus and underestimation of Poisson's ratio.

Orientation dispersion of fibers is assumed to be uniform but bounded symmetrically about a predominant, preferred direction α: that is, in the range of $\alpha-\delta$ to $\alpha+\delta$ where δ is the extent of orientation dispersion. An illustration of dispersed-orientation networks is shown in figure 11. The network, as it might appear to the eye, is shown above while the dispersion angle is depicted in the lower portion of figure 11.

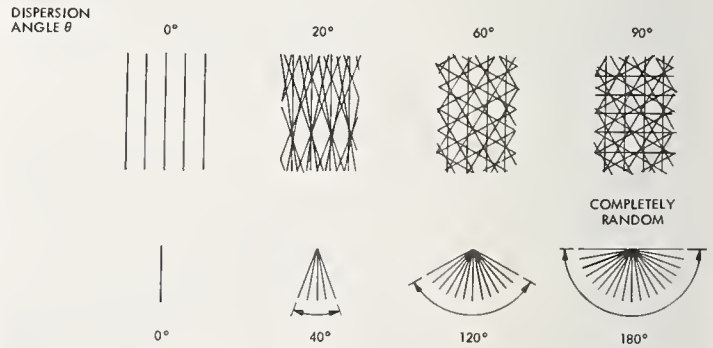

FIGURE 11. *Schematic illustration of dispersed orientation networks.*

In the analysis which is carried out in the following section, two material types are considered and analyzed by the same method (Robinson, [13]). The

TABLE 1. *Basic unidirectional lamellar properties used in analyses*

Material	Longitudinal elastic modulus, $GN/m^2(10^6psi)$	Transverse in-plane elastic modulus, $GN/m^2(10^6psi)$	Shear modulus, $GN/m^2(10^6psi)$	Major Poisson ratio
Carbon/polyethylene	69.0 (10)	0.69 (0.1)	0.69 (0.1)	0.3
Bone tissue	47.5 (7)	5.1 (0.75)	3.45 (0.5)	0.1

first is a synthetic fiber-reinforced, polymer-matrix material, a type which is becoming of great interest in biomedical and prosthetic application; see, for example, Giltrow [14], Musikant [15], and Sclippa [16]. One of the attractions of the material is the prospect of being able to tailor material properties to meet specific and individual objectives. This is achieved, in principle, by varying the quantity of fiber reinforcement and the degree and nature of fiber orientation. In reality, many additional, subtle factors can influence resultant properties of a fiber-composite material. The material considered here is a carbon fiber-reinforced polyethylene.

The second material is a hypothetical bone-tissue model built up of idealized fiber-reinforced lamellae. The basic orthotropic properties ascribed to an ideal unidirectional lamella of each material are shown in table 1. The data in this table are determined in part from published data on collagen, hydroxyapatite and highly oriented tissue, and in part estimated, since complete orthotropic characterization of natural tissues could not be found in a fairly persistent literature search.

4. Formulation and Analysis

In current engineering structural application of fiber-reinforced composites, the material is usually in the form of a multilayer laminate containing parallel, unidirectional fibers in each layer or ply (lamina or lamella). Consequently the analysis for such materials is referred to as laminate theory or laminate analysis. Published work in this field was strongly influenced within the last decade by substantial U.S. Air Force research and development sponsorship directed toward improved lightweight materials for aircraft and space applications. The introduction of carbon and graphite fibers, boron filaments, new single-crystal whiskers and other new fiber types is a direct result of this sponsorship. Also, for many years U.S. Forest Products Laboratory personnel have investigated theoretical and experimental behavior of nonisotropic materials related to plywood and fiberglass analysis. They are an excellent source of useful analysis and copious experimental data.

Lamination theory is covered in the *Structural Design Guide for Advanced Composite Materials* [17] and Ashton et al. [18]. Some elements of laminate analysis are given here to provide a useful description of the equations appropriate to partly random layer orientation. A two-dimension generalized Hooke's Law is used, with material stiffness elements $Q(ij)$ defined by the matrix equation

$$\sigma(i) = [Q(ij)][\epsilon(j)].$$

(See Glossary for definitions of symbols and terms used in this article.)

The 3×3 stiffness elements of $Q(ij)$ depend on the orientation of the principal elastic axes (natural directions of each layer or ply) relative to the applied forces. When these directions coincide (i.e., $\theta = 0$), the matrix elements are the natural direction orthotropic properties given by

$$Q(11) = \frac{E_1}{1-\xi\nu_1^2} \qquad Q(22) = \frac{E_2}{1-\xi\nu_1^2} \tag{1}$$

$$Q(12) = \frac{\nu_1 E_2}{1-\xi\nu_1^2} \qquad Q(66) = G_1.$$

When the natural direction is oriented at θ, the transformed stiffness coefficients of each layer, $Q(ij)$, are given by.

$$\left.\begin{aligned} Q'(11) &= U_1 + U_2 \cos(2\theta) + U_3 \cos(4\theta) \\ Q'(22) &= U_1 - U_2 \cos(2\theta) + U_3 \cos(4\theta) \\ Q'(12) &= U_4 - U_3 \cos(4\theta) \\ Q'(66) &= U_5 - U_3 \cos(4\theta) \\ Q'(16) &= +1/2\, U_2 \sin(2\theta) + U_3 \sin(4\theta) \\ Q'(26) &= +1/2\, U_2 \sin(2\theta) - U_3 \sin(4\theta) \end{aligned}\right\} \tag{2}$$

U_1, U_4, U_5 are invariants, independent of orientation. The coefficients $U(i)$ are given in terms of the natural direction orthotropic parameters by

$$
\left.
\begin{aligned}
U_1 &= 1/8\ [3Q(11) + 3Q(22) + 2Q(12) \\
&\qquad + 4Q(66)] \\
U_2 &= 1/8\ [4Q(11) - 4Q(22)] \\
U_3 &= 1/8\ [Q(11) + Q(22) - 2Q(12) - 4Q(66)] \\
U_4 &= 1/8\ [Q(11) + Q(22) + 6Q(12) - 4Q(66)] \\
U_5 &= 1/8\ [Q(11) + Q(22) - 2Q(12) + 4Q(66)] \\
U_5 &= \frac{[U(1) - U(4)]}{2}.
\end{aligned}
\right\} \quad (3)
$$

In this formulation, the problem is limited to two-dimensional elastic behavior.

The stiffness properties of the two-dimensional multilayer laminate are calculated by summing the stiffness contributions of each layer. Note that for balanced orientations of similar layers (at $+\theta$ and $-\theta$) the $Q'(16)$ and $Q'(26)$ terms will cancel. These are shear coupling terms discussed earlier.

In order to account for orientation dispersion we consider the case of a large number of hypothetical layers in a laminate of unit thickness, with orientations distributed from $-\delta$ to $+\delta$. The laminate stiffness elements are obtained by summing the stiffness contributions from each hypothetical ply. For large n and small angular interval, we can pass from the sum to the integral:

$$
\bar{Q}(ij) = \int_{-\delta}^{\delta} Q'(ij) f(\theta) d\theta \qquad (4)
$$

where $f(\theta)$ is the normalized frequency distribution of orientation, and $Q'(ij)$ are given by eq (2).

4.1. Quasi-Isotropic Limits

If the dispersion angle extends from $-\pi/2$ to $+\pi/2$, the material becomes apparently isotropic. Therefore, the in-plane isotropic elastic limits of a composite result when the orientation distribution is uniform, $f(\theta) = 1/(2\delta)$, and unbounded:

$$
\bar{Q}(ij) = \frac{1}{\pi} \int_{-\pi/2}^{\pi/2} Q'(ij) d\theta.
$$

The terms from eq (1) including functions of θ will drop and this equation shows that the "invariant" terms U_1, U_4, and U_5 are the unbounded θ averages of the $Q'(ij)$ for symmetrical, uniform probability distributions. The isotropic stiffness matrix is, then,

$$
\bar{Q}(ij)_{\text{isotropic}} = \begin{bmatrix} U_1 & U_4 & 0 \\ U_4 & U_1 & 0 \\ 0 & 0 & \frac{U_1 - U_4}{2} \end{bmatrix}
$$

The quasi-isotropic engineering parameters are

$$
\nu = \frac{U_4}{U_1} \qquad G = U_5 \qquad E = U_1(1 - \nu^2) \qquad (5)
$$

It is instructive to examine the invariants in terms of the conventional engineering constants of the individual orthotropic layers:

$$
\begin{aligned}
U_1 &= \frac{E_1}{8}\left[\frac{3 + 4\frac{G_1}{E_1} + \xi\left(3 + 2\nu_1 - 4\nu_1^2\frac{G_1}{E_1}\right)}{1 - \xi\nu_1^2}\right] \\
U_4 &= \frac{E_1}{8}\left[\frac{1 - 4\frac{G_1}{E_1} + \xi\left(1 + 6\nu_1 + 4\nu_1^2\frac{G_1}{E_1}\right)}{1 - \xi\nu_1^2}\right] \qquad (6) \\
U_5 &= \frac{E_1}{8}\left[\frac{1 + 4\frac{G_1}{E_1} + \xi\left(1 - 2\nu_1 - 4\nu_1^2\frac{G_1}{E_1}\right)}{1 - \xi\nu_1^2}\right].
\end{aligned}
$$

This form exhibits the contribution of element Poisson ratio and anistropy to the invariant parameters. The theoretical value for the isotropic Poisson ratio, given by U_4/U_1, shows a fundamental trend to values around 1/3 which is only slightly altered by varying the anisotropy parameters. This tendency to Poisson ratios around 1/3 is seen to be a structural consequence of combining large numbers of randomly oriented orthotropic lamallae into a quasi-isotropic laminate. For layers of random unbonded filaments ($\xi = E_2 = G_1 = 0$) acting as a contiguous network, eq (5) predicts $\nu = 1/3$. This result sheds light on the well-known fact that nearly all macroscopically isotropic materials exhibit Poisson ratios in the vicinity of 0.3. The isotropic sheet may therefore be modeled as an ensemble of random orthotropic layers. For highly anisotropic constituent layers (small ξ), the quasi-isotropic two-dimensional parameters can be estimated by $E = E_1/3$, $G = E_1/8$, $\nu = 1/3$. Cox [12] gives a classic discussion of both two- and three-dimensional fiber networks and reinforced systems.

If the basic layer properties are known, that is, $E1$, $E2$, $G1$, and $\nu 1$, the quasi-isotropic limits may be computed with equations (1), (3), (5), or (6).

4.2. Off-angle Lamallae Containing Dispersed Fiber Orientation

In the bone tissue model the concern is with random partial orientation of individual layers distributed about an intended nominal direction, as well as the effect of orientation dispersion of the constituent filaments. The orientation dispersion is assumed to be distributed in the interval $-\delta$ to $+\delta$ about the nominal predominat direction angle α.

The stiffness elements for unit thickness laminate are given by

$$\bar{Q}(ij)=\int_{\alpha-\delta}^{\alpha+\delta} Q(ij)f(\theta)d\theta \tag{7}$$

For a uniform distribution, $f(\theta)=1/2\delta$, the integration gives

$$\left.\begin{aligned}
\bar{Q}(11)&=U_1+U_2\cos(2\alpha)\left(\frac{\sin 2\delta}{2\delta}\right)+U_3\cos(4\alpha)\left(\frac{\sin 4\delta}{4\delta}\right)\\
\bar{Q}(22)&=U_1-U_2\cos(2\alpha)\left(\frac{\sin 2\delta}{2\delta}\right)+U_3\cos(4\alpha)\left(\frac{\sin 4\delta}{4\delta}\right)\\
\bar{Q}(12)&=U_4-U_3\cos(4\alpha)\left(\frac{\sin 4\delta}{4\delta}\right)\\
\bar{Q}(66)&=U_5-U_3\cos(4\alpha)\left(\frac{\sin 4\delta}{4\delta}\right)\\
\bar{Q}(16)&=\frac{U_2}{5}\sin(2\alpha)\left(\frac{\sin 2\delta}{2\delta}\right)+U_3\sin(4\alpha)\left(\frac{\sin 4\delta}{4\delta}\right)\\
\bar{Q}(26)&=\frac{U_2}{2}\sin(2\alpha)\left(\frac{\sin 2\delta}{2\delta}\right)-U_3\sin(4\alpha)\left(\frac{\sin 4\delta}{4\delta}\right)
\end{aligned}\right\} \tag{8}$$

As the dispersion limit δ approaches zero, the ideal anisotropic results of eq (2) are obtained. When δ reaches $\pi/2$, the isotropic limits result. Equations (8) are identical in form (homologous) to eq (2) if modified values are used for U_2 and U_3:

$$\bar{U}_2=U_2\frac{\sin(2\delta)}{2\delta}$$

$$\bar{U}_3=U_3\frac{\sin(4\delta)}{4\delta}$$

Equations (8) provide a new generalized form of the constitutive stiffness elements given by eq (2). The homologous formulation allows simple alteration of existing computation procedures to incorporate effects of uniform, bounded dispersion and for analysis of partially oriented multilayer laminates (lamellar materials).

The laminated material description is greatly simplified if the orientation at $+\alpha$ is balanced by orientation at $-\alpha$. In such cases, the material is said to be orthotropic, instead of generally anisotropic, and the conventional engineering constants may be computed by

$$\left.\begin{aligned}
&\bar{\nu}_1=\frac{\bar{Q}(12)}{\bar{Q}(22)}\qquad \bar{\xi}=\frac{\bar{Q}(22)}{\bar{Q}(11)}\\
&\bar{E}_1=\bar{Q}(11)[1-\bar{\xi}\nu_1^2]\qquad \bar{E}_2=\bar{\xi}\bar{E}_1\qquad \bar{G}=\bar{Q}(66)
\end{aligned}\right\} \tag{9}$$

using the $\bar{Q}(ij)$ values from eq (8).

5. Results of Numerical Computations

Figures 12 to 14 show the results obtained with the equations of Section 4 applied to the idealized material given in table 1 of section 3. Two types of structural arrangements were analyzed. In the first, the multilayer laminate was assumed to contain perfectly oriented (no dispersion) unidirectional fibers in each layer, with the orientation of alternate layers changing from $+\theta$ to $-\theta$ with respect to the laminate principal direction. In the second case the fibers within the lamellae were assumed to have dispersed orientation, ranging uniformally from $-\delta$ to $+\delta$. Figures 12a and 12b show the computed results for these two structure types for a carbon fiber/polyethylene matrix composite. The quantity and type of carbon fiber reinforcement was chosen to yield the particular set of orthotropic layer properties shown in table 1. The properties of these fibers offer a very broad range of reinforcement and property control with polymeric matrix composites. Figures 13a and 13b illustrate the analogous results for a hypothetical fibrous bone-tissue model.

The two structure types are combined to show the range of orthotropic properties which might be observed in a lamellar structure, wherein each lamella contains orientation dispersion and the preferred layer orientation alternates from layer to layer. The graphical result for such a fibrous bone tissue model is shown in figure 14.

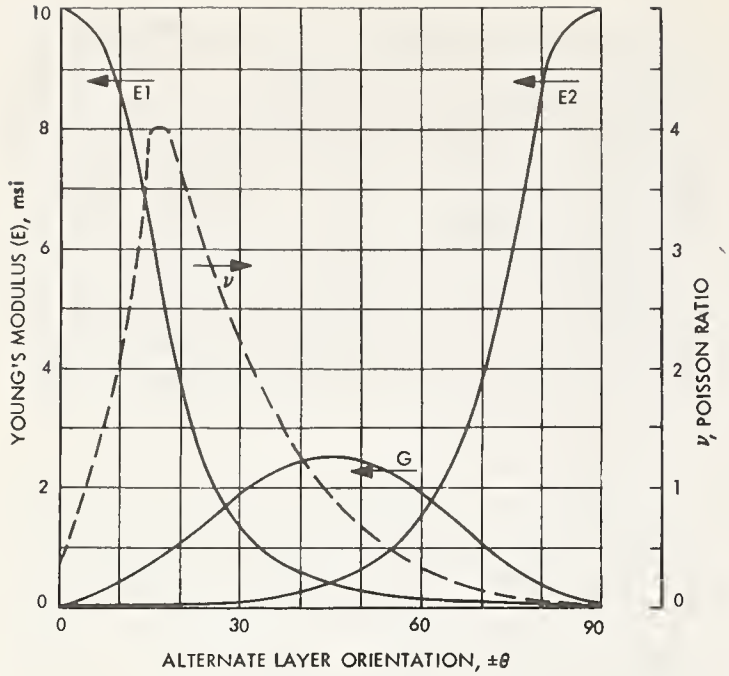

FIGURE 12a. *Calculated in-plane properties of a carbon fiber-polyethylene matrix composite.*

$\pm\theta$ layering, no orientation dispersion.

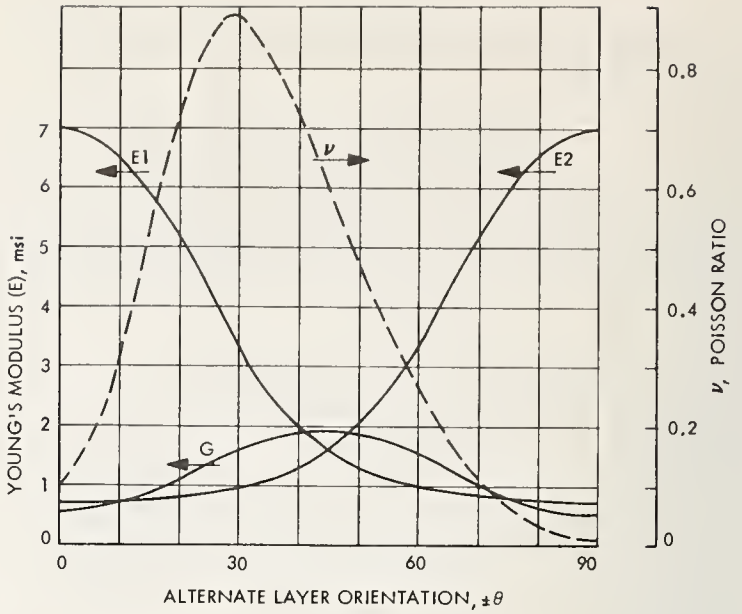

FIGURE 13a. *Calculated in-plane orthotropic properties of a fibrous bone tissue model.*

$\pm\theta$ layering, no orientation dispersion.

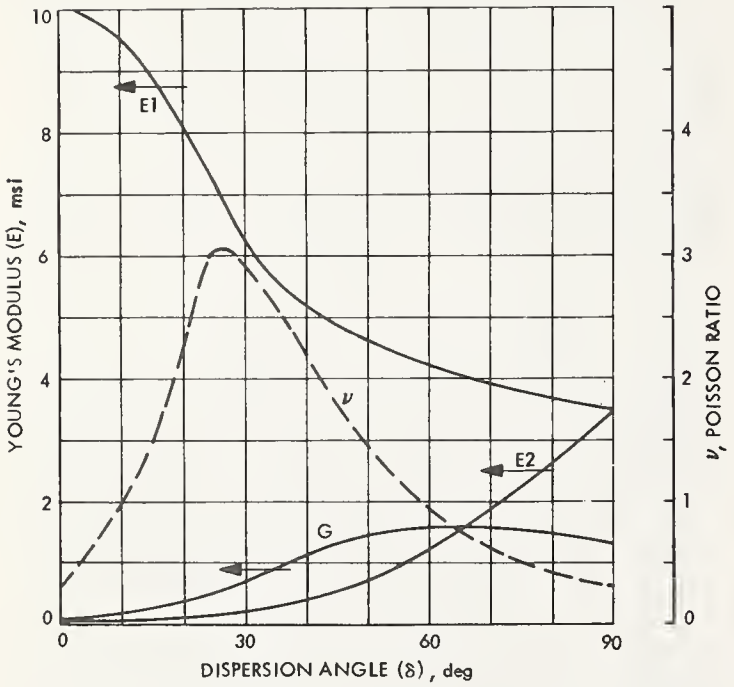

FIGURE 12b. *Calculated in-plane properties of a carbon fiber-polyethylene matrix composite.*

Bounded uniform orientation dispersion (preferred orientation is 0°)

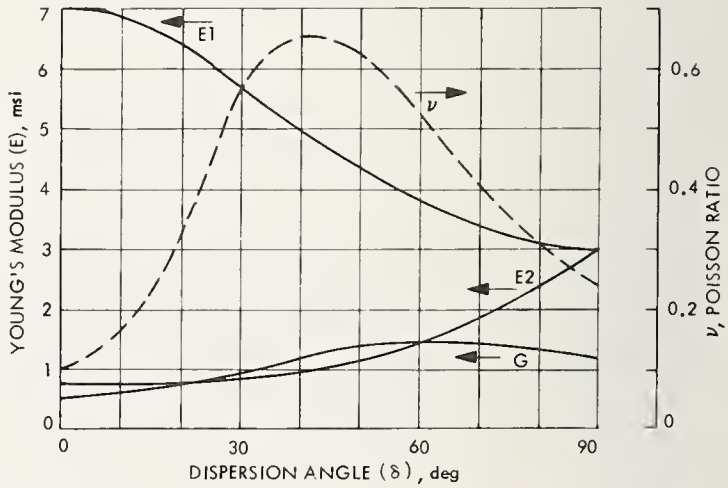

FIGURE 13b. *Calculated in-plane orthotropic properties of a fibrous bone tissue model.*

Bounded uniform orientation dispersion (preferred orientation is 0°)

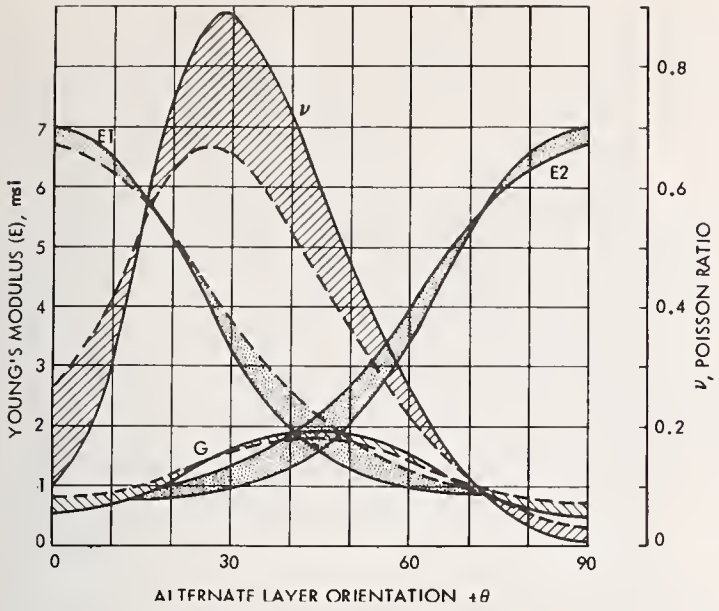

FIGURE 14. *Calculated in-plane orthotropic bone properties showing range of values for $\pm\theta$ layers having up to ± 15 degrees orientation dispersion.*

6. Discussion of Results

The analytical results presented in section 5 illustrate the ranges of material property variations implied by the idealized fibrous structures considered. It should be noted that the resultant orthotropic properties are interrelated. Experimental data on real bone tissue samples can present combinations of properties which are not describable by the type of model considered here. This should not be surprising in view of the photomicrographs presented in section 1 showing twisted, kinked, irregular fibers, with varying degrees of cross-linking. The layering is also irregular in thickness and physical arrangement, and even the highly lamellar osteons may curve and change direction rather sharply within the cortex. The range of properties shown in figure 14 appears to be typical, more or less, of much bone-tissue data published in the literature. However, the applicability of this model is limited, and many of its underlying assumptions are probably too idealized. Nevertheless, a basis is provided for calculating detailed interaction between synthetic materials used in prostheses and adjacent bone tissue. Examination of the equations in section 4 and results in section 5 reveals that direct, axial loads in a laminate will be borne primarily by the stiffest lamallae; however, the transverse stresses, induced by differential contraction according to individual layer Poisson ratios, may be much more equally shared if the lamellae act contiguously. The price for transverse load sharing when axial properties of the layers differ sharply will be induced internal stress and a tendency for the interface to delaminate in efforts to relieve these induced stresses.

The material properties selected for the basic unidirectional lamella are, to some degree, based on published data for collagen and hydroxyapatite (or similar crystalline materials). The analysis provides a logical connection between the properties of a lamellar material and the nature and degree of orientation dispersion which is present. Conversely, if the dispersion is characterized a priori and the properties measured, it is possible to use the analytical model in reverse to infer the maximal properties of constituent reinforcements.

Another potentially important feature of the analytical results is the behavior of Poisson's ratio. In certain regions of orientation dispersion, as shown in figure 14, the value of this parameter becomes very high and is sensitive to orientation. Thus, as orientation of the fibrous tissue changes under the action of applied forces, the instantaneous elastic properties also change in correspondence with the instantaneous orientation. Poisson ratio for the model analyzed would be expected to increase with applied tension loads if the dispersion angle was less than about 35 degrees. If the angle exceeded 35 degrees, the Poisson ratio would be expected to decrease. This could be a significant factor in bone remodeling dynamics, since a high (and possibly increasing) Poisson ratio would cause the fibrous network to close up under tension and to open up under compression. In a flexural loading situation (as in the femur or tibia) the tensile side would inhibit the flow of nutrients into and through the tissue fine-structure, while on the compressive side the "opening" of the structure should encourage the flow of nutrients. This type of structural response may affect localized resorption and bio-electric behavior.

This is consistent with some observed cases of bone remodeling in which apposition occurs on the compressive side and resorption on the tensile side of a flexurally loaded bone. This direction of remodeling acts to reduce flexure arising from eccentric compressive loads until equilibrium is reached.

7. Conclusions and Recommendations

It is a well-known fact that natural tissue is comprised of fibrous networks of various types, including systems of well-defined lamellae (laminates). The mathematical approach to analyzing fiber-reinforced laminates has been presented and extended to include the effect of bounded uniform orientation dispersion. The model analysis was here confined to linear, elastic, small-deflection, two-dimensional conditions.

The resultant equations (sec. 4) may be easily used to infer the orthotropic engineering elastic properties of a fairly arbitrary class of lamellar materials containing dispersed orientation. The same analytical procedure is also applicable to the new types of synthetic biomaterials which in-

corporate fiber reinforcements in a polymer matrix (e.g., carbon fiber/polyethylene matrix). These materials are convenient to mold and, by selection of reinforcing fiber quantity and length, the resultant properties may be tailored over a fairly broad range. This property range can be estimated, at least to a first approximation, by the methods developed here.

Finally, further extension of this work should respond to the explicit limitation described above. Methods for three-dimensional analysis with nonlinear material behavior will yield more faithful simulations of real tissue behavior and will be applicable to soft tissue. Analytical development should be guided by experimental determination of actual orientation and orientation dispersions as well as the degree of interlamellar contiguity and individual fiber configurations. Basic properties of unidirectional bone-tissue microstructural elements should be measured, and procedures should be developed for the reliable experimental characterization of bone tissue samples as orthotropic (or anisotropic) lamellar materials.

8. References

[1] Evans, F. G., Ed., Studies on the Anatomy and Function of Bone and Joints, pp. 92–112, 121–141 (Springer Verlag, New York, N.Y., 1966).

[2] Buckles, R. G., Ed., Formation and Structure of Calcified Tissue, Advances in Bioengineering, (American Institute of Chemical Engineers Symposium, Series No. 114, **67**, 1971).

[3] Currey, J. D., Three analogies to explain the mechanical properties of bone, Biorheology **2**, 1–10 (1964).

[4] Dempster, W. T. and Liddicoat, R. T., Compact bone as a non-isotropic material, American J. Anatomy **91**, 331 (1952).

[5] Evans, F. G. and Vincentelli, R., Relation of collagen fiber orientation to some mechanical properties of human cortical bone, J. of Biomech. **2**, 63 (1969).

[6] Bonfield, W., Mechanism of deformation and fracture in bone, Composites **2**, No. 3, 173–175 (June 1971).

[7] Bonfield, W. and Clark, E. A., Elastic deformations of compact bone, J. Mat. Sci. **8**, 1590 (1973).

[8] Cooke, F. W., et al., The fracture mechanics of bone—another look at composite modeling, J. Biomedical Mat. Research Symposium: Materials and Design Considerations for the Attachment of Prostheses to the Musculoskeletal System (Interscience, New York, N.Y., 1973).

[9] Currey, J. D., The relationship between the stiffness and the mineral content of bone, J. Biomech. **2**, 477–480 (1969).

[10] Lees, S. and Rollins, F. R., Jr., Anisotropy in hard dental tissues, J. Biomech. **5**, 557 (1972).

[11] Kenedi, R. M., Ed., Advances in Biomedical Engineering, pp. 162–168, 202–212 (Academic Press, New York, N.Y., 1971).

[12] Cox, H. L., The elasticity and strength of paper and other fibrous materials, Brit. J. Appl. Phys. **3**, 72–79 (1952).

[13] Robinson, E. Y., On the Elastic Properties of Fiber Composite Laminates with Statistically Dispersed Orientations, (Proc. of the 28th Annual Technical Conference, Reinf. Plast. and Composites, Soc. of the Plastics Industries, New York, N.Y., 1973).

[14] Giltrow, J. P. and Lancaster, J. K., Friction and wear of polymers reinforced with carbon fibers, Nature **214**, 1106 (1967).

[15] Musikant, S., Quartz and Graphite Filament Reinforced Composites for Orthopedic Surgical Application, J. Biomed. Mat. Research Symposium; Medical Application of Plastics (Interscience, New York, N.Y., 1972).

[16] Sclippa, E., and Piekarski, K., Carbon fiber reinforced polyethylene for possible orthopedic uses, J. Biomed. Mat. Research **7**, 59 (1973).

[17] Structural Design Guide for Advanced Composite Materials, Second Edition Prepared under AF Material Laboratory Contract No. F33615–69–C–1368 by Los Angeles Division of North American Rockwell Corp., Los Angeles, Ca., January, 1971.

[18] Ashton, J. E., Halpin, J. C. and Petit, P. H., Primer on Composite materials (Technomic Publishing Co., Stamford, Conn., 1969).

[19] Haut, C. H., and Little, R. W., A Constitutive Equation for Collagen Fibers, J. Biomech **5**, 423 (1972).

[20] Lukes, R. S. and Katz, J. L., Transformation of the Viscoelastic Functions of Calcified Tissues and Interfacial Biomaterials into a Common Representation (Fifth Annual Clemson Biomaterials Symposium, April, 1973).

NATIONAL BUREAU OF STANDARDS SPECIAL PUBLICATION 415,
Biomaterials, Proceedings of a Symposium held in conjunction with the Ninth Annual Meeting of the Association for the Advancement of Medical Instrumentation, New Orleans, La., April 19–20, 1974
(Issued May 1975).

A Simple *In Vitro* Test for Screening the Blood Compatibility of Materials

H. Kambic, T. Komai, R. J. Kiraly, and Y. Nosé

Department of Artificial Organs
The Cleveland Clinic Foundation, 9500 Euclid Avenue,
Cleveland, Ohio 44106

An *in vitro* blood compatibility test was developed to evaluate thromboresistant properties of materials. This method is called the closed-cell kinetic blood coagulation test. A closed cell system eliminates any air-blood interface. The blood is withdrawn directly from the animal into the cell, minimizing the exposure to foreign surfaces other than the one being studied and eliminating the use of anticoagulants through the process.

The technique includes the simultaneous blood filling of eight cells with the test materials, and eight cells lined with a control material. As a control material we have selected silicone rubber, which has reasonably good thromboresistant properties, is widely accepted, and commercially available. The cells are opened at different predetermined times, and the clot formation is then measured by two complimentary methods: weighing the clot and colorimetry of the unclotted blood. The two methods correlate and can differentiate between red and white thrombus.

The results are presented as clot formation curves versus time for the material under test and for the control. The variability of blood properties makes this control curve essential.

Detailed analyses of the curves will offer a new approach to the understanding of the mechanism of thrombus formation on various types of materials. Results will be presented for tests conducted on Hydron®, segmented polyurethane, purified natural rubber, as well as chemically treated tissue.

Key words: Blood coagulation; Blood compatibility; Blood platelet consumption; kinetic clotting test.

1. Introduction

A large number of materials is available for use in intravascular devices. Since the processes occurring when materials are brought in contact with blood are not well known, a screening test is required in order to establish their material blood compatibility.

The advantages of an *in vitro* screening test are obvious: low cost, independence of flow dynamics, and short time. However, questions have been raised as to their reliability as well as their correlation with the actual behavior of the materials once implanted *in vivo*.

A simple technique designed in our laboratory has been reported [5].[1] Further refinement has resulted in a more reliable and reproducible test [11]. This present report describes the results obtained studying candidate materials with the technique.

2. Materials and Methods

The technique employed is the kinetic clotting test, as described by Nosé et al. [11]. Basically, the test consists of the simultaneous filling with donor blood of eight cells containing the candidate material and eight cells containing the control material (Silastic 372®).[2, 3] The cells are sequentially opened at predetermined intervals to follow the kinetics of clot formation.

The test cells consist basically of two sheets of the material under study, enclosed within an acrylic chamber (fig. 1). Blood is drawn in between the material sheets by aspirating saline from the acrylic chamber as shown in figure 2. The blood comes directly from the donor dog, contacting only the venous puncture needle and a short segment of

[1] Figures in brackets indicate the literature references at the end of the paper.

[2] Dow Chemical Co., Midland, Mich.

[3] Certain commercial materials and instruments may be identified in this publication in order to adequately specify the experimental procedure. In no case does such identification imply recommendation or endorsement by the National Bureau of Standards, nor does it imply that the equipment or instruments identified are necessarily the best available for the purpose.

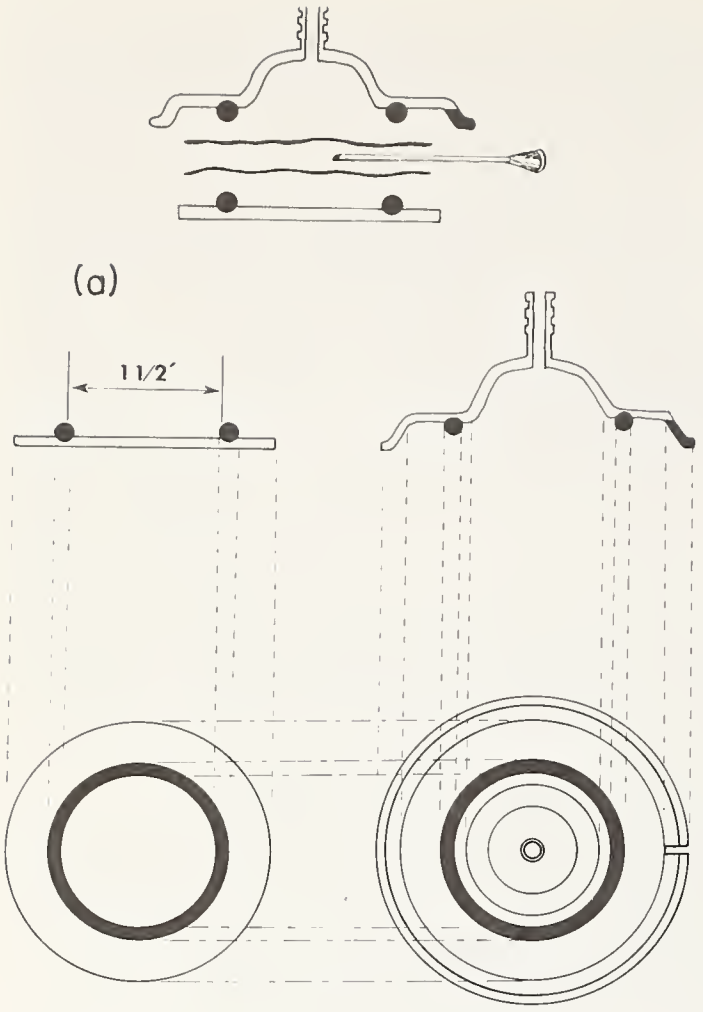

FIGURE 1. *Closed cell kinetic test chamber; (a) expanded view showing test material and filling needle; (b) assembled cell.*

flexible Silastic tubing. No anticoagulants are used throughout.

All test cells are weighed before and after filling to determine the amount of blood within each cell.

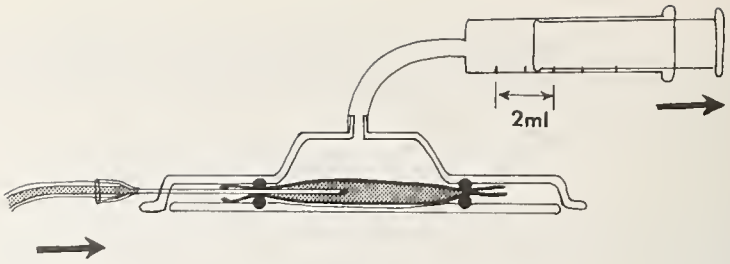

FIGURE 2. *The cell filling technique. Two ml of saline are withdrawn from around the test sample, resulting in blood being drawn between the test sample sheets.*

Afterward, they are placed in a slowly rotating device to prevent sedimentation.

Two cells, one with Silastic and one with the test material, are opened every twenty minutes over a two-hour period. The clot formation is ascertained using two techniques. The first is the *direct* measurement of the amount of clot formed. This is done by determining the dry weight of the clot, normalized by the amount of blood in the cell.

$$\text{Normalized clot weight} = \frac{\text{Dry clot weight (gm)}}{\text{Total blood weight (gm)}}$$

The actual values of normalized clot weight are plotted versus time. The difference between the clot weights obtained with the test material and the Silastic control is also plotted as a function of time; the area under the difference curve provides a quantitative *direct* index for comparing different materials. The more negative the number obtained with one particular material, the better its blood compatibility.

Second, the amount of unclotted blood which remains within the test cell is measured. The content of the cell is immersed in 100 ml of distilled water, where the unclotted blood hemolyzes. The resulting hemoglobin concentration is measured spectrophotometrically at 5400 Å. The hemoglobin readings are normalized by the initial amount of blood, and plotted as functions of time. The differences between the amounts of unclotted hemoglobin obtained with the test material and Silastic control are also plotted, and the area under the curve

provides an *indirect* index where positive numbers predict better blood compatibility than Silastic.

The test materials and Silastic control sheets were cut 2½-in in diameter and soaked in saline overnight prior to use. All test materials were prepared at one time and stored in covered glass jars. The materials used were:

1. Hydron® (2—type E hydrophilic polymer, polyhydroxyethyl-methacrylate). [4]
2. Purified Natural Rubber—double centrifuged, prevulcanized latex;[5] 50 percent solids exposed to a 4 percent formaldehyde solution after curing and then saline rinsed.
3. Segmented Polyether-polyurethane Ethicon [6]—prepared according to the method of Boretos [1].
4. Silastic 372, MDX4–4156—vulcanized at 150 °C, coated with $NaHCO_3$, and washed in saline several days before use (control material).
5. Bovine Pericardium—exposed to 4 percent glutaraldehyde solution (24 h) and saline rinsed.

Healthy 20–25 kg dogs were fasted overnight and anesthetized intravenously with 300 mg of sodium thiamylal.[7] Six donor dogs were used in total; one dog was used for each test.

3. Results

Figure 3a shows the weight of clot formed by Hydron and that formed by Silastic. The difference in the clot weights is shown in figure 3b. The direct index was −3.02 min. The comparison of unclotted hemoglobin is shown in figure 3c. The difference in the amounts of unclotted hemoglobin between Hydron and Silastic (fig. 3d) yields an indirect index of 16.14 min, figures 4, 5, and 6a, b, c, and d show the results for segmented polyurethane, glutaraldehyde treated pericardium and formaldehyde treated natural rubber, respectively. All results are presented as mean values; the bars represent standard errors of the means. The clotting indices for all materials tested are outlined in table 1.

[4] Hydro Med Sciences, Inc., New Brunswick, N.J.
[5] Hygienic Dental Manufacturing Company, Akron, Ohio.
[6] Ethnor Medical Products, Somerville, N.J.
[7] Surital ®, Parke Davis, Detroit, Mich.

TABLE 1. *120 Minute kinetic clotting modulus*

Material	Direct clotting modulus	Indirect clotting modulus (min)
Hydron®	−3.02	+16.4
4 percent glutaraldehyde treated pericardium	−3.33	+24.7
Segmented polyurethane	−3.72	+11.2
4 percent formaldehyde treated natural rubber	+0.66	+6.8

(Silastic 372 Control)

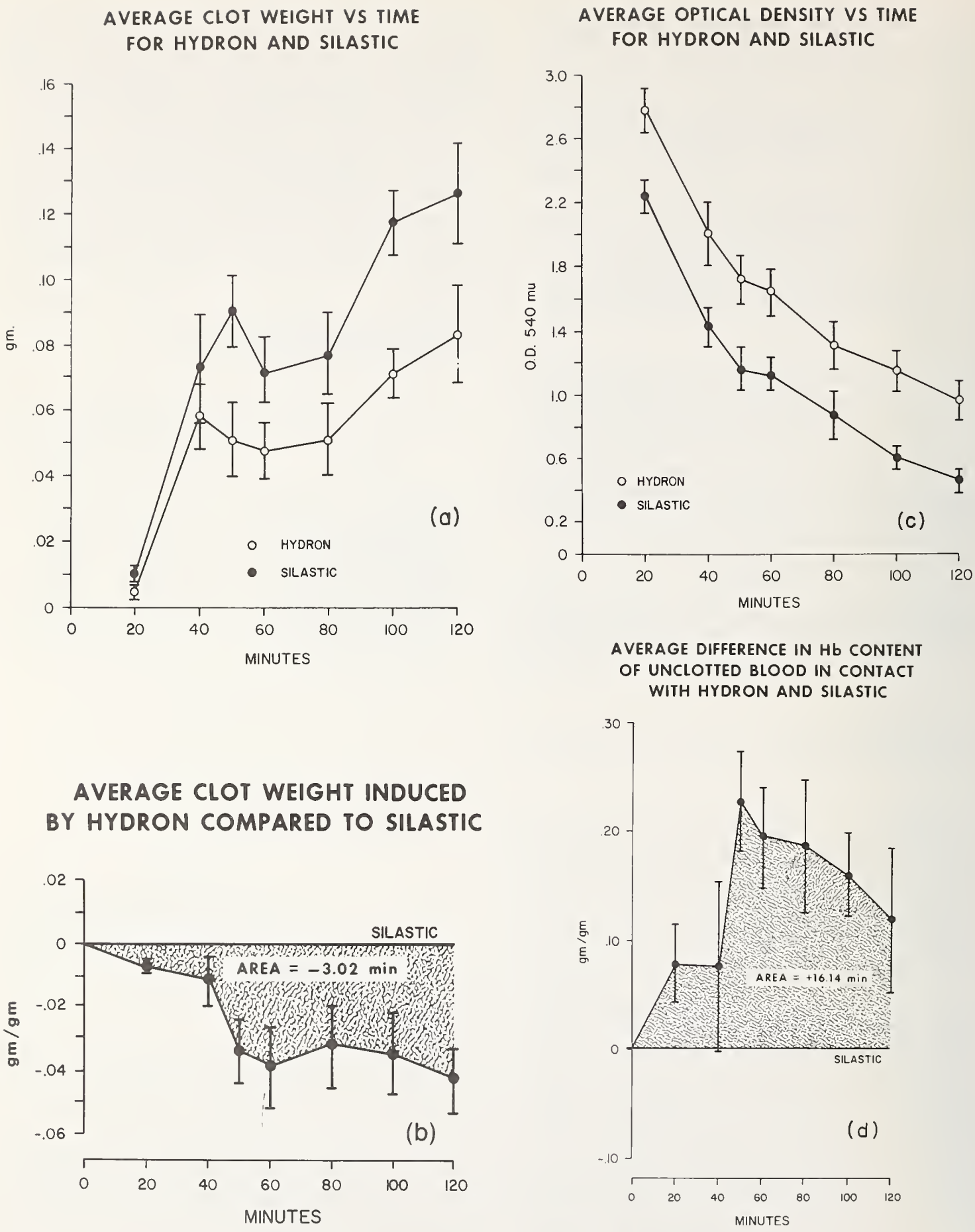

FIGURE 3. *Comparative blood compatibility of Hydron and Silastic.*

(a) average clot weight as a function of time; (b) average clot weight induced; (c) average optical density (hemoglobin content of unclotted blood) as a function of time; (d) average difference in hemoglobin content of unclotted blood.

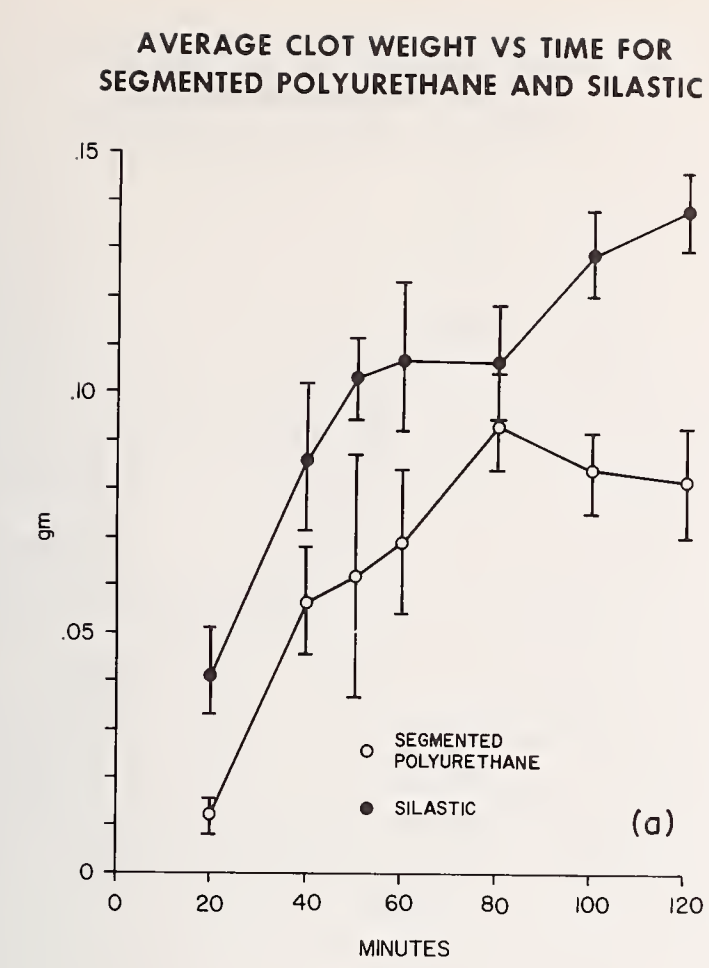

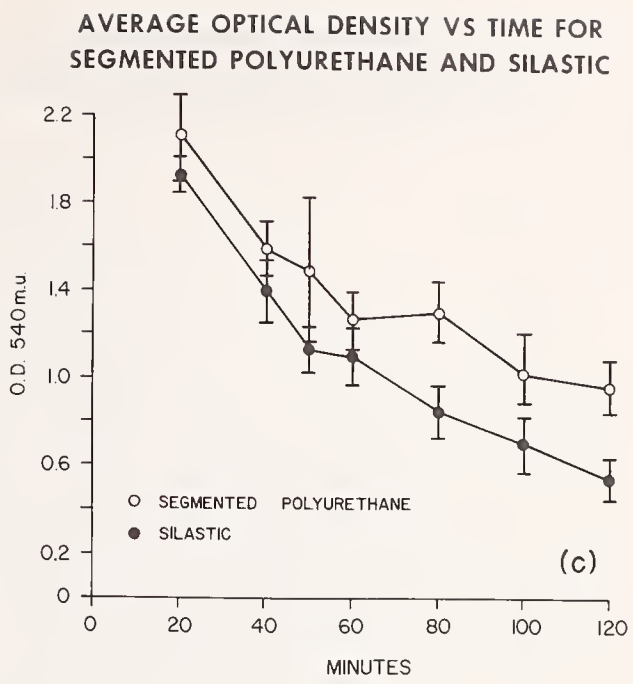

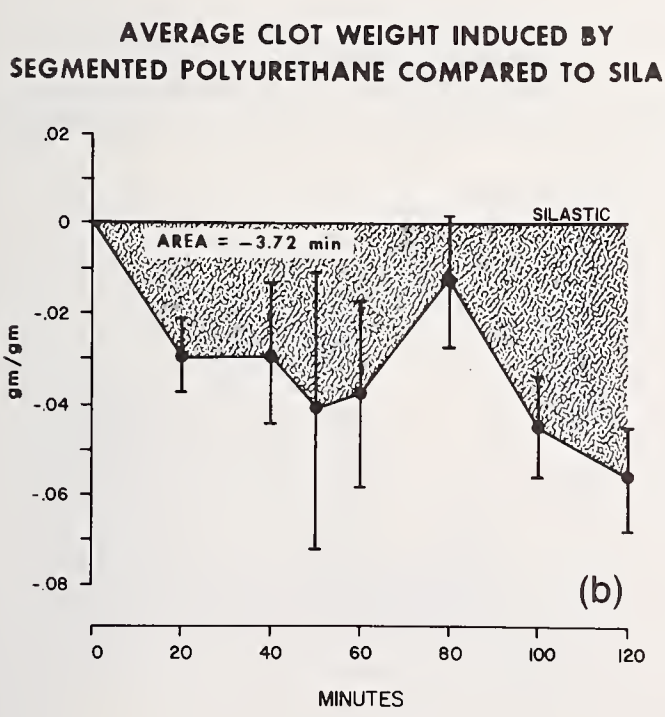

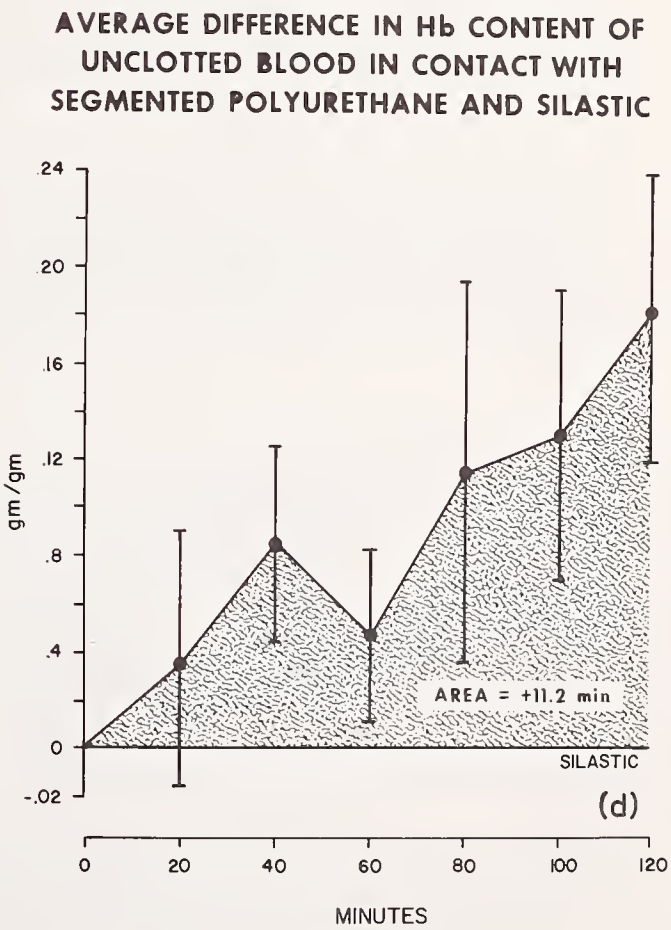

FIGURE 4. *Comparative blood compatibility of segmented polyurethane and Silastic.*

(a) average clot weight as a function of time; (b) average clot weight induced; (c) average optical density (hemoglobin content of unclotted blood) as a function of time; (d) average difference in hemoglobin content of unclotted blood.

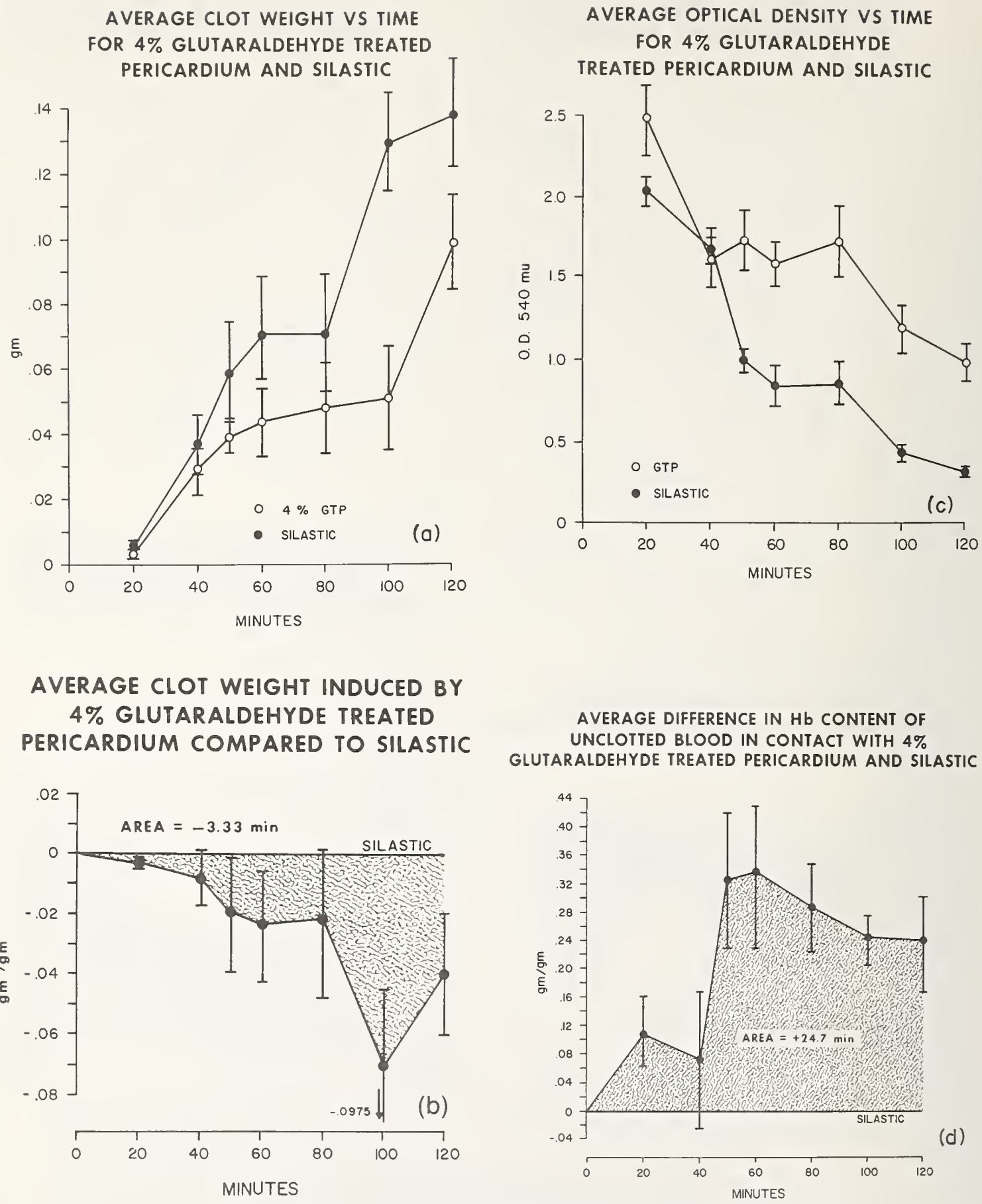

FIGURE 5. *Comparative blood compatibility of 4 percent glutaraldehyde-treated pericardium and Silastic.*

(a) average clot weight as a function of time; (b) average clot weight induced; (c) average optical density (hemoglobin content of unclotted blood) as a function of time; (d) average difference in hemoglobin content of unclotted blood.

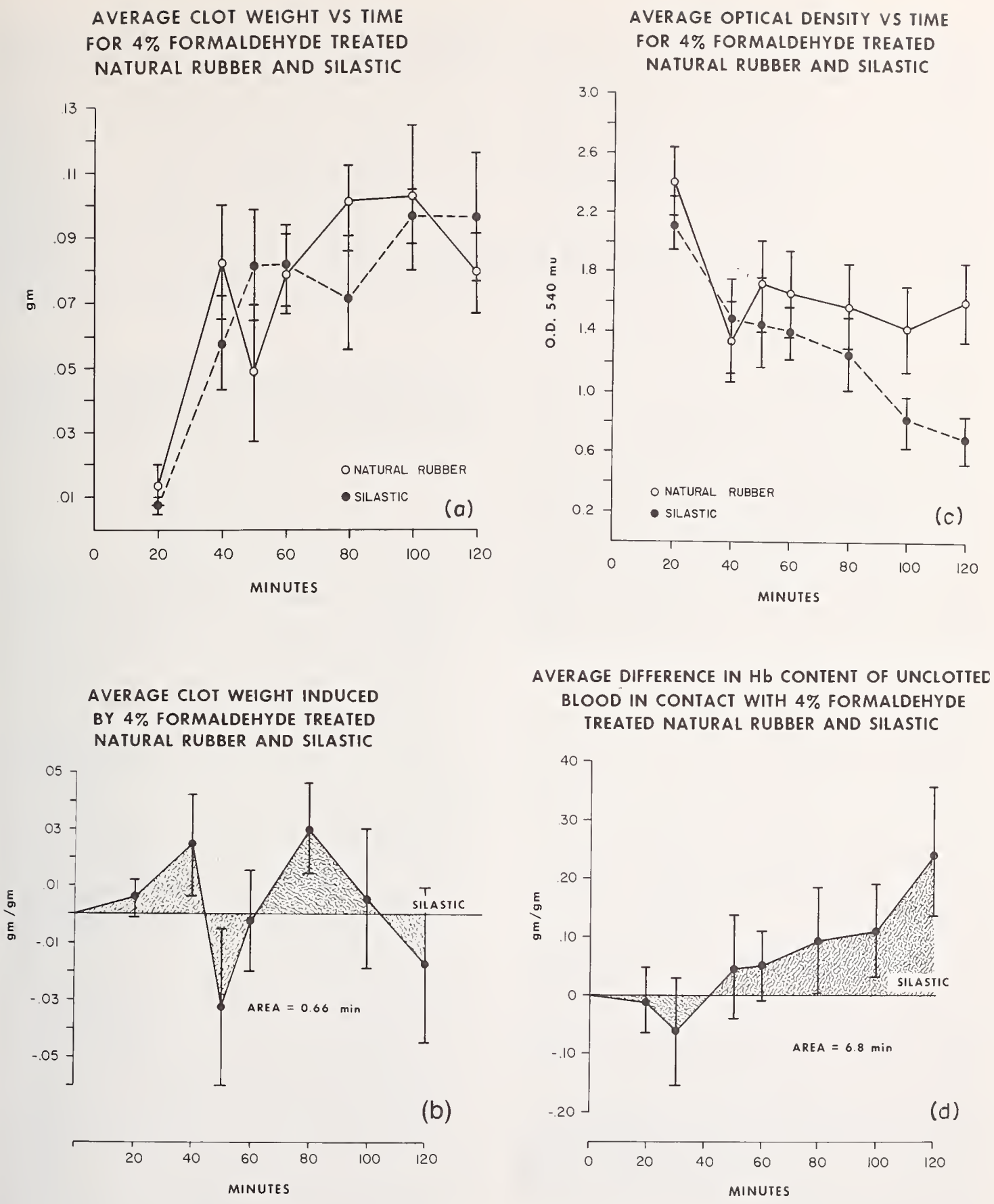

FIGURE 6. *Comparative blood compatibility of 4 percent formaldehyde-treated natural rubber and Silastic.*

(a) average clot weight as a function of time; (b) average clot weight induced; (c) average optical density (hemoglobin content of unclotted blood) as a function of time; (d) average difference in hemoglobin content of unclotted blood.

4. Discussion

In vivo screening tests for determining the thrombogenicity of materials have been proposed [4, 6]. Previous *in vitro* systems, even though simpler and less expensive, have not been readily adapted because of some experimental drawbacks such as blood-air interface, exposure to materials other than the one under study, and the need for anticoagulants [5, 7]. The kinetic closed cell test described herein minimizes these drawbacks [11]. Furthermore, the kinetics of the coagulation process can be followed; thereby determining the beginning, slope, and the end point of the reaction. This is not possible with *in vivo* tests. Moreover, *in vivo* testing involves variables which are extremely difficult to control, such as the blood flow patterns on the surface of the material analyzed.

The test uses material in sheet form; the need for special configurations is eliminated. Also, the ratio of material surface to the amount of blood is increased over previous methods [7]. The same cells can be utilized for analyzing other parameters of material blood compatibility. Preliminary data (fig. 7) illustrates the decrease in platelet counts induced by the listed materials, showing a significant difference between pericardium and the other three.

The variability of the blood properties requires that all tests be run with a simultaneous control. Silastic was selected as a control material, since it

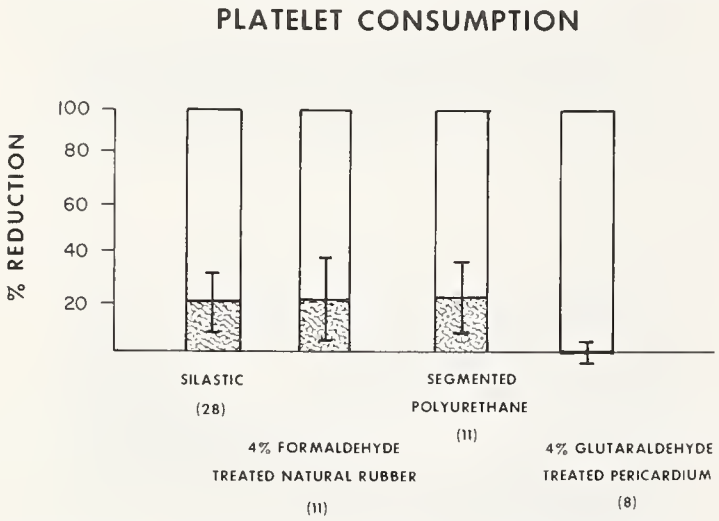

FIGURE 7. *Average platelet consumption by tested biomaterials.*

Numbers in parentheses indicate the number of individual tests made on each.

is readily available, and widely used for blood contacting devices. Results from individual tests can be affected by uncontrolled variables; therefore, a minimum of 10 tests is desirable for statistical evaluation of the data.

The results presented here show that this test can discriminate between different materials. If these *in vitro* results correspond with experimental and clinical results obtained by using the same materials in blood contacting applications remains to be demonstrated.

These materials can be rated quantitatively as to the rate of clot formation on their surface. Natural rubber proved to be the least desirable material with a direct modulus of 0.66 min. The blood compatibility of natural rubber is considered to be inferior to the other materials tested [2, 3, 8, 9, 10]. The direct clot modulus of polyurethane, Hydron, and glutaraldehyde treated pericardium was similar. The indirect modulus for the glutaraldehyde treated pericardium, however, was twice that of the polyurethane, suggesting a higher percentage of white clot formation.

The authors wish to thank T. Agishi, I. Koshino, and C. Carse for their technical assistance. Dr. J. Urzua provided advice in the preparation of the manuscript.

5. References

[1] Boretos, J. W., and Pierce, W. S., Segmented polyurethane: A polyether polymer, J. Biomed. Mater. Res. **2**, 121–130 (1968).

[2] Boretos, J. W., Detmer, D. E., and Donachy, J. H., Segmented polyurethane, II. Two years experience, J. Biomed. Mater. Res. **5**, 373–387 (1971).

[3] Bruck, S. D., Rabin, S., Fergusin, R. J., Evaluation of biocompatible materials, Biomat. Medical Devices and Artificial Organs **1**, 191–222 (1973).

[4] Gott, V. L., Keopke, D. E., Daggett, R. L., Zarnstorff, W., and Young, W. P., The coating of intravascular prosthesis with colloidal graphite—The relative importance of electrical charge in the prevention of clot formation, Surgery **50**, 382 (196).

[5] Imai, Y., and Nosé, Y., A new method for evaluation of antithrombogenicitv of materials, J. Biomed. Mater. Res. **6**, 165 (1972).

[6] Kusserow, B., Larrow, R., Nichols, J., Analysis and measurement of the effects of materials of blood, Proceedings of the Artificial Heart Program Conference (R. J. Hegyeli, Ed.), (National Institutes of Health, Bethesda, Md., June 9–13, 1969), U.S. Government Printing Office, Washington, D.C., p. 233.

[7] Lee, R., and White, P., A clinical study of the coagulation time of blood, Am. J. Med. Sci. **145**, 495 (1913).

[8] Leininger, R. I., Polymers as surgical implants, CRC Critical Reviews in Bioengineering (October 1972).

[9] Levowitz, B. S., La Guerre, J. N., Calem, W. S., Gould, F. E., Scherrer, J., and Schoenfield, H., Biologic compatibility and applications of Hydron, Trans. Amer. Soc. Artif. Int. Organs **14**, 82–87 (1968).

[10] Nosė, Y., Tajima, K., Ogawa, H., Klain, M., von Bally, K., and Effler, D. B., Cardiac prosthesis utilizing biological material, J. Thor. Cardiov. Surg. **62**, 714–724 (1971).

[11] Nosé, Y., Kambie, H., Kiraly, R., Komai, T., and Urzua, J., In vitro test of compatibility of blood with various natural and synthetic surfaces in: P. Didisheim, T. Shimamoto, and H. Yamazaki, Editors, Platelets, Thrombosis, and Inhibitors, Seminar Proceedings, Honolulu, Hawaii, Dec. 19–21, 1973 (Stuttgart-New York: F. K. Schattauer Verlag, 1974), pp. 87–95.

NATIONAL BUREAU OF STANDARDS SPECIAL PUBLICATION 415,
Biomaterials, Proceedings of a Symposium held in conjunction with the Ninth Annual Meeting of the Association for the Advancement of Medical Instrumentation, New Orleans, La, April 19–20, 1974
(Issued May 1975).

Conformation of Adsorbed Blood Proteins

B. W. Morrissey, L. E. Smith, C. A. Fenstermaker, R. R. Stromberg, and W. H. Grant

National Bureau of Standards, Institute for Materials Research, Washington, D.C. 20234

The likelihood that surface-induced blood coagulation results from specific interactions between proteins and materials has led to a study of the conformation of adsorbed blood proteins. Infrared difference spectroscopy was used to determine the bound fraction, i.e., the fraction of carbonyl groups of an adsorbed molecule directly interacting with a silica surface, and ellipsometry was used to measure the average extension (thickness) of adsorbed protein films. *In situ* measurements were made on serum albumin, fibrinogen, and prothrombin as a function of the amount adsorbed, time of adsorption, and surface energy.

The bound fraction results obtained for serum albumin and prothrombin indicate that the internal bonding of these globular proteins is sufficient to prevent changes in conformation while adsorbed. even at low surface population. The bound fraction of fibrinogen increases with increasing adsorbance, suggesting possible interfacial aggregation. The conformation of all three proteins was found by both I. R. difference spectroscopy and ellipsometry to be independent of the time of adsorption. In addition, the ellipsometric studies show that while the adsorbance of fibrinogen and prothrombin does not vary for a number of surfaces, their extensions increase with decreasing surface energy.

Studies of cross-linked and denatured serum albumin have shown that changes in conformation concomitant with adsorption of the native protein, if they occur, are small.

Key words: Adsorbed protein conformation; blood protein; protein conformation.

1. Introduction

Proteins and enzymes localized at interfaces play an important role in many biological phenomena. Matrix insolubilized enzymes are utilized clinically and commercially [1],[1] glyco-proteins on the cell surface can promote and control both cellular aggregation [2] and cellular growth [3], the cytochrome enzyme system for oxidative phosphorylation is localized on the mitochondrion membrane [4], while the deleterious effect of materials on blood resulting in surface-induced coagulation has long been recognized [5–7]. The possible effects of a given surface on a protein mixture include permanent or reversible adsorption with or without denaturation, preferential adsorption of specific proteins, and changes in the protein microenvironment. The details of these interactions can best be understood by determining the conformation of the adsorbed molecule and the conformational changes concomitant with adsorption.

Various techniques have been utilized for the determination of the conformation of adsorbed proteins. Adsorbed molecular area and solution dimensions have been compared by Bull [8] for egg albumin using film balance techniques, and by Brash and Lyman [9] for numerous serum proteins using infrared internal reflection spectroscopy. Perturbations in the transmission fluorescence spectrum arising upon adsorption of trypsin and chymotrypsin were analyzed by Katchalski [10] to demonstrate conformational changes, while Loeb and Harrick [11] induced fluorescence of adsorbed serum albumin using internal reflection techniques and showed that the protein is apparently native when adsorbed. Kochwa and coworkers [12] applied potentiometric titrations to show that γG-globulin apparently unfolds upon adsorption to a polystyrene latex under conditions of low surface coverage and acquires an antigenicity similar to that of heat denatured material. Ellipsometry has been used qualitatively by Vroman [13] to study sequential, competitive adsorption of blood proteins. As indicated by these studies, protein adsorption is a complex process and each technique provides only partial answers. As a result, a consistent model of protein adsorption at the solid-solution interface does not exist at present.

In general, an adsorbed polymer is attached to the surface at a number of locations along the chain. Adsorbed segments can occur singly or in runs with attached portions separated by loops of unattached segments which extend away from the surface into the solution as shown in figure 1. The number and arrangements of the attached portions and the size and distribution of the unattached

[1]Figures in brackets indicate the literature references at the end of the paper.

FIGURE 1. *Schematic representation of a random coil polymer adsorbed with few attachments and large loops.*

loops and tails define the conformation of the adsorbed polymer molecule [14]. In the case of proteins, numerous internal constraints limit the accessible conformations, both in solution and on the surface, and make the prediction of the adsorbed conformation more difficult.

In this paper we review some of our studies [15] of the direct measurement of both the number of protein carbonyl group-surface attachments made using infrared difference spectroscopy, and the average dimensions of the adsorbed protein layer determined ellipsometrically for a number of blood proteins and materials. These results are viewed as providing essential information on the conformation and conformational changes of the adsorbing molecule. These studies have been carried out *in situ* on individual proteins as a function of the amount adsorbed, time of adsorption, and surface energy of the adsorbent. Additional information on blood-protein-material interactions is essential to an understanding of surface-induced coagulation and the development of a rational approach to the selection of thromboresistant materials.

2. Techniques

The interaction of the chromophores of an adsorbed molecule with a surface frequently results in a shift of their characteristic spectral absorption bands. For the protein studies presented here, a shift of -20 cm^{-1} of the amide I band for free and bound carbonyl groups was typically observed. Since there is a significant overlap of these two bands, difference techniques must be utilized. From the data obtained, one determines the bound fraction, i.e., the fraction of carbonyl groups of an adsorbed protein directly interacting with the surface. The number of carbonyl attachments may then be calculated using the known amino acid composition of the protein.

Fontana and Thomas [16] originally described a method whereby a polymer is adsorbed from solution on a high surface-area powder, the suspension centrifuged, and an infrared difference spectrum recorded for the resulting gel. To prevent the introduction of uncertainties in polymer concentration, this method has been modified [17] to permit a direct analysis of the suspension. This modification has been used by a number of investigators [18–20] to study the conformation of synthetic polymers adsorbed from organic solvents.

For the determination of the bound fraction for an adsorbed protein, it is necessary to use D_2O solutions of deuterated proteins to obtain a window in the 1650 cm^{-1} region. The difference spectrum resulting from a protein solution-silica suspension in the sample beam versus the same protein solution in the reference beam (fig. 2) was resolved using a Beer's Law analysis of the optical density of the unbound peak.

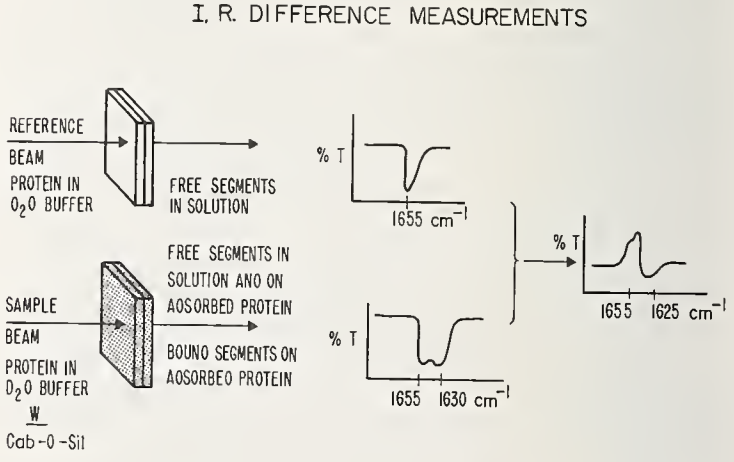

FIGURE 2. *Schematic of infrared difference spectroscopy measurements showing idealized signals and actual resulting difference spectrum.*

The technique of ellipsometry has been described in detail [21], and its application to the study of polymer adsorption from solution *in situ* has been

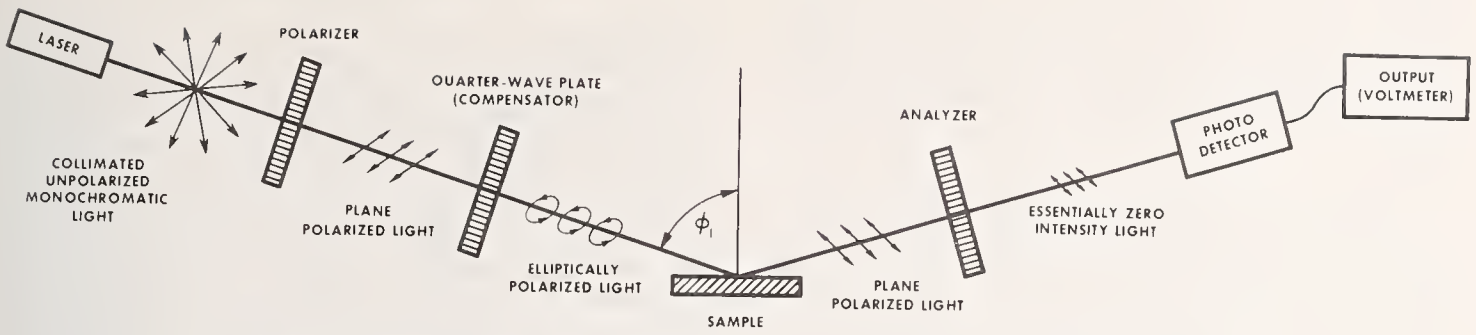

FIGURE 3. *Schematic showing arrangement of ellipsometer components used in protein studies.*

discussed [22]. Briefly, ellipsometry is an optical technique in which changes in the state of polarization of light upon reflection from a surface (fig. 3) are analyzed to characterize the surface and to determine the thickness and refractive index of a thin film on the surface. The thickness of a protein film on a surface is related to the extension and distribution of loops as shown in figure 1. This average extension of the adsorbed molecule normal to the surface is therefore a measure of the dimensions of an undisturbed protein layer on the surface. Calculations of the average extension utilize an iterative solution [23] of the Drude equations [24]. Additionally, one calculates the amount of protein adsorbed using the experimentally measured film refractive index and the refractive index increment for the protein at the wavelength of light of the measurements. These calculations are, however, based upon the model of a homogeneous film of constant refractive index and discrete boundaries. Since an adsorbed protein film would probably be an inhomogeneous film with refractive index decreasing with distance from the surface, the calculated values reported represent an upper bound for the thickness. Appropriate inhomogeneous film models [25] may be utilized to relate the average extension to actual molecular dimensions.

3. Experimental Detail

The proteins selected for study are either major constituents of blood plasma or are implicated as being important in the clotting process.

3.1. Ellipsometry

Human serum albumin (4× crystallized) and bovine prothrombin (Cohn III–2) were obtained from Nutritional Biochemicals (NBC)[2] and used without further treatment. Human fibrinogen (NBC) was purified by the procedure of Batt, et al. [26], a modification of a procedure developed by Laki [27].

Commercial ferrotype plate consisted of chromium electroplated on either brass or stainless steel. Platinum was 99.95 percent pure and rolled to a mirror finish. The quartz was fused silica. These materials were cleaned before use with hot 50:50 HNO_3:H_2SO_4 followed by three rinses in boiling distilled water. They were then heated for 5 minutes at 500° in a muffle furnace and placed while still warm into the adsorption cell filled with buffer.

Low temperature laminar (LTL) type pyrolytic graphite was kindly supplied by Dr. Jack Bokros of General Atomic Corp. Commercial polyethylene sheet was cleaned in ethanol and cast under vacuum at 180° between plate glass sheets. Several samples were prepared from NBS Standard Reference Material 1475 linear polyethylene which has a density of 0.978 g/cm^3, also by casting against glass under vacuum. All results on these two types of polyethylene were identical. The carbon and polyethylene samples were cleaned before use by refluxing with ethanol for two weeks in a Soxhlet extractor followed by a similar washing with distilled water.

All solutions were made up in pH 7.4 phosphate buffer and concentrations were determined by UV spectroscopy. All adsorption measurements were made in a cell thermostatted at 37 ± 0.1 °C.

3.2. Infrared Difference Spectroscopy

Bovine serum albumin (4× crystallized), bovine fibrinogen (Cohn fraction I, 60% clottable), and bovine prothrombin (fraction III–2) were obtained from NBC. The serum albumin was deuterated [28], lyophilized, and stored in vacuo at 4 °C. The prothrombin was dissolved in 0.1*M* D_2O phosphate buffer pD 7.4, dialyzed overnight against buffer, and filtered through a well washed 0.8 μm pore size filter just prior to use. Fibrinogen was purified by the method of Laki [27] with the following modifi-

[2]Certain commercial materials and instruments are identified here and elsewhere in this publication in order to adequately specify the experimental procedure. In no case does such identification imply recommendation or endorsement by the National Bureau of Standards, nor does it imply that the equipment or instruments identified are necessarily the best available for the purpose.

cations: The ammonium sulfate precipitate was resuspended in the pD 7.4 phosphate buffer and dialyzed overnight against the same buffer. The resulting solution was filtered and used immediately. These protein solutions were prepared using 0.1*M* D_2O phosphate buffer which was standardized using NBS standard reference materials 2186–I and 2186–II. Adjustments of pD were made with DCl or NaOD. Ionic strength was adjusted with KCl.

The mild heat denaturation of serum albumin was carried out at 66 °C [28]. The quantitative, limited, reduction of disulfide bonds of serum albumin was performed by the method of Sela et al. [29], using a reaction time of 1.5 hours and omitting the urea.

Serum albumin was cross linked using diethyl malonimidate dihydrochloride. This reagent was prepared from malononitrile and HCl gas in anhydrous ethanol-dioxane according to McElvain and Schroder [30]. The reaction of diethyl malonoimidate dihydrochloride with serum albumin generally followed Dutton et al. [31], using a 1.5 percent protein solution and a reaction time of 1 hour.

The adsorbent used for all experiments was a fumed, nonporous silica with a nominal particle size of 0.012 μm (Cab–O–Sil M–5, Cabot Corp.). The adsorbent was heated in vacuo at 110 °C overnight and cooled over silica gel just prior to use. The surface area, as determined by BET N_2 analysis, was 204 ± 20 m^2/g.

The adsorption isotherms were determined at 23.5 ± 0.5 °C. Known amounts of silica and protein solution were shaken for three hours and the silica then removed by filtration through a 0.8 μm filter. The amount of adsorbed protein was determined from the protein concentration changes measured spectrophotometrical at 280 nm. Changes in the ratio of silica to protein solution volume produced no effect on the protein adsorption isotherms. For studies of adsorbance as a function of time, the quantities of silica and protein solution were suitably scaled up and aliquots withdrawn and filtered with time.

For bound fraction studies, 0.029 grams of silica per ml protein solution was found generally to give stable suspensions suitable for infrared analysis. The difference spectrum of the protein-silica suspension versus the same protein solution was obtained for the region 1750–1550 cm^{-1} using matched 0.1 mm CaF_2 cells at 10× ordinate expansion. The extinction coefficient of the adsorbed carbonyl group was obtained by scanning successive dilutions of the reference solution against the protein-silica suspensions and noting the dilution at which the peak due to the unbound chromophores disappeared. Each reported bound fraction value represents the average of from two to four infrared scans on the same protein suspension.

4. Results and Discussion

4.1. Number of Attachments

The isotherms of serum albumin and prothrombin are given in figure 4 along with values of the bound fraction. The bound fraction of fibrinogen was found in general to depend on the equilibrium concentration (and hence the adsorbance). The results of a set of four experiments on fibrinogen are shown in figure 5. In each experiment, purified protein was utilized to prepare solutions covering a range of concentrations. Portions of the fibrinogen isotherm were inaccessible for bound fraction measurements using the technique described above because of the large adsorbance of this protein coupled with the limited solubility of fibrinogen in the D_2O–phosphate buffer which prevented the preparation of highly concentrated solutions for the adsorption experiments.

For serum albumin and prothrombin, no systematic change in the bound fraction was apparent over the measured portion of each isotherm. The mean values with their computed standard deviations were 0.11 ± 0.02 and 0.11 ± 0.03 for serum albumin and prothrombin respectively. Results for fibrinogen show an increase in the bound fraction with increasing amount adsorbed. The dashed line in figure 5 represents a least-squares linear fit to the data. The unstable nature of the fibrinogen-silica suspension is at least partially responsible for the large scatter in the bound fraction values, and, in conjunction with the high adsorbance, prevented measurements of the bound fraction at larger adsorbance values.

The number of carbonyl contacts made per molecule with the silica surface can be calculated using the bound fractions reported and the total number of carbonyl groups per protein obtained from the amino acid compositions. The bound fraction data reported then translate into a minimum of 77 contacts with the silica surface for serum albumin, 80 for prothrombin, and 176–703 for fibrinogen, as shown in table 1. If the adsorbed protein molecules were spread nearly flat on the surface, large values of the bound fraction would be expected. Adsorption of poly(ethylene o-phthalate) [19], poly(methyl methacrylate) [18], polystyrene [20], and poly(4-vinyl pyridine) [17] on Cab–O–Sil gave bound fractions of 0.37, 0.35, 0.24, and 0.35 respectively. In each of these cases, the synthetic molecules appear to lie close to the surface in a presumably spread condition. Since bound fractions of 0.11 were obtained for prothrombin and serum albumin, the adsorbed protein molecules were still relatively unchanged by the surface, despite the large number of attachments and great interaction.

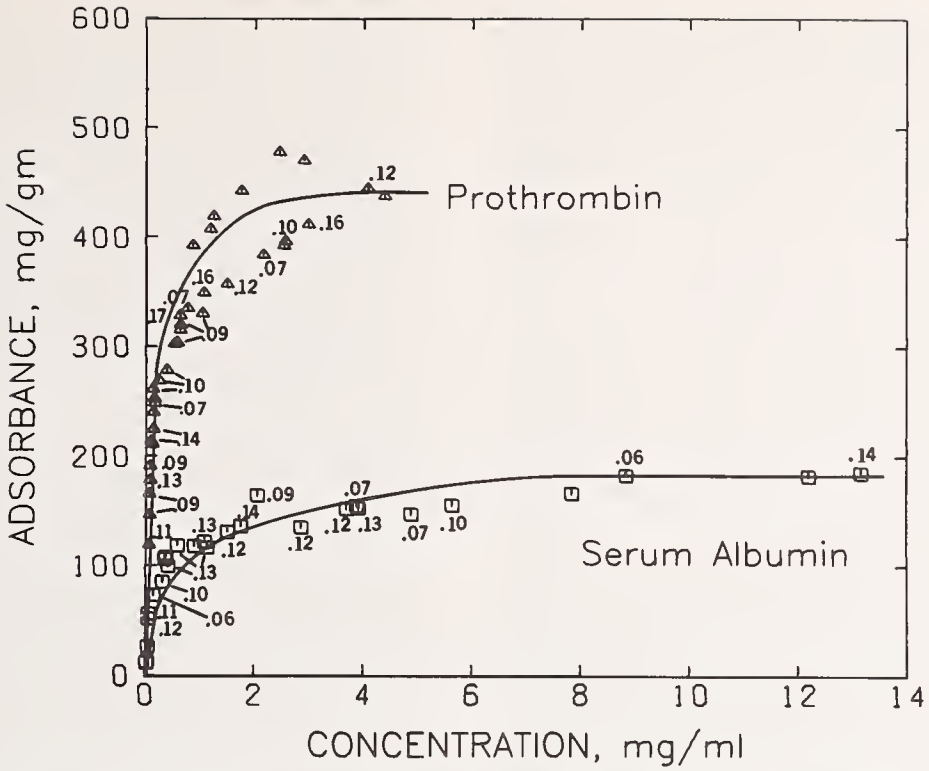

FIGURE 4. *Adsorption isotherms for bovine serum albumin and prothrombin at pD 7.4 on silica.*

Values of bound fraction given for isotherm points.

The bound fraction data can yield information on changes in the conformation of the adsorbed protein molecule as a result of increasing competition for surface sites. A decrease in the bound fraction values with increasing surface population would be expected if changes in conformation were to occur. Such changes in conformation of synthetic random coil polymers have been observed [17, 18, 22]. It has been argued [33, 34] that an adsorbed serum albumin molecule should initially unfold, thereby increasing the value of p, the bound fraction, which would presumably then decrease with increased surface population. Our results for serum albumin and prothrombin, figure 4, show that the bound fraction remains constant, indicating that the conformation does not change as the surface population increases. The relatively low value of the bound fraction for these proteins as compared to the synthetic polymers, and the constant value of the bound fraction over the isotherms, strongly suggests that the internal bonding and disulfide

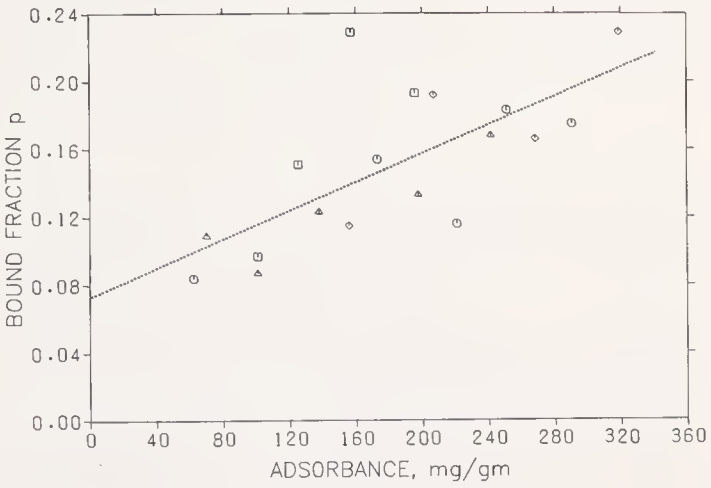

FIGURE 5. *Bound fraction versus adsorbance of bovine fibrinogen for four different experiments.*

Each symbol represents a separate run. Adsorption at pD 7.4 on silica. [Reprinted from Ref. 15, J. Colloid Interface Sci.]

TABLE 1. *Summary of adsorption and bound fraction data for proteins*

Protein	Maximum adsorbance mg/g	Maximum adsorbance mg/m²	Equil. Conc. for Maximum adsorbance mg/ml	Bound fraction	No. Carbonyl contacts per molecule with surface
Serum albumin	180	0.88	11.0	0.11	77
Prothrombin	440	2.16	4.0	0.11	80
Fibrinogen	890	4.36	1.0	0.05–0.20	176–703

crosslinks of the globular proteins are sufficient to preserve the basic tertiary structure of the molecules.

The adsorption behavior of fibrinogen (fig. 5), which shows a direct dependence of bound fraction on adsorbance, does not necessarily represent a conformational change. As noted above, previous experience with synthetic polymers has shown that conformational changes resulting from increases in surface population are accompanied by decreases in the bound fraction. The bovine fibrinogen molecule is rodlike with a length of between 400–600 Å [35] and can easily interact with more than one silica particle. It has been postulated [36] that the solubility of fibrinogen is due to electrostatic repulsion between regions of high negative charge density localized in fibrinopeptides A and B. If adsorption and interaction with the hydrophilic surface were to effectively neutralize this repulsion, fibrinogen molecules adsorbed to different silica particles could interact like fibrin, thereby increasing the surface attachments of each fibrinogen molecule. Such an interfacial aggregation [34] could result in an increase in bound fraction values with increasing adsorbance, without significantly hindering further adsorption to the remaining available surface.

Our data for maximum adsorbance can be converted to amounts/unit area using the measured surface area. These results are presented in table 1 and agree quite favorably with those found for adsorption of human blood proteins on quartz using the ellipsometric techniques. Results obtained by MacRitchie [34] for adsorption of bovine serum albumin on a silica surface (also 200 m^2/g) at pH 7.5 were only one third as great as that found in the present study, while adsorption on flat polymer surfaces determined using internal reflection techniques [9] gave generally higher amounts. The reasons for these differences are not obvious.

The possibility that the conformation of the adsorbed protein might vary as a function of the time of adsorption was tested by determining the bound fraction for each protein periodically following the formation of a suspension. Figure 6 illustrates some typical results obtained for serum albumin, prothrombin, and fibrinogen where the bound fraction values are listed over each curve at the time of measurement. The rates of adsorption cannot be compared since the initial conditions are different for each experiment. It is clear that there is no variation in the bound fraction for any of the proteins over the time period investigated at

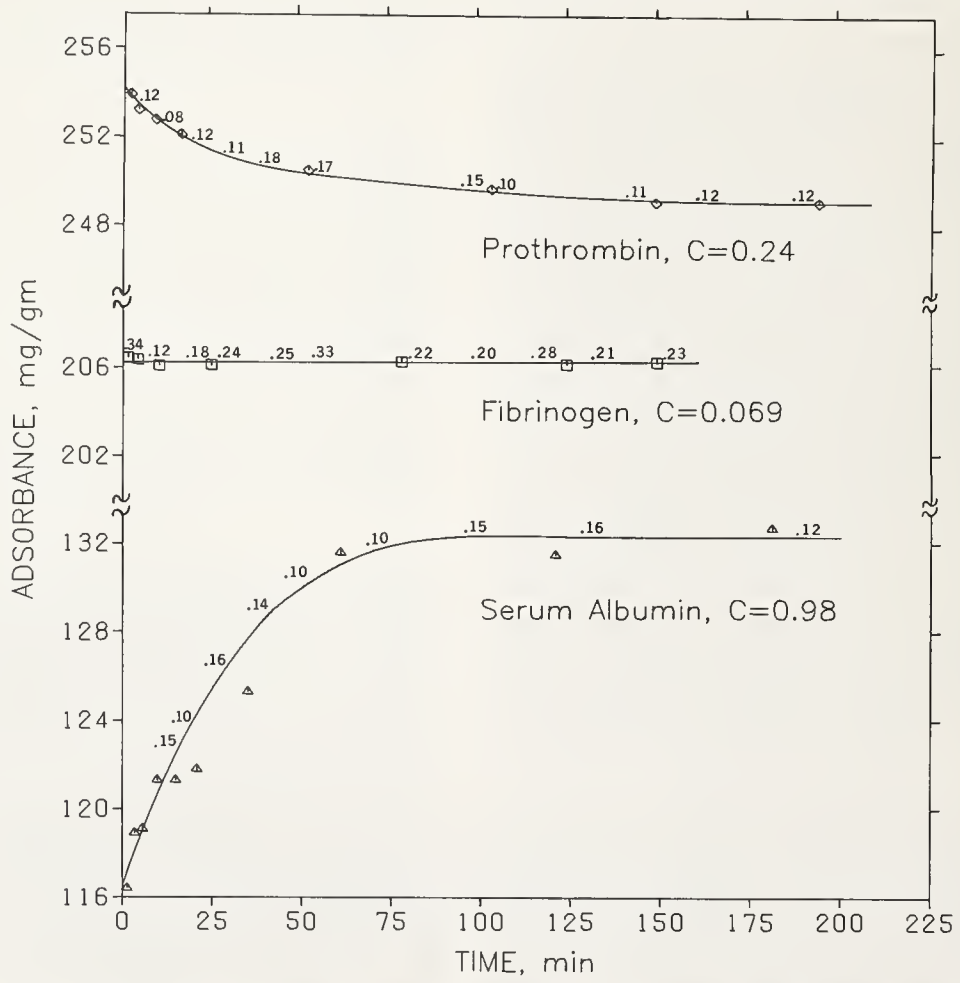

FIGURE 6. *Adsorbance versus time for bovine serum albumin, prothrombin, and fibrinogen.*

Values of bound fraction are given over each curve at the time measured. Adsorption at pD 7.4 on silica. [Reprinted from ref. [15], J. Colloid Interface Sci.]

these conditions. This indicates that molecular rearrangements do not occur following adsorption at the concentrations studied. Although the adsorption rates for prothrombin and fibrinogen were extremely high as a result of the conditions required for bound fraction measurements, the relatively slow adsorption of serum albumin allows measurements of the bound fraction as a function of time which shows that the conformation is not dependent upon the surface population, as was found in the equilibrium adsorption studies (fig. 4). The slight decrease in adsorbance of prothrombin with time in figure 6 is possibly caused by a dissociation at the low final solution concentration. Prothrombin has been reported [37] to associate reversibly at low ionic strengths.

The conformational changes of blood proteins upon adsorption are extremely important to any understandting of surface induced coagulation. A *priori*, one does not know how much denaturation, if any, occurs upon adsorption of native proteins. The effects of any such denaturation are necessarily included in our values of the bound fraction. The presence of an infrared shift in the difference spectrum for the bound carbonyl group does not necessarily mean that protein denaturation has occurred upon adsorption. The shift may occur for adsorbed protein, even if the tertiary structure has not changed. It is possible, however, with the aid of certain assumptions to gain some insight regarding the amount of distortion of the molecule that occurs upon adsorption.

The observed bound fraction for serum albumin can be considered to be the sum of two contributions: the first due to contacts permitted by the native tertiary structure with the surface and the second resulting from surface induced rearrangements that occur as a consequence of adsorption. These contributions can be separated by determining the bound fraction of a highly cross-linked, and therefore rigid, material. Cross-linking of serum albumin with diethyl malonimidate dihydrochloride [32] produces a protein which is resistant to denaturation, has the same electrophoretic mobility, and most important, retains the same antigenic activity as native serum albumin. We prepared such a cross-linked material which had 45% of its free amino groups blocked [38]. The average result of six experiments shown in table 2 gave a bound fraction which was experimentally indistinguishable from that of the native protein. We conclude that surface induced rearrangements, if present in native serum albumin, are small.

As a further means of assessing the conformational change of native serum albumin upon adsorption, we have denatured the protein under mild conditions and determined the bound fraction of the denatured material when adsorbed. Table 2 lists the results for heat denaturation at 66 °C and thioglycollic acid reduction. It is clear that the bound fraction for a given protein is strongly dependent on its tertiary structure. Heating, which causes the irreversible aggregation of serum albumin [39], leads to a bound fraction one third that of native material. Mild reduction, where one disulfide bond was broken as determined by a *p*-chloromercuribenzoate titration [30], leads to a bound fraction of about 1½ times that for native protein.

TABLE 2. *Bound fraction of modified serum albumin*

Sample	Bound fraction
Native (control)	0.11
Cross-linked	0.10
Heated at 66 °C (2–60 min)	0.04
TGA reduced	0.19

These studies also shed light on the conformation of native adsorbed serum albumin. If the native protein were unfolded by an amount equivalent to the breaking of one disulfide bond, an increase of 55 contacts (tables 2 and 1) would result. On the other hand, pretreatment of the serum albumin in a manner which produces aggregates resulted in a decrease of 50 surface contacts, implying that no aggregation occurs upon adsorption of the native serum albumin. These results for denatured serum albumin show that bound fraction is sensitive to what in our view are small conformational changes.

3.2. Molecular Extension

Two aspects of the ellipsometric results should be considered, viz. the time dependence of the adsorption process and the long time or equilibrium value.

In general, no change in extension was observed during the time period from 10 minutes to 24 hours. However, there was a small, but definite increase in adsorbance. The absence of change in extension with adsorption time is a general feature found for all three proteins on all of the surfaces examined to date. Rates could not be inferred from these results as the ellipsometer cell was not stirred for these experiments. Extension measurements made at adsorption times shorter than 20 minutes generally showed poor reproducibility due to refractive index gradients present in the cell before temperature equilibrium is reached.

This behavior can be interpreted as indicating a lack of significant molecular rearrangement of the protein molecule once adsorption has taken place. In the early time periods, additional molecules are still arriving at the surface as evidenced by the increasing adsorbance, but the surface pressure of these molecules is not sufficient to cause the molecules already adsorbed to change their conformation. Nor, apparently, do the late arrivals adopt a significantly more extended conformation

than the majority of the adsorbed molecules. It should be noted that a random coil homopolymer has been shown to undergo a significant change in extension with the adsorption time indicating more conformational freedom [22].

Two general features are noted in the equilibrium adsorbance and extension values of the three proteins adsorbed on the various surfaces studied. First, in spite of the varied nature of the surfaces, the measured adsorbances covered only a small range. Typical results were from 2–4 mg/m^2 and the variations in adsorbance showed no relation to the surface energy. If surface energy is estimated by the critical surface tension for wetting, then the surface energies ranged from the high energy metals, chromium and platinum, to the low surface energy of polyethylene. There was, however, a correlation of surface energy with extension—the extension of a given protein increased with decreasing surface energy. Typical extensions vary from approximately 200 Å on the high energy surface to 5–600 Å on the lowest energy surface. This would be in accord with flat, tightly held conformations on the higher energy surfaces and looser, more extended conformations on the lower energy surfaces.

Secondly, the measured extensions cannot be construed as molecular dimensions of the adsorbed protein. The model assumed for the calculation of this extension is that of a film of homogeneous refractive index with discrete boundaries. Obviously, any large adsorbed molecule will show some refractive index inhomogeneities normal to the surface and this will affect the calculated extensions directly. This problem has been considered by McCrackin and Colson [25] who have shown that extensions calculated assuming a homogeneous film may be converted to root-mean-square segment to surface distances if the actual refractive index distribution is known. For example, the homogeneous film thicknesses have to be divided by factors of from 1.5 to 1.7 if the refractive index distributions are linear, gaussian, or exponential. As we have no estimate of the refractive index distribution of an adsorbed protein, we have no way of making such a conversion, but the homogeneous extensions may perhaps be considered an upper limit approximation to molecular dimensions. The relative values of the extension on the different surfaces may properly be compared assuming that the refractive index distribution does not change markedly from one surface to another.

This work was supported in part by the Biomaterials Program of the Division of Blood Diseases and Resources of the National Heart and Lung Institute.

4. References

[1] Mosbach, K., Sci. Amer. **224** (3), 26 (1971).
[2] Pessac, B., and Defendi, V., Science **175**, 898 (1972).
[3] Schnebli, H. P., and Burger, M. M., Proc. Nat. Acad. Sci. USA, **69**, 3825 (1972).
[4] Green, D. E., and Young, J. H., Amer. Sci. **59**, 92 (1971).
[5] Hulbert, S. F., King, F. M., and Klawitter, J. J., J. Biomed. Mater. Res. Symp. No. 2 (Part 1), 69 (1971).
[6] Bruck, S. D., Biomaterials, Med. Devices and Artificial Organs **1**, 79 (1973).
[7] Brash, J. L., and Lyman, D. J., in The Chemistry of Biosurfaces —M. L. Hair, Ed. (Marcel Dekker, Inc., New York. N.Y. 1971), p. 177.
[8] Bull. H. B., J. Colloid Interface Sci. **41**, 305 (1972).
[9] Brash, J. L., and Lyman, D. J., J. Biomed. Mater. Res. **3**, 175 (1969).
[10] Gable, D., Steinberg, I. Z., and Katschalski, E., Biochem. **10**, 4661 (1971).
[11] Loeb, G. I., and Harrick, N. J., Anal. Chem. **45**, 687 (1973).
[12] Kochwa, S., Brownell, M., Rosenfield, R. E., Wasserman, L. R., J. Immun. **99**, 981 (1967).
[13] Vroman, L., and Adams, A. L., Thrombos, Diathes. Haemorrh. **18**, 510 (1967).
[14] DiMarzio, E. A., and Rubin, R. J., J. Chem. Phys. **55**, 4318 (1971).
[15] A more complete account of part of this work has appeared in J. Colloid Interface Sci. **46**, 152 (1974).
[16] Fontana, B. J., and Thomas, J. R., J. Phys. Chem. **65**, 480 (1961).
[17] Thies, C., Peyser, P., and Ullman, R., Proceedings of the 4th International Congress on Surface Activity, Brussels, 1964, Vol. 2, Gordon and Breach, N.Y. 1967, p. 1041.
[18] Thies, C., J. Phys. Chem. **70**, 3783 (1966).
[19] Peyser, P., Tutas, D. J., and Stromberg, R. R., J. Poly. Sci. A–1, **5**, 651 (1967).
[20] Herd, J. M., Hopkins, A. J., and Howard, G. J., J. Poly. Sci. Part C, **34**, 211 (1971).
[21] McCrackin, F. L., Passaglia, E., Stromberg, R. R., and Steinberg, H. L., J. Res. Nat. Bur. Stand. (U.S.), **67A** (Phys. and Chem.), No. 4, 363–377 (July–Aug. 1964).
[22] Stromberg, R. R., Tutas, D. J., and Passaglia, E., J. Phys. Chem. **69**, 3955 (1965).
[23] McCrackin, F. L., A Fortran Program for Analysis of Ellipsometer Measurements, Nat. Bur. Stand. (U.S.), Tech. Note 479, 83 pages, (April 1969).
[24] Drude, P., Ann. Physik **272**, 532 (1889); **272**, 865 (1889); **275**, 481 (1890).
[25] McCrackin, F. L., and Colson, J. P., in Ellipsometry in the Measurement of Surfaces and Thin Films (Symposium Proceedings), E. Passaglia, R. R. Stromberg, and J. Kruger, Ed., Nat. Bur. Stand. (U.S.), Misc. Publ. 256, 365 pages (Sept. 1964), p. 61.
[26] Batt, C. W., et al., J. Biol. Chem. **245**, 4857 (1970).
[27] Laki, K., Arch. Biochem. Biophys. **32**, 317 (1951).
[28] Susi, H., Timasheff, S. N., and Stevens, L., J. Biol. Chem. **242**, 5460 (1967).
[29] Warner, R. C., and Levy, M., J. Amer. Chem. Soc. **80**, 5735 (1958).
[30] Sela, M., White, F. H., and Anfinsen, C. B., Biochem. Biophys. Acta **31**, 417 (1959).
[31] McElvain, S. M., and Schroeder, J. P., J. Amer. Chem. Soc. **71**, 40 (1949).
[32] Dutton, A., Adams, M., and Singer, S. J., Biochem. Biophys. Res. Comm. **23**, 730 (1966).
[33] Baier, R. E., Loeb, G. I., and Wallace, G. T., Fed. Proc. **30**, 1523 (1971).
[34] MacRitchie, F., J. Colloid Interface Sci. **38**, 484 (1972).
[35] Laki, K., Fibrinogen, p. 4, (Marcel Dekker, Inc., New York, N.Y., 1968).
[36] Laki, K., Op. Cit. p. 6.
[37] Tishkoff, G. H., Williams, L. C., and Brown, D. M., J. Biol. Chem. **243**, 4151 (1968).
[38] Shick, A., and Singer, S. J., J. Biol. Chem. **236**, 2477 (1961).
[39] Neet, K. E., and Putnam, F. W., J. Biol. Chem. **210**, 2883 (1965).

NATIONAL BUREAU OF STANDARDS SPECIAL PUBLICATION 415,
Biomaterials, Proceedings of a Symposium held in conjunction with the Ninth Annual Meeting of the Association for the Advancement of Medical Instrumentation, New Orleans, La., April 19–20, 1974
(Issued May 1975).

A Nerve Implant Prosthesis for Facilitating Peripheral Nerve Regeneration* Part I. Development of the Prosthetic Device and System of Repair

W. E. Kuhn

Department of Materials Science and Metallurgical Engineering

and

James L. Hall

Department of Anatomy, University of Cincinnati, Cincinnati, Ohio 45221

The design rationale and requirements of a system of sutureless nerve repair employing a special thin walled porous stainless steel tube and a vacuum technique for applying the tube and approximating the nerve ends will be outlined. A description of the tubular prosthesis, its fabrication, the surgical instruments and neurorrhaphical procedures will be presented.

A slurry dipping process has been developed for the production of uniform "green" tubes in quantity. These are sintered in a hydrogen atmosphere to impart the strength required to retain their tubular configuration under the forces imposed by the surgical procedures and the vacuum pressure. Placing the porous tube on the nerve and drawing the nerve ends into approximation is both simple and rapid.

Key words: Neurorrhaphical procedures; peripheral nerve repair; tubular prosthesis.

1. Introduction

The problem of peripheral nerve regeneration has been studied intensively by many investigators and has been found to depend on many factors. The most important of these are the patient's age, type of injury, length of tissue, and finally, the technique of nerve repair. A repair is satisfactory when it is executed with as little trauma as possible and when anatomic approximation is achieved. It is difficult to fulfill the requirements without magnification, microsurgical instruments, and the finest of sutures [1, 2][1]. Despite the advances that have have been made to date, the reestablishment of normal function in the damaged nerve is considered poor [3].

According to Hakstian, "One remaining frontier in which a successful breakthrough has" not yet occurred is that of peripheral nerve injury [4]. This is not surprising considering the complex structure of the peripheral nerve over its entire length and the unique manner of healing of this tissue compared to others. Whereas most other tissue, excepting tissue of the central nervous system, survive both distally and proximally of the injury site, nerve tissue (axons) degenerates peripherally [4].

If results are to improve, in addition to gaining greater understanding of the physiology and the pathology of neural tissue and processes of nerve regeneration, it will be necessary to attain greater sophistication in the surgical manipulation of nerve tissue. It is the latter goal that the present research is concerned with. More specifically, it is concerned with the repair of small nerves, that is, nerves 2 mm in diameter and less such as cranial, digital and facial nerves. Digital nerves are the most frequently severed peripheral nerves, and though small in size are of critical importance because of their properties of discriminatory touch [5]. Injury to facial nerves, though less common, is of tragic consequence because of loss of communication through expression, interference with speech and daily activities as eating, drinking, washing and shaving, and the impairment to social and economic welfare produced by psychological effects [6, 7, 8].

Of particular interest to us in the current study has been the use of other tissues or materials to form a channel through which the nerve fibers may grow and bridge the gap between the cut ends. Severed nerves have been drawn through blood vessels [9] or through decalcified bone tubes. Nerve fibers have also been wrapped in sheets of rubber, cargyl membrane, fascia lata or various other materials in an effort to reduce the ingrowth of scar tissue between the ends of the severed fibers. The methods employing organic materials

*This research was supported by the National Science Foundation under Grant GH–33873.

[1]Figures in brackets indicate the literature references at the end of this paper.

have been relatively unsuccessful, largely because phagocytes have removed the nerve covering prematurely. A tubulation method has found some success in neurorrhaphy, whereby sheets of Silastic are wrapped about the anastomosis [10, 11, 12, 13, 14.]. The success of this method for facilitating regeneration of nerves is questionable; further it suffers from the drawback of requiring the use of sutures. Methods employing adhesives, especially the cyanoacrylates, as a sutureless technique to anastomose severed nerves, though highly attractive, has so far been ineffective [15, 16].

2. Principles and Practice of Current Nerve Repair Techniques

In this new system of nerve repair it was considered essential to incorporate the applicable general principles employed in the three types of neurorrhaphy currently practiced, that is, epineurorrhaphy, perineurorrhaphy, and nerve grafts. These principles may be summarized as follows [17, 18, 19].

- Magnification to permit easier, more atraumatic identification, isolation, and preparation of nerve ends.
- Correct anatomic alignment which is mandatory.
- Use of a minimum of fine sutures to achieve approximation or eliminate sutures entirely.
- Tension across a suture line lends to the proliferation of connective tissue within the nerve and a decrease in axon regeneration.
- Ideal nerve repair occurs only when there is no tension at the repair site.
- Axons pass through two suture lines without tension more easily than through one suture line under tension.
- Fibrin adherance is of sufficient strength to maintain the approximation if the repair is accomplished without tension.
- Epineurium contributes to scar formation and should be resected.
- Fasicular grafts can survive without an established blood supply as a free graft, whereas larger grafts undergo central necrosis.

The surgeon using the epineural technique has little or no control over alignment and hence can never be fully confident that correct anatomical approximation has been achieved. Correct tension is essential for successful epineural nerve repairs. If the repair is too loose, a gap results, which will be filled with scar tissue. If the repair is too tight, buckling of the fascicles occurs. According to Bora, even if tension is exactly right, the chances of correct orientation of a fascicular level is only one in four [20]. To overcome the problems of epineural repair, such as gap, overriding, buckling and straddling of fascicles, the fascicular suture technique has been devised [4], whereby two sutures are placed in the perineurium on opposite sides of each fascicle and the severed ends approximated.

The use of sutures is minimized by techniques developed by Millessi, which depends on the use of grafts to eliminate tension [18, 19].

Nerve injuries are commonly repaired by approximating the severed nerve stumps with sutures through the epineurium, and through the perineurium where the fascicular suture technique is used. The very act of suturing destroys nerve fibers. Only the larger nerves can be sutured without serious damage to axons, and even these require a highly skilled surgeon. Thus, ideally, complete elimination of sutures is desired.

The most critical factor of technique in neurography is the accurate approximation of the cut ends of the fascicles. Even though other factors may be ideal, the neurography will fail if a significant number of fascicles do not match up. This is because motor axons regenerating through the sheaths of sensory nerves and vice versa will give no return of sensory or motor function. The fascicles of the larger nerves, such as the median and ulnar nerve, are large enough in cross sectional area that the cut ends of individual fascicles can be matched up by using the epineural vascular pattern for rotational orientation and microsurgical suture techniques. The fascicles of the small diameter nerves however, are too small to be matched by suturing. The best that can be done is to approximate the nerve ends using recognizable vascular patterns for correct anatomical alignment. If the peripheral nerve is cleanly and squarely severed, a primary repair can be made with good approximation of the fascicles. However if a segmental deficit exists, the likelihood of surgical orientation or matching of fascicles becomes a matter of chance. This is attributed to the twisting and plexiform course of the fascicles and axons within the nerve trunk [3]. It is apparent then, except in the instance of a clean cut followed by a primary repair, that a repair of nerves, successful in all other respects, will depend on the chances that the fascicles will match up, unless some natural mechanism exists for directing the axons to sheaths of their own. In this regard Peacock reports evidence of rotation and reorientation into good anatomical alignment prior to a secondary suture of a nerve previously joined at a single point of junction, even when the ends were 180° apart when the suture was first placed [21].

The matching fascicles becomes less of a problem with the smaller nerves, since there are fewer fascicles, often no more than one, to contend with. Thus the chief hazard to the successful repair of fine nerves is the trauma produced by sutures and manipulation of the nerve and invasion of the field of regeneration by epineural and extraneural connective tissue. Many attempts have been made, almost entirely with larger nerves, to shield the region of anastomosis from connective tissue and facilitate longitudinal directional growth of the epineural and nervous tissue.

A most recent and promising approach by Millessi dispenses with wrappings altogether, eliminates tension in the field of regeneration, and uses a minimum of sutures [19]. This approach has been extended experimentally to the sciatic nerves of rabbits to the complete elimination of sutures. This technique depends on the use of a graft to eliminate tension and the natural adhesive properties of the nerve ends to hold them in a position of close anatomical approximation. The strength of the union can amount to several grams after the first 15 to 30 minutes, sufficient to prevent separation of the ends and allow closure of the incision [22].

3. Design Requirements for Tubular Nerve Prosthesis

Consideration and understanding of anatomical and functional features, pathophysiology of nerve degeneration and regeneration, and the principles behind current techniques of nerve repair, suggested the following design requirements for a porous thin-walled tube that could, with proper surgical procedures, facilitate nerve repair and regeneration in small diameter nerves:

- The tube material must be compatible with its biological environment and be nontoxic. No residual substances must remain after processing that will react deleteriously with the nerve tissue or the biological processes contributing to healing.
- The technique of application must facilitate approximation of nerve ends quickly with a minimum of manual manipulation. A method of vacuum approximation has been developed which successfully accomplishes the approximation procedure.
- The tube design must incorporate means to remove the tube without damage to the nerve after healing has progressed sufficiently to permit its removal.
- The tube must possess a combination of porosity and wall thickness that imparts to the tube a sufficient degree of permeability to provide adequate diffusion and flow of intraneural and extraneural fluids.
- The tube must possess a combination of porosity and wall thickness that minimizes the surface area of the tube consistent with enough strength to withstand physical insults. Minimum surface area minimizes the release of toxic substances to the surrounding tissue.
- The pore size of the tube walls must be such as to prevent ingrowth of extraneural connective tissue and, thereby, shield the field of regeneration.
- The pore size of the tube must be such as to discourage the ingrowth of intraneural connective tissue and, thereby, avoid the occurrence of adhesions between the inner wall of the porous tube and epineural tissue.
- The tube must possess strength to rigidly support and shield the joined nerve against buckling and crushing by outside as well as internal forces.
- The method of fabricating tubes must satisfy the requirements of the models selected for evaluating the efficacy of this method of nerve repair. This method of fabrication must be capable of producing many tubes simultaneously having a uniform size and configuration to a wide range of specifications determined by transverse dimensions and shape of the nerve. A standard size is essential for biostatistical comparison studies of nerve repair parameters.

4. Method of Approach and Organization of Research Effort

The general approach taken was to first undertake an exploratory program encompassing all essential activities that would lead to a system of neurorrhaphy employing porous thin-walled tubes. The main development activities, outlined in figure 1 are summarized in table 1.

TABLE 1. *Major development activities*

- Development of tube Fabrication Process
  - Development of comminution process for metal coating slurries
  - Development of coating process for making green tubes
  - Development of sintering process for thin walled tubes of controlled porosity and pore size.
- Development of Surgical Instruments for Applying Porous Tubes.
- *In-vivo* testing of porous tube, surgical instruments and surgical procedures.
- Study of post operative functional behavior of rats and post sacrificial histological studies of anastomosed nerves.

Parallel development and study of the four main activities shown in table 1 permitted earlier production of tubes and hence, an earlier start on surgical and histological procedures than otherwise

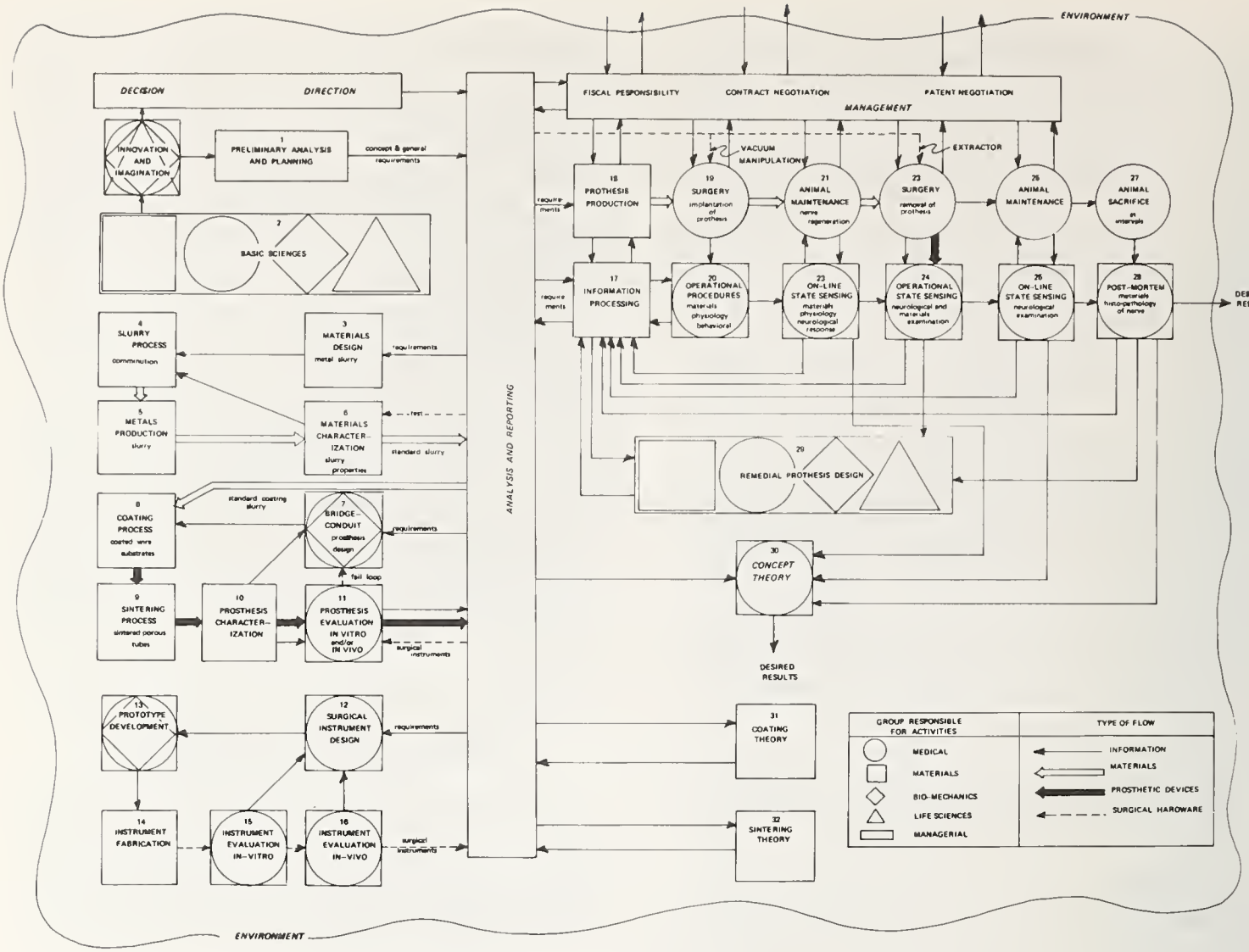

FIGURE 1. *Activity chart.*

would be possible. Further, the feedback of information, especially from surgical experiments, hastened the solution of many problems related to the design of the surgical instruments and prosthetic device.

5. Concept of Method of Nerve Repair and Evaluation Model

Essentially, the method employs a porous thin-walled tube similar to that shown in figure 2. A small hole is drilled through one side of each tubular sleeve at the ⅓ point along its length to serve as a vacuum port. The porous tube is fitted snugly into a matching groove in an adapter at the termination of the barrel of the "anastomizer" making a "T" connection with it. (See figs. 3 and 4). The vacuum port in the porous tube is positioned to match the opening at the bottom of the groove in the adapter.

FIGURE 2. *Porous tube having two diametrically opposite longitudinal micro-slots made by a spark discharge machining technique.*

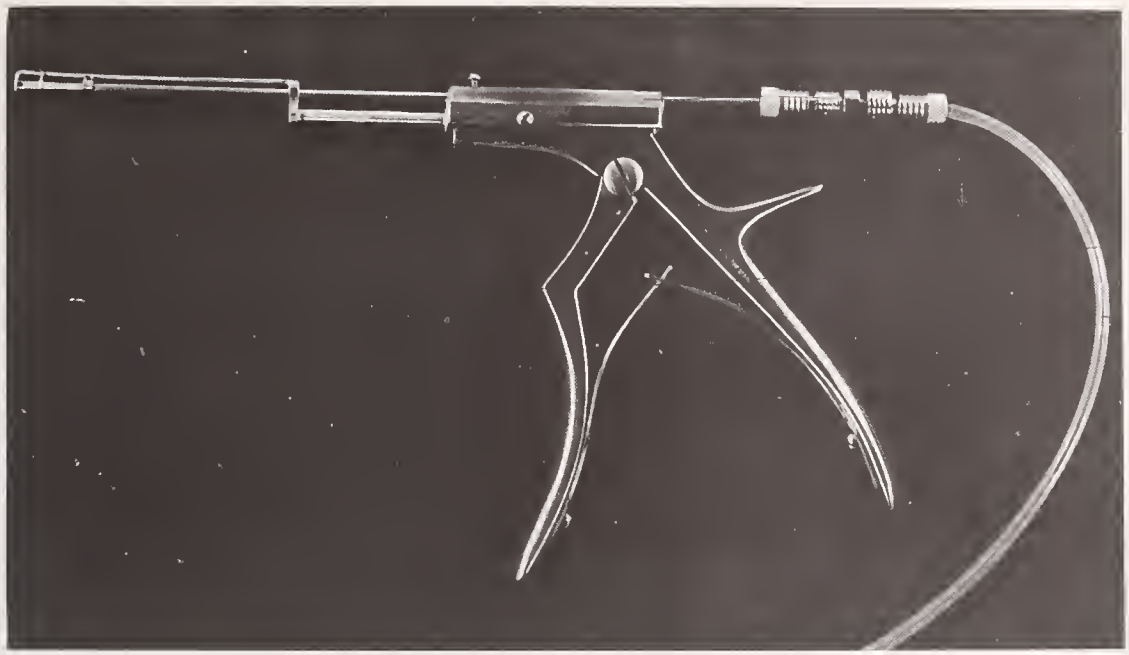

FIGURE 3. *Photograph of "vacuum approximator" showing vacuum tube, spring loaded handle for clamping tube to replaceable tube support.*

Squeezing the handle releases the tube from the tip of the applicator.

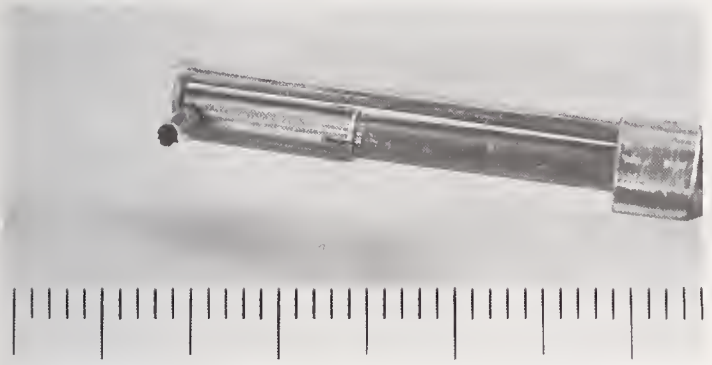

FIGURE 4. *Photograph showing porous tube clamped to tip of vacuum tube or barrel.*

Porous tube fits into the groove at end of a replaceable tube support, which may be removed from the tip of the barrel.

When the vacuum is applied to the barrel, suction at the ends of the porous tube first draws the proximal and then the distal nerve end into abutment within the tube. The nerve is then secured to the tube, either with an adhesive or mechanically by surrounding supporting tissue structure. An important feature of the instrument is the small size of the tube and holding device, thereby allowing access to spaces too small for the application of sutures.

Presently, experiments are being conducted with porous tubes 9 mm long and shorter by 1 mm internal diameter and having a wall thickness about 100 to 125 μm. The porosity of the tubes range between 20 and 30 percent. The pores were elongated circumferentially and longitudinally as a consequence of the platelet shape of the particles and the nature of the tube forming process as shown in figure 5. The average length of the pores ranged from 8.4 to 14 μm and the width from 2 to 2.5 μm for those tubes implanted to date.

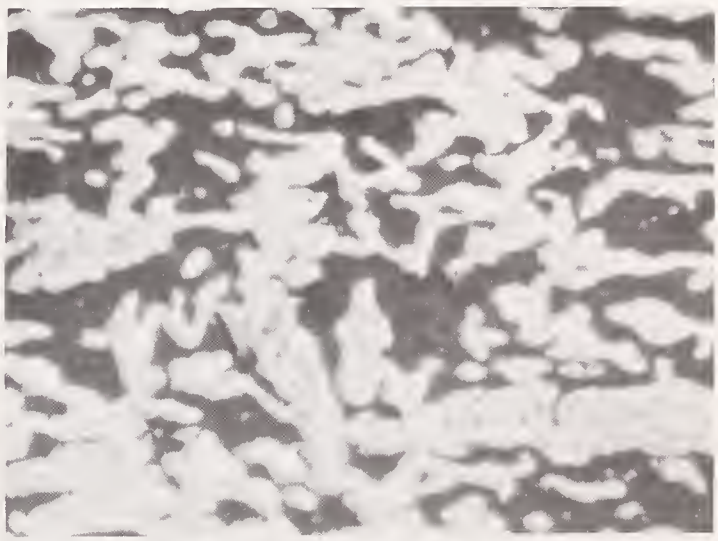

FIGURE 5. *Photomicrograph showing pore structure of cross section of wall of tube taken from Rat No. 7.*

Tube was fabricated from SS 316–L powder milled 192 hours and sintered at 1100°C for 1 hour in pure hydrogen.

6. Device Fabrication

The process steps for tube fabrication are outlined in figure 6.

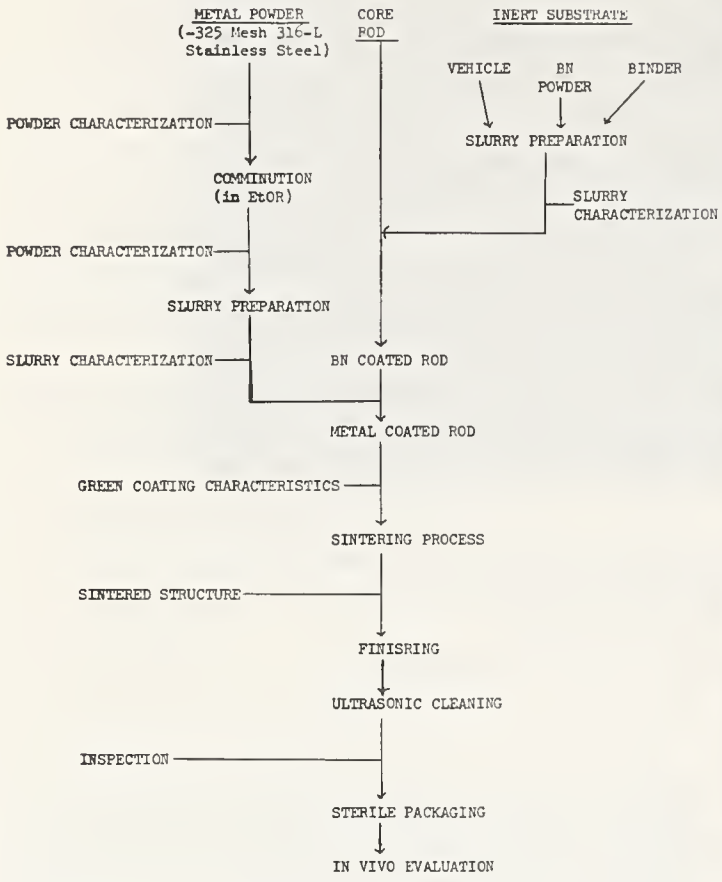

FIGURE 6. *Flow chart for porous tube fabrication and evaluation.*

It has been indicated earlier in relation to the factors contributing to successful nerve repair, that porosity and permeability of the tube wall are presently considered to be essential properties of the tube. Thus, powder characteristics and sintered pore structure have been an important part of the experimental investigation.

The finest powders commercially available in grade 316 L stainless steel are nominally −325 mesh (44 μm and less). Figure 7 shows the appearance of the commercial stainless steel powder as revealed with a scanning electron microscope (SEM). For a tube with a wall thickness of approximately 100 μm a much finer powder must be used. Since ball milling is a common, inexpensive method of reducing particle size in metal powders, it has been used to produce fine metal powder in the form of a coating slurry, a form which facilitates the pressureless forming technique used to fabricate the tubes. Figure 8 shows a Megapact [2,3] high

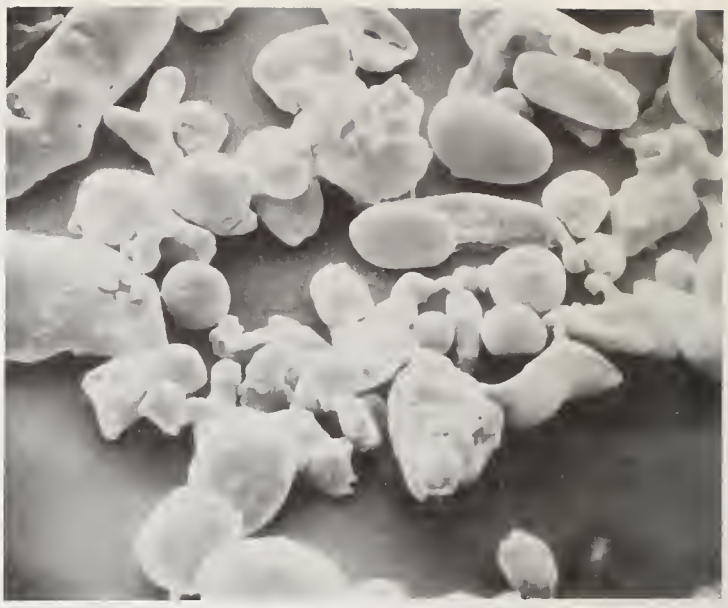

FIGURE 7. *SEM micrograph of as-received 316L powder.*

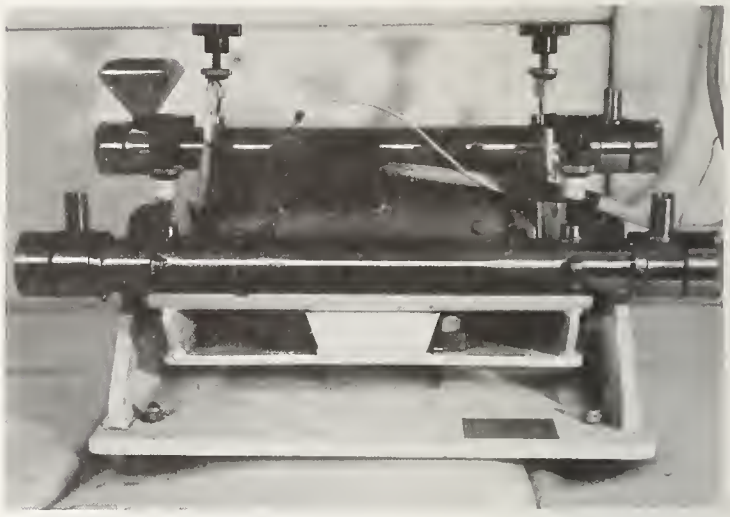

FIGURE 8. *High energy vibratory mill used to mill stainless steel powder.*

energy vibratory mill used to wet grind the stainless steel powder into a stainless steel slurry of particles having the size and shape shown in figure 9. The platelet shape of the particles facilitates the coating process.

Fabrication from fine powder permits adjustments to be made to the pore size, wall thickness, and surface area such that the tube is permeable to body fluids as well as resistant to the ingrowth of glial and extraneous (scar) tissue which inhibits regeneration.

A coating of inert material such as boron nitride is first applied to the core rod to prevent reaction and alloying between the core rod material and the stainless steel coating during sintering.

A dipping machine, shown in figure 10, is used to coat short core rods mounted vertically on a boron

[2] Available from Dymatron Inc., Box 11158, Lexington, Ky. 40511.

[3] Certain commercial materials and instruments may be identified in this publication in order to adequately specify the experimental procedure. In no case does such identification imply recommendation or endorsement by the National Bureau of Standards, nor does it imply that the equipment or instruments identified are necessarily the best available for the purpose.

nitride furnace boat. Coating is achieved by dipping and then withdrawing the core rods, first in the inert coating slurry, then, after drying, in the stainless steel slurry. After thoroughly drying, the double coated core rods are introduced into a furnace chamber and sintered in an atmosphere of hydrogen at temperatures between 1100 and 1200 °C for about 1 hour. After sintering, the sintered tubes are withdrawn from the core rods, facilitated by the slippery nature of boron nitride. The tubes are next cut to size, the vacuum port drilled, and sharp edges resulting from the cutting and drilling operations removed. Finally, the tubes are ultrasonically cleaned to remove the inert coating powder and stored in absolute alcohol until needed. Typical tubes are shown in figure 11.

FIGURE 9. *Stainless steel 316L ball milled for 192 hours in a rotary ball mill.*

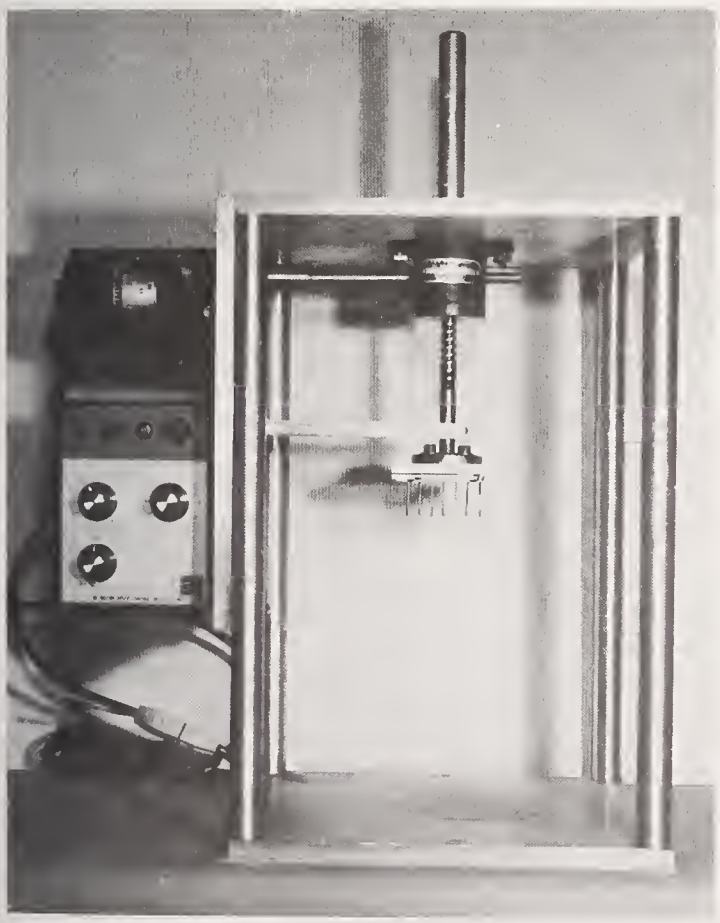

FIGURE 10. *Dipping machine used to multiple coat core rods in tube fabrication process.*

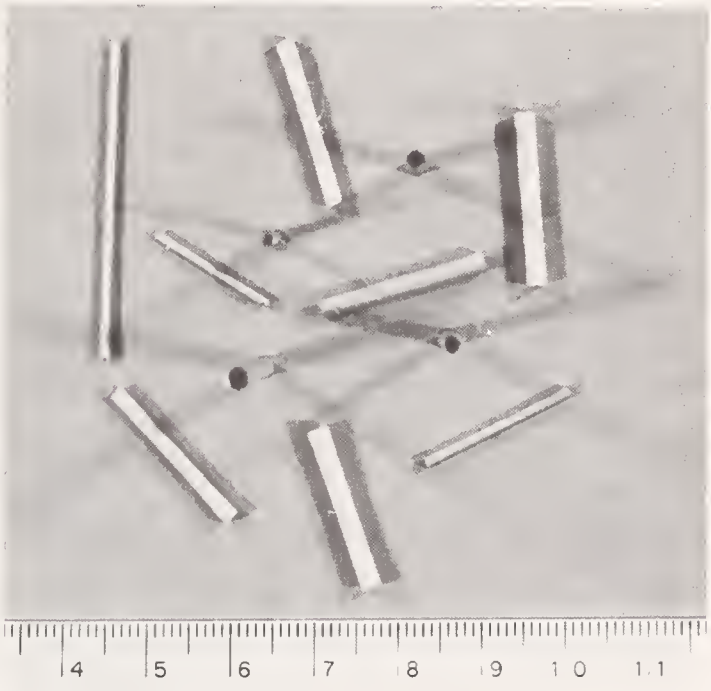

FIGURE 11. *Various porous tubes made by slurry coating-sintering process.*

7. Summary

The need for a more reliable method of neurography capable of significantly increasing the quality and number of neurorrhaphies that result in useful function was indicated. The general principles of nerve repair as currently practiced were reviewed briefly for consideration in the design of a tubular device to facilitate the repair of severed nerve tissue. The method of approach and organization of a research program to create and achieve fabrication of a device that attempts to satisfy the device design and functional requirements was briefly outlined. The concept of the repair technique was also briefly described. Finally the process employed to fabricate the tubes was briefly outlined. Part II of the paper describes some early results obtained using the method to repair the severed sciatic nerves of Wistar rats.

It should be mentioned that, although the system described herein was originally designed for the epineurorrhaphy of small nerves with one or two fascicles, there is the possibility of employing it for the repair of cleanly cut larger multifascicular nerves without segmental loss. Possibly application can be made to joining individual resected fascicles in instances of segmental loss necessitating nerve grafts to replace the deficiency of nerve tissue. The absence of tension would ensure abutment of the nerve within the porous tube, since no tension force is acting on them to cause separation of the nerve endings.

8. References

[1] Kleinert, H. E., Serafin, D., and Daniel, R. K., The place of microsurgery in hand surgery, Orthopedic Clincs of North America **4,** No. 4 (October 1973).

[2] Khodadad, Ghahriman, Microsurgical techniques in repair of peripheral nerves, Surgical Clinics of North America **52,** 1157–1166 (1972).

[3] Brown, Paul W., Factors influencing the success of the surgical repair of peripheral nerves, Surgical Clinics of North America **52,** 1137–1155 (1972).

[4] Hakstian, R. W., Perinaural neurrorhaphy, Orthopedic Clinics of North America **4** (October 1973).

[5] Buncke, Harry J., Digital nerve repairs, Surgical Clinics of North America **52,** 1267–1285 (1972).

[6] Smith, James W., Advances in facial nerve repair, Surgical Clinics of North America **52,** 1287–1306 (1972).

[7] Drake, Charles G., A caustic neuroma—repair of facial nerve with autogeneous graft, J. of Neurosurgery **17,** 836 (1960).

[8] Campbell, James B., Facial nerve repair: new surgical techniques, Trans. Am. Acad. Opthal. Ololaryng. **68,** 1068 (1964).

[9] Mayer, E. K., and Kimmel, D. L., The repair of severed motor and sensory spinal nerve roots by the arterial sleeve method of Anastomous, J. Comp. Neural **88,** 285–317 (1948).

[10] Carlsson, C. A., and Thulin, C. A., Studies on the bridging of irreducible gaps in severed ventral roots: an experimental study in cats, J. Neurol. Sci. **12,** 163 (1971).

[11] Campbell, James B., Peripheral nerve repair, Clinician Neurosurgery **17,** 77 (1969).

[12] Campbell, James B., Andrew, C., Bassett, L., and Bohler, J., Frozen-irradiated homographs shielded with microfilter sheaths in peripheral nerve surgery, J. of Trauma **3,** 303 (1963).

[13] Campbell, J. B., et. al., Microfilter sheaths in peripheral nerve surgery, J. of Trauma **1,** 139 (1961).

[14] Bassett, C. A., and Campbell, J. B., Calcification of millipore in vivo, Transplantation Bulletin **26,** 132 (1960).

[15] Lehman, R. A. W., Hayes, G. J., Leonard, F., Toxicity of alkyl 2-cyanoacrylates-peripheral nerve, Archives of Surgery **93,** 441 (1966).

[16] Leonard, F., Hemostatic applications of alpha cyanoacrylates: bonding mechanism and physiological degradation of bonds, Chapter 11, Handbood of Biomedical Plastics, (Pasadena Tech. Press, Pasadena, Ca.).

[17] Kleinert, H. E., and Griffin, J. M., Technique of nerve anastomosis, Orthopedic Clinics of North America **4** (October 1973).

[18] Millesi, H., Berger, A., and Meissel, G., Fascicular nerve grafting, Transitions of the Fifth International Congress of Plastic and Reconstructive Surgery, (London, Butterworth and Company, Ltd., 1971).

[19] Millesi, H., Meissel, G., and Berger, A., The interfascicular nerve grafting of the median and ulnar nerves, J. Bone Joint Surg. **54A,** 727 (1972).

[20] Bora, W. F., Peripheral nerve repair in cats, J. Bone Joint Surgery **49A,** No. 4 (1967).

[21] Peacock, E. F., and Van Winkle, W., Surgery and biology of wound repair (W. B. Saunders Co., Philadelphia, Pa., 1970).

[22] Visit with Dr. Millesi in Vienna, Austria, January 31, 1973.

NATIONAL BUREAU OF STANDARDS SPECIAL PUBLICATION 415,
Biomaterials, Proceedings of a Symposium held in conjunction with the Ninth Annual Meeting of the Association for the Advancement of Medical Instrumentation, New Orleans, La., April 19–20, 1974
(Issued May 1975).

A Nerve Implant Prosthesis for Facilitating Peripheral Nerve Regeneration * Part II. Development of the Prosthetic Device and System of Repair Neuroanatomical Aspects

James L. Hall

Department of Anatomy, College of Medicine, University of Cincinnati, Cincinnati, Ohio 45219

William E. Kuhn

Department of Materials Science and Metallurgical Engineering, University of Cincinnati, Cincinnati, Ohio 45219

The principal neuroanatomical aspects of peripherical nerve repair are the approximation of the severed ends and the minimizing of trauma during the approximation. The method of using vacuum to draw the severed ends down a porous tube seems to take these two factors into consideration. The porous tube provides a shielded environment for the regenerating nerve to grow into the approximated distal end. The porosity allows for the escape of edematous fluids, prevents the invasion of scar tissue and provides for the flow of nutritional fluids.

Histological and statistical results of the procedures are presented. In most instances the axons of the regenerating nerve grow across the gap and occupy the intact neurilema sheaths of the degenerating distal segments.

Key words: Histological evaluation; nerve axons; surgical procedure.

Any discussion of a method to facilitate peripheral nerve regeneration should first take cognizance of the fact peripheral nerves are capable of regenerating under ordinary circumstances. Our prosthesis and the method of application is an attempt to capitalize and enhance that capability.

Peripheral nerves, unlike their counter-parts in the central nervous system, are ensheathed in a connective tissue covering called the neurilemma or sheath of Schwann. This sheath effectively serves as a conduit or pipeline through which axons or fibers of a severed peripheral nerve can grow if no obstacles are encountered enroute to the target tissue.

If the damage or insult to the nerve has not occurred too close to the spinal cord and its accompanying dorsal root ganglion, the nerve cells or neurons in these locations will attempt to reconstitute themselves. The degree of success of the reconstitution will depend on the severity of the injury, the general health of the individual, and, as mentioned, the proximity of the injury to the cells themselves. An injury within two or three centimeters of the nerve cells will elicit greater damage to the cells and thus result in a poorer chance for functional recovery than would an injury some distance away.

Our study is centered on nerve separations that occur some distance from the cell bodies, so we may assume that a very large percentage, if not all, of the cells will recover from the injury.

The axons of the nerve begin to grow very tenuously from the proximal end of a severed nerve in about 3–5 days. At first these are very delicate strands. Such delicate tendril-like fibers have been called fibers of Von Bungner. They are groping or seeking a direction for further growth. It is at this early stage of regeneration that our prosthesis must satisfy the principal requirements. The tube provides a guide for the neurilemmal sheath to follow thus bridging the gap between the proximal intact nerve and the distal severed end. The neurilemma grows along the long axis of the tube. It is critical, of course, that the two ends of the nerve be brought in as close approximation as possible to provide the optimal situation so that the rapidly proliferating neurilemma will bridge the gap between the two nerve ends prior to the emerging regenerating axon.

It is also critical that the edematous fluids which accompany any injury to living tissue escape through the pores in the tube. If these fluids are confined within the tube or any other membrane they will act as a physical barrier to axon growth during the early phase of regeneration. Such fluids may indeed crush the axons and prevent regeneration if the volume is sufficient and no provision is made for

* This research was supported by the National Science Foundation under Grant GH-33873.

release. This undesirable possibility has prompted many workers to search for either natural or synthetic membranes that could be wrapped around the nerves and still permit escape of fluids.

Surgical Approach.—The sciatic nerve of the rat has been used for our experimental model. The nerve has approached through a midline incision in the posterior thigh, the musculature reflected, and the nerve cleared of any fascia or excessive connective tissue. The sciatic nerve in the rat is approximately 1 mm in diameter. The nerve was exposed for a distance of about 13–15 mm., and was then severed distal to the branch to the long head of the biceps femoris. Care was taken to produce a clean cut, so that the edges of the nerve were smooth. Usually the two separated ends of the nerve retracted and a gap of from 5–7 mm developed between them. The field was cleaned of blood or debris.

Method.—The method of nerve repair described in Part I was followed to bring the nerve ends into apposition. A fluid trap preceded the pressure gauge and vacuum pump. The pressure differential between the interior of the tube and ambient atmospheric pressure was adjusted to give a value between 50 and 75 mm Hg. This pressure range sufficed to draw the nerves firmly into the tube.

The anastomizer with the attached tube was placed in the field, and the two ends of the severed nerve were drawn into the long axis of the tube by suction. The distance the nerves are drawn into the tube can be gauged visually but it is not possible for us to determine accurately whether the ends meet. The nerve will adhere to the tube naturally, but we are experimenting with various adhesives to fix them in place. The wounds were sutured and the animals were given veterinary penicillin at the site of the wound and also intramuscularly.

Recovery.—The animals were examined frequently during the 120 day survival period. At first the animals dragged the operated limb. The limb becomes swollen, sores may develop, and care must be taken to prevent infection. Usually after 3–4 weeks signs of recovery could be seen. The limbs became functional and recovery was fairly complete by the end of 6 weeks. During the 120 day period a number of the animals regained full use of the limb, and responded to pinching or a pin prick by withdrawal. The rats could stand, walk, run, wash, and in every way demonstrated a functional recovery.

Histological Results.—The animals were anesthetized with nembutal, and sacrificed by perfusion with 10 percent formalin through the left ventricle of the heart, after a wash with warm normal saline to prevent blood clotting.

Photographs similar to that in figure 1 were taken of the gross experimental limbs with the tubes *in situ*. The nerve was removed and fixed for 10 days in 10 percent formalin. The excess connective tissue was cleaned off the tubes and the nerves were gently extracted from them. Figure 2 shows a

FIGURE 1. *Photograph of disected hind limbs of Rat No. 27 after 110 days showing the experimental leg with implanted tube T on the left and the normal leg on the right.*

Nerves N can be observed. Full function was restored to the operated leg with no indication of atrophy of muscles in the toes, foot or posterior thigh.

FIGURE 2. *Photograph showing sciatic nerve withdrawn from porous tube taken from Rat #15*

Before sacrifice rat exhibited withdrawal reflex, could support weight on operated leg, displayed no clawing of toes, and exhibited normal walking gait. Post mortem examination revealed no discernible atrophy of muscles of foot or thigh.

segment of nerve that has been withdrawn from a porous tube.

The nerves were then cut in three sections:— proximal to the cut, at the level of the cut but with proximal and distal tissue on either side of the cut, and distal to the cut. The tissues were blocked in paraffin and positioned to provide cross sections of the proximal and distal ends and longitudinal sections of the area around the cut. The tissues were impregnated with silver according to the Holmes modification of the Bielchowsky silver method.

Preliminary histological results seem to indicate that if the procedure described is done properly there is a minimal axonal loss in the regenerated nerve. Comparisons of proximal and distal ends indicate a diminution of axons so slight as to make it difficult to distinguish between the two levels.

Longitudinal sections (fig. 2) at the level of the cut also show no appreciable difference between the proximal and distal ends. The level of the cut, however, can be identified. Axonal counts are in progress but we are not able to report on them in this paper. However, it would appear that the axonal difference between the proximal and distal ends will be less than 20 percent. (See figs. 3 and 4).

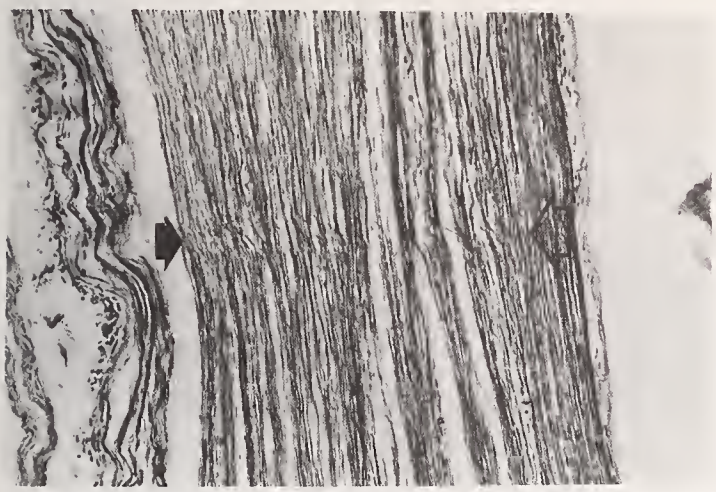

FIGURE 3. *Photomicrograph at the level of sectioning of rat sciatic nerve.*

Note relative similarity between two portions of axons above and below the cut. (Holmes Silver Impregnation 100×)

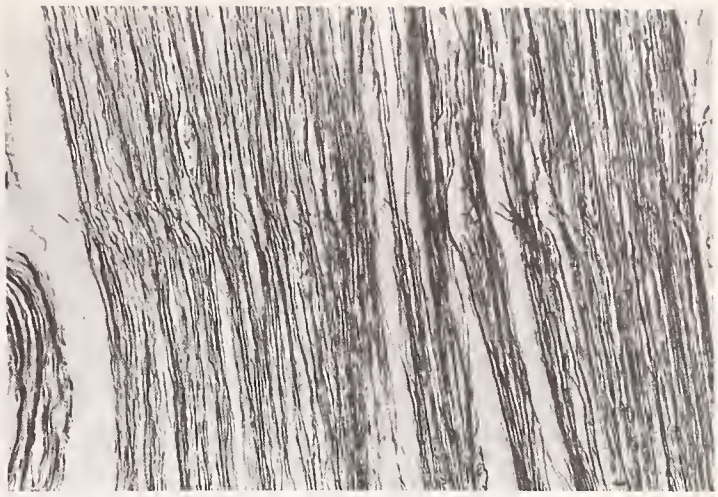

FIGURE 4. *Hieber power magnification at level of cut of regenerated rat sciatic nerve.*

Only a few axons do not show effective repair. (Holmes Silver Impregnation 220×)

Further work is needed, but we suggest that this method of facilitating peripheral nerve regeneration holds great promise. It may be possible to repair small nerves where current surgical methods often produce further axonal loss due to the manipulation involved. Further, certain cranial nerves inside the cranial cavity are practically inaccessible for surgical repair but could be joined with our tube. In addition, this method may result in the repair and restoration of many nerves that now must be sacrificed in order to achieve more significant surgical objectives.

☆ U.S. GOVERNMENT PRINTING OFFICE : 1975 O—565-800

NBS-114A (REV. 7-73)

U.S. DEPT. OF COMM. BIBLIOGRAPHIC DATA SHEET	1. PUBLICATION OR REPORT NO. NBS SP-415	2. Gov't Accession No.	3. Recipient's Accession No.

4. TITLE AND SUBTITLE
Biomaterials (Proceedings of the Symposium on Biomaterials, 9th Annual Meeting, Association for Advancement of Medical Instrumentation, New Orleans, LA. April 19-20, 1974)

5. Publication Date
May 1975

6. Performing Organization Code

7. AUTHOR(S)
E. Horowitz and J. L. Torgesen, Editors

8. Performing Organ. Report No.

9. PERFORMING ORGANIZATION NAME AND ADDRESS

NATIONAL BUREAU OF STANDARDS
DEPARTMENT OF COMMERCE
WASHINGTON, D.C. 20234

10. Project/Task/Work Unit No.

11. Contract/Grant No.

12. Sponsoring Organization Name and Complete Address (Street, City, State, ZIP)

As Above

13. Type of Report & Period Covered
N/A

14. Sponsoring Agency Code

15. SUPPLEMENTARY NOTES

Library of Congress Catalog Card Number: 74-30305

16. ABSTRACT *(A 200-word or less factual summary of most significant information. If document includes a significant bibliography or literature survey, mention it here.)*

This volume is based on papers presented at the Symposium on Biomaterials, held in conjunction with the Ninth Annual Meeting of the Association for the Advancement of Medical Instrumentation, New Orleans, LA. April 19-20, 1974. It provides a review of special topics in biomaterials research selected to focus attention on some noteworthy achievements. The topics covered include plasma-polymerized polymers and their application in biomedicine; biocompatibility of ceramic materials and their application both as inert coatings for synthetic implants and as porous materials for bone repair; the selection of metallic implant materials through engineering and medical considerations; in vitro testing of thromboresistance; adsorption of blood proteins on synthetic substrates; a prosthesis for nerve regeneration; and properties of fibrous biomaterials.

17. KEY WORDS *(six to twelve entries; alphabetical order; capitalize only the first letter of the first key word unless a proper name; separated by semicolons)*

Key words: Biocompatibility; biomaterials; blood protein; ceramic implants; implantable electrodes; metallic implants; nerve prosthesis; synthetic implants; thromboresistance.

18. AVAILABILITY

[X] Unlimited

[ ] For Official Distribution. Do Not Release to NTIS

[X] Order From Sup. of Doc., U.S. Government Printing Office Washington, D.C. 20402, SD Cat. No. C13.10:415

[ ] Order From National Technical Information Service (NTIS) Springfield, Virginia 22151

19. SECURITY CLASS (THIS REPORT)
UNCLASSIFIED

21. NO. OF PAGES
109

20. SECURITY CLASS (THIS PAGE)
UNCLASSIFIED

22. Price
$1.75

USCOMM-DC 29042-P74

NBS TECHNICAL PUBLICATIONS

PERIODICALS

JOURNAL OF RESEARCH reports National Bureau of Standards research and development in physics, mathematics, and chemistry. It is published in two sections, available separately:

• Physics and Chemistry (Section A)

Papers of interest primarily to scientists working in these fields. This section covers a broad range of physical and chemical research, with major emphasis on standards of physical measurement, fundamental constants, and properties of matter. Issued six times a year. Annual subscription: Domestic, $17.00; Foreign, $21.25.

• Mathematical Sciences (Section B)

Studies and compilations designed mainly for the mathematician and theoretical physicist. Topics in mathematical statistics, theory of experiment design, numerical analysis, theoretical physics and chemistry, logical design and programming of computers and computer systems. Short numerical tables. Issued quarterly. Annual subscription: Domestic, $9.00; Foreign, $11.25.

DIMENSIONS/NBS (formerly Technical News Bulletin)—This monthly magazine is published to inform scientists, engineers, businessmen, industry, teachers, students, and consumers of the latest advances in science and technology, with primary emphasis on the work at NBS. The magazine highlights and reviews such issues as energy research, fire protection, building technology, metric conversion, pollution abatement, health and safety, and consumer product performance. In addition, it reports the results of Bureau programs in measurement standards and techniques, properties of matter and materials, engineering standards and services, instrumentation, and automatic data processing.

Annual subscription: Domestic, $9.45; Foreign, $11.85.

NONPERIODICALS

Monographs—Major contributions to the technical literature on various subjects related to the Bureau's scientific and technical activities.

Handbooks—Recommended codes of engineering and industrial practice (including safety codes) developed in cooperation with interested industries, professional organizations, and regulatory bodies.

Special Publications—Include proceedings of conferences sponsored by NBS, NBS annual reports, and other special publications appropriate to this grouping such as wall charts, pocket cards, and bibliographies.

Applied Mathematics Series—Mathematical tables, manuals, and studies of special interest to physicists, engineers, chemists, biologists, mathematicians, computer programmers, and others engaged in scientific and technical work.

National Standard Reference Data Series—Provides quantitative data on the physical and chemical properties of materials, compiled from the world's literature and critically evaluated. Developed under a world-wide program coordinated by NBS. Program under authority of National Standard Data Act (Public Law 90-396).

NOTE: At present the principal publication outlet for these data is the Journal of Physical and Chemical Reference Data (JPCRD) published quarterly for NBS by the American Chemical Society (ACS) and the American Institute of Physics (AIP). Subscriptions, reprints, and supplements available from ACS, 1155 Sixteenth St. N. W., Wash. D. C. 20056.

Building Science Series—Disseminates technical information developed at the Bureau on building materials, components, systems, and whole structures. The series presents research results, test methods, and performance criteria related to the structural and environmental functions and the durability and safety characteristics of building elements and systems.

Technical Notes—Studies or reports which are complete in themselves but restrictive in their treatment of a subject. Analogous to monographs but not so comprehensive in scope or definitive in treatment of the subject area. Often serve as a vehicle for final reports of work performed at NBS under the sponsorship of other government agencies.

Voluntary Product Standards—Developed under procedures published by the Department of Commerce in Part 10, Title 15, of the Code of Federal Regulations. The purpose of the standards is to establish nationally recognized requirements for products, and to provide all concerned interests with a basis for common understanding of the characteristics of the products. NBS administers this program as a supplement to the activities of the private sector standardizing organizations.

Federal Information Processing Standards Publications (FIPS PUBS)—Publications in this series collectively constitute the Federal Information Processing Standards Register. Register serves as the official source of information in the Federal Government regarding standards issued by NBS pursuant to the Federal Property and Administrative Services Act of 1949 as amended, Public Law 89-306 (79 Stat. 1127), and as implemented by Executive Order 11717 (38 FR 12315, dated May 11, 1973) and Part 6 of Title 15 CFR (Code of Federal Regulations).

Consumer Information Series—Practical information, based on NBS research and experience, covering areas of interest to the consumer. Easily understandable language and illustrations provide useful background knowledge for shopping in today's technological marketplace.

NBS Interagency Reports (NBSIR)—A special series of interim or final reports on work performed by NBS for outside sponsors (both government and non-government). In general, initial distribution is handled by the sponsor; public distribution is by the National Technical Information Service (Springfield, Va. 22161) in paper copy or microfiche form.

Order NBS publications (except NBSIR's and Bibliographic Subscription Services) from: Superintendent of Documents, Government Printing Office, Washington, D.C. 20402.

BIBLIOGRAPHIC SUBSCRIPTION SERVICES

The following current-awareness and literature-survey bibliographies are issued periodically by the Bureau:

Cryogenic Data Center Current Awareness Service

A literature survey issued biweekly. Annual subscription: Domestic, $20.00; foreign, $25.00.

Liquefied Natural Gas. A literature survey issued quarterly. Annual subscription: $20.00.

Superconducting Devices and Materials. A literature survey issued quarterly. Annual subscription: $20.00. Send subscription orders and remittances for the preceding bibliographic services to National Technical Information Service, Springfield, Va. 22161.

Electromagnetic Metrology Current Awareness Service Issued monthly. Annual subscription: $100.00 (Special rates for multi-subscriptions). Send subscription order and remittance to Electromagnetics Division, National Bureau of Standards, Boulder, Colo. 80302.

U.S. DEPARTMENT OF COMMERCE
National Bureau of Standards
Washington, D.C. 20234

OFFICIAL BUSINESS

Penalty for Private Use, $300

POSTAGE AND FEES PAID
U.S. DEPARTMENT OF COMMERCE
COM-215

FOURTH CLASS MAIL